Trends in Optics and Photonics
TOPS Volume 36
Series Editor: Tingye Li

Laser Applications to Chemical and Environmental Analysis

Technical Digest Postconference Edition

February 11–13, 2000

Eldorado Hotel
Santa Fe, New Mexico

Sponsored by
Optical Society of America

Partial support from
Air Force Research Laboratory
Army Research Office

OSA®
Optical Society of America

Trends in Optics and Photonics

TOPS Volume 36

Series Editor: Tingye Li

Laser Applications to Chemical and Environmental Analysis

Technical Digest Postconference Edition

February 11–13, 2000

Eldorado Hotel
Santa Fe, New Mexico

Sponsored by
Optical Society of America
2010 Massachusetts Avenue, NW
Washington, DC 20036-1023

Partial support from
Air Force Research Laboratory
Army Research Office

OSA®
Optical Society of America

Articles in this publication may be cited in other publications. To facilitate access to the original publication source, the following form for the citation is suggested:

> Name of Author(s), Title of Paper, OSA *Trends in Optics and Photonics (TOPS) Vol. 36, Laser Applications to Chemical and Environmental Analysis*, Technical Digest, Postconference Edition (Optical Society of America, Washington, DC 2000), pp. xx-xx.

ISSN	1094-5695
ISBN	1-55752-626-5
LCCN	00-102220

Printed in the USA

REPORT DOCUMENTATION PAGE

Form Approved
OMB NO. 0704-0188

1. AGENCY USE ONLY (Leave Blank)	2. REPORT DATE	3. REPORT TYPE AND DATES COVERED
	January 16, 2001	Final 12/15/99 - 12/14/00

4. TITLE AND SUBTITLE
Organization of the 2000 Laser Applications to Chemical Environmental Analysis

5. FUNDING NUMBERS
DAAD19-00-1-0011

6. AUTHOR(S)
John A. Thorner

7. PERFORMING ORGANIZATION NAME(S) AND ADDRESS(ES)
Optical Society of America
2010 Massachusetts Ave., NW
Washington DC 20036

8. PERFORMING ORGANIZATION REPORT NUMBER

9. SPONSORING / MONITORING AGENCY NAME(S) AND ADDRESS(ES)
U. S. Army Research Office
P.O. Box 12211
Research Triangle Park, NC 27709-2211

10. SPONSORING / MONITORING AGENCY REPORT NUMBER
ARO 41043.1-EV-CF

11. SUPPLEMENTARY NOTES
The views, opinions and/or findings contained in this report are those of the author(s) and should not be construed as an official Department of the Army position, policy or decision, unless so designated by other documentation.

12 a. DISTRIBUTION / AVAILABILITY STATEMENT
Approved for public release; distribution unlimited.

12 b. DISTRIBUTION CODE

13. ABSTRACT (Maximum 200 words)

The seventh topical meeting on Lasers and Applications to Chemical and Environmental Analysis continued the tradition of state-of-the-art research and applications and was presented in an informal atmosphere designed to foster communication among researchers and practitioners in the field. New developments in optical sources, instrumentation, and spectroscopic techniques are principal driving forces for the increased use of lasers in chemical analysis and environmental monitoring
Topics that were covered:

- Application of new laser sources to analytical spectroscopy
- Diode laser applications in combustion, industrial, and atmospheric measurements
- Laser diagnostics for combustion
- Laser based detection coupled to microanalytical separations
- Microoptical systems for chemical analysis
- Laser based detection for high density chemical sensing arrays
- Development and applications of single-molecule spectroscopy
- Fluorescence based methods for detection of individual biomolecules (including imaging)

14. SUBJECT TERMS

15. NUMBER OF PAGES

16. PRICE CODE

17. SECURITY CLASSIFICATION OR REPORT	18. SECURITY CLASSIFICATION ON THIS PAGE	19. SECURITY CLASSIFICATION OF ABSTRACT	20. LIMITATION OF ABSTRACT
UNCLASSIFIED	UNCLASSIFIED	UNCLASSIFIED	UL

Contents

Agenda		v
FA	Microanalytical and Single Molecule Techniques 1	1
FB	Microanalytical and Single Molecule Techniques 2	11
FC	Advances in Spectroscopic Sources	21
FD	Ringdown and Polarization Spectroscopy	37
SaA	Quantum Cascade Lasers and Applications	49
SaB	Environmental and Industrial Applications of Diode Lasers	67
SaC	Poster Session	87
SuA	Combustion Diagnostics 1	125
SuB	Combustion Diagnostics 2	139
SuC	Analytical Applications 1	155
SuD	Analytical Applications 2	169
Key to Authors and Presiders		184

Technical Program Committee

Mark G. Allen, *Physical Sciences Inc., USA, General Chair*

Robert W. Shaw, *Oak Ridge Natl. Lab., USA, General Chair*

Volker Sick, *Univ. of Michigan, USA, General Chair*

David J. Rakestraw, *Sandia Natl. Labs., USA, Program Chair*

Markus Sauer, *Univ. of Heidelberg, Germany, Program Chair*

Alan C. Stanton, *Southwest Sciences, Inc., USA, Program Chair*

William P. Ambrose, *Los Alamos Natl. Lab., USA*

Douglas S. Baer, *Stanford Univ., USA*

Jay B. Jeffries*, *SRI Intl., USA*

Kevin L. McNesby, *ARL, USA*

Peter Werle, *Fraunhofer Inst. for Atmospheric Environmental Res., Germany*

**Denotes OSA Technical Council Representative*

Agenda

■ Friday
■ February 11, 2000

7:00am–6:00pm
Registration

9:30am–4:00pm
Exhibit Hours

7:50am–8:00am
Opening Remarks

8:00am–9:40am
Room: Anasazi North
FA ■ Microanalytical and Single Molecule Techniques 1
David J. Rakestraw, Sandia Natl. Labs., USA, Presider

FA1 8:00am (Invited)
Microfabricated fluidic devices: New approaches to chemical measurements, *J. Michael Ramsey, Oak Ridge Natl. Lab., USA.*
Micromachining tools have led to a number of silicon devices for state variable measurement. The impact of microfabrication tools on the acquisition of chemical and biochemical information will be discussed. **(p. 2)**

FA2 8:30am (Invited)
Micro-optical systems for laser-induced fluorescence in capillary separations, *M.E. Warren, W.C. Sweatt, J.R. Wendt, C.G. Bailey, D.W. Arnold, C.M. Matzke, S.A. Kemme, A.A. Allerman, T.R. Carter, R.E. Asbill, S. Samora, Sandia Natl. Labs, USA.*
We describe the design and fabrication of a micro-optical system for an integrated capillary-channel electrochromatograph with laser-induced fluorescence detection. The design uses substrate-mode propagation and utilizes vertical-cavity surface-emitting lasers and high performance microlenses. **(p. 3)**

FA3 9:00am
Fluorescence lifetime imaging microscopy (FLIM) on the single molecule level, *P. Tinnefeld, V. Buschmann, D.-P. Herten, J.-P. Knemeyer, M. Sauer, Univ. of Heidelberg, Germany.*
We present time-resolved measurements on individual dye molecules and labeled oligonucleotides of different sequence immobilized on amino silanized and streptavidin coated glass surfaces. In order to investigate the dynamical fluorescence behavior of individual fluorescent probe molecules with high temporal resolution, i.e. dark state formation and quenching due to different interaction geometries between the dye and the biomolecule, a single molecule search program was developed. Our data clearly indicate that the additional parameter fluorescence decay time provides detailed information about the microenvironment of individual probe molecules. **(p. 5)**

FA4 9:20am
Time-resolved photon counting for multiplexed DNA electrophoreses separations, *Lloyd M. Davis, Univ. of Tennessee Space Inst., USA; Jim L. Amen, Dan L. Draney, Lyle R. Middendorf, Rex A. Peterson, LI-COR, Inc., USA.*
Monte Carlo simulations are used to evaluate time resolved photon counting as a means for identifying and quantifying overlapping electropherogram bands, which have been labeled by dyes with disparate fluorescence lifetimes. **(p. 8)**

9:40am–10:10am
Concourse Area
Coffee Break

10:10am–11:50am
Room: Anasazi North
FB ■ Microanalytical and Single Molecule Techniques 2
Markus Squer, Univ. of Heidelberg, Germany; William P. Ambrose, Los Alamos Natl. Lab., USA, Presiders

FB1 10:10am (Invited)
DNA fragment sizing by single molecule detection, *Erica J. Larson, Janetta R. Penttila, Hong Cai, James H. Jett, Stefan Burde, Babetta L. Marrone, Richard A. Keller, Los Alamos Natl. Lab., USA.*
We have developed the capability to detect and identify single fluorescent molecules as they flow through a focused laser beam. The application of single molecule detection to DNA fragment sizing (fingerprinting) will be described. **(p. 12)**

FB2 10:40am (Invited)
Multidimensional fluorescence spectroscopy of single molecules, *C.A.M. Seidel, S. Berger, C. Eggeling, J. Schaffer, E. Schweinberger, A. Volkmer, J. Widengren, Max-Planck-Inst. for Biophysical Chemistry, Germany.*
Multichannel-detection for simultaneous registration of all information on a signal burst (intensity, lifetime, anisotropy *r* and spectral range) is used for analytics and studies of conformational dynamics of a single fluorescent labeled molecule in solution. **(p. 14)**

FB3 11:10am
Detection of target molecules on the single molecule level using confocal fluorescence microscopy in combination with microelectrophoresis, *A. Schulz, V. Buschmann, T. Hubner, H. Neuweiler, M. Sauer, J. Wolfrum, Univ. of Heidelberg, Germany.*
We present a new method for highly sensitive detection of target molecules (antibodies, etc.) in the concentration range < 10-11 M in homogeneous assays. Upon modification of the labeled probe molecules (antigens, etc.) by addition of positive charges a separation between bound and free probe molecules is possible. Applying a microcapillary with an inner diameter of 0.5 æm at the small end in combination with microelectrophoresis individual streptavidin/biotin complexes were detected on the single molecule level even in a 200-fold excess of free labeled biotin molecules. **(p. 15)**

FB4 11:30am
Single molecule DNA sequencing in microcapillaries, *M. Sauer, F. Göbel, K.-T. Han, Univ. of Heidelberg, Germany; C. Zander, Univ. Gesamthochschule Siegen, Germany.*
We present efficient detection and identification of single dye labeled mononucleotide molecules released from DNA strands bound to an optical fiber in a cone shaped microcapillary with an inner diameter of 0.5 æm at the small end. Cy5-dCMP and MR121-dUMP were degraded enzymatically with the 3'-5' proofreading activity of T4-DNA-polymerase from statistically labeled DNA strands and identified due to their characteristic fluorescence decay times of 1.43±0.28 ns (CY5-dCMP) and 2.21±0.85 ns (MR121-dUMP). **(p. 18)**

11:50am–1:30pm
Lunch Break (on your own)

1:30pm–3:20pm
Room: Anasazi North
FC ▪ Advances in Spectroscopic Sources
Peter W. Werle, Fraunhofer Inst. for Atmospheric Environmental Res., USA, Presider

FC1 1:30pm (Invited)
"W" quantum well diode and optically-pumped mid-IR lasers operating at high temperatures, *J.R. Meyer, W.W. Bewley, L.J. Olafsen, I. Vurgaftman, C.L. Felix, D.W. Stokes, M.J. Yang, NRL, USA; H. Lee, R.J. Menna, R.U. Martinelli, D.Z. Garbuzov, J.C. Connolly, Sarnoff Corp., USA; M. Maiorov, A.R. Sugg, G.H. Olsen, Sensors Unlimited, Inc., USA.*
Type-II antimonide diode lasers have achieved pulsed operation at a wavelength of 3.3 microns, and optically-pumped devices have operated cw up to 210 K at a wavelength of 6.1 microns. **(p. 22)**

FC2 2:00pm
High power mid-IR interband cascade lasers, *J.D. Bruno, R.Q. Yang, J.L. Bradshaw, J.T. Pham, D.E. Wortman, ARL, USA.*
Mid-IR (3.9 micron) type-II interband cascade lasers based on InAs/GaInSb heterostructures are demonstrated. Devices, under differing conditions, show lasing up to 217K, peak output powers exceeding 4W/facet at 80K, and cw operation at 70K. **(p. 24)**

FC3 2:20pm
Guided-wave difference-frequency sources for infrared spectroscopy, *Konstantin P. Petrov, Arti Prasad Roth, Thomas L. Patterson, Douglas J. Bamford, Gemfire Corp., USA.*
Reported are design, performance, and spectroscopic application of guided-wave, diode-pumped difference-frequency sources. They employ channel waveguides in lithium niobate and operate at room temperature, with over 100 microwatts of power at 3.6 microns. **(p. 27)**

FC4 2:40pm
Development of infrared chemical sensors based on quasi-phasematched, periodically poled lithium niobate sources, *Scott E. Bisson, Thomas J. Kulp, Ken Aniolek, Uta-Barbara Goers, Karla Armstrong, Bruce Richman, Sandia Natl. Labs, USA; Peter Powers, Univ. of Dayton, USA.*
We describe the development of novel infrared chemical sensors based on the non-linear optical material periodically poled lithium niobate. **(p. 30)**

FC5 3:00pm
Diode-pumped 214.8-nm Nd:YAG/Cr^{4+}:YAG microchip-laser system for the detection of NO, *J. Wormhoudt, J.H. Shorter, Aerodyne Res., Inc., USA; J.J. Zayhowski, MIT, USA.*
A passively Q-switched Nd:YAG/Cr^{4+}:YAG microchip laser at 214.8-nm (46556 cm^{-1}, the fifth harmonic of 1.074-μm) was developed. NO was detected by laser-induced fluorescence at a sensitivity of ~15 ppb^{v} in a simple, compact optical system. **(p. 33)**

3:20pm–3:50pm
Concourse Area
Coffee Break

3:50pm–5:10pm
Room: Anasazi North
FD ■ Ringdown and Polarization Spectroscopy
Robert W. Shaw, Oak Ridge Natl. Lab., USA, Presider

FD1 3:50pm
Cavity ring-down spectroscopy with a continuous wave laser and analysis of the uncertainty in concentration measurement, *Jae Won Hahn, Jae Wan Kim, Korea Res. Inst. of Standards and Science, Korea.*
We demonstrate a new-design cw cavity ringdown spectrometer. Coupling efficiency of the cw CRDS system and uncertainties in the concentration measurements are analyzed. **(p. 38)**

FD2 4:10pm
CW integrated cavity output spectroscopy, *A. O'Keefe, J.J. Scherer, J.B. Paul, H. Jiao, Los Gatos Res., USA.*
An approach is described that enables continuous, narror band laser sources to be used in conjuction with the recently demonstrated integrated cavity output spectroscopy (ICOS) technique to obtain sensitive quantitative absorption spectra. **(p. 41)**

FD3 4:30pm
Broadband ringdown spectral photography for real-time environmental monitoring, *James J. Scherer, Joshua B. Paul, Hong Jiao, Anthony O'Keefe, Los Gatos Res., USA.*
A new technique capable of obtaining high sensitivity, high resolution "ringdown" absorption spectra over a large optical bandwidth is presented. Data demonstrating sensitivity, spectral coverage, and energy requirements of the light source are presented. **(p. 44)**

FD4 4:50pm
Saturated polarization spectroscopy with a picosecond laser for quantitative concentration measurements, *Thomas A. Reichardt, Roger L. Farrow, Fabio Di Teodoro, Sandia Natl. Labs, USA; Robert P. Lucht, Texas A&M Univ., USA.*
The collisional dependence of saturated polarization spectroscopy with a picosecond laser is investigated by probing hydroxyl in a flow cell. **(p. 46)**

■ Saturday
■ February 12, 2000

7:30am–5:30pm
Registration

9:30am–12:30pm
Exhibit Hours

8:00am–9:40am
Room: Anasazi North

SaA ■ Quantum Cascade Lasers and Applications

Mark G. Allen, Physical Sciences Inc., USA, Presider

SaA1 8:00am
Mid-infrared, single-mode, continuously tunable Quantum Cascade distributed feedback lasers, *Claire Gmachl, Federico Capasso, Rüdeger Köhler, Alessandro Tredicucci, Deborah L. Sivco, James N. Baillargeon, Albert L. Hutchinson, Alfred Y. Cho, Bell Labs., Lucent Tech., USA*
High performance, continuously tunable, single-mode Quantum Cascade distrubed feedback lasers at 5-10 μm wavelength and operating either in pulsed mode up to room temperature or in continuous wave around liquid nitrogen temperature are reported. **(p. 50)**

SaA2 8:20am
Trace gas detection in ambient air using a 7.9 micron QC-DFB laser, *A.A. Kosterev, R.F. Curl, F.K. Tittel, Rice Univ., USA; C. Gmachl, F. Capasso, D.L. Sivco, J.N. Baillargeon, A.L. Hutchinson, A.Y. Cho, Bell Labs, Lucent Tech., USA.*
Spectroscopic trace gas detection in the 7.9 micron spectral region with a single frequency quantum cascade distributed feedback (QC-DFB) laser was demonstrated. A 100-m multipass cell and a "zero-air" background subtraction technique were used to enhance the detection sensitivity. **(p. 54)**

SaA3 8:40am
Sensitive absorption spectroscopy using the quantum cascade laser, *Edward A. Whittaker, Stevens Inst. of Tech., USA; James F. Kelly, Richard M. Williams, Steven W. Sharpe, John S. Hartman, Pacific Northwest Natl. Lab., USA; Claire Gmachl, Federico Capasso, Deborah L. Sivco, James N. Baillargeon, Alfred Y. Cho, Bell Labs, Lucent Tech., USA.*
We have used frequency modulated quantum cascade lasers to make sensitive absorption spectroscopy detection of H_20 and NO vapors at low pressure and low concentration. 5 micron and 8 micron lasers show excellent properties for sensitive spectroscopy. **(p. 57)**

SaA4 9:00am
Application of balanced detection to absorption measurements with quasi-cw QC lasers, *D. Sonnenfroh, E. Wetjen, M. Miller, M. Allen, Physical Sciences Inc., USA; Claire Gmachl, Federico Capasso, Albert L. Hutchinson, Deborah L. Sivco, James N. Baillargeon, Alfred Y. Cho; Bell Labs, Lucent Tech., USA.*
We have demonstrated directed absorption measurements of NO at 5.4 μm using QC lasers in combination with a balanced detection technique. Peak absorptions of 100 ppm have been measured with excellent signal-to-noise ratio. **(p. 60)**

SaA5 9:20am
Pound–Drever–Hall frequency stabilization of a quantum-cascade laser to an infrared ro-vibrational molecular resonance, *Richard M. Williams, James F. Kelly, John S. Hartman, Steven W. Sharpe, Pacific Northwest Natl. Lab., USA; Matthew S. Taubman, John L. Hall, JILA, Univ. Colorado, NIST, USA; Claire Gmachl, Federico Capasso, Deborah L. Sivco, James N. Baillargeon, Alfred Y. Cho, Bell Labs, Lucent Tech., USA.*
A frequency modulation method (Pound-Drever-Hall) has been used to frequency-stablize and lock a quantum-casade laser (QCL) to a ro-vibrational resonance on nitrous oxide at 8.5μm. Experiments with stablized QCLs (kilohertz linewidths) will be discussed. **(p. 63)**

9:40am–10:10am
Concourse Area
Coffee Break

10:10am–12:20pm
Room: Anasazi North

SaB ■ Environmental and Industrial Applications of Diode Lasers

Alan C. Stanton, Southwest Sciences Inc., USA, Presider

SaB1 10:10am (Invited)
A fast chemical sensor for atmospheric trace gas flux measurements, *Peter N. Werle, Fraunhofer Inst. for Atmospheric Environmental Res., Germany.*
A fast response chemical sensor based on tunable diode laser spectroscopy will be described and results from field eddy correlation measurements of methane fluxes from rice paddy fields located in Vercelli, Italy will be presented. **(p. 68)**

SaB2 10:40am

A portable, LN_2–free, multi-chemical sensor based upon mid-infrared laser absorption spectroscopy, *John S. Hartman, Timothy L. Stewart, James F. Kelly, Steven W. Sharpe, Richard M. Williams, Pacific Northwest Natl. Lab., USA; Claire Gmachl, Federico Capasso, Deborah L. Sivco, James N. Baillargeon, Alfred Y. Cho, Bell Labs, Lucent Tech., USA.*

The development of a field-portable, cryo-cooled infrared tunable laser absorption spectrometer (TLAS) will be presented. The configuration includes either multi-quantum-cascade or multi-lead-salt lasers, a 36 m Herriott-cell with integrated laser/detector with cooling via Stirling cryo-coolers. **(p. 71)**

SaB3 11:00am

Pseudo-random code-based differential absorption LIDAR in the LWIR spectral region, *E.T. Wetjen, M.G. Allen, W.J. Marinelli, C.M. Gittins, Physical Sciences Inc., USA; C. Gmachl, F. Capasso, A.L. Hutchinson, D.L. Sivco, J.N. Baillargeon, A.Y. Cho, Bell Labs, Lucent Tech., USA.*

Using a quantum cascade laser operating near 8 æm, we have demonstrated intensity modulation of the transmitted beam and deconvolution of backscattered return necessary for developing a quasi-continuous wave DIAL transceiver for remote sensing applications. **(p. 74)**

SaB4 11:20am

***In-situ* monitoring of water vapour and gas temperature in a coal fired power-plant using near-infrared diode lasers,** *T. Fernholz, H. Pitz, V. Ebert, Univ. of Heidelberg, Germany.*

We report approaches towards quantitative absorption spectroscopy under very low transmission conditions using base band diode laser modulation spectroscopy. Water absorption lines in the 800 nm region were used to derive number-densities and gas temperatures. **(p. 77)**

SaB5 11:40am

Rapid high sensitivity laser absorption measurements of broad band absorbers in the near infrared spectral region, *Kevin L. McNesby, Andrzej W. Miziolek, ARL, USA; Ian A. McLaren, McLaren Res., USA.*

The development of a gas sensor to measure concentrations of binary mixtures of oxygen and several volatile organic compounds is described. The sensor is diode laser-based, all signal processing is performed digitally, and control of the sensor and electronics, data collection, and real time readout is by a laptop computer. **(p. 80)**

SaB6 12:00pm

Measurement of NO, COF_2, and H_2O with a single mid-infrared laser, *Patrick J. McCann, I-Na Chao, Khosrow Namjou, Univ. of Oklahoma, USA.*

A single IV-VI semiconductor mid-IR laser was used to measure NO, COF_2, and H_2O molecules. Potential applications for such measurements include medical diagnostics and plasma etching endpoint detection in semiconductor manufacturing. **(p. 84)**

6:00pm–8:30pm
Room: Sunset

SaC ■ Poster Session

SaC1

IRMA: a tunable infrared multi-component acquisition system for plasma diagnostics, *J. Röpcke, L. Mechold, Inst. f. Niedertemperatur-Plasmaphysik, Germany; J. Anders,F.G. Wienhold, FhG Inst. for Physikalische Meßtechnik, Germany; D. Nelson, M. Zahniser, J. Wormhoudt, Aerodyne Res., Inc., USA.*

IRMA is an InfraRed Multi-component Acquisition system for plasma diagnostics and control. Four independent tunable diode lasers can be temporally multiplexed, and directed into plasma reactors or into a multipass cell for exhaust gas detection. **(p. 88)**

SaC2

Pseudo-random tone burst modulation for active remote sensing of gases using diode lasers, *Chris Hovde, Southwest Sciences, Inc., USA.*

Applying bursts of wavelength modulation to a diode laser in a pseudo-random pattern measures the spectrally narrow, wavelength dependent part of the power absorption that can be used to compute range-resolved trace gas concentrations. **(p. 91)**

SaC3

Development of a real-time continuous emissions monitor for polychlorinated dioxins and furans, *Harald Oser, Michael J. Coggiola, Gregory W. Faris, David R. Crosley, SRI Intl., USA.*

A real-time continuous emissions monitor for polychlorinated dioxins and furans is under development based on resonance enhanced multiphoton ionization of jet-cooled vapors coupled with time of flight mass spectrometry. **(p. 94)**

SaC4

Robust external cavity diode laser (ECDL) and their application in water vapor absorption and saturated-rubidium spectroscopy, *F. Schael, Univ. of Erlangen-Nurnberg, Germany; L. Hildebrandt, R. Knispel, J. Sacher, Sacher Lasertechnik, Germany.*

External cavity diode laser (ECDL) in Littman and Littrow configuration are optimized for optical sensor applications in industrial environments. The performance of the ECDL is demonstrated by water vapor absorption and rubidium saturated-absorption spectroscopy. **(p. 97)**

SaC5
The effect of laser pulse shape on the saturation of the forward degenerate four-wave mixing signal, *Dai-Hyuk Yu, Jai-Hyung Lee, Joon-Sung Chang, Seoul Natl. Univ., Korea; Jae-Seok Ryu, Jae Won Hahn, Korea Res. Inst. of Standards and Science, Korea; Paul M. Danehy, Australian Natl. Univ., Australia.*
We investigate the effect of laser pulse shape on the forward degenerate four-wave mixing(DFWM) in two-level media. Saturation behavior of the DFWM signal generated with the square top and Gaussian pulses are analyzed. **(p. 99)**

SaC6
MIR-evanescent-field spectroscopy for environmental analysis, *Ulrike Willer, Torsten Blanke, Wolfgang Schade, Technische Univ., Germany.*
Evanescent-field spectroscopy in the mid-infrared (MIR) spectral range is applied for online and in-situ gas detection. Tunable MIR laser radiation is generated by difference frequency generation of two single mode diode lasers in $AgGaS_2$. **(p. 102)**

SaC7
Quantitative minor species concentration measurements in atmospheric pressure flames with time-resolved LIF, *A. Brockhinke, A. Bülter, U. Rahmann, Univ. of Bielefeld, Germany.*
Energy transfer and quenching processes are studied with simultaneous wavelength, temporal and polarization resolution. A method to obtain quench-free data is devised. Quantitative OH and H concentration profiles in a counterflow burner interacting with a vortex are presented. **(p. 105)**

SaC8
Spherical cavity ringdown spectroscopy experiments, *Robert W. Shaw, W.B. Whitten, M.D. Barnes, J.M. Ramsey, Oak Ridge Natl. Lab., USA; L.J. Wang, Univ. of Tennessee–Chattanooga, USA.*
Cavity ringdown absorption spectroscopy was investigated using picosecond laser pulses and whispering gallery modes propagating in glass and liquid spheres. Evanescent wave loss for glass spheres was not detected, but preliminary liquid sphere absorption appears promising. **(p. 108)**

SaC9
Diode-laser-based in-situ-CH_4-detection for the surveillance of ignition processes in gas-fired power-plants, *H. Pitz, T. Fernholz, C. Giesemann, V. Ebert, Univ. Heidelberg, Germany.*
We demonstrate the first simultaneous in-situ detection of methane and water in a full-scale 1 GW_{th} gas-fired power plant with an absorption resolution in the order of 10^{-4} OD corresponding to less than 5 ppmV at 400K. **(p. 111)**

SaC10
Laser spectroscopy of magnesium oxide in magnesium metal combustion, *Christopher B. Dreyer, John W. Daily, Angel Abbud-Madrid, Melvyn C. Branch, Univ. of Colorado–Boulder, USA.*
Presented are B-A fluorescence excitation scans of magnesium oxide performed in a seeded acetylene-air flame. This work is motivated by the development of laser diagnostics for a study of magnesium combustion in carbon dioxide. **(p. 114)**

SaC11
NO detection by cavity ringdown laser spectroscopy, *Alexandre D. Usachev, Tracy S. Miller, Jagdish P. Singh, Fang-Yu Yueh, Ping-Rey Jang, David L. Monts, Mississippi State Univ, USA.*
As an initial step in our effort to measure gas-phase 2,4,6-trinitrotoluene (TNT) by means of UV-CRDLS, we have investigated UV-CRDLS detection of NO in 226.5-227 nm spectral region. **(p. 117)**

SaC12
Pressure dependence of polarization spectroscopy signals, *J. Walewski, C. Kaminski, M. Aldén, Lund Inst. Tech., Sweden.*
In this work investigations on the dependence of polarization spectroscopy signal on gas pressure and species concentration are presented and compared with results from laser-induced fluorescence. **(p. 120)**

SaC13
An IR imaging system for remote sensing of chemicals, *S. Kalem, O. Yavuzcetin, Tubitak Inst. of Tech., Turkey.*
An IR active imaging system with separate optical pathways is constructed and tested for remote sensing of chemicals. The technique, which is based on laser light selective heating and its application to the detection of chemicals are discussed. **(p. 123)**

Sunday
February 13, 2000

7:30am–5:30pm
Registration

9:30am–4:00pm
Exhibit Hours

8:00am–9:50am
Room: Anasazi North
SuA ■ Combustion Diagnostics 1
Douglas S. Baer, Stanford Univ., USA, Presider

SuA1 8:00am (Invited)
Diode laser-based tunable ultraviolet sources for combustion diagnostics, *Kristen A. Peterson, Daniel B. Oh, Southwest Sciences Inc., USA.*
Tunable, wavelength modulated ultraviolet sources have been developed based on nonlinear conversion of high power diode lasers and were used to probe key combustion radicals by high sensitivity absorption and phase-sensitive fluorescence methods. **(p. 126)**

SuA2 8:30am
Measurement of SO_2 and SO_3 in aircraft engine exhausts using a tunable diode laser system, *J. Wormhoudt, T.A. Berkoff, R.C. Miake-Lye, Aerodyne Res., Inc., USA.*
We used a mid-infrared (lead-salt) diode laser and multipass cell to measure few ppmv SO_2 concentrations in an aircraft engine exhaust in an altitude test chamber, and demonstrated the possibility of similar sensitivity for SO_3. **(p. 127)**

SuA3 8:50am
Real-time 2-D imaging of water vapor in diffusion flames, *Jeffrey S. Goldmeer, Daniel J. Kane, Southwest Sciences, Inc., USA.*
An imaging Wavelength Modulation Spectroscopy system was developed for measuring combustion species concentrations in flames. Images taken at 23 Hz by a diode laser are used to generate "movies" of strong absorbers within the flame. **(p. 130)**

SuA4 9:10am
Application of RF frequency-division multiplexing for multiple species measurements in large pool fires, *P.J. Santangelo, P.D. Ludowise, C.R. Shaddix, S.W. Allendorf, D.K. Ottesen, Sandia Natl. Labs, USA; G.L. Hubbard, Hubbard Assoc., USA.*
This paper focuses on multiplexing design issues, such as the determination of the minimum modulation frequency separation to prevent crosstalk and resolution of 2f lineshape. The system employed was tested in both an optical furnace and in a buoyant, turbulent diffusion flame. **(p. 133)**

SuA5 9:30am
***In-situ* combustion diagnostics using diode laser absorption sensors,** *M.E. Webber, S. Kim, D.S. Baer, R.K. Hanson, Stanford Univ., USA.*
The availability of extended wavelength DFB diode lasers makes in-situ flame measurements of important combustion species such as CO_2 possible. This work presents recent measurements near 2 micron of CO_2 concentration above flat-flame burners. **(p. 136)**

9:50am–10:20am
Concourse Area
Coffee Break

10:20am–12:00pm
Room: Anasazi North
SuB ■ Combustion Diagnostics 2
Volker Sick, Univ. of Michigan, USA, Presider

SuB1 10:20am
Atmospheric pressure laser induced fluorescence measurements of CH in flames using $B^2\Sigma^-$ levels near predissociation, *Robert J.H. Klein-Douwel, Jorge Luque, Jay B. Jeffries, Gregory P. Smith, David R. Crosley, SRI Intl., USA.*
Laser-induced fluorescence of CH $B^2\Sigma^-v'=1$ is excited in flames using rotational levels above and below the predissociation limit. At atmospheric pressure rotational energy transfer produces a variation in the fluorescence quantum yield with rotational level and gas temperature. **(p. 140)**

SuB2 10:40am
Simultaneous laser-induced fluorescence visualization of acetone and OH for a study on a crevice flow in an SI engine, *Masayuki Tamura, Teruhiro Sakurai, Hideo Tai, Tokyo Gas Co., Ltd., Japan.*
A crevice flow in a spark ignition gas engine was visualized by LIF of OH and acetone. Oxidation of crevice flow was found to be stopped at timing of exhaust valve opening. **(p. 143)**

SuB3 11:00am
Laser-induced incandescence non-intrusive measurements of particles in exhausts, *John D. Black, Rolls-Royce plc, UK; Vartan Grigorian, Cranfield Univ., UK.*
Laser-induced incandescence (LII) measurements of carbonaceous particle concentrations have been made in the exhaust of a currrent large civil aero-engine on a sea level test bed. Comparison of LII with conventional gas sampling is discussed. **(p. 146)**

SuB4 11:20am
Vibrational temperature imaging using two-line laser-induced fluorescence of seeded NO, *Wolfgang Bessler, Frank Hildenbrand, Christof Schulz, Univ. of Heidelberg, Germany.*
Two-dimensional distributions of vibrational temperatures are measured in sooting flames via two-color planar laser-induced fluorescence using seeded NO with excitation in the A-X v'=0 and v'=2 band. Possibilities using a single laser are discussed. **(p. 149)**

SuB5 11:40am
Comparison of particle image velocimetry and optical flow velocimetry for turbulent flows and flames, *J. Fielding, M.B. Long, Yale Univ., USA.*
Optical flow velocimetry based on two-dimensional scalar imaging has been proposed as an alternative to particle image velocimetry in oooturbulent flows. Results comparing these two approaches are presented from experiments in an isothermal air jet. **(p. 152)**

12:00pm–1:30pm
Lunch Break (on your own)

1:30pm–3:10pm
Room: Anasazi North
SuC ▪ Analytical Applications 1
Jay B. Jeffries, SRI Intl., USA, Presider

SuC1 1:30pm
Industrial and environmental analysis by diode laser atomic absorption spectrometry, *Joachim Koch, Kay Niemax, Alexandr Zybin, Inst. of Spectrochemistry and Applied Spectroscopy, Germany; Christoph Schnürer-Patschan, LaserSpec Analytik GmbH, Germany.*
Diode laser spectrometry is applied in process analysis of surface contaminants on silicon wafers, in direct and rapid measurements of chlorine in polymers by laser ablation, and for the analysis of toxic metal species in environmental samples. **(p. 156)**

SuC2 1:50pm
Photoacoustic applications in industrial and atmospheric measurement, *Jeffrey S. Pilgrim, David S. Bomse, Joel A. Silver, Southwest Sciences, Inc., USA.*
Photoacoustic spectroscopy (PAS) is a well-known technique for trace gas detection. In its usual implementation PAS suffers several drawbacks that limit sensitivity. Southwest Sciences has developed techniques that recover the inherent sensitivity of photoacoustic spectroscopy. **(p. 159)**

SuC3 2:10pm
A laser-based system for chemical imaging, *P.D. Ludowise, J.S. Robinson, D.K. Ottesen, T.J. Kulp, U.B. Goers, K. Armstrong, S.W. Allendorf, Sandia Natl. Labs, USA.*
An imaging instrument is being developed to provide in situ assessment of hydrocarbon contaminants on metallic surfaces. A widely-tunable infrared laser system is interfaced with a focal plane array camera to perform non-invasive analysis by reflectance spectroscopy. **(p. 160)**

SuC4 2:30pm
A systematic approach to characterize the flame structure of partially premixed flames based on holographic interferometry measurements, *Xudong Xiao, Ishwar K. Puri, Univ. of Illinois–Chicago, USA.*
In order to describe the flame structure, a systematic approach is developed that is expressed in the form a = a(x), where a denotes any scalar for which a state relationship is pertinent. **(p. 163)**

SuC5 2:50pm
Gas temperature measurements by spontaneous Raman spectra of carbon dioxide, *Hansheng Zhang, Fang-Yu Yueh, Jagdish P. Singh, Robert L. Cook, Mississippi State Univ., USA.*
A spontaneous Raman spectroscopy probe has been developed to measure the gas temperature in large oxygen-fed glass furnaces using the spectra of carbon dioxide. The system was tested and the results are presented. **(p. 166)**

3:10pm–3:40pm
Concourse Area
Coffee Break

3:40pm–5:20pm
Room: Anasazi North
SuD ▪ Analytical Applications 2
Kay Niemax, Inst. of Spectrochemistry and Applied Spectroscopy, Germany, Presider

SuD1 3:40pm
Laser-induced fluorescence detection of atmospheric NO_2 at parts per trillion mixing ratios, *Ronald C. Cohen, Univ. of California–Berkeley, USA.*
A laser-induced fluorescence instrument designed for continuous, autonomous, in situ observations of atmospheric NO_2. The instrument sensitivity is 10 parts per trillion (ppt) in 10 seconds of integration (S/N=2) with a detection limit below 1 ppt. **(p. 170)**

SuD2 4:00pm

Applications of laser multiphoton ionization to fast analysis of environmental samples, *Israel Schechter, Vladimir V. Gridin, Valery Bulatov, Salah Hasson, Takanori Inoue, Michal Fisher, Chanan Sluzny, Iris Litani-Barzilai, Alona Korol, Michal Kadosh, Technion–Israel Inst. of Tech., Israel.*

Laser multiphoton ionization-fast conductivity technique was directly applied to environmental samples, under ambient conditions, resulting in fast analysis. Ultra-sensitive analysis of PAH and pesticides in soils, in aerosols, in liquids and on vegetables are reported. **(p. 173)**

SuD3 4:20pm

Laser-induced breakdown spectroscopy of trace metals, *Randall L. Vander Wal, NASA- Glenn, USA; Thomas M. Ticich, Joseph R. West, Jr., Centenary Col. of Louisiana, USA.*

An alternative approach for laser-induced breakdown spectroscopy (LIBS) determination of trace metal determination in liquids is demonstrated. The limits of detection (LOD) for the technique ranged from 10 ppb to 10 ppm for 15 metals (Mg, Al, Si, Ca, Ti, Cr, Fe, Co, Ni, Cu, Zn, As, Cd, Hg, Pb) tested. **(p. 176)**

SuD4 4:40pm

Improved laser-induced-breakdown analysis of environmental samples by plasma imaging, *Israel Schechter, Valery Bulatov, Liang Xu, Vladimir V. Gridin, Rievie Krasniker, Technion--Israel Inst. of Technology, Israel.*

A new application of chemical vision to plasma spectroscopy, and introduction of spatial resolution, result in considerable improvement of analytical figures. The technique was evaluated for environmental samples and matrixes, such as aerosols and soils. **(p. 178)**

SuD5 5:00pm

Laser analysis and cleaning of nineteenth century daguerreotypes, *Valerie V. Golovlev, John C. Miller, Oak Ridge Natl. Lab., USA; Grant Romer, Intl. Museum of Photography and Film, USA; Paul Messier, Boston Art Conservation, USA.*

Laser ablation mass spectrometry and surface-enhanced Raman spectroscopy have been used to characterize both modern and 150 year old daguerreotypes. Such investigations are a necessary prelude to attempts to clean them of tarnish by laser ablation. **(p. 181)**

5:20pm–5:35pm

Closing Remarks

Laser Applications to Chemical and Environmental Analysis

Microanalytical and Single Molecule Techniques 1

Friday, February 11, 2000

David J. Rakestraw, Sandia Natl. Labs., USA
Presider

FA
8:00am–9:40am
Anasazi North

Microfabricated fluidic devices: new approaches to chemical measurements

J. Michael Ramsey
Oak Ridge National Laboratory, P.O. Box 2008, Oak Ridge, TN 37831-6142
ramseyjm@ornl.gov

Abstract:

Microfabricated fluidic devices (microchips) may allow a paradigm shift that greatly enhances the ability to acquire chemical and biochemical information similar to the ways in which the transistor and integrated circuit have influenced access to electronically coded information[1,2]. Our work on moving conventional bench-top liquid phase assays to microfabricated fluidic devices will be described. The implementation of chemical separation strategies on microfabricated platforms is a key element of this so-called lab-on-a-chip technology. Many separations concepts have now been demonstrated on microfabricated structures, including capillary electrophoresis, capillary gel electrophoresis, micellar electrokinetic capillary chromatography, open channel electrochromatography, solvent programmed micellar electrokinetic capillary chromatography[3] and open channel electrochromatography[4], free flow electrophoresis, and isoelectric focusing. In most cases, these separation techniques were transferred from conventional approaches to microstructures with increased levels of performance. Moreover, microfabricated fluidic structures provide the added advantage of allowing monolithic integration of chemical processing functional elements with essentially zero dead volume interconnects. Chemical processing elements that have been integrated with chemical separations on microchips include pre- and post-separation derivitization, enzymatic digestion[5], polymerase chain reaction amplification, antigenic reactions[6], and preconcentration by stacking, solid phase extraction, and electrokinetic accumulation on a microfabricated membrane[7]. Fundamental advantages and disadvantages of microfabricated fluidic devices will be discussed.

OCIS codes; (000.1570) Chemistry, (170.1420) Biology, (120.1880) Detection,

[1] J. Michael Ramsey, Stephen C. Jacobson, and Michael R. Knapp, "Microfabricated chemical measurements systems," Nat. Med. (N. Y.) **1** (10), 1093-1096 (1995).
[2] Stephen C. Jacobson and J. Michael Ramsey, "Microfabricated Chemical Separation Devices," in *High-Performance Capillary Electrophoresis*, edited by Morteza G. Khaledi (John Wiley & Sons, Inc., New York, 1998), Vol. 146, pp. 613-633.
[3] J. P. Kutter, S. C. Jacobson, and J. M. Ramsey, "Integrated Microchip Device with Electrokinetically Controlled Solvent Mixing for Isocratic and Gradient Elution in Micellar Electrokinetic Chromatography," Anal. Chem. **69** (24), 5165-5171 (1997).
[4] Joerg P. Kutter, Stephen C. Jacobson, Norio Matsubara *et al.*, "Solvent-Programmed Microchip Open-Channel Electrochromatography," Anal. Chem. **70** (15), 3291-3297 (1998).
[5] Stephen C. Jacobson and J. Michael Ramsey, "Integrated microdevice for DNA restriction fragment analysis," Anal. Chem. **68** (5), 720-723 (1996).
[6] Nghia H. Chiem and D. Jed Harrison, "Microchip systems for immunoassay: an integrated immunoreactor with electrophoretic separation for serum theophylline determination," Clin. Chem. **44** (3), 591-598 (1998).
[7] J. Khandurina, S. C. Jacobson, L. C. Waters *et al.*, "Microfabricated Porous Membrane Structure for Sample Concentration and Electrophoretic Analysis," Anal. Chem. **71** (9), 1815-1819 (1999).

Micro-optical systems for laser-induced fluorescence in capillary separations

M. E. Warren, W. C. Sweatt, J. R. Wendt, C. G. Bailey, D. W. Arnold, C. M. Matzke,
S. A. Kemme, A. A. Allerman, T. R. Carter, R. E. Asbill, and S. Samora

Sandia National Laboratories, Albuquerque, New Mexico 87185-0603
Ph: 505-844-7208, Fax: 505-844-8985
mewarre@sandia.gov

A miniaturized, highly integrated free space optical system has been developed to detect laser-induced fluorescence as part of a liquid phase chemical analysis system for portable field use. The system uses electrokinetic capillary separations in conjunction with the optical detection. In this technique, narrow capillary channels are used to perform chromatographic separations of fluids on a planar chip fabricated by microlithographic processes. In these techniques the analyte fluid is driven electrokinetically by applying a voltage across the fluid channels. Until now, the optical detection systems available were too large for portable applications. This work describes micro-optical fluorescence detection systems developed for integration with capillary-channel separation systems. These systems are optimized for detection of explosive residues in solution by indirect fluorescence, in which the presence of explosive residues is detected by the quenching of fluorescence from a dye present in the solution. The use of indirect fluorescence with dyes allows for the use of laser diode sources. The other keys to the compact design of the system are the use of substrate-mode propagation for the optical path, high performance diffractive microlenses and the use of electronic surface-mount techniques for assembly. Vertical-cavity surface-emitting lasers (VCSELs) are used as the optical sources. The design is shown in Fig. 1. The 750 nm VCSEL array is flip-chip bonded to a submount that is then bonded to a ceramic frame that provides the spacing to the first optical surface. The two microlenses are diffractive elements that are etched into the surface of the fused silica substrate. The off-axis lens directs the VCSEL output into the channel via two thin film metal mirrors. The collection lens collimates the fluorescence for the high performance interference filter. Fig. 2 shows a photograph of the micro-optical system, without any active components.

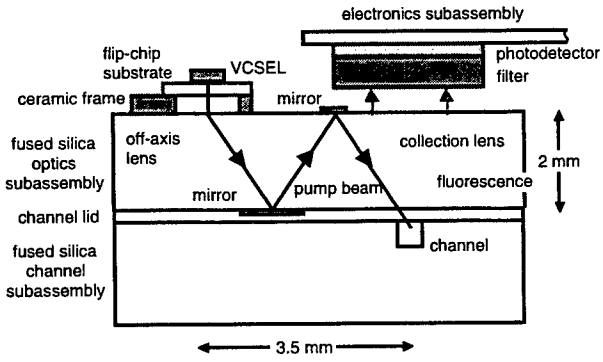

Figure 1. Schematic cross section along the optical path of the fluorescence detection system.

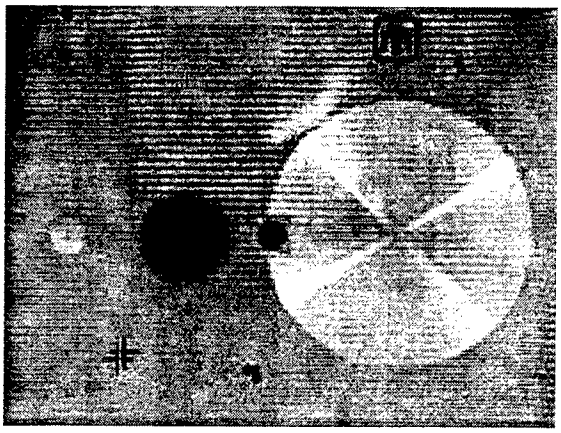

Figure 2. Photograph of the top of the 6 mm X 14 mm optical system. Visible from left to right are the off-axis lens (small light circle), the two metal mirrors (black circles), and the collection lens (large notched circle). The large lens is 2.8 mm diameter.

Fig. 3 shows the results from an open channel separation of a 50 ppm solution of explosives, using the micro-optical system for detection via indirect fluorescence with CY-7 dye.

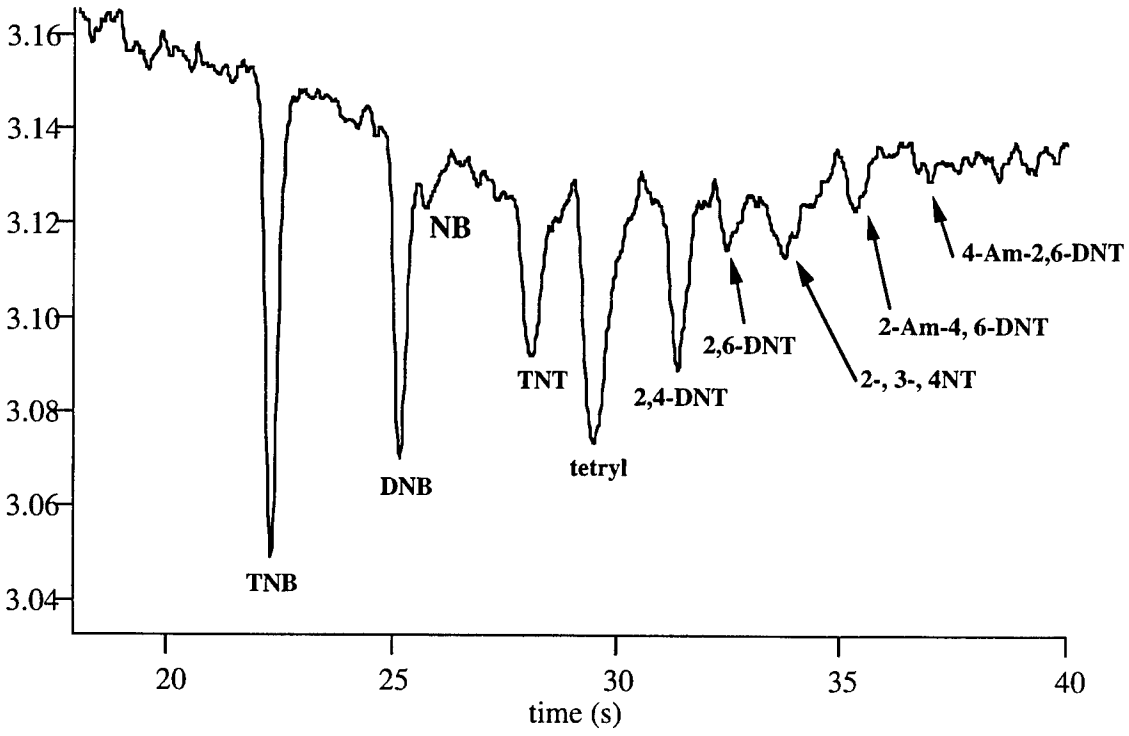

Figure 3. Open channel separation of a 50 ppm solution of explosives detected using indirect fluorescence with CY-7 dye showing separation into components on a timescale of less than one minute. Data was obtained with the micro-optical system. The vertical axis is fluorescence signal in arbitrary units.

Sandia National Laboratories is a multiprogram laboratory operated by Sandia Corporation, a Lockheed Martin Company, for the United States Department of Energy under Contract DE-AC04-94AL85000.

Fluorescence Lifetime Imaging Microscopy (FLIM) on the Single Molecule Level

P. Tinnefeld*, V. Buschmann, D.-P. Herten, J.-P. Knemeyer, M. Sauer
Physikalisch-Chemisches Institut, Universität Heidelberg, Im Neuenheimer Feld 253, 69120 Heidelberg, Germany
**Tel. (49)-6221-545042, Fax. (49)-6221-544255, e-mail: ptinnefe@ix.urz.uni-heidelberg.de*

Summary

During the last years, several methods for the detection of individual fluorescently labeled molecules have been developed. Especially, for the study of inhomogeneous complex systems single molecule spectroscopy can provide information that is difficult to obtain from ensemble measurements. Due to the limited observation time of individual freely diffusing molecules in solution fluorescence scanning systems including single molecule search programs have been developed to monitor the dynamical behavior of individual immobilized probe molecules on surfaces (for review [1]). Besides polarization measurements, so far only the spectral characteristics, i.e. different emission maxima of different dyes, have been used to detect, identify, and monitor the dynamics of individual fluorescent molecules on surfaces. Therefore we decided to further extend the number of obtainable parameters by developing a scanning system for time-correlated single-photon counting (TCSPC). As shown in Fig. 1 the system consists essentially of an inverted confocal fluorescence microscope and a motion driven controller *x,y*-microscope stage (SCAN 100x100 and MC2000; Märzhäuser, Germany). As excitation source we used a pulsed diode laser emitting at 640 nm with a repetition rate of 50 MHz. The laser diode was driven by an external pulse generator.

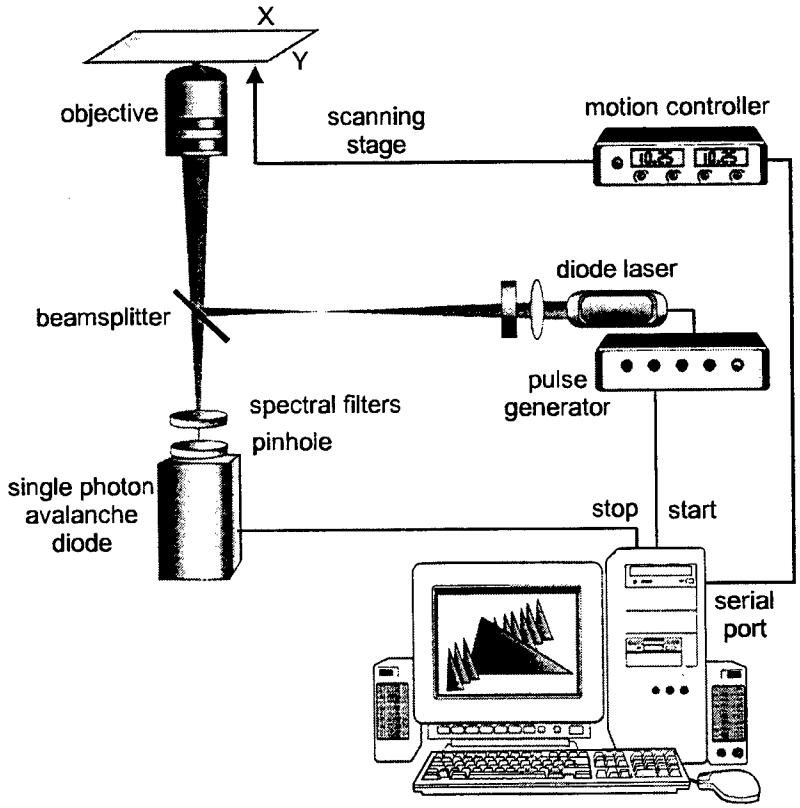

Fig. 1. Schematic diagram of the optical and mechanical setup for time-resolved fluorescence scanning.

Passing an excitation filter the beam was directed to the microscope objective (100x, NA=1.4 oil immersion) by a dichroic beamsplitter. The average laser power for single molecule measurements was adjusted to 5-30 µW at the sample. The fluorescence signal was collected by the same microscope objective, filtered by a bandpass filter and imaged onto a 50 µm pinhole oriented directly in front of an avalanche photodiode. The signal was fed to a time-correlated single photon counting (TCSPC) PC card to acquire time-resolved data [2]. For synchronization of the scanning motion with the detection device a Windows 32® based software with Microsoft Visual C++ 5.0 running under Windows NT® was developed. The communication with the motion controller takes place via the RS-232 serial port at 19600 bps using the built-in command language VENUS-1 of the motion controller. Triggering of the detection device and data acquisition was done through calls to a Windows 32® DLL (Becker & Hickl, Berlin, Germany). The measurement routine was completely written in C to minimize time consuming code overhead. Within the routine the Windows data storage is done in binary format without system cache to avoid arbitrarily gaining control to the operating system. Nevertheless the acquired data can be displayed online within the portions of code that are waiting for a response from the serial port. For data analysis another software is in development, allowing the application of pattern recognition algorithms and other mass data procedures. In the moment a monoexponential maximum likelihood estimator (MLE) algorithm is used for fluorescence decay time determination.

Figure 2a shows a 10 x 10 µm fluorescence intensity image of single Cy5 molecules on an aminopropyl silane (APS) treated cover slip. As can be seen, count rates of up to 30 kHz are obtained from individual Cy5 molecules. In addition, characteristic blinking and bleaching of individual molecules can be observed. By using a MLE-algorithm the fluorescence decay time of each pixel can be calculated. Thus a fluorescence decay time image (Fig. 2b) is obtained.

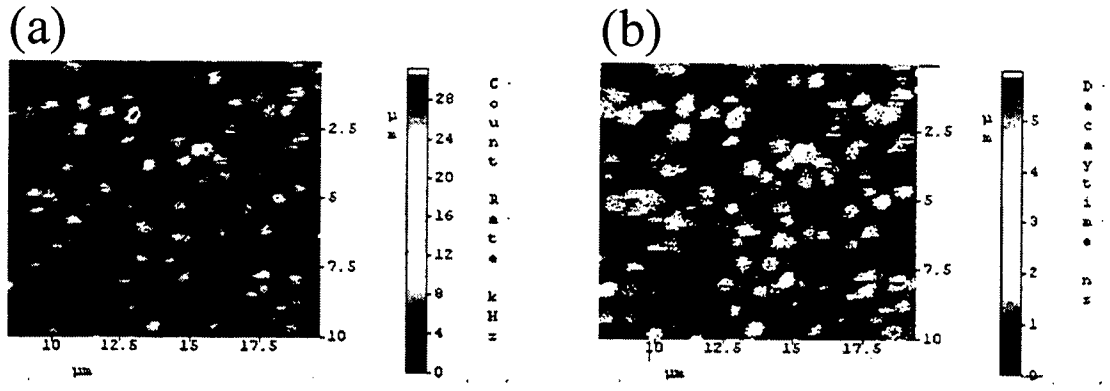

Fig. 2. (a) 10 x 10 µm fluorescence intensity image of single Cy5 molecules. Spatial resolution 50 nm/pixel, temporal resolution: 5 ms/pixel average laser power: 7 µm at the sample. (b) Fluorescence decay time image obtained from each pixel shown in Fig. 2a. with a count rate > 1.25 kHz.

Figure 3 presents the resulting histogram of fluorescence decay times determined in each pixel of Fig. 2b. Using a Gaussian fit we obtain a fluorescence decay time of τ=2.06±0.72 ns for individual Cy5 molecules on an APS treated glass surface. The measured fluorescence decay times are slightly longer than those obtained from single Cy5 molecules in solution [3].

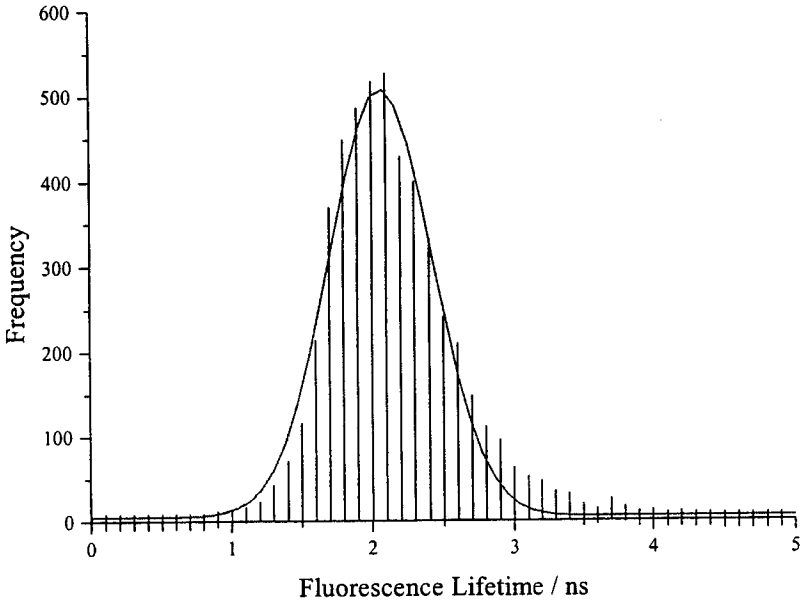

Fig. 3. Fluorescence decay time distribution of fluorescence signals detected from individual Cy5 molecules immobilized on a glass surface.

Besides the detection of single dye molecules on dry surface we also show time-resolved fluorescence scanning of labeled proteins and oligonucleotide molecules in living cells. By use of the appropriate oligonucleotide sequence specific quenching mechanisms can be used to get more insight into the microenvironment of individual probe molecules. Since time-resolved fluorescence scanning is independent of the excitation/detection efficiency and the transition moment of the probe molecule direct information about the system is obtained which is difficult to obtain from intensity measurements.

References

[1] S. Weiss, "Fluorescence Spectroscopy of Single Biomolecules." Science **283**, 1676-1683 (1999).

[2] W. Becker, H. Hickl, C. Zander, K. H. Drexhage, M. Sauer, S. Siebert, J. Wolfrum," Time-resolved detection and identification of single analyte molecules in microcapillaries by time-correlated single-photon counting (TCSPC)," Rev. Sci. Instr. **70**, 1835-1841 (1999).

[3] M. Sauer, J. Arden-Jacob, K. H. Drexhage, F. Göbel, U. Lieberwirth, K. Mühlegger, R. Müller, J. Wolfrum, C. Zander, „Time-resolved identification of individual mononucleotide molecules in aqueous solution with pulsed semiconductor lasers," Bioimaging **6**, 14-19 (1998).

Time-resolved photon counting for multiplexed DNA electrophoreses separations

Lloyd M. Davis
Center for Laser Applications, University of Tennessee Space Institute, Tullahoma, Tennessee 37388

Jim L. Amen, Dan L. Draney, Lyle R. Middendorf and Rex A. Peterson
LI-COR, Inc., Biotechnology Division, P.O. Box 4000, Lincoln, Nebraska 68504

Abstract: Monte Carlo simulations are used to evaluate time resolved photon counting as a means for identifying and quantifying overlapping electropherogram bands, which have been labeled by dyes with disparate fluorescence lifetimes.

OCIS codes: (170.3650) Lifetime based sensing, (170.6920) Time-resolved imaging

1. Introduction

The fluorescence lifetime of a tagging agent can provide an additional dimension of information in many fluorescence-imaging applications. For example, one may measure the fluorescence lifetime of a labeling agent in order to probe spatially its quenching environment. If signal levels are sufficiently high, modulated excitation with phase-sensitive analog detection can be used to obtain precise measurements of the fluorescence lifetime. Maximum-entropy methods have been developed for the determination of the lifetime from such data [1]. When fluorescence signal levels are low, the precision of a measurement becomes limited by shot noise. Photon counting then generally provides superior sensitivity to analog detection. Maximum-entropy methods for the estimation of the lifetime from fluorescence decay profiles measured by time-correlated single photon counting are also available and have been discussed in depth in the literature [2]. In the best case, if the decay profile is measured with adequate resolution, is not truncated, and is free from background, the relative precision in the determined lifetime is equal to the square root of the number of photons [3]. Thus, the fluorescence lifetime can be determined to a useful precision even for a burst of less than 100 photons, as may be collected from a single molecule in solution as it passes through a laser beam [4]. Time-resolved photon counting with maximum entropy determination of the fluorescence lifetime has also been used in capillary electrophoresis to distinguish four different labeling agents in peaks that contain many thousands of photons [5].

The problem of distinguishing between two or more agents with known fluorescence lifetimes or decay profiles is simpler and computationally faster than that of determining the lifetime of a measured decay profile. Maximum entropy methods for deciding which agent has most probably given rise to the measured profile have been discussed [6]. Experiments have been conducted in which the measured decay profiles of photon bursts that are above a preset threshold are used to sort the bursts into groups, corresponding to different lifetimes [6]. Neural network analysis methods for simultaneously utilizing lifetime and other photophysical differences when categorizing photon bursts have also been described [7].

Here, the use of time-resolved single photon counting for increasing the throughput in slab-gel electrophoresis is considered. Dyes that exhibit disparate fluorescence lifetimes would be used to label various constituents and a time-resolved fluorescence decay profile would be collected at each pixel in the read-out of the electropherogram. When bands labeled by different fluorophores overlap spatially, the measured temporal decay profile is expected to exhibit a multi-exponential form, with contributions from each fluorescent agent that is present, and from background. The analysis of the temporal decay profile at each pixel is no longer simply a categorization problem. Instead, the overall shape of the profile is used with maximum entropy methods to estimate the fraction of signal from each agent, assuming a given fluorescence lifetime for each agent. The analysis thereby yields a separate pixilated map of the estimated signal from each fluorophore, and thus would allow two or more electropherogram analyses to be simultaneously conducted in the same gel.

2. Applications

The use of fluorophores with different lifetimes for multiplexing may be useful in fluorescence imaging applications other than slab-gel electrophoresis, such as blotting and griding. However, in this work, we are particularly

interested in the application of the technique to multiplexing DNA sequencing separations. For this case, LI-COR's existing instrument for DNA sequencing [8], which uses infrared fluorescent labeling dyes, and cost-effective laser diodes and silicon avalanche photodiodes for excitation and detection, would require only a relatively small modification. Sub-nanosecond-pulsed laser diodes and single-photon avalanche photodiodes (SPADs) could be used to collect complete fluorescence temporal decay profiles at each pixel of the electropherogram. In order to be able to detect an acceptably low concentration of labeled DNA, and to achieve an acceptably high speed of read-out, signal levels of thousands of photons per pixel at most are anticipated at the center of each electropherogram band.

3. Monte Carlo Simulation

A Monte Carlo simulation has been developed to help determine suitable experimental parameters that would enable electropherogram bands to be clearly and correctly discerned. Of particular interest is the required disparity of the fluorescence lifetimes of the labeling agents, for given levels of fluorescence signal and background, and given temporal width of the instrument impulse response, which is determined by the laser diode pulsewidth and SPAD detector timing jitter. The simulation is also useful for evaluating the robustness of the analysis to changes in such parameters.

To begin, the simulation either reads in experimental electropherogram images, or else generates synthetic images that have approximately Gaussian-shaped bands, with small random variations in shape and size. In the later case, the bands are placed at locations appropriate for particular DNA sequences, which are randomly generated and recorded. The images are scaled to the desired photon brightnesses, and then used to generate the combined electropherogram image and the temporal fluorescence decay profile at each pixel of the combined image. In generating the decay profiles, the model assumes that the number of photons generated at each temporal channel of the decay profile is random with a Poisson distribution. The mean is determined by the weighted-sum of the temporal decay profiles of each labeling agent that is present, as well as the decay profile of the background. The simulation can either read in experimentally measured decay profiles, or else generate profiles by convolution of exponential decays of specified lifetimes with an instrument impulse response function. This in turn can be either read in or generated according to specified parameters.

After the model generates the combined image and temporal decay profiles at each pixel, the maximum entropy analysis routine is executed to recover separate images for each labeling agent. Each such recovered image may then be compared to the "correct" image, which would have been produced if each labeling agent were present alone. A visual comparison is usually adequate to discern the fidelity of the recovered images. The value of chi-squared, which represents the pixel-summed root-mean-square deviation between all recovered images and the corresponding "correct" images, may also be used as a measure of the effectiveness of the multiplexing.

4. General Results

The recovered images in general exhibit varying degrees of cross-talk, depending in part on the disparity of the fluorescence lifetimes, i.e., electropherogram bands that are due to one type of fluorophore lead to false photon intensity in the image of other fluorophores. Such cross-talk is acceptably low for appropriate parameters, but due to the inherent shot noise in the data, it is always present. For example, in the case of just two labeling agents X and Y with different fluorescence lifetimes, if the number of photons in the decay profile at a given pixel is M, the maximum entropy analysis determines the most likely numbers of photons X and Y, assuming that $X + Y + B = M$, where B is the expected number of background photons per pixel. The numbers X and Y are also assumed to be non-negative. Consequently, at pixels where only fluorophore X is present, the analysis must yield $Y \geq 0$. Over many such pixels, the mean value of Y will be finite rather than zero, and the mean value of X will conversely be biased low. However, under appropriate conditions, such errors are minor. Instead, the largest errors are found to occur when electropherogram peaks from X and Y overlap, resulting in a multi-exponential decay profile. Nevertheless, the simulation indicates that electropherogram maps from fluorophores with reasonably closely spaced lifetimes may be successfully separated on a pixel-by-pixel basis under various conditions.

5. Example of Suitable Conditions and Conclusion

The general approach to multiplexing DNA electrophoresis separations, and the capability to resolve overlapping electropherograms that have been labelled by fluorophores with different lifetimes, is illustrated by way of example in Figure 1. The parameters used to generate the images in Figure 1 are listed in Table 1. Despite the existence of cross-talk, the simulation indicates that electropherogram images from fluorophores with lifetimes that differ by only 100 ps can be multiplexed and successfully separated on a pixel-by-pixel basis, even in the case of overlapping bands.

Table 1. Parameters used to generate example

Fluorescence lifetime of X:	700 ps
Fluorescence lifetime of Y:	800 ps
Impulse response:	Gaussian, with FWHM 400 ps, and exponential 130 ps tail
Size of image:	120 × 120 pixels
Mean size of electropherogram bands:	4.5 × 4.5 pixels FWHM
Number of temporal channels:	128
Time calibration:	72 ps/channel
Peak number of photons from X:	3000
Peak number of photons from Y:	3000
Mean background per pixel:	200

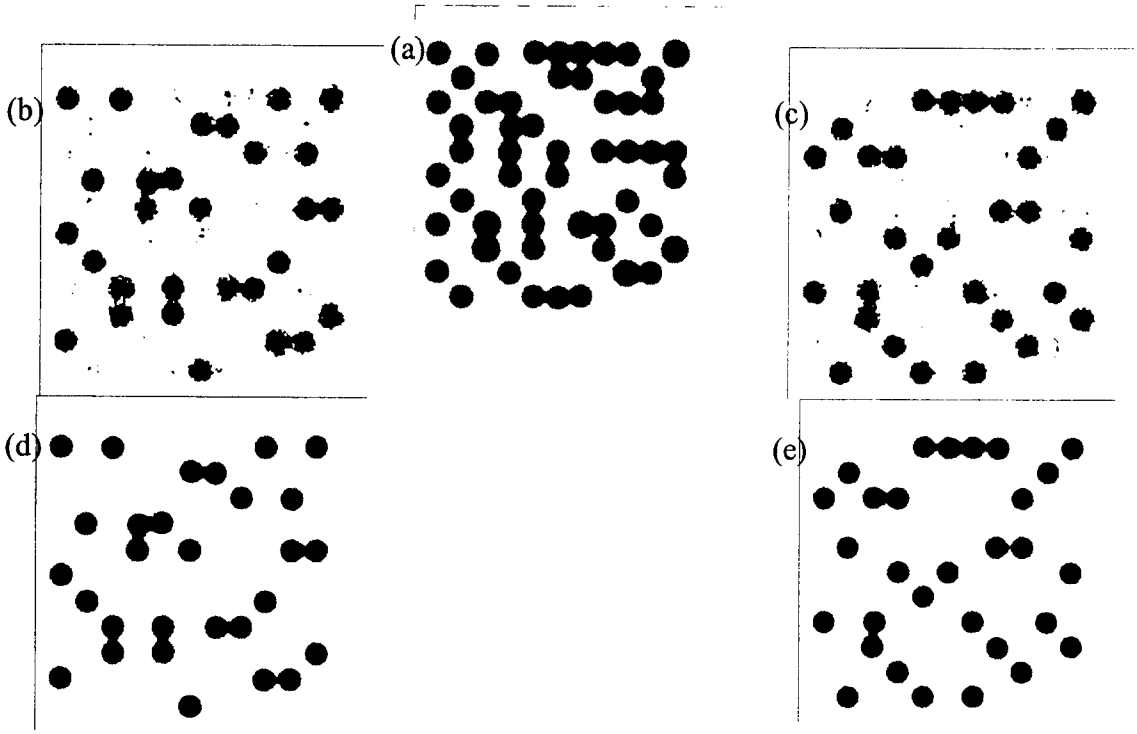

Fig. 1. Example of simulation results of multiplexed electropherogram images. (a) Combined image due to all photons, (b) Recovered image due to X photons, (c) Recovered image due to Y photons, (d) Image that would have been produced by X photons alone, (e) Image that would have been produced by Y photons alone.

6. References

1. J.M. Shaver and L.B. McGown, "Maximum entropy method for frequency domain fluorescence lifetime analysis,"Anal. Chem. **68**, 9-17, 611-620 (1996).
2. J. Tellinghuisen and C.W. Wilkerson, "Bias and precision in the estimation of exponential decay parameters from sparse data,"Anal. Chem. **65**, 1240-1246 (1993).
3. M. Kollner and J. Wolfrum, "How many photons are necessary for fluorescence lifetime measurements?" Chem. Phys. Lett. **200**, 199-204 (1992).
4. S.A. Soper, L.M. Davis, and E.B. Shera, J. Opt. Soc. Am. B **9**, "Detection and identification of single molecules in solution," 1761-1769 (1992).
5. U. Lieberwirth, J. Arden-Jacob, K.H. Drexhage, D.P. Herten, R. Muller, M. Neumann, A. Schulz, S. Siebert, G. Sagner, S. Klingel, M. Sauer, and J. Wolfrum, "Multiplex dye DNA sequencing in capillary gel electrophoresis by diode laser-based time-resolved fluorescence detection," Anal. Chem. **70** 4771-4779 (1998).
6. M. Kollner, Appl. Opt. "How to find the sensitivity limit for DNA sequencing based on laser-induced fluorescence," **32**, 806-820 (1993).
7. J. Enderlein, P.M. Goodwin, A. Van Orden, W.P. Ambrose, R. Erdmann, and R.A. Keller, "A maximum likelihood estimator to distinguish single molecules by their fluorescence decays," Chem. Phys. Lett. **270**, 464-470 (1997).
8. Y. Sun, B.A. Whitehead, and L.M. Davis, "Analysis of ultrasensitive fluorescence experiments," in Advances in Fluorescence Sensing Technology IV, J.R. Lakowicz, S.A. Soper, R.B. Thompson, eds., Proc. SPIE 3602, paper 42,(1999).
9. http://bio.licor.com/

Laser Applications to Chemical and Environmental Analysis

Microanalytical and Single Molecule Techniques 2

Friday, February 11, 2000

Markus Squer, Univ. of Heidelberg, Germany
William P. Ambrose, Los Alamos Natl. Lab., USA
Presiders

FB
10:10am–11:50am
Anasazi North

DNA Fragment Sizing by Single Molecule Detection

Erica J. Larson, Janetta R. Penttila, Hong Cai, James H. Jett, Stefan Burde, Babetta L. Marrone, and Richard A. Keller

Biosciences Division
Los Alamos National Laboratory
Los Alamos, NM 87545

Phone (505) 667-3018
Fax (505) 665-3024
Email keller@lanl.gov

DNA fragment size distribution analysis is a ubiquitous measurement in molecular biology and is typically done using gel electrophoresis. Applications exist in public health, genomics, medical diagnostics, and forensics. We have fully demonstrated a flow cytometric approach for rapidly and accurately sizing DNA fragments.(1-5) Our work has been focused on bacterial species and strain identification. In our approach, a DNA sample of whole bacterial genome DNA is digested into a characteristic set of DNA fragments using a rare-cutting restriction endonuclease. The fragment set is stained with a fluorescent intercalating dye that binds stoichiometrically to the DNA such that the amount of dye incorporated is directly proportional to the fragment size [number of base pairs (bp)]. The large increase (~1000X) in the fluorescence quantum yield of the intercalating dye upon binding to the DNA makes it unnecessary remove unbound dye from the solution before analysis. The stained fragments are diluted to ~10^{-14} molar and introduced into an ultrasensitive flow cytometer developed in our laboratory. Fragments pass individually through the laser illuminated detection region of the flow cytometer, each fragment producing a fluorescence burst as it transits the laser beam. Fluorescence bursts from individual fragments are detected and recorded. A histogram of the individual burst sizes is generated that displays the distribution of fragment sizes in the sample (i.e. a DNA fingerprint). For large DNA fragments, our approach is more sensitive (femtograms vs. micrograms), faster (analysis time of five minutes vs. tens of hours), and more accurate (size uncertainty 2% vs. 10%) than pulsed-field gel electrophoresis, commonly used for these analyses.

REFERENCES:

1. Goodwin, P. M., Johnson, M. E., Martin, J. C., Ambrose, W. P., Marrone, B. L., Jett, J.

H., and Keller, R. A., Rapid sizing of individual fluorescently stained DNA fragments by flow cytometry, *Nucleic Acids Res., 21*, 803-806 (1993).

2. Petty, J. T., Johnson, M. E., Goodwin, P. M., Martin, J. C., Jett, J. H., and Keller, R. A., Characterization of DNA Size Determination of Small Fragments by Flow Cytometry, *Anal. Chem., 67*, 1755-1761 (1995).

3. Huang, Z., Petty, J. T., O'Quinn, B., Longmire, J. L., Brown, N. C., Jett, J. H., and Keller, R. A., Large DNA fragment sizing by flow cytometry: application to the caracterization of P1 artificial chromosome (PAC) clones, *Nucleic Acids Res., 24*, 4202-4209 (1996).

4. Huang, Z., Jett, J. H., and Keller, R. A., Bacterial Fingerprinting by Flow Cytometry: Bacterial Species Discrimination, *Cytometry, 35*, 169-175 (1999).

5. Kim, Y., Jett, J. H., Larson, E. J., Penttila, J. R., Marrone, B. L., and Keller, R. A., Bacteria Fingerprinting by Flow Cytometry: Bacterial Species Discrimination, *Cytometry, 36*, 324-332 (1999).

OCIS Codes: 020.0020, 170.0170

Multidimensional fluorescence spectroscopy of single molecules

C. A. M. Seidel, S. Berger, C. Eggeling, J. Schaffer, E. Schweinberger, A. Volkmer, J. Widengren
Max-Planck-Institut fuer Biophysikalische Chemie, Am Fassberg 11, D-37077 Goettingen, Germany
phone ..49/(0)551/201-1774, Fax ..49/(0)551/201-1006, EM: cseidel@gwdg.de

Abstract: Multichannel-detection for simultaneous registration of all information on a signal burst (intensity, lifetime, anisotropy *r* and spectral range) is used for analytics and studies of conformational dynamics of a single fluorescent labeled molecule in solution.

OCIS codes: (300.6280) Spectroscopy, fluorescence and luminescence

Using a confocal epi-illuminated microscope with a polarizing beam-splitter and four channel detection of single molecule fluorescence induced by pulsed laser excitation, a new application of the multi-dimensional, real-time spectroscopic technique BIFL (Burst Integrated Fluorescence Lifetime) is introduced [1,2]. BIFL allows the simultaneous registration of fluorescence intensity, lifetime, anisotropy and spectral range of individual single molecules. In feasibility studies it is shown to be well suited to quantitatively identify freely diffusing fluorescent molecules such as Rhodamines and the Enhanced Yellow Fluorescent Protein via their characteristic fluorescence parameters (anisotropy, *r*, and mean lifetime, *tau*) [2].

This multi-dimensional technique is applied to study the conformational dynamics of a set of single- and double-stranded DNA-molecules labelled with the fluorescent dye Rhodamine 6G. Using highly diluted aqueous solutions of the DNA, fluorescence bursts indicating traces of individual molecules are registered and further subjected to a sliding burst analysis to obtain time traces of the fluorescence parameters *r* and *tau* [3] (left Fig.). Constructing frequency histograms of the fluorescence parameters found in the trajectories on the single molecule level, two major conformational states (A,B) with characteristic fluorescence parameters can be identified which are stable on a ms-time scale (right Fig.). State-selective analysis of lifetimes and intensities of these states indicates different photophysical parameters and additional faster dynamics, which is a direct prove for further branching of the energy landscape.

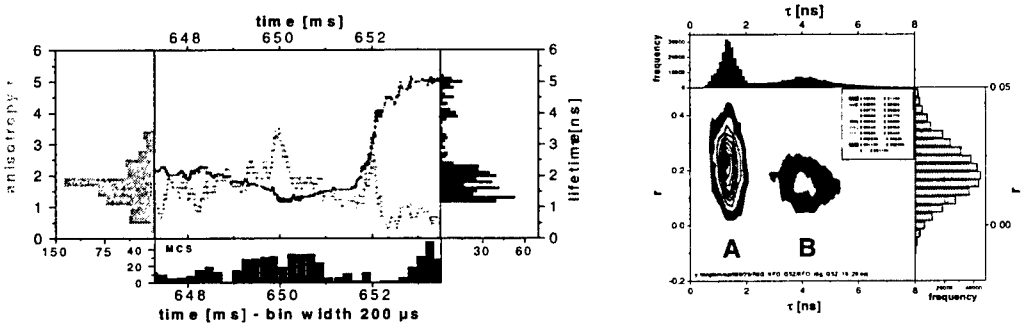

In addition first measurements with four fluorescence parameters are presented to study fluorescence resonance energy transfer (FRET) of single DNA molecules, which can adapt different conformations. Perspectives for monitoring biomolecular dynamics by BIFL are discussed.

1. Fries, J. R., Brand, L., Eggeling, C., Köllner, M., Seidel, C. A. M., J. Phys. Chem. A. **102,** 6601-6613 (1998).
2. Schaffer, J., Volkmer, A., Eggeling, C., Subramaniam,V., Striker, G., Seidel, C. A. M., J. Phys. Chem. A. **103**, 331-336 (1999).
3. Eggeling, C., Fries, J. R., Brand, L., Günther, R., Seidel, C. A. M., Proc. Natl. Acad. Sci. USA. **95,** 1556-1561 (1998).

Detection of target molecules on the single molecule level using confocal fluorescence microscopy in combination with microelectrophoresis

A. Schulz*, V. Buschmann, T. Hübner, H. Neuweiler, M. Sauer, J. Wolfrum
Physikalisch-Chemisches Institut, Universität Heidelberg, Im Neuenheimer Feld 253, 69120 Heidelberg, Germany
**Tel. (49)-6221-545042, Fax. (49)-6221-544255, e-mail: c62@ix.urz.uni-heidelberg.de*

Summary
Improvements in single molecule detection technologies have encouraged several research groups to implement this very sensitive technique for biomedical analysis. Especially, the screening for specific antibodies or nucleic acid sequences on the single molecule level is of great importance for early-stage diagnostic of tumor development [1]. The clinical standard antibody tests utilize enzyme-linked immunosorbent assays (ELISA) which achieve a sensitivity of a few nanogram antigen per milliliter corresponding to a concentration of 10^{-9} to 10^{-10} M. In all these methods the analyte molecules have to be isolated from the serum by binding to specific materials. In addition, several washing-steps are required. It would be desirable to detect and quantify analyte molecules in a homogeneous assay. Using fluorescence correlation spectroscopy (FCS) the binding of fluorescently labeled antibodies or antigens has been successfully demonstrated with analyte concentrations in the nanomolar range [2].
For the detection of antigens and antibodies in the concentration range below 10^{-11} M problems occur. In such diluted solutions the association constant of the complex controls the concentration of the target molecules. To shift the equilibrium to the antigen/antibody complex an excess of labeled probe molecules (antigen or antibody) has to be used. Only a few probe molecules bind to their target, thereby changing their characteristic diffusion time or other detectable parameters. While in heterogeneous assays the excess can be easily removed by washing steps a new detection method, which separates free from bound labeled probe molecules has to be developed for a homogenous assay. One way to circumvent this problem is to combine confocal fluorescence microscopy with microelectrophreses. Electrophoresis, separation based on charge and/or mass of analytes, is a common technique in almost every aspect of basic or applied biomedical research. Figure 1 shows a schematic diagram of our used setup.

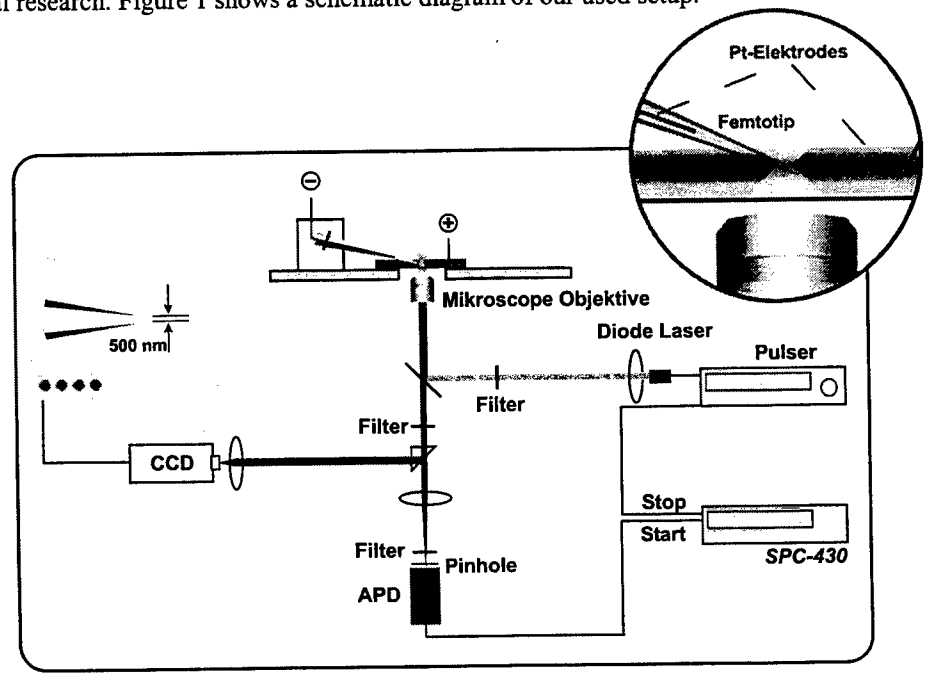

Fig. 1. Schematic diagram of the optical and electronical apparatus.

The experimental set-up consists essentially of a standard inverse confocal fluorescence microscope for TCSPC (Figure 1). A pulsed diode laser emitting at 638 nm served as excitation source. The laser system provided light pulses with a duration of less than 400 ps full width at half maximum (FWHM) at a repetition rate of 57 MHz. The collimated laser beam passes an excitation filter (639DF9; Omega Optics, Brattleboro, VT), entered an inverse microscope (Axiovert 100 TV; Zeiss, Germany) through the back port and was coupled into an oil-immersion objective (100xNA = 1.4; Olympus, Tokyo, Japan) by a dichroic beam splitter (645DRLP; Omega Optics, Brattleboro, VT). The average laser power was adjusted to be 600 µW at the sample. Fluorescence was collected by the same objective, filtered by two bandpass filters (675RDF50; Omega Optics, Brattleboro, VT; 680HQ65; AF Analysentechnik, Tübingen, Germany) and imaged onto a 100 µm pinhole oriented directly in front of an avalanche photodiode (AQ-131; EG&G Optoelectronics, Canada). The detector signal was registered by a PC plug-in card for TCSPC (SPC-430; Becker&Hickl, Berlin, Germany). With this card a minimum collection (integration) time of 150 µs per decay curve (64 channels) for a gap-free measurement is possible. All time-resolved measurements were carried out in the reversed mode, i.e. the detector signal served as start signal, whereas the laser pulse was used as stop signal. The instrument response function of the entire system was determined to be 420 ps. From the data of the TCSPC-card multichannel-scalar (MCS) traces were generated. For this all photons of a decay curve were added up to a bin of the MCS-trace.

The diameter of the detection volume is defined by the optical set-up. In particular the diameter is given by the used pinhole. Therefore in our set-up the diameter of the detection volume is approximately 1 µm, i.e. to ensure detection of all fluorescent molecules a detection channel with a diameter < 1 µm has to be applied. A commercially available channel fulfilling this requirement is given by the so-called "Femtotip" which has an inner diameter of about 500±200 nm at the small end (Eppendorf-Nethler-Hinz, Hamburg, Germany). Femotips are generally used for microinjection into cells. The capillary dips into a tissue culture dish (Petriperm hydrophil; Heraeaus Instruments, Osterode, Germany) containing pure glycerol. The use of glycerol decreases the refractive index differences at the outer capillary wall and minimizes vibrations of the capillary. The capillary was adjusted to meet the focus of the exciting laser beam about 1 µm in front of the exit. Alignment was carried out by a three-axis electrostrictive actuator with a resolution of 20 nm (ESA-CXA-Set; Newport Corporation, Irvine, CA) and a CCD camera (Imager 3, La Vision, Göttingen, Germany). The capillary was filled with a solution of 20 mM Tris-borate pH 8.4, 3% (w/v) polyvinyl pyrrolidone (PVP), containing 69.9% water, 30% glycerol, and 0.1% Tween 20. The solution was degassed under vacuum for 60 min. To avoid blocking of the tip, the solution was filtered through a 200 nm filter. The flow of the charged molecules through the capillary was established by electrokinetic forces using two platinium electrodes. One electrode was inserted into the capillary and the other dipped into the glycerol outside of the capillary.

The basic principle of our method is the use of differently charged probe and target molecules. For example, if a positively charged (either by additional amino acids like lysine residues or the charge of the fluorescent label) antigen molecule is used as fluorescent probe molecule it will move towards the cathode. Upon specific binding to the antibody (target) the excess of negative charges of the antibody should overcompensate the positive charges of the probe molecule. Thus the complex is separated from the probe molecules by moving towards the anode. To demonstrate the principal feasibility of our method we used the well known streptavidin/biotin system. Here we labeled biotin with the positively charged oxazine derivative MR121, i.e. under neutral conditions, the MR121-biotin conjugate moves towards the cathode. The MCS-traces on the right side in Fig. 2 show the time-resolved fluorescence signals observed from a 10^{-10} M solution of MR121-conjugates containing different streptavidin concentrations. With the setup shown on the right side of Fig. 2 (cathode outside and anode inside of the microcapillary) the biotin conjugates move towards the cathode. Upon addition of a solution containing 10^{-10} M streptavidin most biotin conjugates bind. Hence, the signal rate drastically decreases. On the other hand, if we change the polarity of the electrodes (left side in Fig. 2: anode outside and cathode inside of the capillary) a high signal rate is detected. This data clearly demonstrate that a separation of bound and free probe molecules is easily possible with the chosen experimental setup. Even in a 200 fold excess of free unbound probe molecules, i.e. addition of a solution containing 5×10^{-13} M streptavidin, bound biotin/streptavidin complexes can be detected moving towards the anode outside of the microcapillary.

As demonstrated our technique exceeds the sensitivity of the conventional ELISA. At the moment we are working on the early-stage detection of human antibodies directed against a tumor specific antigen. By the use of pulsed laser diode excitation in the red spectral range homogeneous assays are possible, even in undiluted human serum samples [3].

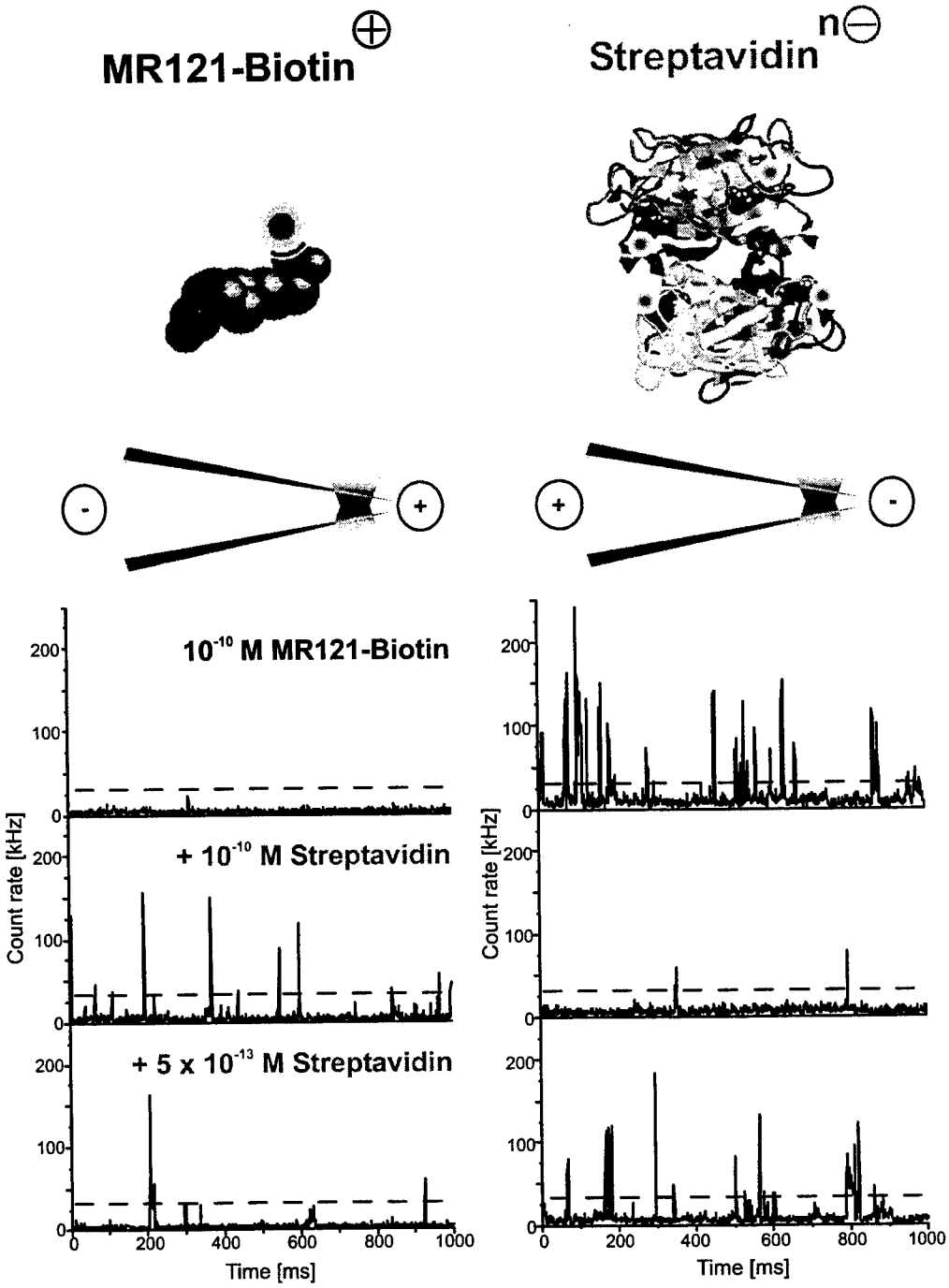

Fig. 2. MCS-traces (1 ms/bin) of a 10^{-10} M MR121 labeled biotin solution containing different concentrations of streptavidin recorded at different polarity in the microcapillary. Average laser power at the sample: 600 µW. As solvent served 20 mM Tris-borate pH 8.4, 3% (w/v) polyvinyl pyrrolidone (PVP), containing 69.9% water, 30% glycerol, and 0.1% Tween 20.

References

[1] R. Rigler, M. Eigen, "Sorting single molecules: Application to diagnostics and evolutionary biotechnology," Proc. Natl. Acad. Sci. USA **91**, 5740-5747 (1994).

[2] J. Briggs, V.B. Elings, D.F. Nicoli, Science **212**, 1267-1269 (1981).

[3] M. Sauer, C. Zander, R. Müller, B. Ullrich, K. H. Drexhage, S. Kaul, J. Wolfrum, "Detection and identification of individual antigen molecules in human serum with pulsed semiconductor lasers," Appl. Phys. B **65**, 427-431 (1997).

Single molecule DNA sequencing in microcapillaries

M. Sauer*[a], F. Göbel[a], K.-T. Han[a], C. Zander[b]

[a] *Physikalisch-Chemisches Institut, Universität Heidelberg, Im Neuenheimer Feld 253, 69120 Heidelberg, Germany*

[B] *Institut für Physikalische Chemie, Universität-Gesamthochschule Siegen, Adolf-Reichwein-Str. 3, 57068 Siegen, Germany*

**Telephone: (49)-6221-548460, fax: (49)-6221-544255, e-mail: sauer@urz.uni-heidelberg.de*

Summary

Since the first measurements of single molecule fluorescence decay times in flowing sample streams [1] several groups have improved the ability to distinguish between differently labeled single molecules due to their characteristic fluorescence decay times using time-correlated single-photon counting (TCSPC) [2,3]. Using confocal excitation/detection techniques detection volumes in the femtoliter region can be easily attained which permit signal-to-background ratios (SBRs) > 100 [4]. For efficient detection of all analyte molecules a technique has to be developed which constrains all analyte molecules to flow through the detection volume. If a detection volume in the picoliter (pl) range is used, hydrodynamic focusing of the sample stream in a sheath flow cuvette has been applied successfully [5]. Recently, efficient detection of single fluorescent molecules eluting off a polystyrene microsphere optically trapped in a flowing sheath stream has been demonstrated [6]. Unfortunately, for the application of femtoliter detection volumes microcapillaries or microchannels with inner diameters smaller than the detection area (< 1 μm) have to be used. Recently [7,8], we were able to demonstrate the time-resolved identification of individual fluorescent dyes as they flow through a microcapillary with an inner diameter of 500±200 nm applying an electrical tension of a few volts. Addition of a nonionic detergent (Tween 20) efficiently suppressed adsorption of molecules to the glass surface of the capillary and reduced the electroosmotic flow.

A very promising but likewise demanding application of the single molecule detection technique is single molecule DNA sequencing which was first proposed by Keller and coworkers [9]. The idea of this method involves the incorporation of fluorescently labeled deoxynucleosidetriphosphate molecules (dNTPs) into a growing DNA strand by DNA polymerases, selection of a single DNA strand, transportation of the selected DNA strand into the detection system (flowing sample stream or detection channel on a microchip) and identification of the individual fluorescently tagged deoxynucleoside monophosphate molecules (dNMPs) as they are cleaved from the DNA strand by an exonuclease enzyme. Since the DNA sequence is determined by the order in which labeled dNMPs are detected, diffusional misordering of sequentially cleaved dNMPs has to be prevented, i.e. the enzymatic cutting rates, flow velocities and the distance to the detection volume have to be optimized. The current bottleneck of the single molecule sequencing scheme appears to be the complete substitution of native dNTPs by fluorescently labeled dNTPs in an enzymatic labeling reaction. However, the sequence information can also be obtained if the DNA is only partly labeled, i.e. if two kinds of nucleotides are substituted completely in varying combinations.

Here we demonstrate efficient sample delivery from an etched optical fiber (diameter < 500 nm at the very end of the tip). The end of the streptavidin coated fiber is dipped for 1 s into DNA containing solutions (10^{-8} – 10^{-10} M) and fixed about 20-40 μm in front of the detection area inside of a conical capillary with an inner diameter of 500 nm at the small end. The experimental setup for single molecule counting and identification consists essentially of a standard inverse confocal fluorescence microscope for time-correlated single photon counting (TCSPC). As excitation source we used a diode laser emitting at 638 nm. The laser system provided light pulses with a duration of less than 400 ps (FWHM) at a repetition rate of 57 MHz. Details of the apparatus are described in Ref. 8. To ensure the detection of all fluorescent molecules we applied a microcapillary with an inner diameter smaller than the detection area (~ 1 μm). The capillary was adjusted to meet the focus of the exciting laser beam about 1 μm in front of the exit. The capillary was filled with a solution of 20 mM Tris-borate, pH 8.4, 3% (w/v) polyvinylpyrrolidone (PVP), containing 68% water, 30% glycerol, and 2% Tween 20. The flow of the negatively charged labeled mononucleotide molecules Cy5-dCTP and MR121-dUTP (Fig. 1) through the detection area was established by electrokinetic forces using two platinum electrodes (cathode inside, anode outside).

For DNA digestion experiments a 5'-biotinylated 1688 bp PCR product labeled with about 30 Cy5-dCTP and 30 MR121-dUTP molecules per DNA strand was used [8]. The amount of incorporated fluorescent nucleotides was determined by absorption measurements in PBS, pH 8.4. In order to demonstrate the feasibility of single-molecule DNA sequencing in microcapillaries a streptavidin coated fiber was dipped

into a 10^{-8} M DNA solution in PBS for 1 s. After this the fiber was washed with the described solvent mixture and inserted into the capillary. To remove adsorbed dNTP and DNA molecules an electrical tension of 15 V was applied for about 3 h. After this a signal count rate of < 0.1 Hz, i.e. one fluorescent signal in 10 s was achieved. Enzymatic degradation was started adding an diluted exonuclease solution. It should be pointed out that the observed cleavage rate of an exonuclease enzyme is controlled by several factors: (a) the relative velocity between the exonuclease and the DNA strand (diffusion and velocity of the solvent), (b) the rate of attachment to the strand, (c) the cleavage rate on the strand, and (d) the processivity. All these factors depend strongly on the chosen experimental conditions, like the applied solvent, temperature, and electrical field. As mentioned in (a), in single molecule DNA sequencing the velocity of the exonuclease molecules may become very important, i.e. attachment of the exonuclease to DNA is more unlikely in case of high relative velocity between them. We assume that the overall cleavage rate is mainly determined by the rate of attachment of the exonuclease molecule to the DNA strand and the processivity.

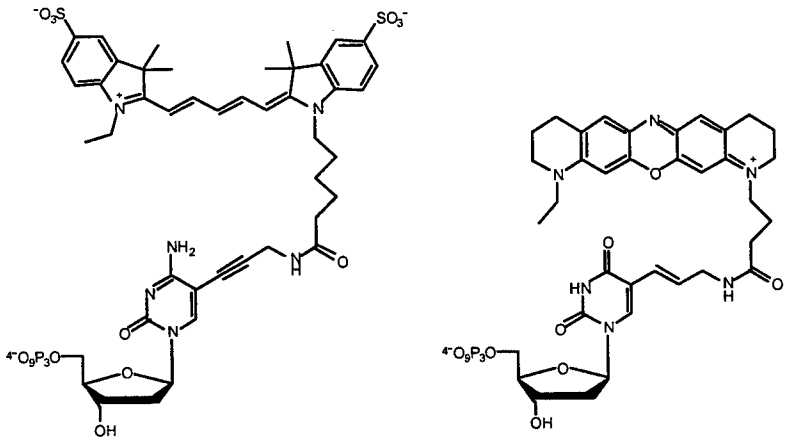

Fig. 1. Molecular structures and spectroscopic characteristics in the used solvent system of labeled mononucleotide molecules Cy5-dCTP (λ_{abs}=652 nm, λ_{em}=671 nm, τ=1.38 ns) and MR121-dUTP (λ_{abs}=661 nm, λ_{em}=673 nm, τ=2.31 ns).

To avoid hairpin structures in single-stranded DNAs, the degradation of double-stranded DNA is generally preferred. On the other hand, we found that the labeled dNTP molecules Cy5-dCTP and MR121-dUTP have a strong tendency to bind to double-stranded DNA fragments. As already mentioned such nonspecific binding might result in sequencing errors. Therefore, we decided to use single-stranded DNA in our sequencing experiments. Due to the applied electrical field and solvent mixture the DNA should be mostly stretched in the capillary. Figure 2 shows time-resolved fluorescence signals observed after addition of T4-DNA-polymerase solution to single-stranded DNA attached to an optical fiber. The exonuclease containing solution was injected into the capillary close by the tip of the fiber (about 2-3 mm). As can be taken from the MCS-trace in Fig. 2a, after about 50 s the first fluorescently labeled dNMP molecules reach the detection area. The number of detected bursts increases during the first 200 s from about 20 Hz to more than 200 Hz. Fig. 2b shows a part of the MCS-trace recorded ~200 s after addition of the exonuclease. Since the high counting rate was detected during a time period of over 5 h we suggest that at least 60.000 DNA strands (each containing about 60 labels) have been bound to the fiber. To estimate the overall cleavage rate we assume that all 60.000 DNA strands would be degraded simultaneously by exonucleases. With a rate of detected conjugates of ~200 Hz we found an average cleavage rate of ~0.1 Hz for T4-DNA-polymerase on statistically labeled DNA strands under our applied experimental conditions. For the fluorescence decay time distribution shown in Fig. 2c we used the first 10.000 detected photon bursts after addition of the exonuclease enzyme. To consider only photon bursts which result from single conjugate events only bursts with a duration between 0.5 and 4.5 ms were utilized. Using this time-filtering two maxima result (Gaussian fits: peak 1: 1.43±0.28 ns, peak 2: 2.21±0.85 ns) which correspond well to the expected values of the fluorescence decay time. By using the average decay time, the peak frequencies and standard deviation of the Gaussian fits a composition of 38% Cy5-dCMP and 62% MR121-dUMP results. This ratio does not correspond to the composition revealed from absorption measurements. From

absorption measurements we calculated an amount of incorporated fluorescent nucleotides of about 30 Cy5-dCMP (50%) and 30 MR121-dUTP (50%) molecules per single-stranded PCR-product. However, in a real sequencing experiment each detected burst with a fluorescence decay time shorter than 1.85 ns (point of intersection of the Gaussians in Fig. 2c) is assigned to be a Cy5-dCMP molecule, whereas all bursts with decay times longer than 1.85 ns are defined to be MR121-dUMP molecules. In this case a ratio of 48:52 for Cy5-dCMP and MR121-dUMP molecules results which is similar to the ratio determined by absorption spectroscopy.

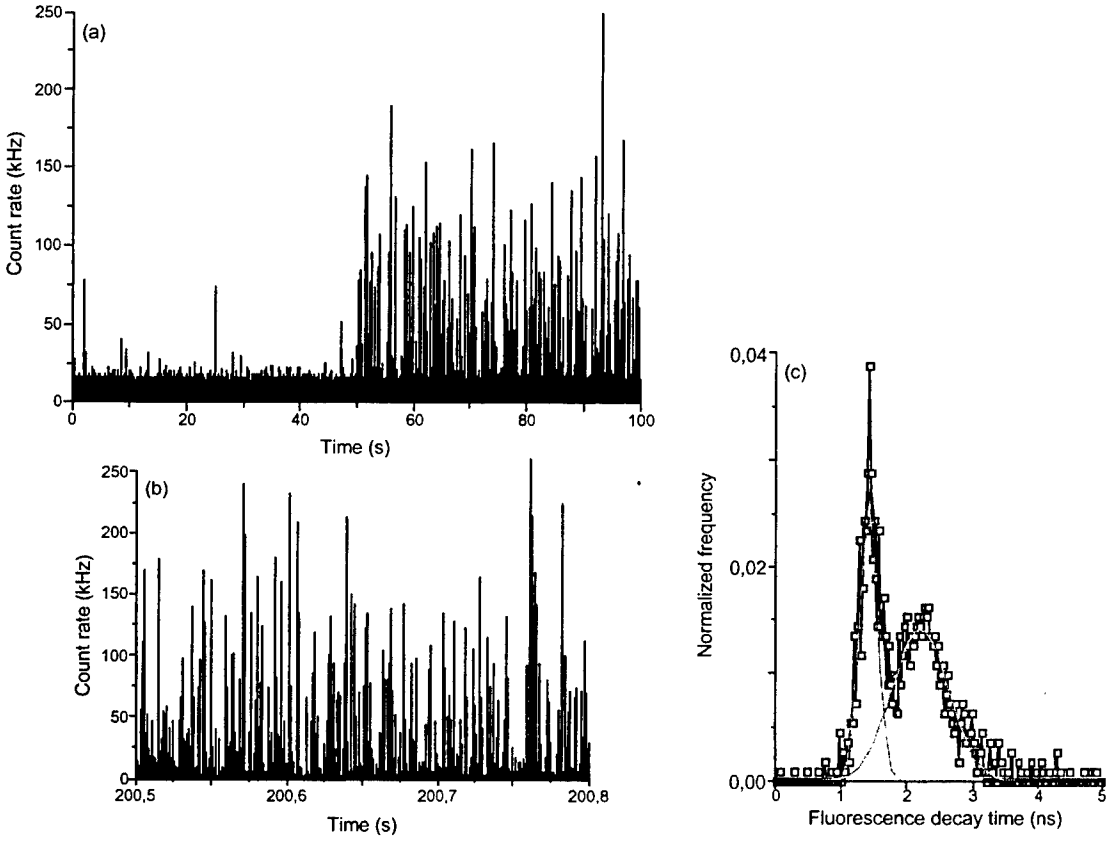

Fig. 2. MCS trace (0.5 ms/bin) recorded after adding 5 µl of a T4-DNA-polymerase solution and normalized fluorescence decay time distribution of the first 10.000 detected photon bursts.

References

[1] C. W. Wilkerson, P. M. Goodwin, W. P. Ambrose, J. C. Martin, R. A. Keller, "Detection and lifetime measurement of single molecules in flowing sample streams by laser-induced fluorescence," Appl. Phys. Lett. **62**, 2030-2032 (1993).

[2] C. Zander, M. Sauer, K. H. Drexhage, D.-S. Ko, A. Schulz, J. Wolfrum, L. Brand, C. Eggeling, C. A. M. Seidel, „Detection and characterization of single molecules in aqueous solution," Appl. Phys. B **63**, 517-523 (1996).

[3] M. Sauer, J. Arden-Jacob, K. H. Drexhage, F. Göbel, U. Lieberwirth, K. Mühlegger, R. Müller, J. Wolfrum, C. Zander, „Time-resolved identification of individual mononucleotide molecules in aqueous solution with pulsed semiconductor lasers," Bioimaging **6**, 14-19 (1998).

[4] Ü. Mets, R. Rigler, "Submillisecond detection of single rhodamine molecules in water," J. Fluoresc., **4**, 259-264 (1994).

[5] P. M. Goodwin, W. P. Ambrose, R. A. Keller, *"Single-molecule detection in liquids by laser-induced fluorescence* ,"Accounts Chem. Res. **29**, 607-613 (1996).

[6] N. P. Machara, P. M. Goodwin, J. Enderlein, D. J. Semin, R. A. Keller., "Efficient detection of single molecules eluting off an optically trapped microsphere," Bioimaging **6**, 33-42 (1998).

[7] W. Becker, H. Hickl, C. Zander, K. H. Drexhage, M. Sauer, S. Siebert, J. Wolfrum," Time-resolved detection and identification of single analyte molecules in microcapillaries by time-correlated single-photon counting (TCSPC)," Rev. Sci. Instr. **70**, 1835-1841 (1999).

[8] M. Sauer, B. Angerer, K.-T. Han, C. Zander, „Detection and identification of single dye labeled mononucleotide molecules released from an optical fiber in a microcapillary: First Steps towards a new single molecule DNA sequencing technique," PCCP **1**, 2471-2477 (1999).

[9] J. H. Jett, R. A. Keller, J. C. Martin, B. L. Marrone, R: K. Moyzis, R. L. Ratliff, N. K. Seitzinger, E. B. Shera, C. C. Stewart, "High-speed DNA sequencing: an approach based upon fluorescence detection of single molecules," J. Biomol. Struc. Dynam. **7**, 301-309 (1989).

Laser Applications to Chemical and Environmental Analysis

Advances in Spectroscopic Sources

Friday, February 11, 2000

Peter W. Werle, Fraunhofer Inst. for Atmospheric Environmental Res., USA
Presider

FC
1:30pm–3:20pm
Anasazi North

"W" Quantum Well Diode and Optically-Pumped Mid-IR Lasers Operating at High-Temperatures

J. R. Meyer, W. W. Bewley, L. J. Olafsen, I. Vurgaftman, C. L. Felix, D. W. Stokes, and M. J. Yang
Naval Research Laboratory, Washington, DC 20375
meyer@sisyphus.nrl.navy.mil, bewley@sisyphus.nrl.navy.mil, vurgaftm@aphrodite.nrl.navy.mil

H. Lee, R. J. Menna, R. U. Martinelli, D. Z. Garbuzov, and J. C. Connolly
Sarnoff Corporation, Princeton, NJ 08543-5300
hlee@sarnoff.com, rmartinelli@sarnoff.com

M. Maiorov, A. R. Sugg, and G. H. Olsen
Sensors Unlimited, Inc., Princeton, NJ 08540-5914

Semiconductor diode technology will some day offer compact, robust, and inexpensive mid-IR sources that are ideal for spectroscopy and chemical sensing applications. The main reason that this has not occurred already is that current cw or quasi-cw mid-IR semiconductor lasers require cryogenic cooling. Before now, no III-V laser emitting beyond 3 μm had achieved cw operation above 180 K, and even for pulsed mode the T_{max} for electrically-pumped interband devices was 255 K. Here we will discuss the rapid recent progress by type-II antimonide lasers toward the goal of higher operating temperatures, and also higher cw output power in the mid-IR.

The active regions of these type-II antimonide lasers employed the "W" configuration,[1] which derives its name from the shape of the conduction band profile. Two InAs electron quantum wells surround a GaInSb hole well to maximize the wavefunction overlap and gain, and are in turn bounded by AlSb, AlAsSb, or AlGaAsSb barrier layers which provide electrical confinement along with a two-dimensional density of states for both carrier types. The Auger decay rate, which governs the high-T lasing thresholds, is suppressed by a factor of 5-10 compared to analogous type-I structures.

While only lead salt lasers and the intersubband quantum cascade laser had previously displayed room-temperature pulsed operation beyond 3 μm, type-II diodes with AlGaAsSb broadened-waveguide separate confinement regions[2] and W active regions recently became the first electrically-pumped interband III-V mid-IR lasers to do so. At 300 K, the 10-quantum-well devices had a peak output power >2 mW and a lasing spectral width of 12 nm centered on $\lambda = 3.30$ μm. The characteristic temperature T_0 over the range 100-280 K was 48 K, which is higher than that of any earlier interband mid-IR device at high T. For cw operation, T_{max} was 170 K and $P_{out} = 90$ mW per uncoated facet was measured at 77 K.

Optically-pumped type-II devices with W active regions recently attained the highest cw operating temperatures of *any* semiconductor lasers emitting between 3 and 6 μm. Using a new diamond-pressure-bond heat-sinking approach, typical T_{max} values were 290 K at $\lambda = 3.0$ μm, 265 K at $\lambda = 4.0$ μm, and 210 K at $\lambda = 6.1$ μm.[3] For a $\lambda = 3.2$ μm device at 77 K, the maximum cw output power was 0.54 W per uncoated facet. Pulsed lasing up to 220 K and cw lasing to 130 K were obtained for $\lambda = 7.3$ μm, which is 2 μm beyond any previous interband III-V lasing wavelength.

[1] J. R. Meyer, *et al.*, *Appl. Phys. Lett.* 67, 757 (1995), "Type-II quantum-well lasers for the mid-wavelength infrared."

[2] D. Z. Garbuzov, *et al.*, *Appl. Phys. Lett.* 69, 2006 (1996), "Ultralow-loss broadened-waveguide high-power 2 μm AlGaAsSb/InGaAsSb/GaSb separate-confinement quantum well lasers."

[3] W. W. Bewley, *et al.*, *Appl. Phys. Lett.* 74, 1075 (1999), "High Temperature Continuous-Wave 3-6.1 μm `W' Lasers with Diamond-Pressure-Bond Heat Sinking."

High Power Mid-IR Interband Cascade Lasers

J. D. Bruno, R. Q. Yang, J. L. Bradshaw, J. T. Pham, and D. E. Wortman

U.S. Army Research Laboratory, 2800 Powder Mill Rd, Adelphi, MD 20783-1197
(301)394-5740, fax (301)394-2103, bruno@arl.mil

Abstract: Mid-IR (3.9 μm) type-II interband cascade lasers based on InAs/GaInSb heterostructures are demonstrated. Devices, under differing conditions, show lasing up to 217K, peak output powers exceeding 4W/facet at 80K, and cw operation at 70K.

OCIS codes: (140.6810) Semiconductor lasers; (250.5980)Semiconductor optical amplifiers

Compact reliable mid-IR ($\lambda > 2.5\mu$m) sources are in growing demand for a variety of military and commercial applications. Most applications require lasers that emit relatively high output powers (multi-Watt peak-power levels) and operate cw (or quasi-cw) at ambient temperatures (or at temperatures accessible with thermoelectric coolers, i.e. T$\geq$200K). Although no presently available diode lasers meet these requirements, the demonstration of a quantum cascade (QC) laser [1] based on intersubband transitions in type-I semiconductor quantum wells (QWs) has produced new opportunities for the development of such mid-IR sources. The novel aspect of these type-I QC devices is their unipolar active regions. Being unipolar, they can be stacked together, one after another, to produce many identical active regions within a single device. This series connection permits the emission of more than one photon for each injected electron; ideally, above threshold, one photon is emitted for each active region in the device. These devices have exhibited impressive performance characteristics and are the subject of considerable current interest [2].

An alternative approach, first suggested by one of the authors [3], takes advantage of the QC configuration used in the type-I devices, but uses type-II heterostructues configured to give interband active regions in series with interband tunneling injection sections (facilitated by the type-II band alignments). This combination leads to a total active/injection region that is unipolar in nature and hence can be stacked as occurs in the type-I QC devices. This type-II interband cascade (IC) laser offers several advantages not shared by the type-I QC laser. The interband nature of the active region laser-transition eliminates the fast phonon relaxation from the upper-laser-level present in the type-I device. This significantly reduces unwanted heating in the device's active region and allows for the possibility of efficient devices. The interband design also eliminates constraints associated with intersubband-transition-induced polarization selection rules. In addition, the type-II materials used in the structure have wide band offsets. This feature significantly reduces thermionic emission from the upper laser level (and associated heating), and permits the development of devices which lase at wavelengths in the 3-5μm region, wavelengths that are generally too short for the band offsets present in the type-I QC devices. The first demonstration of the IC concept was reported in 1997 [4]. Since that time, significant progress has occurred [5, 6, 7].

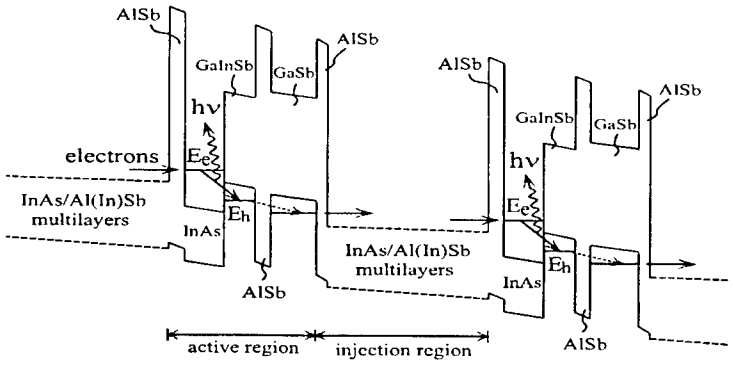

Fig. 1. Schematic band-edge profile of the active and injection regions in an interband cascade laser

In this work, we present recent results, some of which are already documented [8], on IC lasers based on

InAs/GaInSb type-II QWs and grown in a Varian Gen-II MBE system at the Army Research Laboratory (ARL). The devices we have demonstrated exhibit significantly higher differential quantum efficiency and peak power than previous IC lasers, and have lased under cw conditions. To our knowledge, this is the first report of cw operation from an IC laser.

The IC laser structure described below .consists of 23 repeated periods of active regions separated by n-type doped injection regions as shown in Figure 1. The injection regions consist of digitally graded InAs/Al(In)Sb layers. Each active region comprises coupled QWs, stacked sequentially with 23ÅAlSb, 25ÅInAs, 36Å$Ga_{0.7}In_{0.3}Sb$, 15ÅAlSb, and 58ÅGaSb layers, and is designed to lase at a wavelength $\lambda \approx 3.9\mu$m.The optical mode is confined by top and bottom cladding layers consisting of n-type InAs/AlSb superlattices with overall thicknesses of 1.6μm and 2.0μm, respectively. At ARL, we have grown three nominally similar device structures labeled ICL1, ICL2, and ICL3. All three MBE growths were on (001) GaSb substrates; however, the substrates were not all from the same vendor. MBE growth ICL1 was on a vendor-"A" substrate while growths ICL2 and ICL3 were were on vendor-"B" substrates. All three growths showed excellent structural characteristics as evidenced by high resolution x-ray diffraction measurements. Many gain-guided and mesa-defined laser devices (with uncoated facets) were fabricated from each growth. Devices were mounted with silver epoxy epi-side up onto a Au-coated Al chip carrier that was itself mounted onto the copper cold finger of a cryostat. All devices tested lased near the design wavelengths (3.8-3.9μm) and were robust in their performance. This fact demonstrates the reproducibility/viability of the type-II cascade design. Significantly, several devices survived current densities in excess of 12kA/cm^2 and performed repeatedly showing no signs of degradation despite these high current levels.

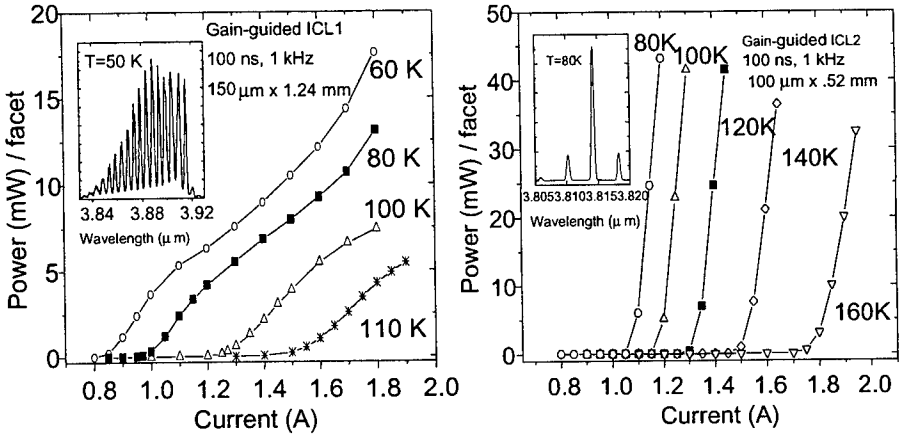

Fig. 2. Optical output power vs. current for gain-guided ICL1 and ICL2 devices. The insets show high resolution lasing spectra under pulsed excitation conditions (see text).

Figure 2 shows optical output power vs. injection current (L-I curve) for a gain-guided ICL1 device(left) and ICL2(right) device. The insets show high resolution lasing specra obtained under pulsed excitation conditions; the ICL1 spectrum(left) is from a mesa-defined device. The general appearance of L-I curves obtained from other ICL1 devices is similar to that shown for the ICL1 device in the figure. The same can be said regarding ICL2 devices. L-I curves from ICL3 devices (not shown) were qualitatively similar to those of ICL2 devices, but with higher threshold currents. Generally, ICL1 devices had lower threshold current densities and lower slope efficiencies than exhibited by ICL2 and ICL3 devices. Whether this behavior can be traced to the different vendor substrates used in the growths is currently being investigated. Among devices from ICL2, several 1-mm long devices were able to lase at temperatures up to 210 K, which is considerably higher than the previous record (182 K) for an IC laser [7] at this wavelength. The threshold current densities of devices from ICL3 are the largest in comparison to devices from ICL1 and ICL2; however, lasers from ICL3 could be operated at temperatures up to 217 K, the highest among any III-V diode lasers at this wavelength. Figure 3 shows the L-I curve from a 200μm-wide mesa-defined ICL2 device. As can be seen in the figure, at low duty cycle where device heating is not as significant an issue, peak output power exceeded 4W/facet. For

another 100μm wide ICL2 mesa-defined laser, a slope efficiency of 735 mW/A was observed from one facet at 150 K. Assuming identical facets, and correcting for the transmission coefficients of the collection optics, this corresponds to a differential external quantum efficiency greater than 458%, i.e. above threshold, more than 4.5 photons were emitted per additional injected electron. Finally, in a preliminary attempt to better heat sink the devices, an ICL1 device was mounted epi-side up on a Cu heat sink (as opposed to a Au-coated Al chip carrier). Because ICL1 devices had the lowest current thresholds, we expected that these devices would have the lowest unwanted heating. The 100μm wide mesa-defined device lased under cw conditions at 70K. This and other devices are currently being further investigated to better understand their performance characteristics.

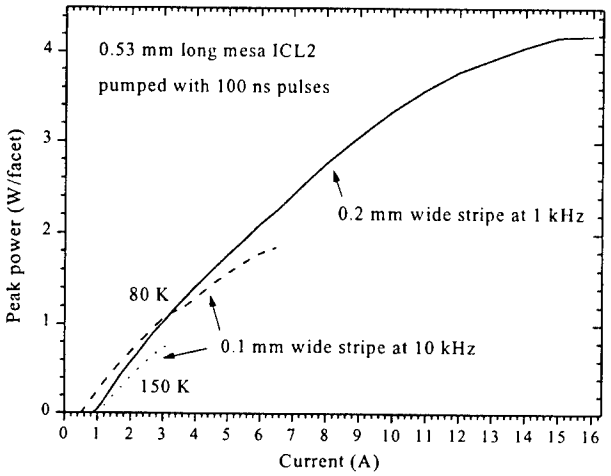

Fig. 3. Optical output power vs. current for mesa defined ICL2 devices.

Although the device results described above do not yet meet current application requirements, they are very encouraging. First, heat sinking of these devices can be significantly improved by using an epi-side down design. This will enhance heat flow out of the device's active region keeping the device temperature closer to that of the heat sink. Secondly, device structures incorporating higher gain than obtained from a single indirect QW transition as depicted in Figure 1 can be designed and grown. Additionally, there seems to be significant room for improvement with respect to threshold currents Devices we have looked at showed significant device-to-device variability This suggests that further research on these devices and their fabrication processes may significantly improve their performance from present levels. These considerations lead us to speculate that these type-II IC lasers may one day become the laser of choice in the mid-IR spectral region for most applications

References

1 J. Faist, F Capasso, D L. Sivco, C Sitori, A L Hutchinson, and A Y Cho, Science **264**, 553 (1994)
2 see for example, Proceedings of the 5th International Conference on Intersubband Transitions in Quantum Wells (ITQW'99, http://www hlphys.uni linz ac at/hl/itqwprogram.htm)
3. R. Q. Yang, Superlattices and Microstructures **17**, 77 (1995).
4. C. H. Lin, R. Q. Yang, D. Zhang, S. J. Murry, S. S. Pei, A. A. Allerma, S. R. Kurtz, Electron. Lett. **7**, 598 (1997).
5. C. L. Felix, W. W. Bewley, I. Vurgaftman, J. R. Meyer, D. Zhang, C.-H. Lin, R. Q. Yang, and S. S. Pei,IEEE Photonics Technol. Lett. **9**, 1433 (1997).
6. R. Q. Yang, B. H. Yang, D. Zhang, C.-H. Lin, S. J. Murry, H. Wu, and S. S. Pei, Appl. Phys. Lett. **71**, 2409, (1997).
7. B. H. Yang, D. Zhang, R. Q. Yang, C.-H. Lin, S. J. Murry, and S. S. Pei, Appl. Phys. Lett. **72**, 2220, (1998).
8. Some of these results have been reported in R. Q. Yang, J. D. Bruno, J. L. Bradshaw, J. T. Pham, and D. E. Wortman, Electron. Lett. **35**, 1254 (1999).

Guided-wave difference-frequency sources for infrared spectroscopy

Konstantin P. Petrov, Arti Prasad Roth, Thomas L. Patterson, Douglas J. Bamford
Gemfire Corporation, 2471 East Bayshore Road, Suite 600, Palo Alto, CA 94303
tel. 650-849-6800, fax 650-849-6900, k.petrov@gemfirecorp.com

Abstract: Reported are design, performance, and spectroscopic application of an infrared source based on difference-frequency mixing of diode lasers. The source employs an annealed proton exchanged channel waveguide in periodically poled lithium niobate and operates in the 3.2-3.9 μm wavelength region at room temperature. Device efficiency of up to 4 $\%\cdot W^{-1}$ and output power of up to 145 μW were obtained. Spatial and spectral characteristics of the output beam were examined. High-resolution spectroscopy and detection of several trace gases were performed.

OCIS codes: (130.3120) Integrated optics devices; (130.3730) Lithium niobate; (140.2020) Diode lasers; (190.2620) Frequency conversion; (300.6340) Spectroscopy, infrared

1. Introduction

Diode-pumped difference-frequency generation (DFG) [1] is a simple and effective method for producing mid-infrared light for spectroscopic applications, although the generally low level of output power (microwatts) has prevented its use in field applications. Output power and device efficiency have been the focus of intense development over the last five years. Important technological advances made in this area include quasi-phase-matched nonlinear optical materials and channel waveguides [2]. Annealed proton exchange (APE) is widely used for fabrication of waveguides in lithium niobate. Our goal was to develop channel geometry and fabrication recipes which would yield devices with high DFG conversion efficiency. A waveguide channel design has been investigated that is based on the principle first proposed by Chou et al [3]. It employed three stages: a single-mode filter, an adiabatic taper that transforms the mode size, and a mixing region capable of carrying the product of frequency mixing. The waveguide investigated in this work differs from those previously described in the literature in the design of these stages.

2. Waveguide fabrication

Waveguide arrays were fabricated in five steps, as described below. First, a three-inch-diameter, 0.5-mm-thick wafer of z-cut congruent lithium niobate was periodically poled from the +z surface, with periods ranging from 17.4 to 20.1 μm. Second, a 1500-Å-thick layer of nichrome was sputtered on the +z surface of the wafer, and the waveguide channel openings were lithographically patterned in the layer. Each waveguide had a 5-mm-long, 2-μm-wide mode filter followed by a 2-mm-long, 2→20 μm linear width taper and a 17-mm-long, 20-μm-wide output channel. The wafer was then diced into individual chips. In step three, the chips were proton-exchanged in pure benzoic acid at 160°C for 34 hours. The exchange occurred in capped, but not sealed, test tubes placed in a heated circulating oil bath. In step four, the mask material was stripped, and the chips were annealed in an air-filled tube furnace at 340°C for 75 hours. In step five, both ends of each chip were optically polished.

3. Source performance

Characterization of difference-frequency mixing was performed in a setup similar to that described in our earlier work [4]. Diode lasers were used as pump and signal sources. The pump laser was a 775-795 nm semiconductor master oscillator power amplifier. The signal laser was a grating-stabilized tapered semiconductor oscillator operating in the 1000-1020 nm wavelength range. By difference-frequency mixing of these lasers it was thus possible to cover the 3.2-3.9 μm mid-infrared spectroscopic region. Collimated pump and signal laser beams were combined on a dichroic beamsplitter, passed through an f=75 mm focusing lens, and imaged onto the waveguide input facet by a 2.5× or a 4.3× microscope objective. Total uncorrected waveguide throughput of 63% was observed. Throughputs of tapered waveguides were compared with those of straight channel waveguides of the same width as the input mode filter, 2 μm. The throughputs were the same, suggesting that no excess loss was

incurred by the taper.

Quasi-phase-matching for the idler wavelength of 3.6 μm occurred in waveguides with a 19.5-μm domain grating period at room temperature. With 42 mW pump power at 787 nm and 48 mW signal power at 1008 nm coupled in the waveguide, the maximum generated idler power was 80 μW. The corresponding device conversion efficiency was 4 %·W^{-1}. Up to 145 μW of idler power were generated with higher pump and signal power (105 mW and 112 mW, respectively), although the device efficiency was lower due to the onset of photo-refraction. At these levels of output power, the measured device efficiency was typically a factor of four lower than predicted.

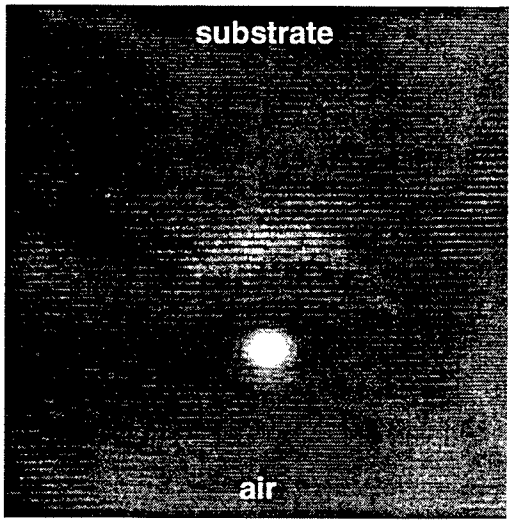

Fig. 1. Infrared camera image of a 3.5-μm idler beam at the output of a tapered waveguide.

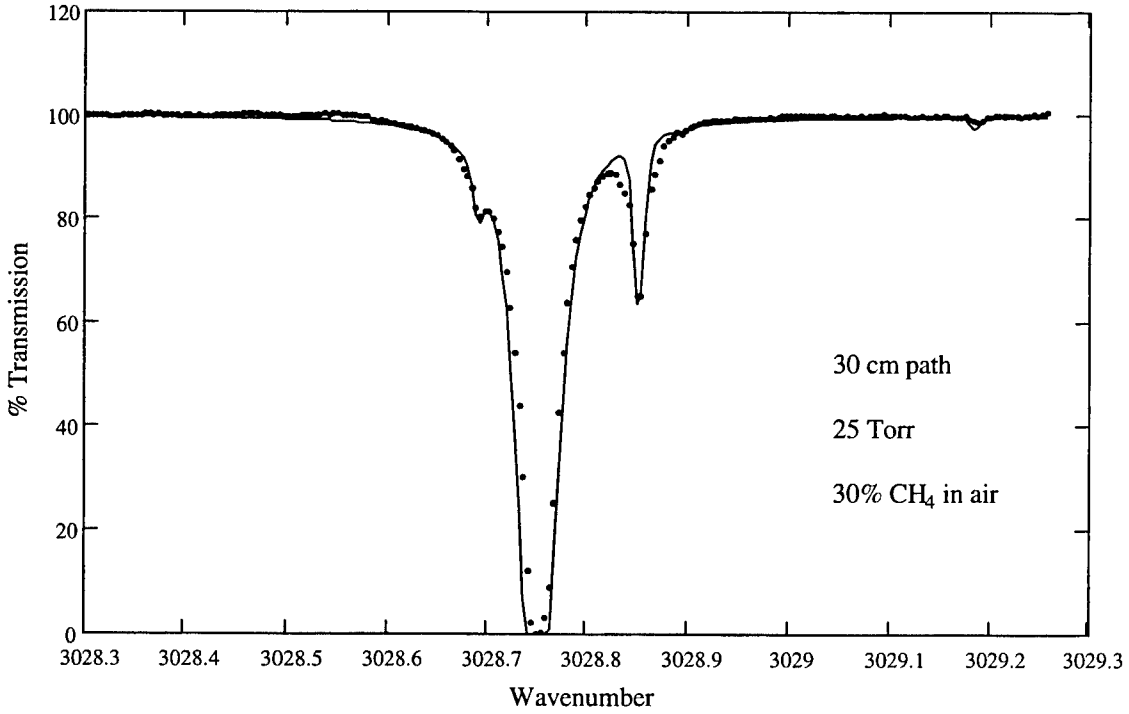

Fig. 2. Measured (dots) and calculated (line) spectra of methane in air. The data shown are a 256-sweep average acquired in 2.6 s.

The spatial profile of the idler beam was analyzed using a liquid-nitrogen-cooled InSb array camera. The waveguide output face was imaged onto the array by a CaF_2 lens and through a germanium filter. Fig. 1 shows the

camera image. The waveguide carries a single spatial mode at 3.5 μm which is observed as a bright, slightly elliptical spot in the image. The weak semi-circular halo above the waveguide core is Cerenkov-idler emission produced by interaction of higher-order modes at the pump wavelength with the fundamental mode at the signal wavelength.

4. Spectroscopic measurements

The output power, spatial characteristics, and spectral quality of the output beam were sufficient for use in high-resolution spectroscopy. Fig. 2 shows a spectrum of an air sample in a 30-cm-long absorption cell at room temperature. The sample pressure is 25 Torr, and it contains 30% methane by volume. The wavelength of the pump laser was scanned at a rate of 100 Hz by rotation of the piezo-driven diffraction feedback grating in its master oscillator. The beam was synchronously chopped, such that no light was incident on the detector during scan retrace, allowing the measurement of detector dark voltage. The dc-coupled detector output waveform was averaged over 256 cycles using a 8-bit digital oscilloscope. The detector dark voltage was subtracted from the entire waveform. Baseline normalization was performed by fitting it with a fifth-order polynomial outside the region of strong absorption. Dots in Fig. 2 plot the normalized spectrum. Good agreement between calculated and experimental spectra is evident, both in terms of line intensity and line width. High-resolution spectroscopy and sensitive detection of other gases, including water vapor, carbon dioxide, and formaldehyde, were also performed.

1. U. Simon, C.E. Miller, C.C. Bradley, R.G. Hulet, R.F. Curl, F.K. Tittel, "Difference-frequency mixing in $AgGaS_2$ by use of single-mode diode-laser pump sources," Opt. Lett. **18**, 1062-1064 (1993)
2. R.L. Byer, Journal of Nonlinear Optical Physics and Materials **6**, 549 (1997)
3. M.H. Chou, M.A. Arbore, M.M. Fejer, "Adiabatically tapered periodic segmentation of channel waveguides for mode-size transformation and fundamental mode excitation," Opt. Lett. **21**, 794-796 (1996)
4. K.P. Petrov, A.T. Ryan, T.L. Patterson, L. Huang, S.J. Field, D.J. Bamford, "Spectroscopic detection of methane by use of guided-wave diode-pumped difference-frequency generation," Opt. Lett. **23**, 1052-1054 (1998)

Development of infrared chemical sensors based on quasi-phasematched, periodically poled lithium niobate sources

Scott E. Bisson, Thomas J. Kulp, Ken Aniolek, Uta-Barbara Goers, Karla Armstrong and Bruce Richman
Sandia National Laboratories
7011 East Ave.
Livermore, CA 94550
Ph. (925) 294-2467
e-mail sebisso@sandia.gov

Peter Powers
University of Dayton, Dayton, OH 45469-2314

Abstract

Periodically poled lithium niobate (PPLN) is a relatively new non-linear optical material which can be used for such processes as second harmonic generation, sum and difference frequency generation and optical parametric oscillation. The use of periodically-poled lithium niobate in spectroscopy and chemical sensing offers many potential advantages over systems employing more traditional laser sources. When pumped by the fundamental of a Nd:YAG laser PPLN offers the promise of high efficiency, high power, broad tunability (1.5-3.5 μm) and compact size. The broad tunability over the C-H stretch region is an important advantage for many chemical sensing applications. At Sandia, we are developing IR sources based on PPLN for both remote and in-situ chemical sensing.

Introduction

There are many applications in both remote sensing and in-situ monitoring which require rapid measurement capability, high sensitivity, selectivity to a broad range of species and portability. Until recently, such technology was deficient in one or more areas. However, with the advent of novel non-linear optical materials such as PPLN, sensors with the required attributes are now becoming a reality. At Sandia we are employing PPLN in three sensor systems: a mid-IR imaging system for short range standoff detection and imaging of methane and VOC's, a high sensitivity in-situ detection system for compliance monitoring of VOC's and NOx as mandated by the Clean Air Act Amendments (CAAA), and an extremely high performance system for atmospheric trace gas monitoring. Common to all of these systems is the ability to tune over broad spectral regions (thus allowing access to a wide range of species), with high sensitivity to species with both broad and narrow spectral features.

PPLN operates by converting light from a fixed frequency pump source and converting it to two tunable waves, termed the signal and idler. The pump source is typically a Nd:YAG laser operating at 1μm in either pulsed or continuous wave (cw) format. The pump light is split into a signal wave which for our applications is usually near 1.5μm and an idler wave near 3.3μm. PPLN operates in the mid-IR which is ideal for many chemical sensing applications since many functional groups (i.e. C-H) absorb there. The exact wavelengths of the signal and idler are determined by the wavelength of the pump and more importantly by the period of the domain reversal of the optical axis. This is illustrated in Figure 1 which shows a PPLN crystal with a variable period structure. By translating the crystal to a new period the signal and idler waves are thus tuned. In this laboratory, crystals with periods varying continuously from 29.1 to 30.2μm are used which yields an idler tuning range of approximately 2800 cm^{-1} to 3100 cm^{-1}, covering the important C-H stretch region.[1] A typical crystal has dimensions of 5 cm X 2cm X 0.05 cm and has several thousand of periods running lengthwise .

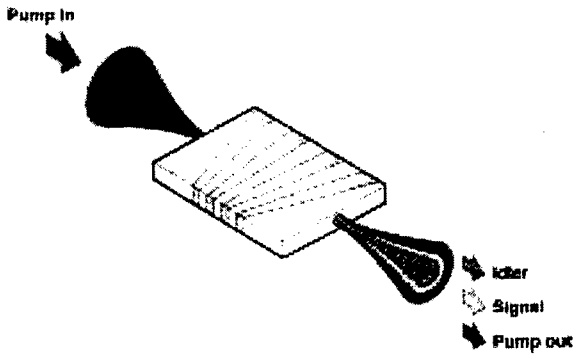

Figure 1. Schematic representation of a PPLN crystal illustrating the conversion of pump light into two longer IR wavelengths. The shaded domains have their optical axis vertical and are oriented opposite to those of the unshaded regions.

Applications to Chemical Sensing

The need to detect a broad range of species with high sensitivity places certain requirements on both the laser and spectroscopic method employed. Namely, the system must tune over a broad spectral region and must also be sensitive to species with both broad and narrow spectral features. This last requirement is perhaps the most difficult to achieve. While broad tuning of PPLN has been demonstrated, a combined coarse and fine tuning capability has not been demonstrated over significant spectral ranges. At Sandia, we have developed a broadly tunable, single longitudinal mode OPO based on PPLN for use in a photoacoustic spectrometer. A schematic of the laser system is shown in Figure 2. The basic configuration of the OPO was a bow-tie ring geometry[2] employing a FAN type PPLN crystal[1] with periods ranging from 29.3 μm to 30.1 μm. Coarse tuning was achieved by translating the PPLN crystal to a new period. For fine tuning, an air-spaced, intra-cavity etalon was used to mode-hop tune the OPO in steps on the order of .02-.1 cm^{-1}, depending on how many cavity modes were jumped. The high power output of this system at 3μm (100-200mW) makes this system ideal for use in photoacoustic spectroscopy where higher power is preferred.

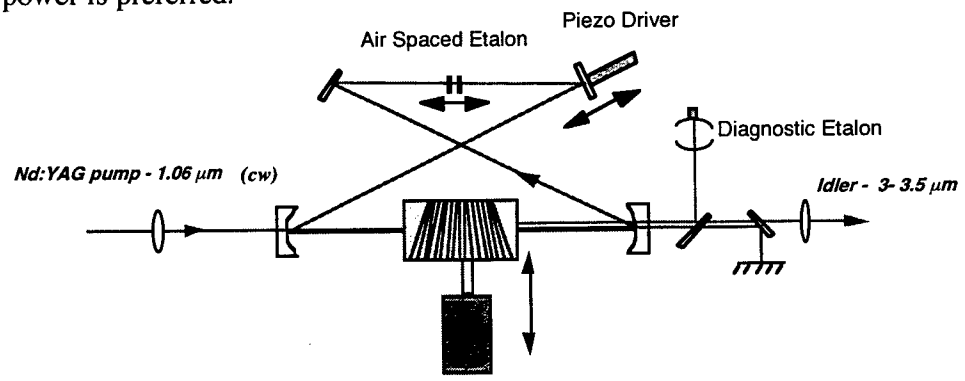

Figure 2. Schematic of the broadly tunable, cw PPLN OPO used in both the photoacoustic and gas imaging systems.

We are also employing PPLN in a pulsed, IR cavity-ringdown spectrometer.[3] This system contrasts sharply with the cw system in that there is no optical cavity and hence no modes. The system employs two PPLN stages with the first stage generating broadband (~15cm^{-1}) light at both 1.5 and 3.3μm through an optical parametric generation (OPG) process. The 1.5μm radiation is then spectrally filtered through the use of a tunable etalon

to produce narrowband light (~.08cm^{-1}). This is then amplified with a second stage optical parametric amplifier (OPA) to produce ~10μJ of 3.3μm light. The OPG/OPA configuration makes an ideal source for cavity-ringdown spectroscopy since it does not require much power. Figure 3 illustrates the configuration of the combined OPG/OPA system and cavity-ringdown cell. The coupling of a PPLN OPG/OPA system with cavity-down spectroscopy is a first and has many advantages over more traditional laser based methods such as simplicity (there is no cavity), sensitivity (absorptions down to 10^{-9} per pass) and rapid tunability (i.e. 15cm^{-1}/sec). This is illustrated in Figure 4 which shows an absorption spectrum of the Q-branch of methane acquired in only 1s.

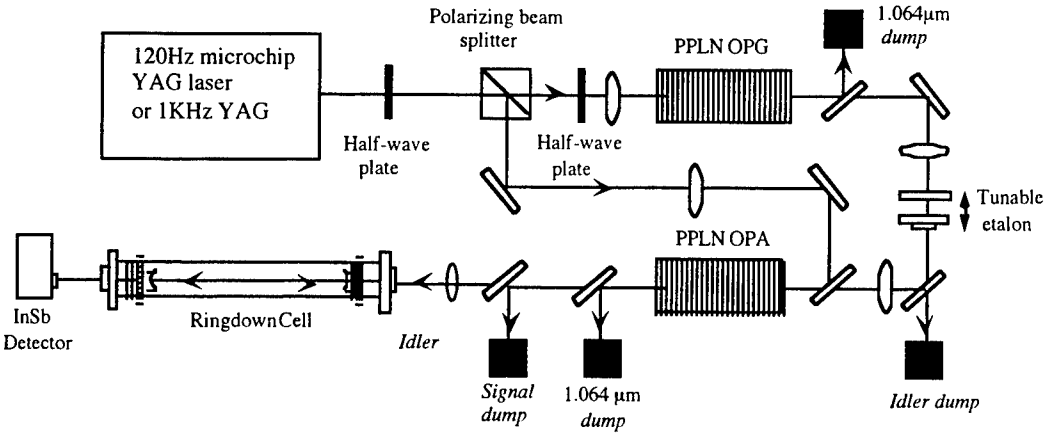

Figure 3. Configuration of the PPLN OPG/OPA cavity-ringdown spectrometer.

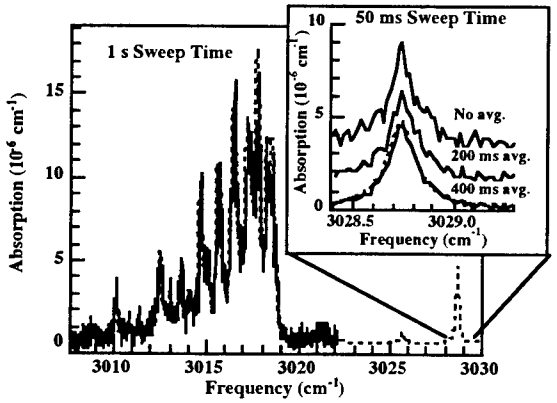

Figure 4. Cavity-ringdown absorption spectrum of the Q-branch of methane obtained with the PPLN OPG/OPA system.

1. P. E. Powers, Thomas J. Kulp, and S. E. Bisson, Opt. Lett., **23**, 159-161 (1998)

2. W. R. Bosenberg, A. Drobshoff, J. I. Alexander, L. E. Myers, and R. L. Byer, Opt. Lett., **21**, 1336-1338, (1996).

3. K. W. Aniolek, P. E. Powers, T. J. Kulp, B. A. Richman and S. E. Bisson, Chem. Phys. Lett. **302**, 555-562 (1999)

Diode-Pumped 214.8-nm Nd:YAG/Cr^{4+}:YAG Microchip-Laser System for the Detection of NO

J. Wormhoudt and J. H. Shorter
Center for Materials Technology, Aerodyne Research, Inc., Billerica, MA 01821-3976
jody@aerodyne.com, shorter@aerodyne.com

J. J. Zayhowski
Lincoln Laboratory, Massachusetts Institute of Technology, Lexington, MA 02420-9108
zayhowski@ll.mit.edu

Abstract: A passively *Q*-switched Nd:YAG/Cr^{4+}:YAG microchip laser at 214.8-nm (46556 cm^{-1}, the fifth harmonic of 1.074-μm) was developed. NO was detected by laser-induced fluorescence at a sensitivity of ~15 ppb_v in a simple, compact optical system.

OCIS Codes: (300.2530) Fluorescence, laser-induced; (140.3580) Lasers, ultraviolet

1. Introduction

We describe the development and characterization of a microchip-laser system delivering the fifth harmonic of the 1.074-μm Nd:YAG transition. Analysis of NO fluorescence spectra covering a range of almost 3 cm^{-1} identified the fifth-harmonic nominal frequency as 46556 cm^{-1}. This is an excellent position for sensitive and selective detection of NO, since it lies between two strong absorption lines, with either peak being easily accessed by temperature tuning the laser. Laser-induced fluorescence is a well-known technique for sensitive detection of trace gases, but NO requires excitation in the ultraviolet, where typical laser sources are large and complex. Field applications require systems that are compact, robust, portable, low-power, inexpensive, and operable over a large range of ambient conditions. Passively *Q*-switched Nd:YAG/Cr^{4+}:YAG microchip lasers meet all of these requirements and provide all-solid-state sources of coherent, subnanosecond, multikilowatt pulses at high repetition rates [1].

Prior to this work, all of the passively *Q*-switched Nd:YAG/Cr^{4+}:YAG microchip lasers operated at 1.064 μm or 946 nm. The harmonics of these sources do not overlap the NO absorption bands and are not useful for NO detection. Nd:YAG has a gain peak at 1.074 μm, whose fifth harmonic at 214.8 nm falls within the NO absorption bands. A frequency-quintupled passively *Q*-switched Nd:YAG/Cr^{4+}:YAG microchip laser operating at this wavelength provides a compact, robust light source for the measurement of NO. The main challenge in building such a source is the close proximity of the dominant 1.064-μm gain peak, whose effective gain cross section is about twice as large. Since a microchip laser has no intracavity frequency selective elements that can be used to discriminate between the two lines, all of the discrimination must be done with the laser mirror coatings.

2. Laser development

The laser consists of 2 mm of undoped YAG, 1.5 mm of Nd:YAG, 0.6 mm of Cr^{4+}:YAG, and 2 mm of undoped YAG, diffusion bonded to each other in the order listed. The input coating of the laser must be highly transmitting at the pump wavelength of 808 nm and highly reflecting at the oscillating wavelength. Since there are already dual wavelength requirements on this coating, we perform all of the discrimination against the 1.064-μm Nd transition with the output coating. A coating was designed with theoretical parameters of <5% reflectivity at 1.064 μm and 70% reflectivity at 1.074 μm. Diagnostic tests showed that these goals were achieved, and the ability of several devices in the coating run to operate as 1.074-μm lasers confirmed it. Details of the coating technique are given in Ref. 2.

The microchip lasers were longitudinally pumped with the fiber-coupled output of a 12-W diode-laser array. The minimum pump duration required for the passively *Q*-switched lasers to produce an output pulse is 120 μs. The lasers can be operated at repetition rates up to 2 kHz, and produce an output pulse

with a typical pulse energy of 30 μJ and duration of 1.6 ns, in a single longitudinal mode with a linearly polarized, 85-μm-radius, diffraction-limited transverse mode.

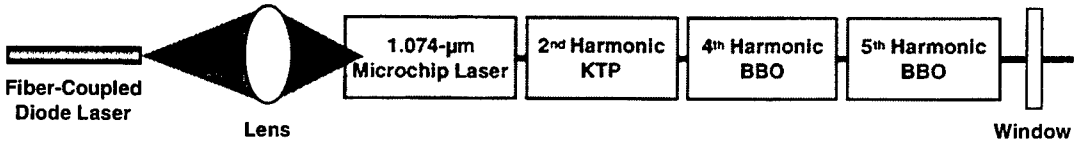

Fig. 1. Schematic of optical head of fifth-harmonic 214.8-nm microchip laser source.

One of the microchip lasers was used to construct the 214.8-nm source. A schematic of the source is shown in Fig. 1. The 1.074-μm output of the microchip laser is frequency converted with a set of antireflection-coated nonlinear crystals. Second-harmonic generation in KTP results in 8 μJ/pulse of 537-nm light, and a second frequency doubling in a 5-mm length of BBO produces 1.2 μJ/pulse of 268-nm light. This is frequency summed with the fundamental (1.074 μm) in a second 5-mm-long piece of BBO. The result is 50 nJ (±20%) of fifth-harmonic light at the desired 214.8-nm wavelength. The entire optical head (fiber-imaging optics, microchip laser, and nonlinear crystals) is packaged in a 1.5-cm-diameter × 8-cm-long stainless steel can, whose only input is the pump-delivery fiber.

3. NO fluorescence observations

Fluorescence observations were made using a 1-cm-diameter, 15-cm-long quartz fluorescence cell with integral Brewster-angle windows and inlet and outlet tubes to allow a flow of gas through the cell. A gas mixture containing 200 ppm_v NO was further diluted with air to make NO mixtures. A highly compact photomultiplier tube (Hamamatsu R5600U-03) was used to detect the fluorescence, with an Oriel 51122 bandpass filter.

3.1 Spectral position

A key to understanding the detection capabilities of devices using this laser is an accurate knowledge of its frequency relative to the NO spectral lines. Our approach was to temperature tune the laser fundamental by changing the pump-laser repetition rate, thus generating excitation spectra with an unknown frequency scale. Because the fractional changes in repetition rate were small (from about 800 to 1200 Hz), the temperature changes were also small and we expected a linear relationship between repetition rate and laser frequency.

The frequency scale was set by comparison of experimental data to the predictions of a model of the spectrum. Three types of parameters had to match: line-frequency separations, line widths, and relative line intensities. Only one set of NO features matched within the spectral range considered, leading to a positive identification of the nominal fifth-harmonic frequency under our operating conditions, 46556 cm^{-1}. The result of this procedure is shown in Fig. 2. Two experimental spectra, shown in dots and dashes, are compared with a model spectrum (solid line). We also made observations of the same two lines at three more pressures, up to 740 Torr. The expected broadening of the lines with increasing pressure was observed, in acceptable agreement with the model.

3.2 Detection sensitivity

A calibration curve generated by diluting the standard NO mixture showed linear behavior in the 0.2–4 ppm_v range. The detection sensitivity determined by these observations was used to set the concentration scale in Fig. 3, which gives an example of the detection sensitivity observed with the current system. On the left is the photomultiplier signal due to scattered light only; on the right is the signal after NO has been added to the flow through the cell. The boxcar averaging was set to give a 1-s time constant. Under these conditions, the standard deviation in fluorescence signal corresponds to an NO concentration of 15 ppb_v.

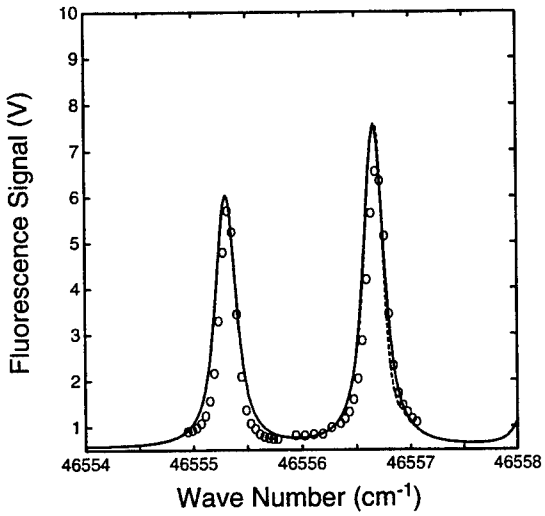

Fig. 2. Observed NO fluorescence excitation spectrum at 122 Torr (dots, discrete tuning; dashes, continuous tuning) and model prediction.

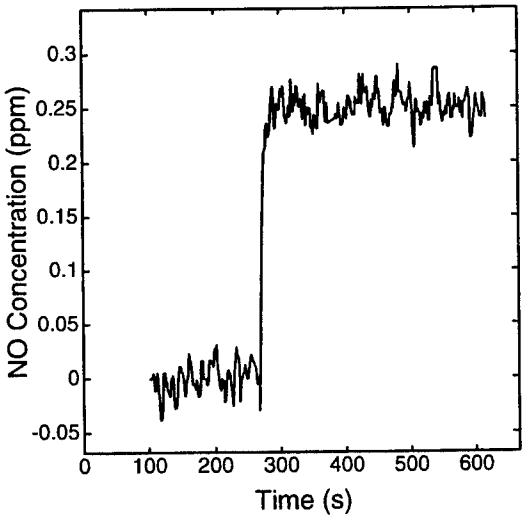

Fig. 3. Fluorescence intensity trace as NO concentration changed from 0 to 0.247 ppm_v.

4. Conclusions

The system we studied lies between two limiting types of interesting systems. Higher sensitivity is possible using multiple passes of the excitation beam, averaging for much longer times than the 1 s used in our data acquisition, and other modifications which might add to system size, weight, and expense. On the other hand, we expect the compact size of the current laser will lead to applications in which the detection system is reduced in size from the layout we studied, and the major advantages are not high sensitivity but small size and rugged construction.

This work was supported by the U. S. Army Research Office under contract DAAG55-97-C-001. The Lincoln Laboratory portion of this work was performed under a Cooperative Research and Development Agreement with Aerodyne Research.

1. J. J. Zayhowski, "Passively *Q*-switched microchip lasers and applications," Rev. Laser Eng. **26**, 841–846 (1998).

2. C. C. Cook and J. J. Zayhowski, "High-accuracy, high-stability optical discriminator coatings for passively *Q*-switched 1.074-μm Nd:YAG/Cr^{4+}:YAG microchip lasers," Thin Solid Films, to be published.

Laser Applications to Chemical and Environmental Analysis

Ringdown and Polarization Spectroscopy

Friday, February 11, 2000

Robert W. Shaw, Oak Ridge Natl. Lab., USA
Presider

FD
3:50pm–5:10pm
Anasazi North

Cavity ring-down spectroscopy with a continuous wave laser and analysis of the uncertainty in concentration measurement

Jae Won Hahn and Jae Wan Kim
Optical High Temperature Measurement Group, Korea Research Institute of Standards and Science
P.O. Box 102, Yusong, Taejon 305-600, Korea
Phone: 82-42-868-5221, Fax: 82-42-868-5118, E-mail: jwhahn@kriss.re.kr

Abstract: We demonstrate a new design of a cavity ringdown spectrometer with a continuous wave (cw) laser. Coupling efficiency of the cw CRDS system and uncertainties in the concentration measurements are analyzed.

OCIS codes: (300.6360) laser spectroscopy; (120.0120) instrumentation, measurement, and metrology; cavity ringdown spectroscopy

1. Introduction

CRDS is now being widely used for studying chemical kinetics and absorption bands of molecules and for measuring the concentration of minor species in flames, etc[1,2]. It is also considered one of the most promising techniques for detecting the absolute concentrations of trace species for measurement standards. After O'Keefe and Deacon demonstrated CRDS with a pulsed laser source[3], most CRDS experiments performed used pulsed lasers because the pulsed laser is a convenient source of high-intensity photon bursts, even though the energy coupling efficiency is small.

Recently CRDS with a continuous-wave (cw) laser was successfully demonstrated by several authors[4-6]. In 1997 Romanini *et al.* produced photon decay signals with an acousto-optic modulator interrupting the cw laser beam introduced into the cavity. Paldus *et al.* also performed cw CRDS by locking a high-finesse resonator to a cw laser source. Using the cavity-locking technique, they could greatly improve the system performance by reducing the shot-to-shot fluctuation in the photon decay signal. A single-mode cw laser has a narrow linewidth of ~ 1 MHz, and a cavity used for the CRDS experiment has a narrow bandwidth because of its high finesse ~ larger than 10^4. Hence locking the cavity mode directly to the narrow laser linewidth is extremely difficult, because a small thermal drift of the cavity length or a tiny mechanical vibration can cause the cavity mirror to go off resonance.

In the present work, we demonstrate a new simple CRDS setup that yields photon decay signals by using only a PZT instead of an acousto-optic modulator as an optical switch. For efficient operation of the cw CRDS spectrometer, we numerically calculate the coupling efficiency of a cw CRDS system. We also analyzed the uncertainties in the concentration measurement of the cw CRDS technique.

2. Basci principle of a cw CRDS spectrometer

To realize CRDS technique with a cw laser source, we need to accumulate high-intensity photon flux in the cavity and then quickly switch off the cw laser source to obtain a photon decay signal. Here we pay attention to the two well-known intrinsic properties of a Fabry-Perot cavity. One is trapping of photons in the cavity, and the other is fast switching of a cw laser beam. To understand the basic concept of trapping a burst of photons in the cavity, let us assume that the light source is purely monochromatic and that the energy loss by absorption and scattering upon the cavity-mirror surface is negligibly small. When a Fabry-Perot cavity stays on resonance at the wavelength of the light source for a time comparable with the cavity ring-down time, the photon intensity coupled into the cavity increases by a factor equal to the finesse of the cavity, then almost the same intensity of the light as was incident upon the cavity emerges from the cavity. When the cavity stays off resonance, however, only a small fraction of the cw light will be transmitted through the cavity; the transmittance of the cavity is given by multiplication of the transmisivities of the two mirrors that constitute the Fabry-Perot cavity. This means that, if we quickly scan the cavity from on an resonance position to an off-resonance position, we can rapidly switch off the cw laser source coupling into the cavity. Therefore, by using only these two intrinsic properties of the Fabry-Perot cavity, we can not only accumulate abundant photons from a cw laser in the cavity, but also quickly switch off the cw laser without any additional optical switching device, such as an acousto-optic modulator or an optical Q-switch.

The apparatus for the experiment is shown schematically in Fig. 1. (a) and the electronic circuit for driving the PZT is shown in Fig. 1 (b). We modulated the cavity length with a PZT that had an inherent capacitance of ~ 3.5 nF.

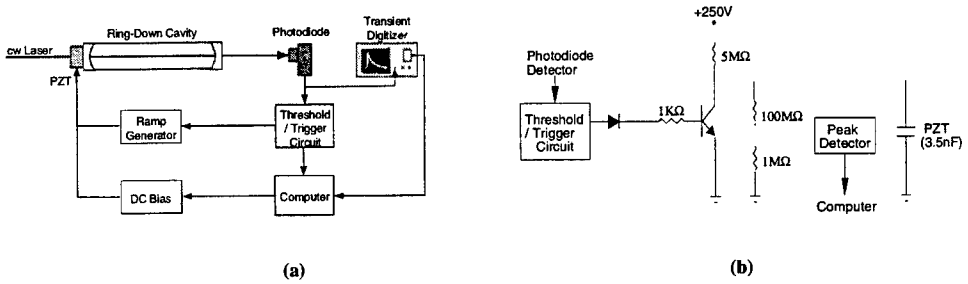

Fig.1. Schematic diagram of cw-CRDS system and the PZT driving circuit.

A high voltage of ~ 250 V was applied to the PZT through a 5 MW resistor. As the applied voltage at PZT increases with a time constant of 17.5 ms, one of the cavity modes can be coincident with the wavelength of the cw laser. We slowly increased the voltage applied to the PZT to sweep the cavity slowly. When the photon intensity coming through the cavity reached a threshold intensity, we triggered only a transistor to decrease the voltage applied to the PZT. The cavity length changed by a quarter wavelength in 1 ms, causing the cavity mirror to move off resonance within a few nanoseconds after the trigger; then it stayed at off resonance until most of the photons in the cavity decayed out. In addition to producing the photon decay signal, the PZT could simultaneously compensate for the thermal drift of the cavity and track the cavity length according to laser frequency tuning. To maintain the photon decay signal at the same position during the cavity sweeping, we add a dc bias voltage to the voltage applied for scanning the cavity.

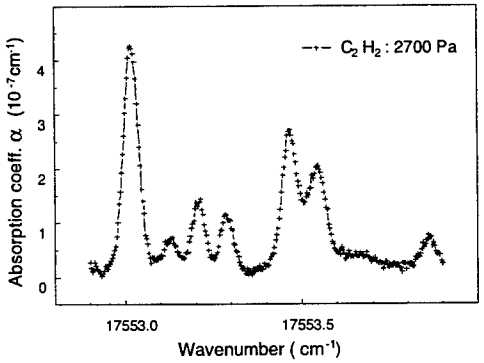

Fig. 2. CRDS spectrum of a weak overtone of acetylene.

We made a performance test of the CRDS spectrometer by recording a spectrum of the overtone transition of acetylene near 570 nm. The measured spectrum is plotted in Fig. 2. The ringdown cavity was filled with acetylene at a pressure of 2700 Pa, and the scanning rate of the cavity was 100 Hz. The detection sensitivity that corresponds to the noise-equivalent absorption is found to be ~ 3 x 10^{-9}/cm.

3. Numerical calculation of coupling efficiency of the cw CRDS system

For a change in cavity length accomplished by moving one mirror, some theoretical analyses were performed by several authors. Here we give only a brief description of the analytical equation that was extended it to include the laser linewidth effect. Considering a Fabry-Perot cavity with two mirrors that have identical electric field reflectivity and transmissivity, let us assume a Lorentzian line shape of the excitation laser. We also assume that the cavity is on resonance with the incident field at time t=0 and the cavity round trip time t_r(=$2L_o/c$, where L_o and c are cavity length and velocity of light, respectively) is much smaller than the cavity decay time τ_d(=$L_o/(-c\ln R)$) . Time t is described in units of the cavity round-trip time: $t=t_r l$ (l is integer). Then, we obtain the intensity of the ringdown signal: [6]

$$I_{out}(t)=\frac{1}{\pi}\int_0^{\infty}T^2R^{2[l+\delta(\omega)]}\left|\sum_{n=-[l+\delta(\omega)]}^{\infty}R^n\exp[-i\omega t_r(\frac{\nu}{c})n^2]\right|^2\frac{I_0\Delta\omega d\omega}{(\omega-\omega_0)^2+(\Delta\omega/2)^2} \quad (1)$$

where ω_o is the line center frequency, and $\Delta\omega$ is the FWHM of the Lorentzian lineshape. For the summation and multiplication of R, we take the integer value of $\delta(\omega)$(=$-(c/2\pi)(\omega-\omega_o)/\omega_o$). R and T are the intensity reflectivity and transmissivity, respectively.

We have defined the coupling efficiency of the cw CRDS system as the ratio of the peak power of the photon decay signal to that of the incident cw laser, which is the peak transmissivity of a cw laser through the cavity. By changing the linewidth of the cw laser, the cavity length, and the reflectivity of the mirror, we calculated the coupling efficiencies with Eq. (1). The coupling efficiencies calculated as a function of the linewidth of the cw laser are plotted in Fig. 3. For the calculation, the reflectivity of the mirror and the cavity length were 99.99% and 30 cm,

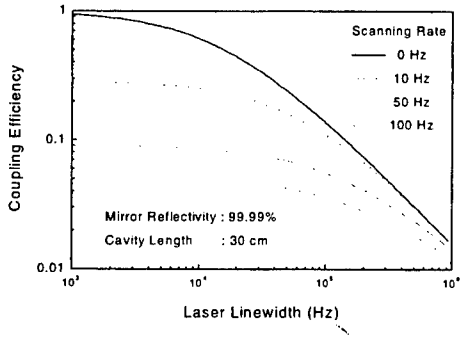

Fig. 3. Coupling efficiency calculated as a function of laser linewidth for various scanning rates.

respectively. The scanning rate of 1 Hz denotes the cavity scanning of one FSR per second. The curve calculated for the scanning rate of 0 Hz illustrates the ratio of integration of multiplication of the transmission function of the cavity and the spectral line-shape function of the cw laser in the frequency domain to the area of the spectral line-shape function.

It is found that, for a fixed FWHM of the transmission peak of the cavity, the coupling efficiencies are correlated with two factors, the spectral density of the laser in unit frequency and the overlap time of the laser linewidth and the transmission peak during the cavity scan. If the laser linewidth increases, the spectral density decreases, leading to decreased coupling efficiency, but the overlap time increases, leading to higher coupling efficiency. Therefore, for efficient operation of a cw CRDS setup, we need to choose the scanning rate properly by taking account of the linewidth of the cw laser and the FWHM of the transmission peak of the cavity. In this manner we can easily expect that the coupling efficiency will be inversely proportional to the cavity length because the FWHM of a transmission peak decreases with an increase in the cavity length.

4. Analysis of the uncertainties in concentration measurement

Using the capability of CRDS technique detecting extremely small change of absorption in the cavity, we can determine the absolute concentration of minor species. From the absorption change, the number density of the molecule under test is given by

$$n = \alpha(\nu,T)/\{S(T)g(\nu)\} \qquad (2)$$

where $\alpha(\nu,T)$ is the absorption change, T is temperature, ν is frequency, $g(\nu)$ is the spectral line shape function, and $S(T)$ is the strength of the line. Assuming the spectral line shape function $g(\nu)$ being Gaussian, we can analytically derive the uncertainties due to several error sources that are listed in Table 1. In the table, E is the ground state energy, k is Boltzmann constant, ν_D is the spectral width, τ is ringdown time, and N is number of data points taken for the spectral line measurement. By controlling temperature within a few tens of mK and increasing number of data points up to 100 or more, we can easily reduce the uncertainties due to the several error sources except the strength of the spectral line to be less than 10^{-4}. The uncertainty caused by the error of the spectral line strength is directly proportional to the magnitude of the error, however.

Table 1. Uncertainty of the cw CRDS

Error sources	Uncertainty
Temperature	$\frac{E/k-2T}{T}\frac{\Delta T}{T}$
Strength of spectral line	$\frac{\Delta S}{S}$
Laser frequency	$\frac{\Delta\nu}{\nu_D}\frac{1}{\sqrt{N}}$
Decay time	$1.56\frac{\Delta\tau}{\tau}\frac{1}{\sqrt{N}}$

5. Conclusion

We have demonstrated a new, simple method for detecting the photon decay in a Fabry-Perot cavity coupled with a cw laser source, and we found that a simple CRDS spectrometer design that uses a PZT instead of an acousto-optic modulator can produce good cavity ringdown signals. The coupling efficiency of a cw CRDS system has been analyzed with a numerical calculation of the peak CRDS signals. We also found that the most dominant error source affecting the uncertainty in the concentration measurement is the error in the strength of the spectral line.

References

[1] P. Zalicki, et al., "Methyl radical measurement by cavity ring-down spectroscopy," Chem. Phys. Lett. **234**, 269-274 (1995).
[2] R. T. Jongma, et al. ,"Trace gas detection with cavity ring-down spectroscopy," Rev. Sci. Instrum. **66**, 2821-2827 (1995).
[3] A. O'Keefe and D.A.G. Deacon, "Cavity ring-down optical spectrometer for absorption measurements using pulsed laser sources," Rev. Sci. Instrum. **59**, 2544-2551 (1988)
[4] D. Romanini, et al., "CW cavity ring-down spectroscopy," Chem. Phys. Lett. **264**, 316-322 (1997).
[5] B.A. Paldus, et al., "Cavity-locked ring-down spectroscpoy," J. Appl. Phys. **83**, 3991-3997 (1998).
[6] J.W. Hahn, et al., "Cavity ring-down spectroscopy with a continuous wave laser: calculation of coupling efficiency and a new spectrometer design," Appl. Opt. **38**, 1859-1866 (1999).

CW INTEGRATED CAVITY OUTPUT SPECTROSCOPY

***Anthony O'Keefe**, James J. Scherer, Joshua B. Paul,and Hong Jiao, Los Gatos Research*
67 East Evelyn Ave., Suite 3,Mountain View, CA, USA 94041
(650) 965-7772 FAX: (650) 965-7074
e-mail: aoklgr@ix.netcom.com
WWW.LGR-HOME.COM

Abstract

An approach is described that enables continuous, narrow band laser sources to be used in conjunction with the recently developed integrated cavity output spectroscopy (ICOS) technique to obtain sensitive, quantitative absorption spectra.

Summary

Recently, the integrated cavity output spectroscopic technique (ICOS) was introduced and demonstrated using pulsed dye laser sources [1] and cw diode laser sources [2]. In the ICOS approach, light is coupled into a highly reflective optical cavity, and the cavity output is measured in order to extract intracavity losses such as molecular or atomic absorption. This work demonstrated that very weak absorptions of less than 10^{-6} per cavity length could easily be quantitatively measured using a pulsed dye laser

In this paper we discuss cw-ICOS, which enables absorption spectra to be obtained using continuous sources such as diode lasers. This cw version of the ICOS method employs two strategies to effectively eliminate the problems traditionally associated with the frequency selectivity or sharp resonances of the optical cavity. Under coherent excitation, cw pumped optical cavities exhibit high-energy buildup when the cavity mode coincides with the excitation wavelength, resulting in near-unity "transmission" when on-resonance and near zero transmission when off-resonance. The resulting contrast of the cavity is a function of the cavity stability as well as the degree of mode matching achieved between the laser and the cavity. Small fluctuations in the cavity can result in large deviations in transmitted energy, making traditional absorption measurements impossible. A high finesse optical cavity also acts as an efficient spectral filter to narrow band light passed through it, which can result in strong variations in transmitted energy with source frequency.

In cw-ICOS, both of these potential problems are eliminated by effectively randomizing the cavity mode structure on a time scale significantly faster than the frequency-scanning rate of the injection light source. This is achieved by dithering both the frequency space of the optical cavity as well as that of the input light source. The modulation of the source laser frequency eliminates transmission fringes with variation in wavelength. In the present study, we demonstrate that the ICOS method of integrating the total cavity output can be employed to obtain accurate, linear absorption spectra. Here absorption spectra are obtained for trace levels of water vapor in the 1.3 micron region using a frequency scanned, narrow bandwidth diode laser source. These studies establish the feasibility of the concepts employed in cw-ICOS, and demonstrate the utility, generality, and simplicity of the technique.

The cw ICOS experimental apparatus is simple employing only a computer A/D card to record the data and an oscilloscope that was

used for diagnostic purposes only. Absorption measurements were made using a two different pairs of mirrors to form the optical cavity (R=99.94% and 99.995%@1.3 μm) employing a single mode, tunable diode laser (New Focus model 6224) as the injection light source. The system was tuned continuously between 7630 cm^{-1}, and 7410 cm^{-1}, and around 7402 cm^{-1}. Absorption measurements were made in air for several cavity sizes and in a closed cell that could be evacuated and filled with controlled pressures of various gases.

RESULTS

Spectra of rovibrational overtone-combination bands of water vapor and carbon dioxide were measured, and were used to characterize the performance of the cw-ICOS technique. These measurements were not normalized to variations in the diode laser output. The diode laser exhibited an output power modulation of 1-5% when scanned over spectral regions of greater than several wavenumbers. While this effect could be easily normalized out for wide spectral scans, no attempt was made to do this in the present study since most absorption strength measurements were made on selected lines in regions where the laser output was stable to at least 1 % here. In the spectral region between 1.30 and 1.35 micron wavelength, absorptions resulting from H_2O and CO_2 were recorded and compared to known absorption strengths calculated using the Air Force HITRAN database [3]. Absorption measurements for single lines were obtained in spectral regions free of laser mode hops, although in some of the wide spectral range data taken of CO_2 some mode hopping is evident

Absorption due to nascent water vapor in the laboratory air were used in some tests, however the rapidly increasing strength of the absorption for probe wavelengths above 1.35 microns effectively turned the ICOS cell black. Weaker water absorption features near 1.346 microns were used to demonstrate the sensitivity and ease of use of the cw-ICOS technique. A typical 30-cm cavity cw-ICOS absorption spectrum due to atmospheric water is shown in Figure 1, where several absorption features near 7526 cm^{-1} are seen. This spectrum was recorded using the pico-motor scan mode of the New Focus laser. In Figure 1 the absorption spectra predicted using the HITRAN database are shown for a 290 meter pathlength of atmospheric broadened water vapor at a relative pressure of 8.75 Torr (50% humidity at 22 degrees Centigrade). The predicted spectra compare well with the observed spectra in both line width and absorption strength.

A section of the CO_2 absorption overtone band near 7580 cm^{-1} is shown in Figure 2, which also shows an overlay trace of the HITRAN predicted absorption spectrum for a 400 meter path length of 1 atmosphere of CO_2. The excellent agreement between the predicted and observed spectrum demonstrates that the "impulsive" ICOS model as well as the traditional Fabry-Perot model (to be discussed) describes the same process. The same process underlies the approach recently demonstrated by Engeln, et al. [4] referred to as Cavity Enhanced Absorption (CEA), which is simply another experimental manifestation of the Fabry-Perot absorption process and differs from ICOS only in the experimental detail employed.

References:

1) O'Keefe, A., Chem. Phys. Lett., 293, (1998) 331
2)O'Keefe, A., Scherer, J.J. Scherer, and J. B. Paul, Chem. Phys. Lett., 307, (1999) 343
7) HITRAN 1996 database, U.S. Airforce
8) Engeln, R., Berden, G., Peeters, R., and Meijer, G., Rev. Sci. Instrum., 69, (1998) 3763

This work supported by US Army Strategic Defense Command under contract #DASG60-97-C-0089 and the US Navy Office of Naval Research under contract #N00014-98-C-0347

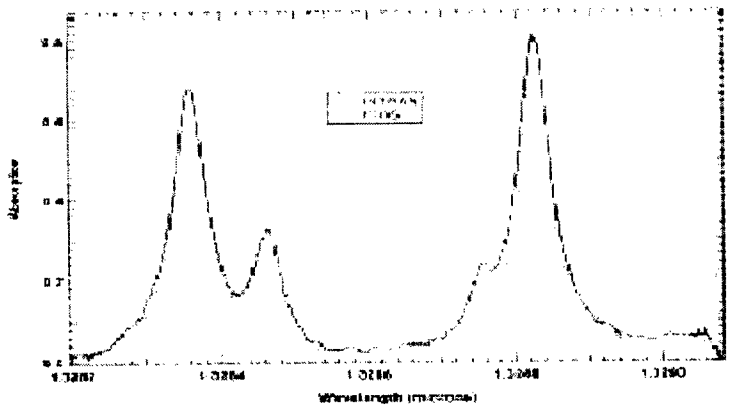

Figure 1. 5 GHz wide scan of three water absorption lines near 7529 cm-1 taken using the cw-ICOS approach. The Y-axis represents fractional transmission through the 30 cm long cavity. The dashed line represents the HITRAN predicted transmission spectrum for a 290 meter long path of air at 50% humidity at 20 degrees Centigrade, at a total pressure of 1 atm.

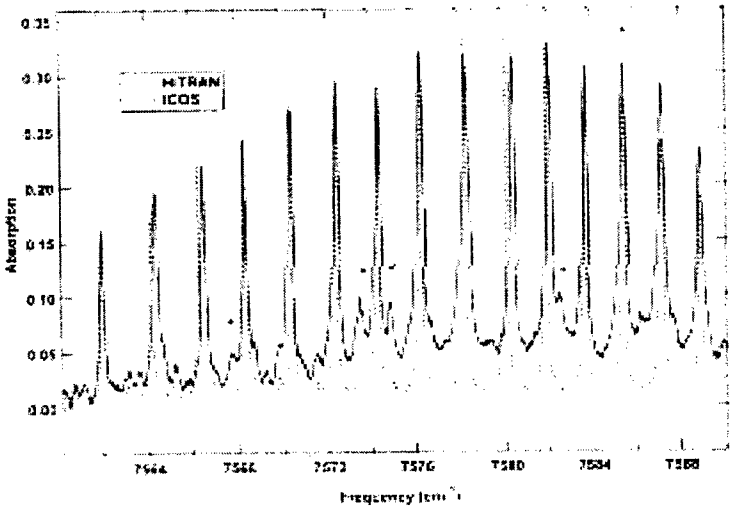

Figure 2. cw-ICOS absorption spectra of CO2 taken around 7580 cm-1. A HITRAN simulated spectrum is overlaid as a dashed line for comparison. The simulated spectrum assumes a 400 m path.

Broadband Ringdown Spectral Photography for Real-Time Monitoring

J. J. Scherer, J. B. Paul, H. Jiao, and A. O'Keefe, *Los Gatos Research*

Over the last decade there has been a significant increase in the implementation of cavity ringdown-based methods for spectroscopic studies in the gas phase[1]. Although these methods have demonstrated high sensitivity in numerous applications and spectral regions, real-time applications of the approach have been hindered by the need to tune the probe laser over the absorption lineshape while the ringdown time is obtained. The resultant pointwise determination of the frequency dependent intracavity loss leads to monitoring times ranging from seconds to minutes, depending on the spectral coverage required. In many cases, large optical bandwidths need be covered in order to differential between absolute absorption intensities for the target species vs. other intracavity losses. In real-world environments, large bandwidths must frequently be measured in order to identify spectral interferences from non-target species, broadband absorption due to soot, or scattering due to particulates. As real-time environmental monitoring requires the need to deal effectively with transient conditions, tuned-frequency approaches can be inadequate.

To address the real-time deficiency of tuned frequency ringdown methods, we have developed a technique, ringdown spectral photography (RSP)[2], which enables ringdown-derived absorption intensities to be determined at high resolution over a large optical bandwidth on the timescale of a single ringdown event (typically microseconds). The RSP technique obtains high resolution cavity ringdown absorption spectrum over a broad spectral region by injecting a single pulse of broadband light into the cavity, and resolving the frequency dependent decay times with an extracavity dispersion assembly and array detector. The RSP method achieves this real-time capability by combining two key concepts in a simultaneous fashion. The first concept involves using a linear detector array (or 1 dimension of a 2-d array) in conjunction with a rapidly rotating mirror to record the decaying cavity signal in a "streak camera" fashion. In this case, the time domain is translated into the spatial domain of the array, effectively using the array as a transient recorder. The second concept employed involves dispersing the cavity output in wavelength with a diffraction grating along an axis orthogonal to the "streak camera" axis. The RSP apparatus combines both of these concepts simultaneously to record the decay times and frequencies on a single two-dimensional detector array. In this fashion, the time and frequency response of the cavity is recorded in a single shot fashion on the timescale of a single ringdown event.

A simplified schematic of the UV-vis RSP instrument is shown in Fig. 1. A pulse of broadband light (produced in a Nd:YAG-pumped broadband dye laser system) is optically coupled into a two-mirror cavity. The light exiting the cavity is deflected off of a rotating mirror and swept across a diffraction grating. The diffracted orders are subsequently imaged into an array detector such that the "frequency" and "time" axes are orthogonal. The

decaying intracavity light intensity (photon lifetime) is thus recorded as a function of wavelength. The resultant "spectral photograph" obtained is analyzed in a manner similar to that used in conventional cavity ringdown methods to yield absolute absorption intensities as a function of frequency. As

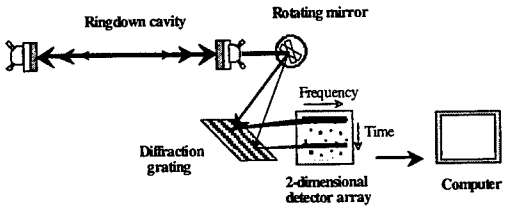

Fig. 1. RSP concept: A single ringdown event is dispersed time with a rotating mirror and in wavelength with a diffraction grating. The wavelength resolved decay times are determined by analyzing the resultant 3-D (frequency vs. time vs. intensity) RSP "photograph".

the number of frequency elements is limited ultimately by the array detector, the RSP approach enables hundreds to thousands of frequency elements to be recorded in a simultaneous fashion. Inherent to all ringdown based methods, a desirable feature of the RSP approach is that it is not effected by large variations in the intensity of a given bandwidth element. Thus, RSP presents a new opportunity for pulsed, broadband light sources that are currently not adequate for sensitive, high-resolution spectroscopic applications.

An RSP spectrum of molecular oxygen is shown in Fig. 2, as obtained with a broadband dye laser operating on a mixture of LDS 698 and methanol. These data display the 690-nm b-X (1,0) rovibronic system, with the doublet structure resolved with an instrumental resolution of approximately 1 cm^{-1}. These data were obtained with a single pulse of broadband light with a total energy of only 100 microjoules over the bandwidth shown. The camera used for the data of Fig. 2 was a ½"-format, uncooled CCD (Pulnix TM7AS), indicating that significant reductions in the input light energy levels can be realized with a more sensitive camera. Similar spectra obtained on propane with both RSP and conventional scanned frequency cavity ringdown have demonstrated the ability to routinely obtain "ringdown-level" absorption sensitivities (10^{-6} absorbance per pass or better) with the RSP method. With presently available cavity ringdown mirrors, light sources, and detectors, the RSP method can be further developed for spectral regions ranging from 200 nm to 8.5 microns and beyond.

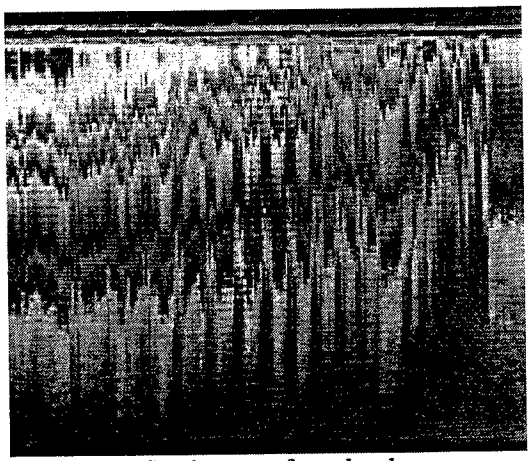

Fig. 2. RSP image of molecular oxygen, obtained in the 690 nm region using a single pulse of broadband light. Here, individual rovibronic transitions are resolved with an instrumental resolution of 1 cm^{-1}.

References

[1] J.J. Scherer, J.B. Paul, A. O'Keefe and R.J. Saykally *Chemical Reviews,* **97**, 25 (1997) and references therein

[2] J. J. Scherer *Chem. Phys. Lett.,* **292**, 143 (1998)

Saturated polarization spectroscopy with a picosecond laser for quantitative concentration measurements

Thomas A. Reichardt
(tareich@sandia.gov)
Ph: 925-294-4776

Roger L. Farrow
(farrow@ca.sandia.gov)
Ph: 925-294-3259

Fabio Di Teodoro
(fditeod@california.sandia.gov)
Ph: 925-294-4816

Combustion Research Facility, Sandia National Laboratories, P.O. Box 969, Livermore, CA 94551-0969, Fax: 925-294-2276

Robert P. Lucht
(RLucht@mengr.tamu.edu)
Ph: 409-862-2623
Department of Mechanical Engineering, Texas A&M University, College Station, TX 77843-3123, Fax: 409-862-2418

Abstract: The collisional dependence of saturated polarization spectroscopy with a picosecond laser is investigated by probing hydroxyl in a flow cell.

OCIS Codes: (120.1740) Combustion diagnostics; (300.6420) Spectroscopy, nonlinear

While nanosecond lasers have been used often for nonlinear diagnostic measurements of flame composition, picosecond lasers provide a potentially superior source for such techniques. Compared to a nanosecond laser, picosecond lasers produce significantly greater peak power for the same pulse energy, and this could improve the signal strength of multi-photon techniques such as degenerate four-wave mixing (DFWM) and polarization spectroscopy (PS). The spectral bandwidth of a transform-limited, 50-150 ps pulsewidth laser [1] is sufficiently narrow to couple effectively with the molecules, and thus such lasers have been successfully used for laser-induced fluorescence (LIF) concentration measurements [2,3]. Such pulse widths are on the order of the characteristic collisional time in an atmospheric combustion environment. It has been suggested that the signal produced by such lasers would be less dependent on the collisional environment because the behavior of the molecular system probed by short-pulse lasers is governed more by the spectral width of the laser and the Doppler effect [4]. To investigate the collisional dependence of the polarization spectroscopy signal generated with a picosecond laser, we probe the $A^2\Sigma^+$-$X^2\Pi$ (0,0) band of OH in a flow cell. In this well-controlled environment, we monitor the change in signal strength as we vary the buffer gas pressure by a factor of 50.

In PS two beams, a high-power pump and a low-power probe, are crossed at the measurement location. The probe beam is passed through two orthogonally oriented linear polarizers positioned on opposite sides of the measurement location. The pump beam is either circularly polarized or linearly polarized 45° with respect to the polarization of the probe beam. When the pump beam is tuned to a resonance of the interaction medium, it induces a change in both the real and imaginary parts of the refractive index. This causes the polarization of the probe beam to rotate as it passes through the medium, and the PS signal is observed as leakage of the probe beam through the second polarizer.

The experimental setup is pictured in Fig. 1. The laser source is the frequency-doubled output of a distributed feedback dye laser (DFDL) with motorized tuning and active wavelength stabilization. The energy of the doubled output is controlled by a polarizer preceded by a quarter-wave plate (to compensate for the slightly elliptical polarization of the beam) and half-wave plate (to rotate the polarization of the beam). The beam is down-collimated and directed toward an uncoated UV 3° wedge. The front surface reflection from the wedge forms the probe beam while the back surface reflection is sent to two photodiodes (Thorlabs DET 110 and DET 210) to monitor the beam energy. The portion of the beam that passes through the wedge forms the pump beam. The pump and probe beams are sent through separate delay lines. Before passing through the vertically-oriented polarizer, the probe beam is directed through a half-wave plate rotated to maintain the probe beam energy at 0.5% of the pump beam energy. A quarter wave plate is placed in the pump beam path to change the vertically polarized pump beam to a circular polarization.

Hydroxyl (OH) is created by photolysis of hydrogen peroxide (H_2O_2) using the softly focussed 266-nm output of a Continuum PL9020 Nd:YAG laser. Hydrogen peroxide is obtained by flowing 8 standard cm^3 s^{-1} argon through a bubbler containing 95 wt. % aqueous H_2O_2. Further details of the photolysis system are

given by Kliner and Farrow [1]. The 266-nm beam crosses the pump and probe beams inside the cell in front of the LIF detection optics. The crossing angle between the pump and probe beams (both 900 μm in diameter) is 0.6°, resulting in an interaction length of 25 cm. The fluorescence signal is captured by an f/2 lens and focused with another f/2 lens onto the entrance slit of a 0.25-m monochromator (Oriel 77250) with a 1200 groove/mm grating (Oriel 77296). The fluorescence is attenuated with neutral density filters before detection by a photomultipler tube (PMT, Hamamatsu R955).

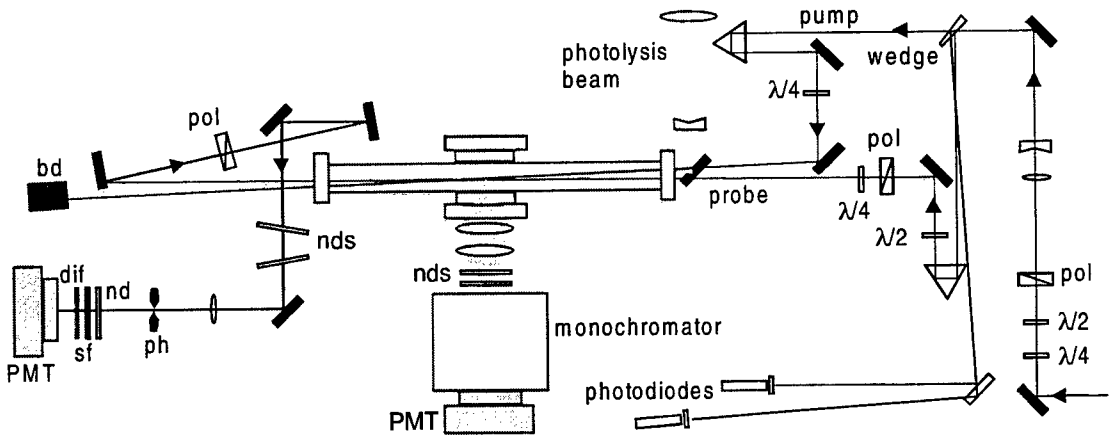

Fig. 1. Schematic diagram of PS experiment. λ/4 – quarter-wave plate, λ/2 – half-wave plate, pol – polarizer, bd – beam dump, nd – neutral density filter, sf – spectral filter, dif – diffuser, PMT – photomultiplier tube.

After exiting the cell, the probe beam is picked off with a mirror, sent through a horizontally-oriented polarizer, attenuated by neutral density filters, and passed through a spatial filter before being detected by another Hamamatsu R955 PMT. A Schott Glass UG-1 filter eliminates ambient light. The rejection ratio of the crossed polarizers is 10^{-7}, but because the windows on the cell are strained by the pressure differential they induce a polarization rotation of the probe beam that would interfere with the PS signal. A quarter-wave plate is placed between the probe beam polarizer and the cell to compensate partially for the birefringence of the cell windows. The resulting rejection ratio is 10^{-6}. The PS and LIF signals, as well as the photodiode output, are amplified and digitized using 12-bit A/D converters. For the results reported in this paper, the laser was tuned to the $P_1(2)$ transition.

Figure 2 displays saturation curves acquired by recording the LIF and PS line-center signal strengths with increasing laser energy. At low laser pulse energies the LIF and PS signals increase with increasing laser energy until the laser radiation significantly populates the upper molecular level of the transition, decreasing the efficiency of the signal generation. The LIF and PS signals experience saturation at a pump beam energy of ~1 μJ, above which the LIF signal becomes nearly independent of laser power. However, the PS signal exhibits a plateau between 1 and 3 μJ pump energy, then increases again until finally rolling over near 10 μJ. We have seen such saturation effects before in theoretical studies of DFWM using short-pulse lasers [4]. Further theoretical studies are underway to analyze these effects for PS, similar to the DFWM analysis but for a multistate molecular system.

Scans of the $P_1(2)$ transition were acquired at different pressures to investigate the collisional dependence of the PS signal. The cell pressure was adjusted with a needle valve on the gas flow output port. The same computer that recorded the digitized signals also incremented and recorded the DFDL wavelength. One hundred laser shots were averaged at each wavelength, and the visible wavelength step size was 7×10^{-4} nm. The PS signals integrated over the spectral line shapes are plotted as a function of cell pressure in Fig. 3. The results are displayed for both an unsaturating pump beam and for a saturating pump beam. The PS signal is proportional to the square of the number density probed, and therefore has been normalized by the square of the OH concentration measured with unsaturated LIF. The LIF signals were corrected for quenching for each cell pressure by measuring the fluorescence decays with a 1-GHz digital oscilloscope (Tektronix TDS 680B). Varying the cell pressure between 10 and 500 torr, we found the unsaturated PS signal decreased by a factor of 15 while the saturated PS signal decreased by only a

factor of 3. This remarkable insensitivity to pressure would correspond to an error of only $\sqrt{3}$, or 70%, in the saturated concentration measurements if the effects of pressure were neglected in data analysis.

The quenching rate and collisional environment in the cell are dependent on the partial pressures of Ar, H_2O, and H_2O_2 in the cell. Because the vapor pressure for 95 wt. % acqueous H_2O_2 is only 1.8 torr, Ar is the major species in the cell for all pressures investigated. The overall collisional width is then expected to vary approximately linearly with cell pressure as 18.5×10^{-5} cm^{-1}/torr given by Shirinzadeh et al. [5]. The quenching rate, on the other hand, is a strong function of the relative concentrations of H_2O and H_2O_2. While Ar is a relatively weak quencher of OH, both H_2O and H_2O_2 are strong quenchers [6,7]. As the cell pressure was increased, the partial pressures of H_2O and H_2O_2 also increased. The quenching rate calculated from the acquired fluorescence decays increased by a factor of 5 from 0.013 ns^{-1} to 0.071 ns^{-1}. The saturated PS signal, which varied by only a factor of 3 over the pressure range, is therefore also quite insensitive to collisional quenching.

In conclusion, saturated PS with a picosecond laser is relatively insensitive to both the overall collisional rate and to collisional quenching. Nonlinear resonance techniques benefit from saturation, because saturating beam intensities both increase the signal intensity and decrease the dependence of the signal on the collisional environment. Saturation is easily achieved with the frequency-doubled DFDL, and the laser pulse energy had to be reduced by 3 orders of magnitude from its peak energy to avoid the effects of saturation even with relatively large beam diameters.

Acknowledgements

This work was supported by the U.S. Department of Energy, Office of Basic Energy Sciences, Chemical Sciences Division.

References

1. D. A. V. Kliner and R. L. Farrow, "Measurements of ground-state OH rotational energy-transfer rates," J. Chem. Phys. **110**, 412-422 (1999).
2. F. Bormann, T. Nielsen, M. Burrows, and P. Andresen, "Single-pulse collision-insensitive picosecond planar laser-induced fluorescence of OH $A^2\Sigma^+$ (v'=2) in atmospheric-pressure flames," Appl. Phys. B **62**, 601-607 (1996).
3. M. W. Renfro, S. D. Pack, G. B. King, and N. M. Laurendeau, "Hydroxyl time-series measurements in laminar and moderately turbulent methane/air diffusion flames," Comb. Flame **115**, 443-445 (1998).
4. T. A. Reichardt and R. P. Lucht, "Degenerate four-wave mixing spectroscopy with short-pulse lasers: theoretical analysis," J. Opt. Soc. Am. B **13**, 2807-2816 (1996).
5. B. Shirinzadeh, D. M. Bakalyar, and C. C. Wang, "Measurement of collision-induced shift and broadening of the ultraviolet transitions of OH," J. Chem. Phys. **82**, 2877-2879 (1985).
6. I. J. Wysong, J. B. Jeffries, and D. R. Crosley, "Quenching of $A^2\Sigma^+$ OH at 300 K by several colliders," J. Chem. Phys. **92**, 5218-5222 (1990).
7. C. B. McKendrick, E. A. Kerr, and J. P. T. Wilkinson, "OH($A^2\Sigma^+ \rightarrow X^2\Pi$) photofragment emission from two-photon photolysis of hydrogen peroxide at 193.3 nm," J. Phys. Chem. **88**, 3930-3932 (1984)

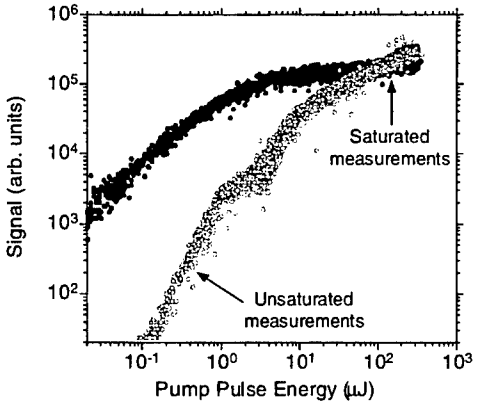

Fig. 2. LIF (closed circles) and PS (open circles) saturation curves of the $P_1(2)$ transition. The cell pressure was 106 torr and the bubbler pressure was 129 torr. Arrows indicate the pump laser energy maintained for the measurements displayed in Fig. 3.

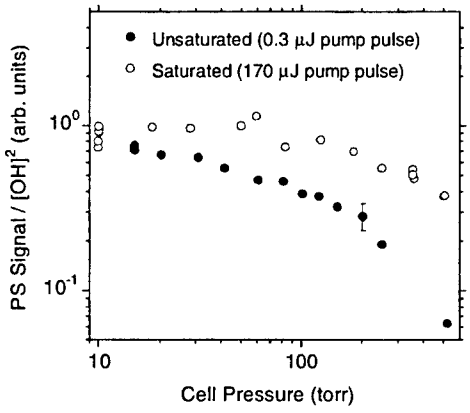

Fig. 3. PS signal (normalized by the square of the OH concentration) as a function of cell pressure. The results are displayed for both an unsaturating pump beam and for a saturating pump beam.

Laser Applications to Chemical and Environmental Analysis

Quantum Cascade Lasers and Applications

Saturday, February 12, 2000

Mark G. Allen, Physical Sciences Inc., USA
Presider

SaA
8:00am–9:40am
Anasazi North

Mid-infrared, single-mode, continuously tunable Quantum Cascade distributed feedback lasers

Claire Gmachl, Federico Capasso, Rüdeger Köhler, Alessandro Tredicucci, Deborah L. Sivco, James N. Baillargeon, Albert L. Hutchinson, and Alfred Y. Cho
Bell Laboratories, Lucent Technologies, 600 Mountain Avenue, Murray Hill, NJ 07974
phone: 908-582-6164, fax: 908-582-7660, email: cg@lucent.com

Abstract – High performance, continuously tunable, single-mode Quantum Cascade distributed feedback lasers at 5 – 10 μm wavelength and operating either in pulsed mode up to room temperature or in continuous wave around liquid nitrogen temperature are reported.
OCIS codes – 140.3070 Infrared and far-infrared lasers; 140.5960 Semiconductor lasers; 140.3600 Lasers, tunable;

Quantum Cascade distributed feedback (QC-DFB) lasers [1, 2] are a rapidly developing new type of semiconductor laser source for the mid-infrared. QC-lasers are based on electronic transitions between quantized conduction band states of a multiple quantum well structure [3, 4]. They are designed through band-structure engineering [5] and grown by molecular beam epitaxy (MBE) [6].

The emission wavelength can be set within the entire mid-infrared (3.5 – 17 μm) by tailoring layer thicknesses in the active region. Furthermore, the cascading scheme, in which electrons are recycled in successive (N = 1 – 75) active regions interleaved with injectors, inherently results in high optical peak power (several 100 mW). These properties, together with the reliability of III-V semiconductor laser materials, make the QC-lasers prime candidates for laser-based, portable and stand-alone environmental monitoring systems.

For gas spectroscopy the lasers have to operate with stable single-mode emission and controlled tunability. This is achieved by fabricating the devices as distributed feedback lasers, where a first-order grating, representing a modulation of the effective refractive index and/or modal gain, selects a single-mode over the usual multiple-mode Fabry-Perot spectrum. QC-DFB lasers at various wavelengths have been reported previously, [1, 2, 7, 8] and they also have been used successfully in various gas sensing applications [9, 10, 11, 12].

Here we present an overview of our latest results on QC-DFB lasers; pulsed lasers operating in the wavelength range of the CO_2 laser ($\lambda \approx 9.5 - 10.5$ μm) and very high power continuous wave (cw) QC-DFB lasers at liquid nitrogen temperature and above at $\lambda \approx 5.2$ μm and $\lambda \approx 7.95$ μm.

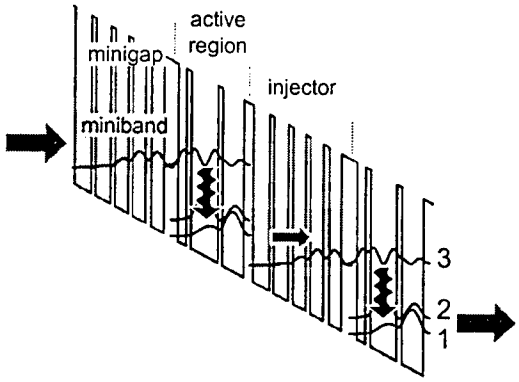

Fig. 1: Two periods of active region and injector of a QC-laser designed with a "three-well-vertical transition" active region at $\lambda \gg 8$ μm. The laser transition is indicated by the wavy dark arrows, the electron flow by the gray arrows. The well and barrier widths in the active region are **3.8**/2.1/**1.2**/6.5/**1.2**/5.3/**2.3** nm (bold font indicates the barriers).

A portion of the conduction band structure is shown in Fig. 1 for sample D2409 emitting at 7.95 μm. The quantum wells are InGaAs, the barriers AlInAs, both grown lattice matched to InP. Typically, 25 – 30 periods of active regions and injectors are employed. Similar active region designs are used also at the other wavelengths [4]. The lasers are processed as conventional deep etched ridge waveguide lasers with stripe widths of ~ 8 – 20 μm. The grating is formed by wet chemical etching either on top of the laser ridge or buried close to the active region by epitaxial regrowth of the top cladding layer on top of the grating.

The lasers are cleaved into bars with a length ~ 2.25 mm and the facets are left uncoated. The laser bars are wire bonded and then mounted epitaxial layer side up in a temperature controlled cold-finger cryostat. For the pulsed (50 ns pulse width, 5 – 100 kHz repetition rate) light output versus current characteristics the light is collected with f/0.8 optics and focused onto a fast room temperature HgCdTe detector. Cw output is collected with non-imaging optics onto a conventional thermopile laser power meter. The

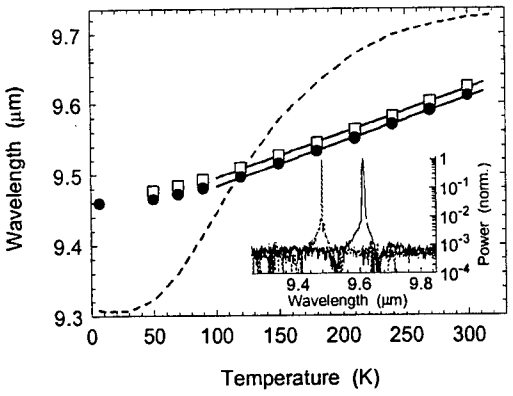

Fig. 2: Single-mode emission wavelength versus heat sink temperature for two QC-DFB lasers operated in pulsed mode (symbols). The lasers differ in ridge width (10 and 11 μm) resulting in the slightly different emission wavelengths. Straight lines are fitted to the data. The dashed line shows the position of the peak gain versus temperature, which was determined from Fabry-Perot-type devices. The insets show the single-mode spectra at 300 K, 5 A (solid) and 90 K, 0.8 A (dashed).

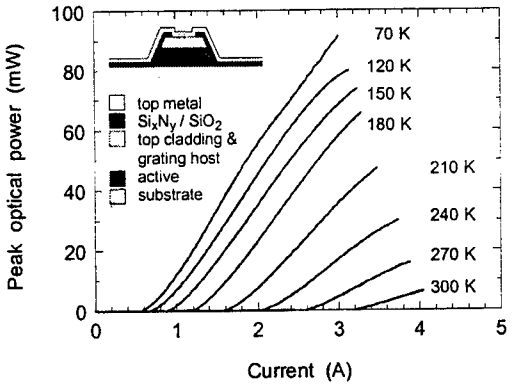

Fig. 3: Peak light output versus current characteristics of a QC-DFB laser operated in pulsed mode (50 ns pulse width, 5 kHz repetition rate) emitting at ~9.5 μm (Fig. 2). Over the entire range shown, the laser emission is single-mode. The inset shows a schematic cross section through the laser ridge. The grating is on top of the ridge, etched into the semiconductor and covered with metal. The latter results in a complex-coupling scheme involving feedback through effective index- and gain-modulation.

spectral characteristics of the devices are measured with a Fourier Transform Infrared (FTIR) Spectrometer.

Fig. 2 shows the single-mode tuning range with heat sink temperature of a pulsed QC-DFB laser emitting around 9.5 μm. The grating period was 1.525 μm. A total continuous single-mode tuning range of 150 nm and an approximately linear tuning coefficient of ~ 0.61 nm/K (above 100 K) was obtained. Fig. 3 shows the pulsed light output versus current characteristics for the laser of Fig. 2. Single-mode peak output power levels of several 10 mW are achieved. Independent of temperature and output power level, a side mode suppression ratio of 30 dB is readily obtained. Similar performance was measured for QC-DFB lasers emitting around 10.2 μm, fabricated with a grating period of 1.6 μm.

If a narrow linewidth of the laser source is important, such as e.g. for very high resolution gas sensing applications, pulsed operation of QC-lasers is not indicated due to the thermal wavelength chirp induced by the current pulse. In this case the lasers are used at liquid nitrogen temperature and above and operated in cw [12]. While the cw current is slowly (~ 10 kHz) raised, the power dissipated in the device is steadily increased, which by rising the temperature tunes the quasi-cw laser output to longer wavelengths [10]. In this way continuous tuning is achieved. Figs. 4 and 5 show such single-mode tuning with current at various heat sink temperatures for two lasers emitting at 5.2 and 7.95 μm wavelength. The inset in Fig. 4 again shows the high mode purity obtained under

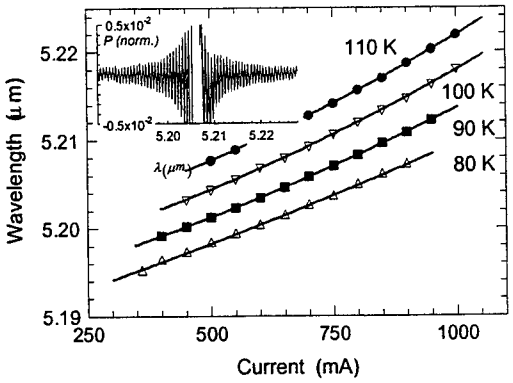

Fig. 4: Single-mode emission wavelength of a QC-DFB laser (D2383) with buried grating versus cw current at various constant heat sink temperatures (symbols). The lines are quadratic functions fitted to the data. The inset shows a close-up of a normalized spectrum (80 K, 850 mA) as measured with a Nicolet Fourier Transform spectrometer. No side-modes are detected.

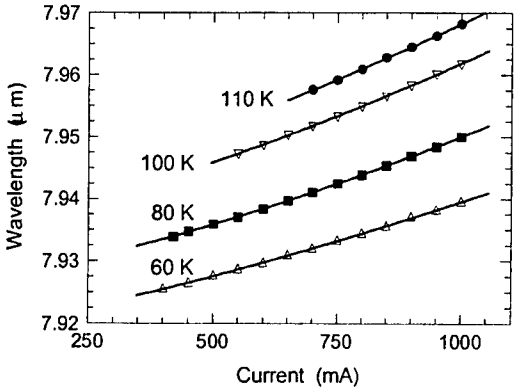

Fig. 5: Single-mode emission wavelength of a QC-DFB laser (D2409) with buried grating versus cw current at various constant heat sink temperatures (symbols). The lines are quadratic functions fitted to the data.

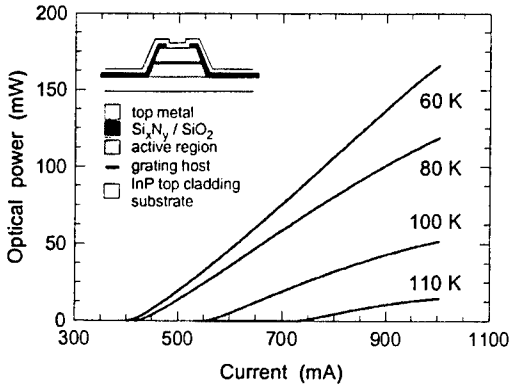

Fig. 6: Cw light output versus current characteristics of a QC-DFB laser operated in pulsed mode (50 ns pulse width, 5 kHz repetition rate) emitting at ~ 7.95 μm (Fig. 5). The inset shows a schematic cross section through the laser ridge.

single-mode emission.

By advantageously engineering the gain spectrum with respect to the Bragg resonance of the grating very high single-mode output power in excess of 100 mW at 80 K can be achieved for these lasers. Fig. 6 gives an example for a 7.95 μm QC-DFB laser.

This material is based upon work supported in part by DARPA/US Army Research Office under Contract No. DAAG55-98-C-0050. R. K. acknowledges support by Studienstiftung des Deutschen Volkes, Germany.

References:

1 J. Faist, C. Gmachl, F. Capasso, C. Sirtori, D. L. Sivco, J. N. Baillargeon, A. L. Hutchinson, and A. Y. Cho, "Distributed feedback quantum cascade lasers", *Appl. Phys. Lett.* **70**, 2670 – 2672, 1997.

2 C. Gmachl, J. Faist, J. N. Baillargeon, F. Capasso, C. Sirtori, D. L. Sivco, S. N. G. Chu, and A. Y. Cho, "Complex-Coupled Quantum Cascade Distributed-Feedback Laser", *IEEE Photon. Technol. Lett.* **9**, 1090 – 1092, 1997.

3 F. Capasso, C. Gmachl, D. L. Sivco, and A. Y. Cho, "Quantum cascade lasers" *Physics World* ***12,*** 27 – 33, June 1999.

4 F. Capasso, C. Gmachl, A. Tredicucci, D. L. Sivco, A. L. Hutchinson, and A. Y. Cho, "Quantum cascade lasers", *Optics and Photonics News, in press*, October 1999.

5 F. Capasso, "Band-Gap Engineering: From Physics and Materials to New Semiconductor Devices", *Science*, **235**, 172 – 176, 1987.

6 A. Y. Cho ed., *Molecular Beam Epitaxy*, Woodbury, NY: AIP Press, 1994.

7 D. Hofstetter, J. Faist, M. Beck, A. Müller, and U. Oesterle, "Demonstration of high-performance 10.16 μm quantum cascade distributed feedback lasers without epitaxial regrowth", *Appl. Phys. Lett.* **75**, 665 – 667, 1999.

8 W. Schrenk, N. Finger, S. Gianordoli, L. Hvozdara, G. Strasser, and E. Gornik, "GaAs/AlGaAs distributed feedback quantum cascade lasers", *submitted to Appl. Phys. Lett.*, 1999.

9 K. Namjou, S. Cai, and E. A. Whittaker, J. Faist, C. Gmachl, F. Capasso, D. L. Sivco, and A. Y. Cho, "Sensitive absorption spectroscopy with a room-temperature distributed-feedback quantum-cascade laser", *Opt. Lett.* **23**, 219 – 221, 1998.

10 S. W. Sharpe, J. F. Kelly, J. S. Hartman, C. Gmachl, F. Capasso, D. L. Sivco, J. N. Baillargeon, and A. Y. Cho, "High-resolution (Doppler-limited) spectroscopy using quantum-cascade distributed feedback lasers", *Opt. Lett.* **23**, 1396 – 1398, 1998.

11 B. A. Paldus, T. G. Spence, R. N. Zare; J. Oomens, F. M. J. Harren, D. H. Parker; C. Gmachl, F. Capasso, D. L. Sivco, J. N. Baillargeon, A. L. Hutchinson, and A. Y. Cho, "Photoacoustic spectroscopy using quantum-cascade lasers", *Opt. Lett.* **24**, 178 – 180, 1999.

12 R. M. Williams, J. F. Kelly, J. S. Hartman, S. W. Sharpe, M. S. Taubman, J. L. Hall, F. Capasso, C. Gmachl, D. L. Sivco, J. N. Baillargeon, and A. Y. Cho, "Kilo-Hertz Linewidth from Frequency Stabilized Mid-Infrared Quantum Cascade Lasers", *Opt. Lett., in press* 1999.

Trace gas detection in ambient air using a 7.9 micron QC-DFB laser

A.A. Kosterev, R.F. Curl and F.K. Tittel
Rice Quantum Institute, Rice University, Houston, TX 77251-1892
akoster@rice.edu

C. Gmachl, F. Capasso, D.L. Sivco, J.N. Baillargeon, A. L. Hutchinson, and A.Y. Cho
Bell Laboratories, Lucent Technologies, 600 Mountain Avenue, Murray Hill, NJ 07974

Abstract: Spectroscopic trace gas detection in the 7.9 μm spectral region with a single frequency quantum cascade distributed feedback (QC-DFB) laser was demonstrated. A 100-m multipass cell and a "zero-air" background subtraction technique were used to enhance the detection sensitivity.

OCIS Codes: (140.5960) Semiconductor lasers; (300.6340) Spectroscopy, infrared; (010.1280) Atmospheric composition

1. Introduction

Infrared laser absorption spectroscopy is an effective tool for monitoring atmospheric trace gas species. Applications of this method are limited mainly by the availability of convenient tunable sources in the spectroscopically important "fingerprint" region from 3 to 20 μm. Recently developed quantum-cascade lasers [1] have been demonstrated to be useful tunable single-frequency light sources for laser-based absorption spectroscopy [2-5]. In this work, we demonstrate the application of a cw single frequency QC-DFB laser operating at 7.9 μm to the sensitive detection of CH_4, N_2O and different isotopic species of H_2O in ambient air.

2. Experimental details

A schematic of the QC-DFB laser based gas sensor configuration is shown in Fig. 1. In these experiments, QC-DFB laser designed for cw operation at cryogenic temperatures in the 7.9 μm spectral region was used. The laser was placed in a liquid N_2 dewar equipped with a broadband AR coated ZnSe window. No active temperature stabilization was applied. Two off-axis aluminum gold-coated parabolic mirrors and an uncoated BaF_2 lens were used to shape the laser beam. To detect trace components of the ambient air, a commercial multipass cell aligned for a 100 m optical path was used. The air was continuously flowing through the cell, and the pressure in the cell was

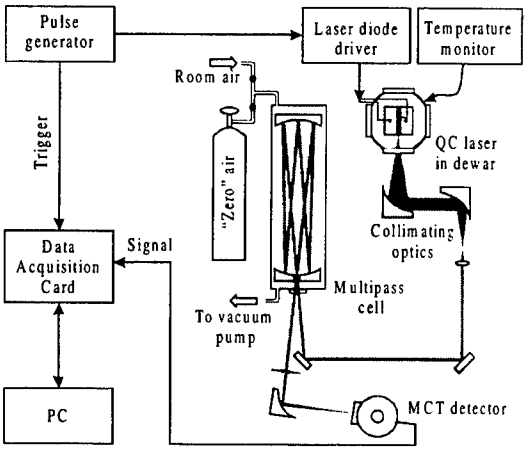

Fig. 1. Schematic of the QC-DFB based gas sensor.

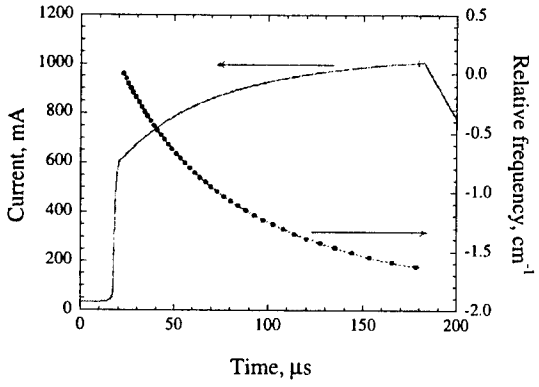

Fig. 2. Laser current and frequency as a function of time when a 200 μs long pulse is applied to the external modulation input of the laser current driver. Circles indicate positions of the etalon fringes. The fitting curve is a 4th order polynomial.

set to 20-40 Torr. After passing the cell, the laser radiation was collected onto a liquid nitrogen cooled photovoltaic MCT detector with a built-in 20 MHz preamplifier. The electrical signal was digitized using a 12 bit data acquisition card capable of a 50 MHz sampling rate.

The laser current was supplied by a low-noise driver (Wavelength Electronics MPL-5000). External modulation of current with this device has a 7 kHz bandwidth limitation. Therefore, when a rectangular pulse is applied to the external modulation input, the laser current grows exponentially from its minimum set value to the steady-state current. This technique was used for fast current scanning of the QC laser frequency using a pulse generator. The use of a pulse generator instead of a function generator enabled the variation of the laser duty cycle and thus its average temperature and frequency. A drawback of this method is an essentially nonlinear frequency-time dependence as depicted in Fig. 2 which is not important when the transition frequencies of interest are well known. All the absorption lines observed in these experiments were readily assigned. Typically, pulses of 120 μs to 235 μs duration were applied at a 800 Hz – 1000 Hz repetition rate. Frequency scans were typically over 2 cm^{-1}.

The main sensitivity-limiting factors for detecting weak absorption lines were optical interference fringes and baseline inhomogeneities caused by optical diffraction and water absorption outside the cell. Higher-frequency fringes were washed out by applying a weak changing mechanical deformation to the multipass cell during the measurements. To suppress the influence of other interfering effects, a "zero-air" background subtraction technique [6] was used. Spectra of ambient air and a pollutant-free "zero air" were alternatively taken. Replacing the air in the 3.3 l multipass cell took ~ 30 seconds. Then the zero-air signal (as a function of a datapoint number) was subtracted from the ambient air signal, and the result was normalized to the zero-air signal, resulting in an absorption spectrum. In most of the measurements, pure air with an addition of 5% CO_2 was used as a zero gas. The resulting weak "negative absorption" CO_2 lines in the spectra aided in the spectral calibration of wavelength scans.

3. Experimental results

A typical absorption spectrum of ambient air obtained with the procedure described in the previous section is shown in Fig. 3. Four strong methane lines, two strong nitrous oxide lines and several water lines corresponding to different isotopic species fall into the spectral range covered by this QC-DFB laser frequency scan. The spectrum depicted is

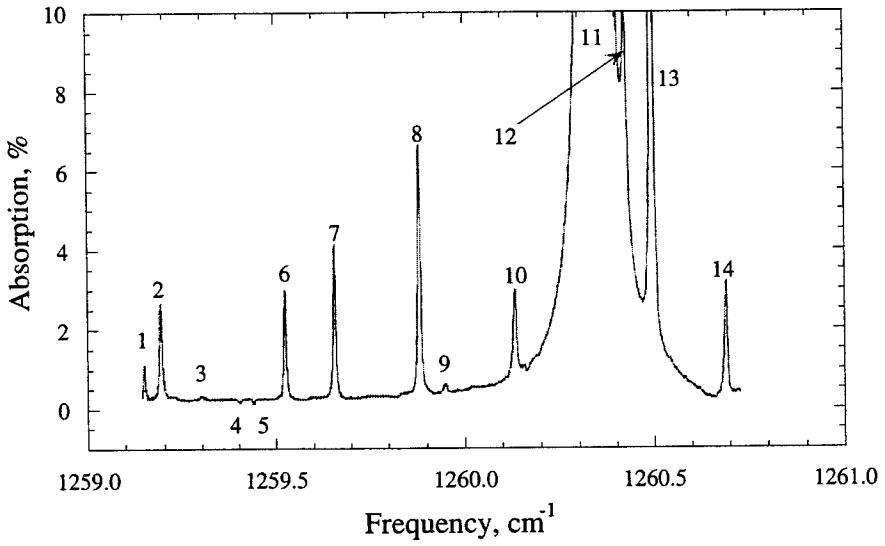

Fig.3. An example of an absorption spectrum of room air obtained with 100 m multipass cell and a zero-air background subtraction technique. The assignment of the strong spectral lines is shown: $H_2{}^{16}O$ - 1, 11, 13; N_2O - 2, 3, 10; CH_4 - 6, 7, 8, 14; $H_2{}^{18}O$ - 9; HDO - 12; and CO_2 in the reference zero-air that appears as a negative absorption - 4, 5.

the result of averaging over 6000 individual scans for both ambient air and zero-air. An acquisition and averaging of 6000 200 μs-long scans at 1 kHz repetition rate, 50 MS/s took approximately 30 seconds, because the software has not yet been optimized for fast data acquisition. The minimum detectable absorption is estimated to be 10^{-4} (0.01%)

for absorption lines with a linewidth of ~0.01 cm^{-1} characteristic for the pressure range from 20 to 40 Torr. The present sensitivity to weak absorption features is limited by an unstable baseline. This limitation can be minimized if a reproducible multipass cell deformation is applied. The current sensitivity achieved corresponds to a minimum detectable concentration of 3.5 ppb for CH_4 and 1.5 ppb for N_2O, based on intensities of the strongest absorption lines present in a given frequency scan.

Experiments were carried out to measure the $[^{13}CH_4]/[^{12}CH_4]$ ratio in the ambient air. The natural abundance of $^{13}CH_4$ is close to 0.01 and can experience up to 10% variation depending on the methane source [7]. A $^{13}CH_4$ line centered at 1260.547 cm^{-1} was chosen for these measurements, because it experiences the least interference from other absorption lines, though it is situated on the wing of a strong H_2O line. Isotopic abundances of $H_2{}^{18}O$ and $HD^{16}O$ could be measured as shown in Fig. 3. Isotopic composition measurements are of interest in determining out a sources and sinks of trace gas constituents in air [7].

The spectral range near 8 μm is also profitable for detection of some more complex organic molecules, such as ethanol (C_2H_5OH). The frequency of our laser falls close to the center of one of the absorption bands of this molecule. Unlike in the C-H and O-H stretch spectral region (~3 μm), this band has a reasonably well resolved rovibrational structure. This is explained by much smaller density of vibrational states at 1200 cm^{-1} compared to 3000 cm^{-1}, where they already form a vibrational quasicontinuum [8]. The resolved spectral features enable to positively distinguish the absorption of ethanol from other organic compounds. To calibrate the gas sensor for ethanol concentration measurements, absorption spectra of 1.1 Torr of ethanol vapor mixed with 30 Torr of air in a 0.43 m single-pass gas cell were recorded. For measurements with the multipass cell, a small amount of ethanol was spilled near the multipass cell air input, and the spectra were acquired at 5, 10 and 15 minutes later. The sensitivity to ethanol vapor concentration in the air was estimated to be 850 ppb.

4. Conclusion

This work demonstrates the successful application of a single-frequency QC-DFB laser to the analysis of trace gases in ambient air. A relatively simple technique was used to operate the QC laser, consisting of a liquid N_2 dewar with optical access, a laser current driver, and a pulse generator. To date the QC-laser based gas sensor has a demonstrated detection sensitivity of 3.5 ppb for CH_4, 1.5 ppb for N_2O and 850 ppb for C_2H_5OH for a ~60 sec data acquisition time. Measurements of the isotopic composition of H_2O and CH_4 in ambient air were also performed.

References

1. F. Capasso, C. Gmachl, D. L. Sivco and A. Y. Cho, "Quantum cascade lasers", Physics World **12**, 27-33 (1999)
2. A. A. Kosterev, R. F.Curl, F. K. Tittel, C. Gmachl, F. Capasso, D.L. Sivco, J.N. Baillargeon, A. L. Hutchinson, and A.Y. Cho, "Methane concentration and isotopic composition measurements with a mid-infrared quantum cascade laser", submitted to Optics Letters
3. B.A. Paldus, T.G. Spence, R.N. Zare, J. Oomens, F.J.M. Harren, D.H. Parker, C. Gmachl, F. Capasso, D.L. Sivco, J.N. Baillargeon, A.L. Hutchinson, and A.Y. Cho, "Photoacoustic spectroscopy using quantum-cascade lasers", Opt. Lett. **24**, 178-180 (1999)
4. S.W. Sharpe, J.F. Kelly, J.S. Hartman, C. Gmachl, F. Capasso, D.L. Sivco, J.N. Baillargeon, and A.Y. Cho, "High-resolution (Doppler-limited) spectroscopy using quantum-cascade distributed- feedback lasers", Opt. Lett. **23**, 1396-1398 (1998)
5. K. Namjou, S. Cai, E.A. Whittaker, J. Faist, C. Gmachl, F. Capasso, D.L. Sivco, and A.Y. Cho, "Sensitive absorption spectroscopy with a room-temperature distributed-feedback quantum-cascade laser", Opt. Lett. **23**, 219-221 (1997)
6. A. Fried, S. Sewell, B. Henry, B.P. Wert, T. Gilpin, and James R. Drummond, "Tunable diode laser absorption spectrometer for ground-based measurements of formaldehyde". J. Geophys. Res., **102**, 6253-6266 (1997)
7. P. Bergamaschi, M. Schupp, and G.W. Harris, "High-precision direct measurements of $^{13}CH_4/^{12}CH_4$ and $^{12}CH_3D/^{12}CH_4$ ratios in atmospheric methane sources by means of a long-path tunable diode laser absorption spectrometer", Appl. Opt. **33**, 7704-7716 (1994)
8. A.A. Stuchebrukhov; S.I. Ionov, V.S. Letokhov, "IR spectra of highly vibrationally excited large polyatomic molecules and intramolecular relaxation", J. Phys. Chem. **93**, 5357-5365 (1989)

Sensitive absorption spectroscopy using the quantum cascade laser

Edward A. Whittaker
Stevens Institute of Technology, Castle Point Station, Hoboken, NJ
201-216-5707, 201-216-5638, ewhittak@stevens-tech.edu

James F. Kelly, Richard M. Williams, Steven W. Sharpe, John S. Hartman
Pacific Northwest National Laboratory, MS K5-25, P.O. Box 999, Richland, WA 99352
509-375-6736, 509-375-2771 jfk@pnl.gov, Richard.Williams@pnl.gov, sw.sharpe@pnl.gov

Claire Gmachl, Federico Capasso, Deborah L. Sivco, James N. Baillargeon and Alfred Y. Cho
Bell Laboratories, Lucent Technologies, 600 Mountain Ave., Murray Hill, NJ 07974
908-582-7737, 908-582-7660 cg@physics.bell-labs.com, fc@physics.bell-labs.com

Abstract: We have used frequency modulated quantum cascade lasers to make sensitive absorption spectroscopy detection of H_20 and NO vapors at low pressure and low concentration. 5μ and 8μ lasers show excellent properties for sensitive spectroscopy.

OCIS codes: (280.3420) Laser sensors; (120.6200) Spectrometers and spectroscopic instrumentation

1. Introduction

The quantum cascade (QC) laser is a promising new source for tunable, infrared laser radiation and the spectroscopic capabilities of the QC laser were demonstrated in two recent reports. Namjou, *et al.*[1] reported on sensitive absorption spectroscopy using thermoelectrically cooled, pulsed mode QC lasers with a weak, low frequency modulation. Sharpe, *et al.* [2] reported absorption spectroscopy using liquid nitrogen cooled, continuous wave operation QC lasers. In this report, we extend the work of reference 2 by demonstrating wideband frequency modulation (FM) of the QC laser and the detection of FM spectroscopic signals from a weakly absorbing sample of molecules.

2. Laser Modulation Characteristics

We used 5.2μm distributed feedback QC lasers fabricated in a structure with 25-30 quantum well periods.[3] The experimental setup was similar to that in reference [2] with the exceptions that the lasers were driven with a current waveform with both a low frequency ramp for laser frequency scanning as well as a high frequency component for laser frequency modulation. We recorded the direct absorption signal by DC coupling the detected light into a high-resolution digitizer. We recorded frequency modulation spectroscopy signals by first demodulating the photocurrent using a zero-span mode radio-frequency spectrum analyzer tuned to the modulation frequency with the output of the spectrum analyzer also recorded by the digitizer.

Large modulation indices with driving frequencies in the range of 200 kHz to 1.6 MHz could be obtained using only a modest amount of RF power. Figure 1 shows the direct absorption signal with the laser center frequency tuned near a water vapor signal and the modulation frequency set to 750 kHz measured for various RF powers. The laser propagated through 140 cm of room air as well as a 10 cm long cell containing about 2 Torr of gas with some water vapor contamination. With no RF power applied to the laser, the ~10% absorbing Doppler broadened H_2O line from the low pressure cell rides atop the atmospherically broadened absorption from the long room air path. As the RF power is increased to only a few milliwatts, the absorption line broadens nearly a factor of 2 as a result of the laser frequency modulation.

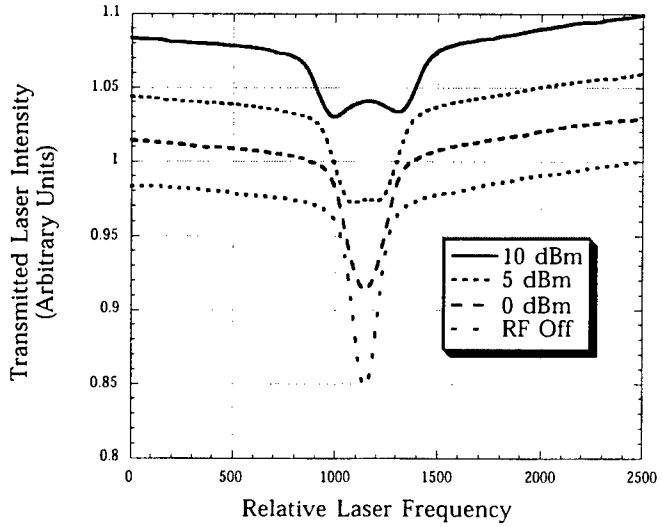

Fig. 1: Absorption spectra obtained with frequency modulated QC laser for various RF powers. The traces have been offset for clarity.

In Figure 2 we show the corresponding frequency modulation signals with the spectrum analyzer tuned to the modulation frequency. Of particular note are the near absence of amplitude modulation off resonance and of the weak signal (shown at x200 greater sensitivity) obtained with no RF modulation. We also observed a weakly resonant behavior of the magnitude of the modulation index as a function of RF frequency. Similar measurements made on an 8.5μm device showed no such resonance and a much smaller modulation index at comparable RF powers.

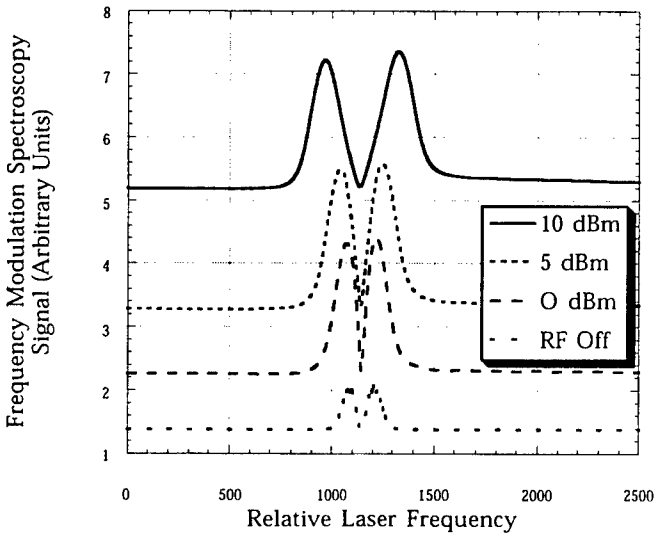

Fig. 2: Frequency modulation spectra corresponding to Figure 1. The RF Off signal has been expanded x200 in sensitivity.

3. Absorption Calibration

In Figure 3 we show a spectral scan of a sample of NO taken with the 5.2 m laser. The 10 cm long sample was at a pressure which resulted in a ~2% absorption. Both the direct absorption signal and the frequency modulation signal are plotted enabling us to calculate a calibration for the frequency modulated signal and to estimate the background limit. The figure shows the

excellent signal-to-noise ratio possible with the FM spectroscopy method. A wider spectral scan reveals the background to be dominated by weak interference fringes arising from windows in the beam path. We estimate the fringe amplitude to correspond to an equivalent absorption of approximately 0.1 %. However, the light induced background riding on top of the fringe signal is about 2 orders of magnitude smaller. Standard methods to reduce fringe interference should allow us to reach this limit.

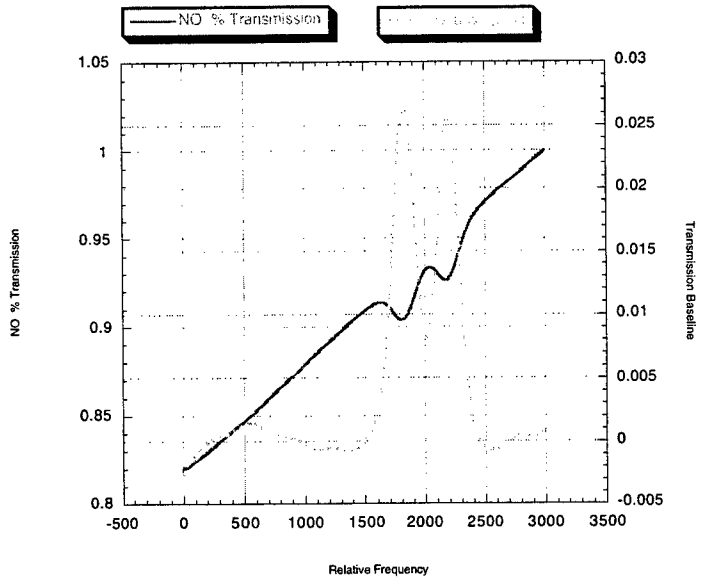

Fig. 3: Direct absorption and frequency modulation spectroscopy signals for a 10 cm path length sample of NO.

---

[1] K. Namjou, S. Cai, E. A. Whittaker, J. Faist, C. Gmachl, F. Capasso, D. L. Sivco, A. Y. Cho, Opt. Lett. **23**, 219 (1998).

[2] S. W. Sharpe, J. F. Kelly, J. S. Hartman, C. Gmachl, F. Capasso, D. L. Sivco, J. N. Baillargeon, A. Y. Cho, Opt. Lett. **23**, 1396 (1998).

[3] C. Gmachl,. J Faist, J. N. Baillargeon, F. Capasso, C. Sirtori, D. L. Sivco, A. Y. Cho, IEEE Photon. Technol. Lett. **9**, 1090 (1997).

Application of Balanced Detection to Absorption Measurements with Quasi-cw QC Lasers

D. Sonnenfroh, E. Wetjen, M. Miller, and M. Allen
Physical Sciences Inc., Andover, MA 01810
978-983-2315, 978-689-0003, sonnenfroh@psicorp.com

Claire Gmachl, Federico Capasso, Albert L. Hutchinson, Deborah L. Sivco, James N. Baillargeon, and Alfred Y. Cho
Bell Laboratories, Lucent Technologies, 600 Mountain Ave., Murray Hill, NJ 07974
908-582-7737, 908-582-7660, cg@physics.bell-labs.com, fc@physics.bell-labs.com

Abstract: We have demonstrated direct absorption measurements of NO at 5.4 μm using QC lasers in combination with a balanced detection technique. Peak absorptions of 100 ppm have been measured with excellent signal-to-noise ratio.

OCIS Codes: (280.3420) Laser Sensors; (120.6200) Spectrometers and spectroscopic instrumentation

1. Introduction

Single frequency DFB-QC lasers are expected to form the heart of the next generation, high sensitivity, mid-IR laser absorption spectrometer, especially as applied to field measurements of trace gases in a variety of environments. Incorporation of room temperature-operable, single frequency laser devices will result in very compact and rugged instruments for real world applications. In this paper, we report preliminary results indicating the absorption sensitivities achievable when using balanced ratiometric detection in combination with a QC laser spectrometer. The QC laser is operated at near room temperature in quasi-cw mode.

2. Pulsed Operation of QC Lasers

From the perspective of developing a practical, truly fieldable sensor, we are interested in room temperature operation of both the QC laser and the detectors. This implies that the laser is operated in pulsed mode. Two issues, both related to thermal management, constrain the design of the injection current pulse train. The pulse width is limited by the need to minimize the frequency chirp that arises from heating in the active region during the pulse. The duty cycle is also limited by the need to manage the heating arising from the large current densities impressed on the device. These lasers have been operated successfully with a negative bias, 1 MHz pulse train with a 1% duty cycle (10 ns pulse width).[1] In order to scan the laser wavelength across an absorption transition, we add a small amplitude, low frequency sawtooth current ramp to the pulse train. The two signals are added using a bias tee.

A block diagram of the laser drive electronics is presented in Figure 1. We use a high power, pulsed diode laser driver (DLD) supply to create the pulse train. The DLD draws power

from both low and high voltage DC supplies. A pulse generator supplies the pulse train which is amplified by the DLD. The DLD is capable of producing peak output currents to 100A. In these initial experiments, we were limited to operation with 50 ns pulses at 5 kHz for a duty cycle of <0.1%. The output of the DLD is carried to the laser via a low impedance copper strip transmission line. We use a precision diode laser current supply to provide the sawtooth ramp for wavelength scanning. A waveform generator is used to provide a voltage control ramp to the precision current supply. This supply then typically produces a 50 mA current ramp at 100 Hz.

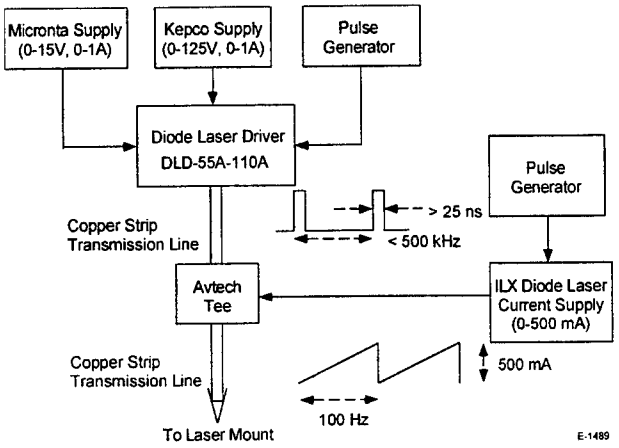

We used a simple dual beam absorption spectrometer for our initial measurements. In this experimental arrangement, the collimated laser beam exits the mount and is split into a signal and a reference beam using an ar-coated Ge beamsplitter. The signal beam propagates through an 0.5 m absorption cell having ar-coated, wedged Ge windows. After exiting the cell, the beam is refocused onto an LN2-cooled InSb detector by an ar-coated Ge f/1 lens. Similarly, the reference beam is refocused onto a second InSb detector using another lens. Each detector was fitted with a cold field-of-view machined to match the f/1 collection optics. This was done to minimize the background current arising from ambient radiation.

We adapted our balanced ratiometric detection (BRD) technique for use with pulsed QC lasers and InSb detectors.[2] Originally designed by Hobbs,[3] we have developed the BRD for operation with cw visible and near-infrared diode lasers. To enable operation with pulsed photocurrents, we decreased the bandwidth of the BRD so that the detector responded to the average input power rather than individual pulses. We found a nominal bandwidth of 5 to 10 kHz worked well with the 15 kHz pulse train. We also modified the BRD for operation with the InSb detectors. The BRD has an internal voltage reference for reverse biasing the photodiodes. While this marginally increases the dark current, it provides for an output current that is linear with respect to the incident photon flux. We modified the voltage reference stage to allow operation at 85 mV of reverse bias. The circuit output was amplified and bandpass filtered.

3. Results

To demonstrate sensitive detection with the BRD we monitored NO using the overlapped grouping of 6 lines of the P branch of the fundamental: P5.5e at 1857.268 cm^{-1} (5.3843 μm) and P5.5f at 1857.280 cm^{-1} (5.3842 μm). A spectrum of these lines for 0.032 Torr NO is presented in Figure 2. The spectrum was obtained for peak current of 1.02 A, 50 ns pulsewidth, 5 kHz pulse repetition rate, and a TEC temperature of -1 C. The peak absorption is 0.0385. The small amplitude high frequency modulation on the lineshape is residual amplitude modulation from the drive current pulsetrain. This could be removed by further decreasing the bandwidth of the BRD but was removed by FFT filtering during post processing. The filtered spectrum is also presented in Figure 2. The rms noise on this spectrum implies a SNR of 550 which yields a minimum measurable peak absorbance of 7 x 10^{-5}. We have used the BRD to record routinely peak absorbances in the range 1 x 10^{-5} under field conditions. It is likely that we did not achieve that performance because the BRD can not cancel the uncorrelated noise present on the relatively large background photocurrents of the two detectors. To further minimize background currents, improvements include using matched responsivity detectors and integral cold bandpass filters.

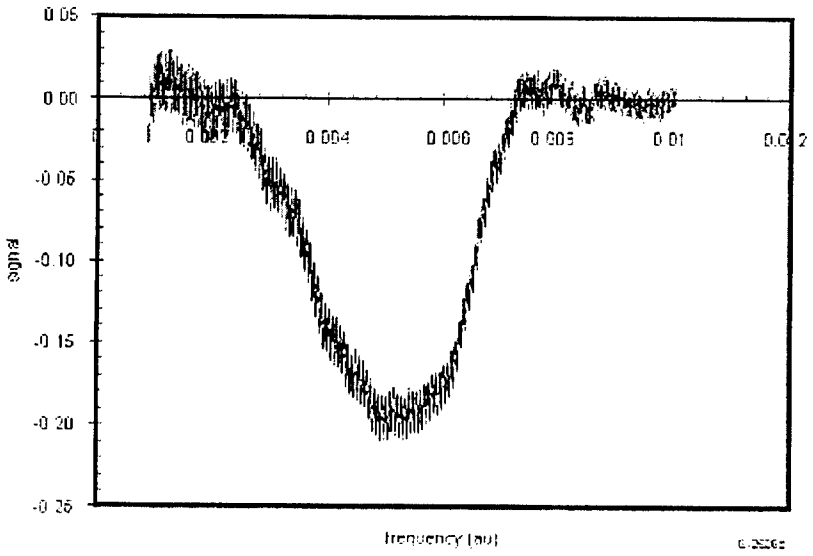

4. References

1. K. Namjou, S. Cai, E.A. Whittaker, J. Faist, C. Gmachl, F. Capasso, D.L. Sivco, and A.Y. Cho, "Sensitive absorption spectroscopy with a room-temperature distributed-feedback quantum-cascade laser," Opt. Letts., 23, 219, (1998).
2. M.G. Allen, K.L. Carleton, S.J. Davis, W.J. Kessler, C.E. Otis, D.A. Palombo, and D.M. Sonnenfroh, "Ultra-sensitive dual-beam absorption and gain spectroscopy: Applications for near-ir and visible diode laser sensors," Appl. Opt., 34, 3240, (1995).
3. P.C.D. Hobbs, "Ultrasensitive laser measurements without tears," Appl. Opt., 36, 903, (1997).

Pound-Drever-Hall frequency stabilization of a quantum-cascade laser to an infrared ro-vibrational molecular resonance

Richard M. Williams, James F. Kelly, John S. Hartman and Steven W. Sharpe
Pacific Northwest National Laboratory, MS K5-25, P.O. Box 999 Richland, WA 99352
509-372-4026, richard.williams@pnl.gov

Matthew S. Taubman and John L. Hall
JILA, University of Colorado and National Institute of Standards and Technology, Boulder, CO 80309-0440
303-497-3126, jhall@jila.colorado.edu

Claire Gmachl, Federico Capasso, Deborah L. Sivco, James N. Baillargeon and Alfred Y. Cho
Bell Laboratories, Lucent Technologies, 600 Mountain Ave., Murray Hill, NJ 07974
908-582-7737, 908-582-7660, cg@lucent.com, fc@lucent.com

Abstract: A frequency modulation method (Pound-Drever-Hall) has been used to frequency-stabilize and lock a quantum-cascade laser (QCL) to a ro-vibrational resonance on nitrous oxide at 8.5 μm. Experiments with stabilized QCLs (kilohertz linewidths) will be discussed.

OCIS Codes: (280.3420) Laser sensors; (120.6200) Spectrometers and spectroscopic instrumentation

1. Introduction

Single-mode, distributed-feedback (DFB) quantum cascade (QC) lasers[1] have the potential for ultra-high resolution (sub-Doppler) spectroscopy due to their high continuous-wave (cw) powers and wavelength tunability. Recently an 8.5 μm DFB-QC laser was shown to have a fast-linewidth of 12 kHz when actively stabilized to the side of a Doppler-limited ro-vibrational resonance of nitrous oxide (N_2O).[2,3] Further improvement in the phase-coherence of these lasers will come with the implementation of more advanced stabilization techniques. We present here recent QC laser stabilization efforts using a frequency-modulation stabilization scheme, known as Pound-Drever-Hall (PDH) stabilization.[4,5] Additionally, we discuss applications of such a stabilized mid-infrared (mid-IR) laser to sensitive chemical sensing using cavity enhanced techniques.

2. Frequency Stabilization

In our previous work, an 8.5 μm DFB-QC laser was actively stabilized to the side of a N_2O ro-vibrational resonance, while here we discuss a technique to stabilize to the top or center of a similar ro-vibrational resonance. Additional circuitry has been added to the previous electronic servo unit which allows for tracking or tuning of the stabilized laser wavelength over a portion of the Doppler-limited absorption profile. This tuning capability will be used in future sub-Doppler saturation-spectroscopy experiments, which will investigate the hyper-fine structure (due to quadrupole coupling) of such molecules as ammonia (NH_3). Spectroscopic applications based upon intra-cavity saturation absorption will also be studied. Ultra-sensitive near-IR cavity-enhanced techniques such as NICE-OHMS [Noise-Immune Cavity-Enhanced Optical Heterodyne Molecular Spectroscopy] have been shown to produce noise-equivalent absorptivities of 5×10^{-13} (1×10^{-14} cm^{-1}).[6,7] Extending this powerful technique to the rich mid-IR spectral region using QC lasers will facilitate the study of fundamental intra- and inter-molecular processes, sensitive chemical detection techniques, laser trapping of molecules or cavity quantum-electro-dynamic (C-QED).

Figure 1 depicts the experimental arrangement used for PDH frequency stabilization. A small fraction (~ 10%) of the total QC laser output (25 mW) is directed, via reflection from a potassium chloride window, through a 15 cm low-pressure (1-2 Torr) gas-cell containing N_2O. This light is focused onto a 1 mm diameter HgCdTe photovoltaic detector fitted with a custom transimpedance amplifier (TIA) having a

sufficient gain-bandwidth product for signal recovery. The absorption signal derived from a Doppler-limited resonance ($\Delta\nu_{DOPPLER}$ [FWHM] ~ 66 MHz) at 1172 cm^{-1} is used as a frequency discriminator for the servo system. The dc portion of this signal is monitored on an oscilloscope, while the ac component is filtered and fed into a 7 dBm double-balanced-mixer (DBM). Two phase-locked signal generators are used to frequency-modulate the QC laser (3-5 MHz) and drive the local oscillator input on the DBM at the same frequency, respectively. The output of the DBM, which appears as a $1f$ harmonic or 1st derivative, is used as the error signal for the custom servo unit. The feedback circuitry produces a correction signal that is fed back into the QC laser current controller acting to reduce frequency fluctuations. The electronic bandwidth of the servo unit is several hundred kHz, although the unity gain frequency has not been measured directly.

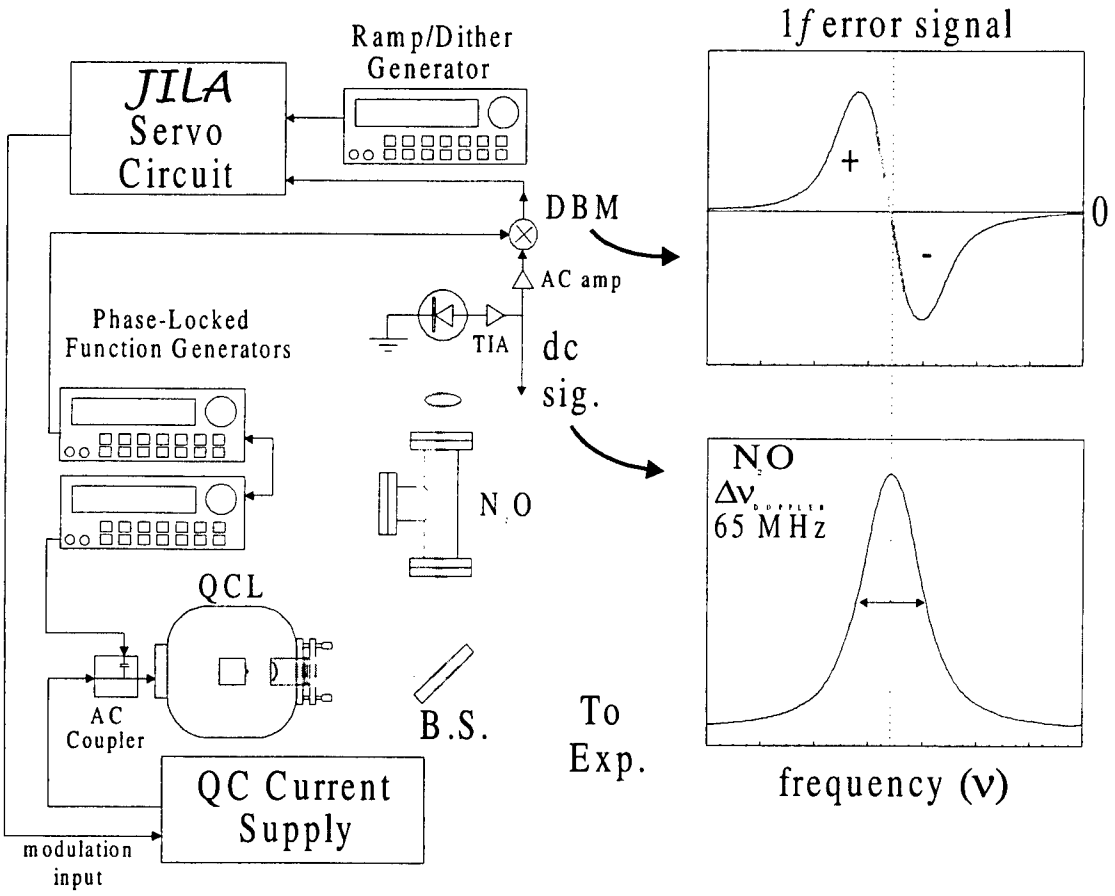

Fig. 1. Schematic representation of a Pound-Drever-Hall frequency stabilization arrangement used to lock and stabilized an 8.5 μm QC laser to the top of a nitrous oxide ro-vibrational molecular resonance.

Additionally, a tracking signal (sine or saw-tooth) in the 10 – 100 Hz range can be superimposed onto the error signal thereby forcing the servo unit to scan the stabilized QC over the quasi-linear portion of the $1f$ error-signal. The amount of this scan is typically 50% of the FWHM of the spectral resonance (e.g., 30–35 MHz for N_2O). Our previous stabilization scheme, which locked the QC laser to the side of a resonance, allowed for a direct measure of the stabilized versus non-stabilized frequency-fluctuation power-spectral-density using an "out-of-loop" frequency discriminator (i.e., the side of the molecular resonance the laser was lock to). In this case the laser is stabilized and referenced to the top of a spectral resonance which has a frequency-to-amplitude discriminator slope of zero. Future efforts to characterized the performance of this PDH stabilization scheme will include a heterodyne beat measurement of two QC lasers stabilized and referenced to the same molecular resonance. These two lasers will be simultaneously

detected on a high-speed IR detector whose output is displayed on a spectrum analyzer, the width of the heterodyne signal is directly related (in a quadruture fashion) to the spectral width of the stabilized lasers.

3. Summary

A mid-IR QC lasers has been successfully stabilized to the center or top of a ro-vibrational resonance of nitrous oxide using a variation of PDH frequency-modulation stabilization. Previous experiments have shown the laser fast-linewidth ($\tau < 1$ ms) to be reduced to 12 kHz when referenced to the side of a similar Doppler-limited resonance.[2] Improvements over the previous results are expected based upon the reduction in uncorrelated errors associated with pointing-jitter from the multiple beams (two laser beam paths required for the previous stabilization scheme instead of just the one used here). Reduction beyond this point will require an enhancement of the frequency-discriminator slope used to generate the error signal and/or a reduction in the shot noise from the "back-ground" limited detector/preamplifier combination.

The present optical powers (10's mW) and stabilized linewidths (< 10 kHz) from mid-IR QC lasers are marginally adequate to perform sub-Doppler saturation spectroscopy experiments on a variety of molecules and efforts are underway to make such measurements. Spectral features from multiple molecular species which are overlapped and unresolvable in the Doppler limit may be resolvable when investigating the hyper-fine sub-structure in the sub-Doppler limit. This type of sensitive absorption spectroscopy would allow measurement to be performed in spectral regions which are normally severely congested by background species such as water and carbon dioxide. Considerable improvements in detection limits can be achieved by performing sub-Doppler saturation-absorption measurements inside of a high Finesse optical cavity. If the laser is stabilized and referenced to the cavity, then the wavelength of the laser can be scanned continuously over a spectral feature thereby allowing a background ratio to be performed and an absolute concentration of the absorbing species to be determined. This technique is also being investigated at Pacific Northwest National Laboratory.

4. Acknowledgements

Work performed at Pacific Northwest National Laboratory (operated by Battelle Memorial Institute) was supported by the U.S. Department of Energy under contract DE-AC06-76RLO 1830. Partial support of the work performed at Bell Laboratories was provided by DARPA/ARO under contract DAAG55-98-C0050.

1. C. Gmachl, F. Capasso, J. Faist, A. L. Hutchinson, A. Tredicucci, D. Sivco, J. N. Baillargeon, S. N. G. Chu, and A. Y. Cho, "Continuous-wave and high-power pulsed operation of index-coupled distributed feedback quantum cascade laser at 8.5 micron" Appl. Phys. Lett. **72,** 1430 (1998).

2. R. M. Williams, J. F. Kelly, J. S. Hartman, S. W. Sharpe, M. S. Taubman, J. L. Hall, F. Capasso, C. Gmachl, D. L. Sivco, J. N. Baillargeon, and A. Y. Cho, "Kilo-Hertz Linewidth from Frequency Stabilized Mid-Infrared Quantum Cascade Lasers" Optics Letters (in press) (2000).

3. R. M. Williams, J. F. Kelly, S. W. Sharpe, J. S. Hartman, C. Gmachl, F. Capasso, D. L. Sivco, J. N. Baillargeon, and A. Y. Cho, in *SPIE*, Vol. (In press, 3758-04), edited by A. Fried (The International Society for Optical Engineering, Denver, CO, 1999).

4. R. V. Pound, "Electronic Frequency Stabilization of Microwave Oscillators" Rev. Sci. Instr. **17,** 490 (1946).

5. R. W. P. Drever, J. L. Hall, F. V. Kowalski, J. Hough, G. M. Ford, A. J. Munley, and H. Ward, "Laser Phase and Frequency Stabilization Using an Optical Resonator" Appl. Phys. B **31,** 97 (1983).

6. J. Ye, L. Ma, and J. L. Hall, "Sub-Doppler optical frequency reference at 1.064 μm by means of ultrasensitive cavity-enhanced frequency modulation spectroscopy of a C_2HD overtone transition" Opt. Lett. **21,** 1000 (1996).

7. J. Ye, L. Ma, and J. L. Hall, "Ultrasensitive detections in atomic and molecular physics: demonstration in molecular overtone spectroscopy" J. Opt. Soc. Am. B **15,** 6 (1998).

Laser Applications to Chemical and Environmental Analysis

Environmental and Industrial Applications of Diode Lasers

Saturday, February 12, 2000

Alan C. Stanton, Southwest Sciences Inc., USA
Presider

SaB
10:10am–12:20pm
Anasazi North

A fast chemical sensor for atmospheric trace gas flux measurements

Peter W. Werle
Fraunhofer Institute for Atmospheric Environmental Research
Phone : ++49-(0)8821-183170, Fax : ++49-(0)8821-183296, E-mail : werle@ifu.fhg.de

Abstract: A fast response chemical sensor based on tunable diode laser spectroscopy will be described and results from field eddy correlation measurements of methane fluxes from rice paddy fields located in Vercelli, Italy will be presented.

OCIS codes: (010.1120) air pollution monitoring; (300.6260) spectroscopy, diode laser

1. Introduction

In order to specify effective greenhouse gas reduction policies, more precise quantification of fluxes from individual sources is required. Among biogenic sources of atmospheric methane, rice paddies have been identified as one of the most important sources. In the future, CH_4 is expected to become an increasingly important greenhouse gas. For example, Asian rice production must increase 60 % over the next 30 years to keep up with population growth. Increased rice cropping intensity and fertilizer use are expected to significantly increase CH_4 emissions from flooded rice paddies. The projected concentration of CH_4 by the year 2030 is 2,2 to 2,5 ppm. In particular, there is a need to better understand and assess CH_4 fluxes from rice paddies since global extrapolations range from 25-150 Tg yr^{-1}. Fortunately, any reductions in CH_4 emissions will be quickly reflected in the atmosphere due to methan's short residence time. A major limitation to atmospheric research on surface-exchange and flux measurements is the lack of sensitive, reliable, and fast-response chemical species sensors. Tunable diode laser absorption spectroscopy (TDLAS) is increasingly being used to measure atmospheric trace gas concentrations down to low ppbv-levels. This optical technique fulfills the requirements for trace gas analysis in the atmosphere for most of the smaller molecules like CH_4, N_2O, CO, CO_2 etc. High frequency modulation (FM-TDLAS) schemes can further improve sensitivity and detection speed of modern instrumentation [1]. Therefore, this technique is ideally suited for flux measurements by the eddy correlation method, which provides a micrometeorological alternative to closed chambers. The eddy correlation technique requires simultaneous fast and accurate measurements of both the vertical velocity and the trace species in question. The technique for the measurement of the turbulence with the necessary resolution is available as sonic anemometers can readily yield air motion data with the required resolution. For the determination of surface emission and deposition fluxes, the eddy correlation method is rigorous when specific criteria are met and the meteorological conditions controlling the state of the turbulence do not vary over the course of the measurements.

2. A fast chemical sensor

A fast laser-optical sensor is the key issue for eddy correlation measurements. Diode laser spectrometers are now at the threshold of routine applications in environmental monitoring. So far the development of this technology has been driven mainly by scientific questions, but increasingly these techniques are applied to a sensitive, selective and fast analysis for monitoring applications. A new spectroscopic method - high frequency modulation spectroscopy (FMS) - was developed in the early 80s. In FMS, the laser is modulated at higher frequencies, typically in the radio frequency (rf) region, thus allowing selective and fast scanning over an absorption line of a molecule. The technique is described in detail in a recent review article [1]. A fast sensor for the spectroscopic detection of atmospheric methane based on this technique with a ppbv precision is shown in Fig. 1. A diode laser is housed in a liquid-nitrogen (LN_2) cooled dewar. The TDL beam is first collimated by an off-axis parabola and then directed by mirrors through the sample cell and onto a LN_2-HgCdTe photo-voltaic detector. For typ. linestrengths ambient concentrations of 1 ppbv produce an absorption of only 1 part in 10^7 over a 10 cm path-length. Conventional absorption spectroscopy will not be able to measure such a small absorption. TDLAS overcomes this problem by using a multi-pass cell with path lengths of 100 m or more. In the Herriott cell used here the optical beam is injected through a hole in one mirror and is reflected back and forth a number of times before exiting from the same hole. Detector signals are fed into a phase sensitive detection electronics, which can be regarded as a high frequency lock-in amplifier [1]. Both channels (sample and reference) are then digitized and further processed by digital filters, line

locking, normalization and calibration procedure. With this spectrometer ambient methane concentrations around 2 ppm can be detected with a precision of about 1 % at a 10 Hz repetition rate. The fast examination of the wind vectors was performed using an ultrasonic anemometer mounted at a measurement height of 3.2 m. The measurement interval of the ultrasonic anemometer is fixed at 48 ms (20.8 Hz). The interval of the spectrometer was therefore chosen to be 96 ms, which easily can be connected to the rate of the anemometer and which is adopted to the possible frequency resolution given by the gas exchange in the measurement cell of the spectrometer. The averaging time scale for the turbulent fluxes was chosen to be about 30 min, interrupted by a calibration procedure of the diode laser spectrometer, which lasted for about 20 s. Fast response measurements of state variables generate time series of data that we can statistically analyze. The first step in the eddy correlation process is to calculate the perturbation values of the data points. For the measured time series of concentration values we can subtract the mean from each data point to yield the time series of perturbations c´. We can similar find a time series of vertical wind velocity perturbations w´. Multiplying the respective values together yields a time series w´c´. The average of this series <w´c´> gives the turbulent vertical flux. An advantage of this method is that it is direct and simple, and fluxes can be calculated at whatever height or location the original time series was measured.

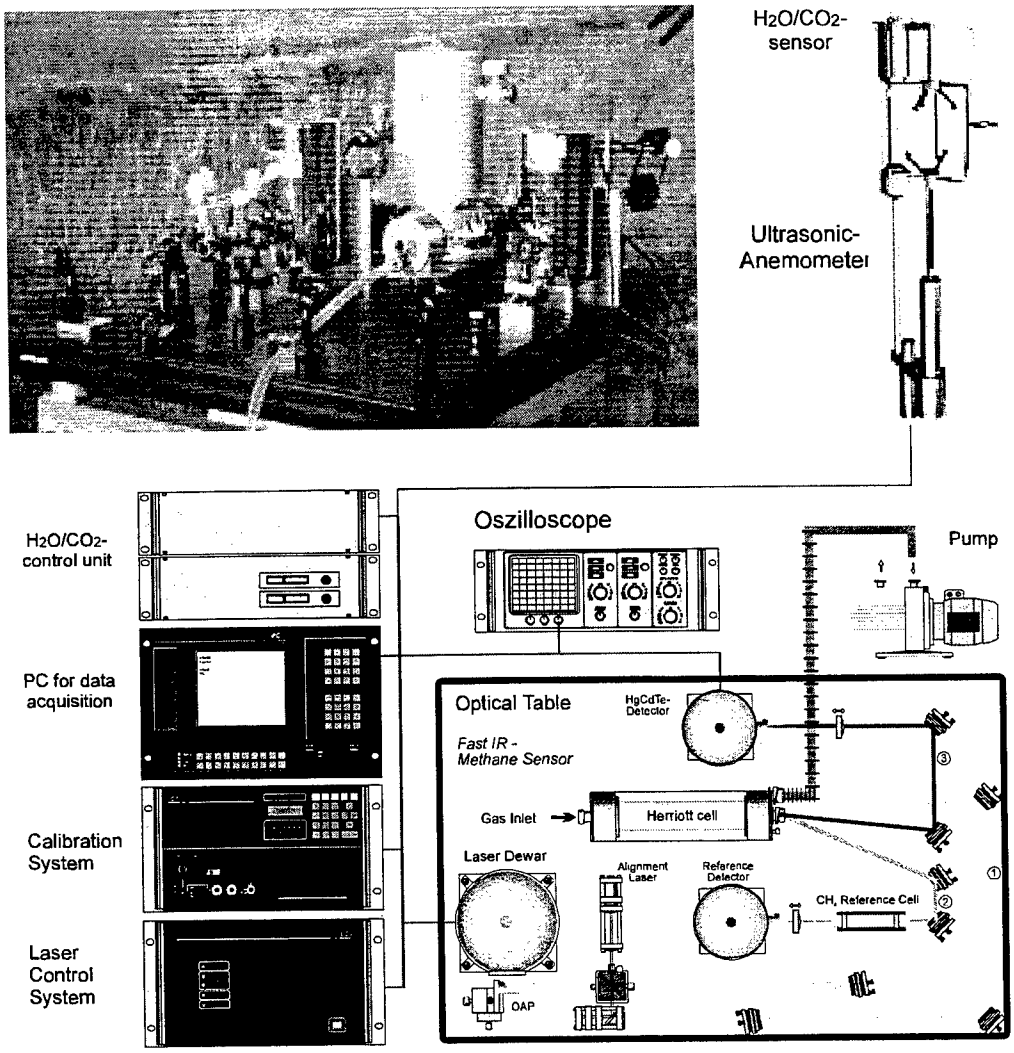

Fig. 1 : A high frequency modulation spectrometer for methane sensing with all control electronics for eddy correlation trace gas flux measurements together with the layout of the optical sensor based on a small volume (0.3 l) Herriott cell during the field campaign in Italy. A non-dispersive infrared H_2O/CO_2 sensor is mounted behind the measurement paths of the ultrasonic anemometer and the gas inlet for the spectrometer.

3. Field Measurements and Results

In the frame of an interdisciplinary research project funded by the European Community eddy correlation measurements of methane emissions from rice paddy fields have been performed during a field campaign in order to allow a comparison with data from continuous monitoring provided by the closed chamber technique. The application of these two in-dependent methods should help to assess and improve the quality of data on methane fluxes. It is doubtless that the closed chamber technique gives valuable results for the understanding of the local processes finally leading to net-methane emissions into the atmosphere and the detection of diurnal as well as seasonal variations in CH_4 flux rates from rice paddy fields. While the chamber technique is highly appropriate to determine the effects of different site treatments on fluxes, site spatial variability is the greatest problem in using chambers to measure fluxes from a field or ecosystem[38]. In addition, chambers disturb the natural air turbulence, decouple the rice plant from the ambient turbulent atmosphere and alter the temperature, solar radiation and gas concentration in the measurement environment. Therefore, the extrapolation of CH_4 emissions, based on flux rates obtained by use of small closed chamber measurements, to field, landscape and regional levels is not so well established. A major objective of the eddy correlation measurements was the exploration of systematic differences between the closed chamber method and a direct micrometeorological technique.

A record of high quality data on methane emissions from irrigated rice paddy fields in Italy has been obtained during a recent field campaign. From the eddy correlation measurements a mean daytime flux of 6.35 ppbv m/s (14.5 mg/m^2h) has been derived, while the measurements based upon the closed chamber technique report about 70% higher methane fluxes. The significantly lower emission measurements of the laser based micrometeorological eddy correlation system shown here have been confirmed in an on-site comparison with two other independent diode-laser based eddy correlation systems. In order to try to explain this difference, we have to recall that closed chambers usually have a fan mounted inside the chamber and during closure, the fan causes rapid mixing of air within the chamber. Thus a strong artificial turbulence is introduced in the chamber, which does not allow natural gradients inside the box. The chamber data may suffer from this experimentally introduced effect, which might have influenced all methane flux measurements by closed chambers in rice paddy fields so far. In addition, during the analysis of the campaign data a positive correlation between the measured methane flux and the friction velocity and also with the horizontal wind and temperature has been found. This result is also well in line with the recent findings of Kahlil et al., who analyzed a 7-year data set on methane emissions from rice fields in Tu Zu, China, and found that greater wind speeds tend to result in greater methane emissions [2]. They conclude that wind can affect fluxes from rice fields by increasing the agitation of the soil and water as the plants are moved in the wind and this effect may be larger in windier locations. While the amount of distortion or turbulence is constant inside the chamber, this is not the case in the free atmosphere, where conditions can be changing with time. From the data we can see, that the ratio of the flux measured by the eddy correlation technique to the flux measured by the closed chamber technique correlates positively with the horizontal wind speed and the friction velocity, a measure for turbulence.

As a conclusion of the work presented here the current hypothesis is that closed chamber measurements might present only an upper level for the methane flux under strong turbulent conditions and, therefore, do not represent the natural emission under normal and low wind conditions, which we encountered in Italian rice paddy fields. Further measurements and studies are needed to more confirm and explain these findings.

4. Summary

The features of TDLAS rendering it such a valuable technique for gas analysis are that it is specific and as a high resolution spectroscopic technique it is virtually immune to interference by other species - a problem that plagues most competing methods. Tunable diode laser absorption spectroscopy based on the FM technique is one of the most powerful spectroscopic techniques for ultra-sensitive and high-speed detection of weak absorption signals. TDLAS has made the transition from a technique mainly of interest to instrument developers into one which produces results of real value to trace gas analysis and atmospheric chemistry studies, where this technique is especially well suited for the measurement of trace gas fluxes from terrestrial ecosystems based upon the eddy correlation technique, because is allows rapid measurements of ambient gas concentrations with frequencies up to 10 Hz with still an accuracy better than 1%.

5. References

[1] P. Werle, "A review of recent advances in semiconductor laser based gas monitors," Spectrochimica Acta **A54**, 197-236 (1998).

[2] M.A.K. Kahlil, R.A. Rasmussen, M.J. Shearer, R.W. Dalluge, L. Ren, C.L. Duan, "Factors affecting methane emissions from rice fields," J. of Geophys. Res. **103**, 25219-25231 (1998).

A portable, LN_2-free, multi-chemical sensor based upon mid-infrared laser absorption spectroscopy

John S. Hartman, Timothy L. Stewart, James F. Kelly, Steven W. Sharpe and Richard M. Williams
Pacific Northwest National Laboratory, MS K5-25, P.O. Box 999 Richland, WA 99352
509-375-2771, john.hartman@pnl.gov

Claire Gmachl, Federico Capasso, Deborah L. Sivco, James N. Baillargeon and Alfred Y. Cho
Bell Laboratories, Lucent Technologies, 600 Mountain Ave., Murray Hill, NJ 07974
908-582-7737, 908-582-7660, cg@lucent.com, fc@lucent.com

Abstract: The development of a field-portable, cryo-cooled infrared tunable laser absorption spectrometer (TLAS) will be presented. The configuration includes either multi-quantum-cascade or multi-lead-salt lasers, a 36 m Herriott-cell with integrated laser/detector with cooling via Stirling cryo-coolers.

OCIS Codes: (280.3420) Laser sensors; (120.6200) Spectrometers and spectroscopic applications

1. Introduction/Design Summary

Portable chemical sensors, based upon tunable infrared (IR) laser absorption spectrometers (TLAS), have the potential to become routinely used as deployable field units if size, weight and cost can be reduced and if the units can be made robust, user friendly and with a minimum amount of maintenance. In fact, many researchers have made considerable progress constructing such devices, some of which may eventually be deployed on the International Space Station (ISS) to monitor the build-up of noxious gases within the crew-habitat.[1,2] Here we discuss recent efforts at Pacific Northwest National Laboratory (PNNL) to produce a high-performance, low-maintenance "IR-sniffer" system which incorporates the latest in infrared laser and electro-mechanical cooling technologies.

An important aspect in the successful design of any mid-infrared (mid-IR) TLAS includes the choice of laser source. Few mid-IR sources are available, these include lead-salt (group IV-VI semiconductor materials) and antimony lasers, laser systems based on non-linear difference-frequency-generation (DFG)[1,3] and quantum cascade (QC) lasers.[4-6]

Lead-salt and antimony diode lasers can be fabricated to operate in specific wavelength ranges over the entire infrared spectral region (3-30 μm), however, these sources produce limited optical power (< 1 mW) and suffer from discontinuous mode-hopping during wavelength scanning. Despite these limitations many working spectrometers based upon these materials have been produced with excellent sensitivities.[7] Infrared DFG sources, like those in references [1,2], produce even less optical power (< 10 μW) and normally operate in the range of 3 to 5 μm using non-linear materials such as periodically-poled lithium niobate (PPLN). An advantage to these sources is their room temperature operation, unlike lead-salt and antimony lasers which need to be kept at cryogenic temperatures (< 120 K) during operation. Wavelength conversion to longer IR wavelengths is possible using more exotic non-linear media, however, these materials possess even lower non-linear conversion efficiencies than PPLN. The low optical powers can severely limit the detection sensitivity of a DFG spectrometer. When used in conjunction with multi-path absorption cells (e.g., Herriott- or White-cells), the detected power can be < 1 μW, producing less photo-current on the detector than the residual black-body- or dark-current (i.e., power-limited absorption sensitivities). The most recent infrared laser source is the QC laser, which has great potential for a myriad of chemical sensing applications because of its greater output power and stability against environmental and operational degradation.

QC lasers are fabricated via a molecular-beam-epitaxy (MBE) growth process involving multiple or cascaded alternating quantum-well structures of AlInAs/GaInAs. The emission wavelength of the QC laser is engineered into the quantum-well structure; to date QC lasers have been shown to emit from 3.4 to 17 μm. QC lasers can operate continuous-wave (cw) up to 120 K and pulsed at room temperature. Continuous single-mode tuning (up to 40 nm) is accomplished via temperature tuning, with efficient side-

mode suppression achieved by incorporating a distributed-feedback (DFB) grating into the waveguide structure of the device. DFB-QC lasers operating at cryogenic temperatures can produce up to 200 mW of cw output power with excellent robustness and wavelength reproducibility during "aging" or cryo-cycling (often a limiting factor in lead-salt diode laser operations). High-power QC lasers have the potential for not only point sensing applications but also in remote chemical sensing using variations of LIDAR technology. PNNL is developing several chemical sensing applications (both remote and point) using QC lasers, and in previous work a minimum-detectable-absorbance of 3×10^{-6} (2×10^{-7} cm^{-1}) was obtained for nitric oxide (NO) at 5.2 μm using a QC laser (log_{10}, 10^5 samples averaged, 15 cm single-pass cell).[8,9]

The TLAS system described here is designed to eventually integrate QC laser technology with high-performance Stirling cryo-coolers (designed to lift ~ 5W at 77K) in conjunction with a long-path (36 m) Herriott cell to yield a chemically-sensitive and selective portable sensor system that is liquid-cryogen-free and designed to operate from standard "wall-plug" power. The custom cryogenic-vacuum-Dewar assembly is designed to house multiple lasers together with a single detector element, all cooled to near 77K with a single cryo-cooler. For applications using lead-salt lasers, a cryo-cooler capable of lifting 1.5 Watts at 77K is sufficient however, for QC lasers (QCLs), a larger unit (~ 5 Watts @ 77K) is necessary due to the increased power consumption (0.5 amps/8 volts) compared to the lead-salt lasers. Platform vibrations from the electro-mechanical cooler are minimized by using a dual-opposed-piston design which passively cancels vibration. Residual jitter of the fixture may in fact be beneficial as many researchers have found that a minimal amount of vibration "washes-out" etalon fringing effects.

The system supports multiple lasers, which is advantageous and necessary to gain broad spectral coverage for multi-analyte interrogation. The IR sources (either lead-salt or QCL) are mounted on a motorized rotating fixture which accurately positions individual lasers in the focal plane of a collimating lens (mounted in a vacuum compatible 5-axis mount). Collimated laser radiation emitted from this source is routed through a 0.3 liter astigmatic Herriott cell with a 36 meter path-length before being focused onto a 1 mm diameter HgCdTe photovoltaic detector element (also housed in the Dewar assembly). Reproducible operating conditions that sample specific molecular resonances are achieved by using custom laser current controller, based on the design of Libbrecht and Hall,[10] used in unison with waveforms superimposed onto the pre-selected laser drive current for limited wavelength scanning and precise temperature regulators.

A small (< 0.5 l s^{-1}) oil-free pump pulls fresh air into the cell while maintaining an optimal operating pressure of 20-40 Torr. Figure 1 shows an excellent example of the effect of sample pressure on line-center absorbance values using carbon monoxide (CO) detected in a lead-salt laser TLAS system. As can be seen in Fig. 1 as the pressure is reduced, from atmospheric values, the line center absorbance is independent of sampling pressure as gas density and linewidth (due to pressure line-broadening effects) decrease

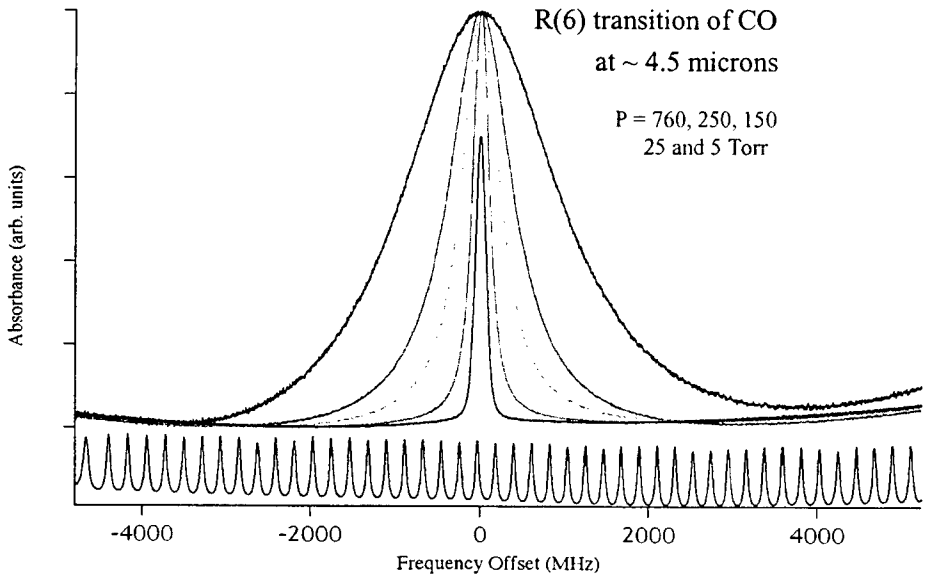

Fig. 1. Absorption profiles of carbon monoxide, showing density and line-broadening effects on the line-center absorbance. Profiles are measured at 760, 250, 150, 25 and 5 Torr from broadest to narrowest, respectively. An etalon fringe pattern is also shown for a frequency reference.

uniformly. As there is no negative impact on peak absorbance values until the Doppler limit is reached, the cell is operated at reduced pressures to mitigate congested spectral features. Approaching the Doppler-limited pressure range (< 25 Torr in this case), the line-center absorbance begins to scale inversely with pressure as the line-broadening contribution becomes negligible. Provisions for "zero" air background subtraction will be considered depending upon the required sensitivity as well as wavelength modulation signal recovery algorithms.

2. Summary

Recent results in the design and development of a robust, field-portable "IR-sniffer" have been outlined. This prototype apparatus takes advantage of several emerging technologies, including quantum-cascade lasers and advanced Stirling cryo-cooler design. An integrated multi-laser/detector Dewar design will facilitate concentration measurements of multiple species absorbing over a potentially broad IR spectral range. Although not complete, many of the key technical milestones have been achieved and will be discussed during the presentation.

3. Acknowledgement

The authors wish to acknowledge the substantial technical contributions made to this project by G. Morgen, T. Kieffer, B. Burghard, B. Gray, J. Reeves and J. Willett. Pacific Northwest National Laboratory is operated by Battelle for the U.S. Department of Energy under contract DE-AC06-76RLO 1830. This work was supported by the U.S. Department of Energy, NN-20 program. Partial support of the work performed at Bell Laboratories was provided by DARPA/ARO under contract DAAG55-98-C0050.

1. D. G. Lancaster, D. Richter, and F. K. Tittel, "Portable fiber coupled diode laser based sensor for multiple trace gas detection" Applied Physics B **In press** (1999).
2. F. K. Tittel, D. G. Lancaster, D. Richter, and R. F. Curl, in *Interdisciplinary Laser Science Conference, Joint symposium on advances in sources and applications in the mid-IR* (Optical Society of America, 1999).
3. T. Topfer, P. P. Konstantin, M. Yasuharu, J. Dieter, R. F. Curl, and F. K. Tittel, "Room-temperature mid-infrared laser sensor for trace gas detection" Appl. Opt. **36,** 8042 (1997).
4. J. Faist, F. Capasso, D. L. Sivco, C. Sirtori, A. L. Hutchinson, and A. Y. Cho, "Quantum cascade laser" Science **264,** 553 (1994).
5. C. Gmachl, F. Capasso, J. Faist, A. L. Hutchinson, A. Tredicucci, D. Sivco, J. N. Baillargeon, S. N. G. Chu, and A. Y. Cho, "Continuous-wave and high-power pulsed operation of index-coupled distributed feedback quantum cascade laser at 8.5 micron" Appl. Phys. Lett. **72,** 1430 (1998).
6. F. Capasso, C. Gmachl, D. Sivco, and A. H. Cho, "Quantum Cascade Lasers" Physics World **12,** 27 (1999).
7. P. Werle, "A review of recent advances in semiconductor laser based gas monitors" Spectrochimica Acta Part A **54,** 197 (1998).
8. S. W. Sharpe, J. F. Kelly, J. S. Hartman, C. Gmachl, F. Capasso, D. L. Sivco, J. N. Baillargeon, and A. Y. Cho, "High-resolution (Doppler-limited) spectroscopy using quantum- cascade distributed-feedback lasers" Opt. Lett. **23,** 1396 (1998).
9. S. W. Sharpe, J. F. Kelly, R. M. Williams, J. S. Hartman, C. Gmachl, F. Capasso, D. L. Sivco, J. N. Baillargeon, and A. Y. Cho, "Rapid scan (Doppler-limited) absorption spectroscopy using mid-infrared quantum-cascade lasers" Proc. SPIE **3758** (1999).
10. K. G. Libbrecht and J. L. Hall, "A low-noise high-speed diode laser current controller" Rev. Sci. Instr. **64,** 2133 (1993).

Pseudo-random code-based differential absorption LIDAR in the LWIR spectral region

E.T. Wetjen, M.G. Allen, W.J. Marinelli, and C.M. Gittins
Physical Sciences Inc., 20 New England Business Center, Andover, MA 01810
Phone: 978-689-0003, Fax: 978-689-3232, E-mail: gittins@psicorp.com

C. Gmachl, F. Capasso, A.L. Hutchinson, D.L. Sivco, J.N. Baillargeon, and A.Y. Cho
Bell Laboratories, Lucent Technologies, 600 Mountain Ave., Murray Hill, NJ 07974

Abstract: Using a quantum cascade laser operating near 8 μm, we have demonstrated intensity modulation of the transmitted beam and deconvolution of backscattered return necessary for developing a quasi-continuous wave DIAL transceiver for remote sensing applications.

OCIS codes: (280.1910) DIAL; (140.3070) Infrared and far-infrared lasers

Differential absorption lidar (DIAL) systems have become extremely useful tools for remote sensing of atmospheric constituents. Using a quantum cascade (QC) laser operating near 8 μm fabricated by Lucent Technologies, Physical Sciences Inc. has demonstrated proof-of-concept for a low peak power, quasi-continuous wave (cw) QC laser-based DIAL transceiver for stand-off detection of chemical vapor plumes. QC lasers are compact, solid-state devices recently developed at Lucent Technologies through a novel combination of band-gap engineering and molecular beam epitaxy [1]. A DIAL system based on LWIR QC lasers would allow remote quantification of organic chemical vapors, many of which have characteristic absorption features in the 8 μm to 12 μm spectral region. Many of these absorption features are presently difficult or impossible to access using other LWIR light sources, e.g., CO_2 lasers and optical parametric oscillators.

Range resolved DIAL measurements are typically accomplished using a pulsed laser source. Time resolved direct detection or optical heterodyning of the backscattered light pulse provides range resolution. Molecular absorption and light scattering are both linear optical processes however and the DIAL signal scales with the average power used in the measurement. A particularly noteworthy operating characteristic of QC lasers is that a single device can provide peak output power >100 mW at high operating temperature ($T \leq 320$ K) [2]. As the thermal management of the QC laser chips continues to improve, average output powers may well approach those of larger, heavier pulsed infrared sources.

The key to the quasi-cw LIDAR measurements described in this presentation is the pseudo-random code-based (PRC) intensity modulation of the transmitted laser beam. (PRC modulation of radio frequency signals is what enables the high positioning accuracy of the GPS.) PRC modulation of the transmitted QC laser beam enables ranging information and 100% duty cycle data acquisition. The most commonly used PRC function is the maximum shift-register sequence, "M-sequence." An M-sequence consists of $2^n - 1$ elements. The sequence is a cyclic function with elements, a_i, equal to 1 or 0. Each M-sequence also has a conjugate with elements $a_i' = 2a_i - 1$; $i = 0, 1, 2, \ldots, 2^n - 1$. The M-sequence has the extremely useful mathematical property that its cross-correlation with its conjugate is proportional to the Dirac delta function:

$$\sum_{i=1}^{2^n-1} a_i \cdot a'_{i-j} = 2^{n-1} \cdot \delta_{0,j} \qquad (1)$$

The binary M-sequence described above has a finite pulse width analogue. The cross-correlation of the sequence with its conjugate yields a triangular peak with FWHM equal to the pulse width. Figure 1 shows a synthetic 31 element PRC sequence with 1 μs fundamental widths. Figure 2 depicts the corresponding cross-correlation function where the Offset axis refers to the imposed temporal delay between the sequence and its conjugate prior to summation. In order to demonstrate proof-of-concept for the QC laser based DIAL system, the output of our PRC modulated QC laser was collimated and directed through a gas flow cell containing a calibrated column density of a

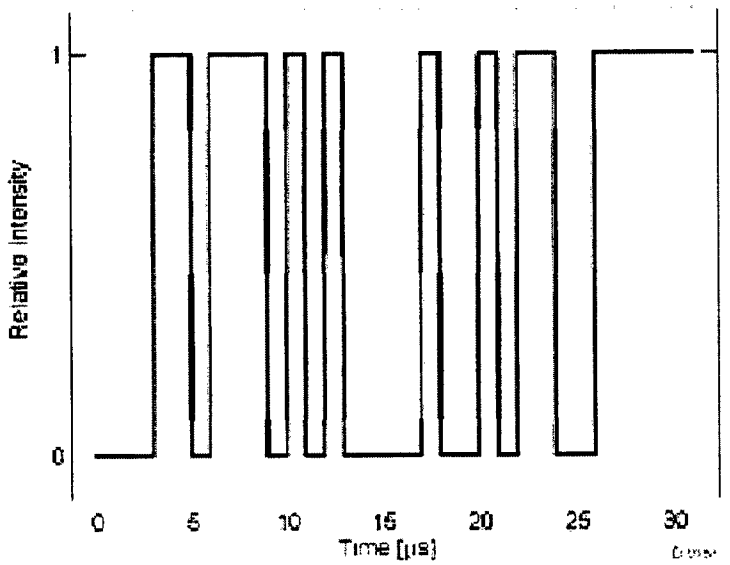

Fig. 1. A finite pulse width (1 μs) analogue of a binary PRC sequence. With reference to DIAL and LIDAR measurements, the "zero" and "one" states of the system correspond to the transmitted beam being on or off, respectively.

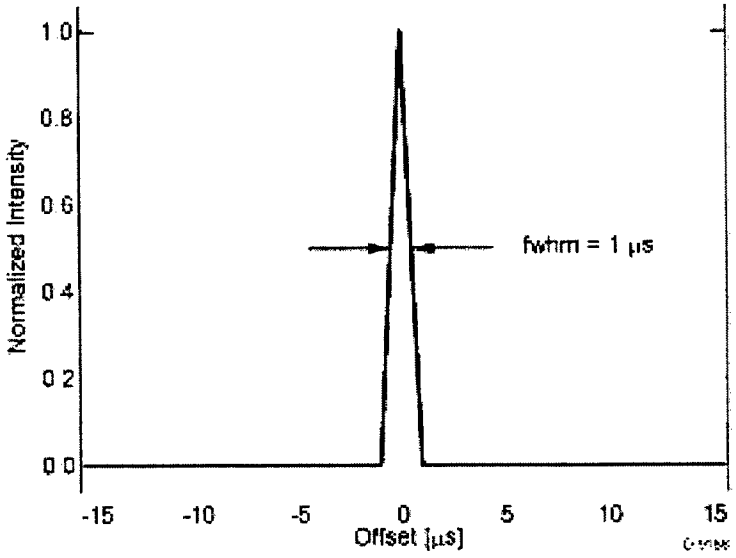

Fig. 2. Cross-correlation function of the 31-bit PRC sequence depicted in Figure 1 with its conjugate. In a LIDAR or DIAL configuration, correlation peaks are temporally shifted by 2L/c, where L is the range to the scattering medium and c is the speed of light.

broadband IR-absorbing chemical vapor and then onto a scatter screen in the near field. The signal generated by collecting backscattered light was processed to recover both ranging information and demonstrate Beer's Law attenuation of the transmitted light by the chemical vapor.

PRC modulation has been successfully implemented to extract range resolved scattering information from atmospheric and anthropogenic aerosols using an eye-safe, diode laser-based cw lidar system [3,4]. It has also been successfully implemented with a cw CO_2-based heterodyne lidar to demonstrate range-resolved scattering from topographic targets [5]. QC lasers are an extremely new technology and the first spectroscopic absorption measurements have just recently been demonstrated [6]. To the best of our knowledge this effort is the first to demonstrate Beer's Law attenuation of a PRC-modulated pulse train in order to show feasibility of a PRC-based DIAL system.

References

1. F. Capasso, C. Gmachl, D. L. Sivco and A. Y. Cho, "Quantum cascade lasers," Physics World **12**, 27-33 (1999).

2. J. Faist, F. Capasso, D.L. Sivco, J. N. Baillargeon, A.L. Hutchinson, S.-N.G. Chu, and A.Y. Cho, "High power mid-infrared (λ~5 μm) quantum cascade lasers operating above room temperature," Appl. Phys. Lett. **68**, 3680-3682 (1996).

3. N. Takeuchi, H. Baba, K. Sakurai, and T. Ueno, "Diode-laser random-modulation cw lidar," Appl. Opt. **25**, 63-67 (1986).

4. N. Takeuchi, N. Sugimoto, H. Baba, and K. Sakurai, "Random modulation cw lidar," Appl. Opt. **22**, 1382-1386 (1983).

5. J.F. Holmes and B.J. Rask, "Coherent, CW, Pseudo Random Code Modulated Lidar for Path Resolved Optical Remote Sensing," SPIE **2222**, 20-28 (1994).

6. K. Namjou, S. Cai, E.A. Whittaker, J. Faist, C. Gmachl, F. Capasso, D.L. Sivco, and A.Y. Cho, "Sensitive absorption spectroscopy with a room-temperature distributed-feedback quantum-cascade laser," Opt. Lett. **23**, 219-221 (1998).

In-situ monitoring of water vapour and gas temperature in a coal fired power-plant using Near-Infrared Diode Lasers

T. Fernholz, H. Pitz, V. Ebert
Institute of Physical Chemistry, University of Heidelberg, Im Neuenheimer Feld 253, 69120 Heidelberg, Germany
Phone: +49-6221-545004, Fax: +49-6221-545050
volker.ebert@urz.uni-heidelberg.de

Abstract: We report approaches towards quantitative absorption spectroscopy under very low transmission conditions using base band diode laser modulation spectroscopy. Water absorption lines in the 800 nm region were used to derive number-densities and gas temperatures.

OCIS codes: (120.0120) Instrumentation, measurement, and metrology; (140.0140) Lasers and laser optics; (120.1740) Combustion diagnostics; (140.2020) Diode lasers

1. Experimental Details

A very simple setup is used to perform in-situ measurements of water -vapour in the combustion chamber of a coal fired power plant. The beam of a Sharp FP-diode laser driven by the Melles Griot DLD06 was directed through the chamber and focused on a silicon detector by means of a gold coated mirror. We used a base band modulation scheme to determine line strengths in the 810 nm region. Two overlapping transition bands (000→112 and 000→211) have their origin in this region. We used lines at 12295.6863 cm^{-1} and 12296.0585 cm^{-1} which could simultanously be observed by modulating the operating current of the laser with a triangular function.

In this application (10 m path, 1100°C-1500°C, 10 Vol.-% H_2O) the peak absorption is about 2%. In addition to that severe and strongly variing interferences (like radiation emission, broad band absorption and scattering by dust and beam deflection by index of refraction fluctuations) are caused by the in-situ absorption path. They lead to transmission fluctuations which are by orders of magnitudes larger than the required absorption resolution. A narrow band filter was used to seperate the laser light from thermal radiation. The signal was digitized by means of a 12-bit ADC. Model functions were fitted to the data after correcting for the stated interferences in order to derive density and temperature data.

2. Characterization of the optical path

Laser light that passes the combustion chamber in a coal combustion process is subject to very strong scattering. This is mainly due to the high content of solid particles in the flue gases as ashes and burning coal particles. There are very strong variations in the intensity of light reaching the detector. The intensity varied at frequencies up to kilohertz, while typical observed transmissions were in the 10^{-4} region. At some conditions overall transmissons of the in-situ path of only 10^{-6} were found. The contrast of detected laser light to specious thermal radiation was about 10. These are very poor conditions compared to those that were found in waste incinerators where thermal radiation was relatively small and transmissions of several 10 per cent were typical [1-4].

The detected signal during a short time interval is shown in the upper part of fig. 1. The very sharp spikes reflect the laser current modulation at 1 kHz. The intensity of the transmitted light changes drastically within few milliseconds. The thermal emission is considered to be constant on short time scales and is insinuated in the graph. The distribution of ocurred transmissions is shown in the lower part of the figure.

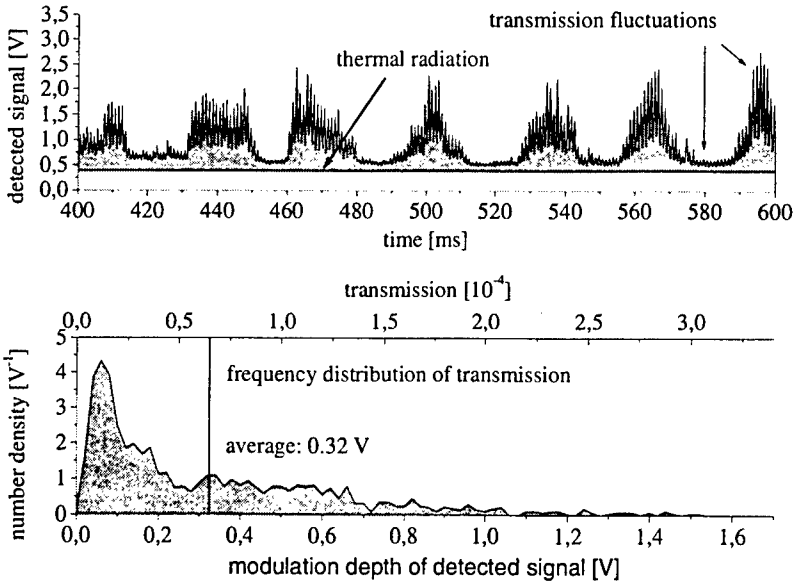

Fig. 1. Transmission properties of the optical path through the combustion chamber. See text for details.

3. Data analysis and results

The signal during a single modulation cycle is shown in fig. 2. It has been averaged over 20 cycles to increase the signal to noise ratio. The number of averaged cycles has to be much higher at lower transmissions to achieve the same signal quality.

The water-vapour absorption lines are so small that they can hardly be seen in the dc-signal. The absorption signal could be revealed at these very demanding conditions by correction for the modulation function and thermal radiation using a new data evaluation strategy. The level of background radiation as well as the laser intensity were derived from the modulation depth of the detected signal. The corrected data and the fitted line functions are shown in the lower part of the figure.

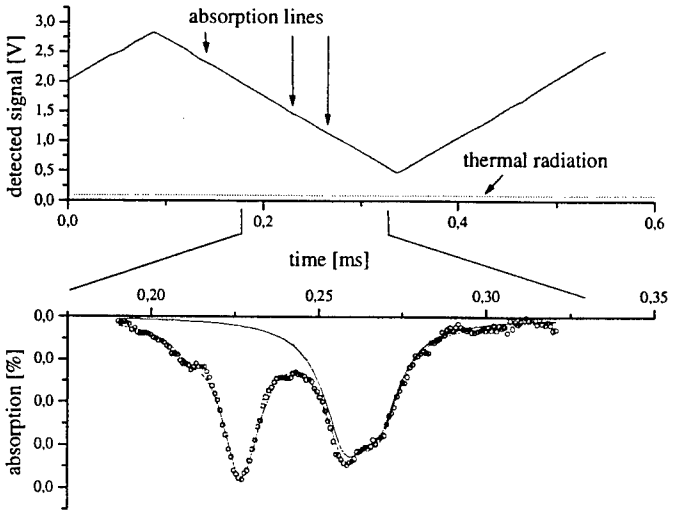

Fig. 2. Data analysis of the detected H_2O signal. Top: DC-Signal. Bottom: transmission corrected signal. See text for details.

Line parameters from the HITRAN compilation were used to obtain values for gas temperature and water-vapour concentration [4]. The line center positions could be used to determine the tuning rate of the diode laser, which is necessary to calculate the pressure independent integrated optical densities. The temperature was derived from the line-strength ratios. The water-vapour number densities were calculated using the isolated absorption line on the left in fig. 1 which is almost temperature independent between 1200 and 1400 Kelvin.

The time evolution of the in-situ H_2O and temperature signal over 4 hours is shown in figure 3. There is a definite correlation between our data and the process parameters. The H_2O number density increased when the coal feed was decreased. This could be due to a pure temperature effect as the density increases at lower temperatures. Temperature changes of about 150 Kelvin would explain the observed variations. In contrast, there is no evidence of this effect in our temperature data. Instead, there is a correlation between temperature and NO_2-concentration which is very temperature sensitive. Further investigation of correlation between these process parameters will be persued.

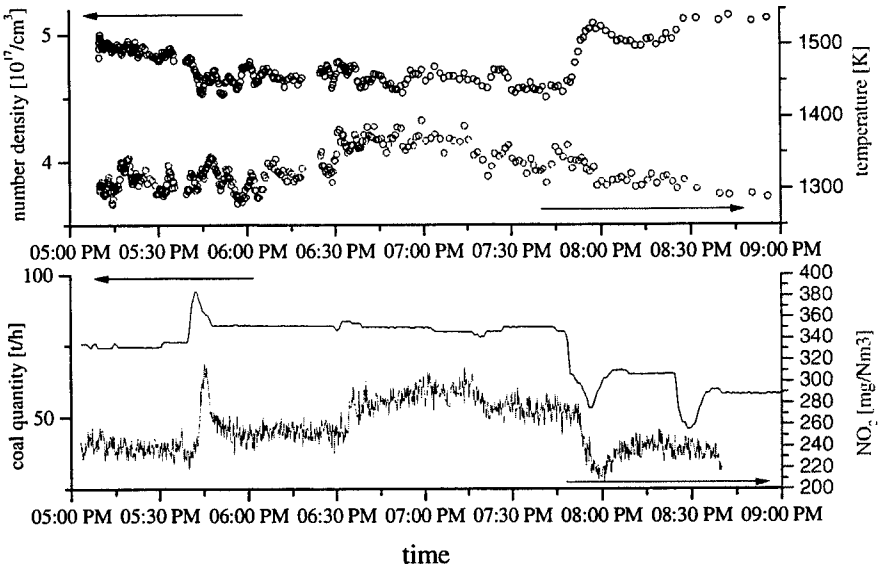

Fig. 3. Time evaluation of the in-situ signals. Top: H_2O concentration and gas temperature. Bottom: coal feed and NO_2 concentration.

4. Conclusions

It has been shown that even under very low transmission conditions (10^{-4} range), high background radiation and strong transmission fluctuations wavelength modulation spectroscopy can be used to quantitatively determine water vapour concentration and gas temperature using a simple base band modulation scheme combined with a new data evaluation strategy. In-situ water vapour and temperature data could be obtained in a 4 hour run in a full scale coal fired power plant and could be correlated to simultanously gathered process parameters. In spite of transmissions as low as 10^{-4} a fractional absorption resolution of 10^{-3} was achieved with a time resolution of 10 seconds.

5. References

[1] V. Ebert, J. Fitzer, I. Gerstenberg, K.-U. Pleban, H. Pitz, J. Wolfrum, M. Jochem, J. Martin, "Online monitoring of water vapour with a fiber coupled NIR-diode laser spectrometer", 5th Intern. Symposium on Gas Analysis by Tunable Diode Lasers, Freiburg, February 25-26 1998, 145.154, (VDI-Berichte 1366)

[2] V. Ebert, K.-U. Pleban, J. Wolfrum, "In-situ Oxygen-Monitoring using Near-Infrared Diode Lasers and Wavelength Modulation Spectroscopy", in *Laser Applications to Chemical and Environmental Analysis*, Technical Digest (Optical Society of America, Washington DC), pp 206-209, March 9-11, 1998, Orlando, Florida, USA, Paper No LWB3

[3] V. Ebert, J. Fitzer, I. Gerstenberg, K.-U. Pleban, H. Pitz, J. Wolfrum, M. Jochem, J. Martin, "Simultanous Laser-based In-Situ-Detection of Oxygen and Water in a Waste Incinerator for Active Combustion Control Purposes", 27th Symposium (Int.) on Combustion, The Combustion Institute, Pittsburgh, pp. 1301-1308 (1998)

[4] L. S. Rothman, R. R. Gamache, R. H. Tipping, C. P. Rinsland, M. A. H. Smith, D. C. Benner, V. M. Devi, J.-M. Flaud, C. Camy-Peyret, A. Perrin, A. Goldmann, S. T. Massie, L. R. Brown, and R. A. Toth, "The HITRAN molecular database: editions of 1991 and 1992," J. Quant. Spectrosc. Radiat. Transfer **48**, 469-507 (1992).

Rapid High Sensitivity Laser Absorption Measurements of Broad Band Absorbers in the Near Infrared Spectral Region

Kevin L. McNesby and Andrzej W. Miziolek
U.S. Army Research Laboratory
Aberdeen Proving Ground, MD 21005-5066

Ian A. McLaren
McLaren Research, Mountain View, CA 94043

Abstract

The development of a gas sensor to measure concentrations of binary mixtures of oxygen and several volatile organic compounds is described. The sensor is diode laser-based and all signal processing is performed digitally.

Introduction

This paper describes efforts towards the development of a high measurement speed binary gas sensor for simultaneous quantitative measurements of fuel and oxygen concentrations. The method of detection relies upon absorption of radiation near a wavelength of 760 nanometers by oxygen, and absorption of radiation near a wavelength of 1700 nanometers by hydrocarbon based fuels [1]. These spectral regions were selected because of the commercial availability of room temperature lasers and detectors operating in this spectral range and because laser radiation in this spectral range may be easily transported at low loss using inexpensive optical fibers. The sensor development consists of two concurrent parts. Part one consists of development of the method of measurement for gases with and without well resolved ro-vibrational transitions, and the design and construction of the light source and fiber optics necessary for remote measurement. Part two consists of the design and implementation of the instrument control electronics, and the interface to allow instrument control and data acquisition using a laptop computer. These efforts are described in what follows.

Background

Large and/or heavy molecules may not posses well resolved ro-vibrational absorption bands because of overlap between fundamental, combination, and overtone vibrations, and because of rotational constants which may be less than typical gas phase linewidths [2]. Figure 1 shows the near-infrared vapor phase absorption spectrum of the hydrocarbon-based turbine fuel JP-8 near a wavelength of 1700 nanometers (measured using a Fourier transform spectrometer), and the calculated absorption spectrum of oxygen near a wavelength of 760 nanometers [1]. For JP-8 vapor, the absorption spectrum near a wavelength of 1700 nanometers is essentially a continuous hump.

Detection

The proposed method for detection of JP-8 vapor, and all other detection methods based upon phase sensitive detection, takes advantage of the following relations:

$$\int_0^{\pi} m(\sin at)n(\sin bt)\,dt = 0 \qquad a \neq b \tag{1}$$

$$2C\int_0^{\pi} m(\sin at)n(\sin bt)\,dt = Cmn\pi \qquad a=b \tag{2}$$

For the discussion to follow, a and b are laser amplitude modulation frequencies, t is time, m and n are amplitudes, and C represents the number of periods over which the integration is carried out.

If the signal of interest is sinusoidal at frequency a (in equation 1), upon multiplication of this periodic signal by a reference sinusoid at frequency b, the resulting integral will be non-zero only when a=b. If the measurement is made at a frequency at which the Fourier component of the broadband noise in the signal is small, the integral of the product of the signal and the reference will exclude broadband signal noise, and only include the signal noise component at the reference frequency. Furthermore, if the signal amplitude is proportional to the desired quantity being measured, the result of the integration in (2) yields a value directly proportional to the quantity of interest.

Experimental Design

The proposed method uses two fixed frequency amplitude modulated lasers, each modulated at the same frequency but out of phase by 180 degrees [3]. These two lasers are combined to produce the probe beam. Ideally, the combined output of the two lasers will have an amplitude that is invariant with time (in the absence of absorption of either laser output intensity).

The key to the method is selection of one laser wavelength coincident with a wavelength absorbed by the gas of interest, and selection of the second laser wavelength in a region where no absorption is anticipated. When the mixed, modulated probe beam is passed through a gas which preferentially absorbs the laser radiation from laser one, the signal at the detector is modulated at the laser modulation frequency and, for small absorptions, has an amplitude proportional to the concentration of absorbing gas.

Modulation Design

A time (t) dependent square wave, S(a,n,t) at frequency a with amplitude n may be expressed as a sum of sine waves:

$$S(a,n,t) = 0.636n\sin(at) + 0.212n\sin(3at) + 0.1273n\sin(5at) + \ldots. \quad (3)$$

The signal at the detector, in the absence of any absorption, from two combined square wave amplitude modulated lasers differing in phase by 180 degrees is:

$$S1(a,n,t)+S2(a,m,t) = (0.636n\sin(at) + 0.212n\sin(3at) + 0.1273n\sin(5at) + \ldots.) + (0.636m\sin(at+\pi) + 0.212m\sin(3at+\pi) + 0.1273m\sin(5at+\pi) + \ldots. \quad (4)$$

Using the relationship $-\sin(ax) = \sin(ax + \pi)$, multiplying by the reference sine wave (frequency locked to the laser modulation) and integrating gives:

$$2C \int_0^{\pi} (S1(a,n,t) + S2(a,m,t))p\sin(at)\, dt = Cp\pi(.636n-.636m) \quad (5)$$

Here, p is the amplitude of the reference sine wave and C is the number of periods over which the integration is carried out. Equation 5 shows that for a probe beam composed of modulated lasers with equal amplitude, the signal at the detector is zero in the absence of any absorption. When the amplitudes of the modulated lasers differ, then the zero absorption signal must be corrected for offset. When the output radiation of laser two is preferentially absorbed by an analyte gas in the path of the probe beam, equation 5 becomes:

$$2C \int_0^{\pi} (S1(a,n,t) + S2(a,m,t))\, (\exp-\alpha cl)p\sin(bt)\, dt = Cp\pi(.636n-.636m(\exp(-\alpha cl))) \ , \quad (6)$$

Where α is the absorption coefficient of the analyte gas (cm^2/molecule), c is analyte gas concentration (molecules/cm^3), and l is the probe beam path length through the analyte gas (cm).

When the product $\alpha cl << 1$, $\exp(-\alpha cl)$ may be rewritten as1-A, (where A is absorbance = (αcl)) so equation 6 may be rewritten:

$$2C \int_0^{\pi} (S1(a,n,t) + S2(a,m,t)) (\exp-\alpha cl)\text{psin}(bt)\, dt = Cp\pi(.636n-.636m + .636mA) \quad (7)$$

For component lasers of equal amplitude, equation 7 becomes:

$$2C \int_0^{\pi} (S1(a,n,t) + S2(a,m,t)) (\exp-\alpha cl)\text{psin}(bt)\, dt = .636Cp\pi mA \quad (8)$$

Equation 8 shows that the summation of the amplitudes of the two out of phase lasers is directly proportional to the absorbance, A, and hence to the concentration of the analyte gas. Additionally, the signal is directly proportional to the amplitude of the reference sine wave, to the base amplitude of the detector laser signal, and to the number of periods over which the integration is carried out. Using sine wave modulation of the component lasers instead of square wave modulation changes equation 8 to:

$$2C \int_0^{\pi} (S1(a,n,t) + S2(a,m,t)) (\exp-\alpha cl)\text{psin}(bt)\, dt = Cp\pi mA \quad (9)$$

Equation 9 may be considered the working equation for using this simple method of analysis. It is interesting to note that changing from square wave to sinusoidal amplitude modulation results in almost a 40% increase in signal intensity.

This work is supported by the Next Generation Fire Suppression Technology Program (NGP).

Bibliography

[1] L.S. Rothman, R.R. Gamache, R.H. Tipping, C.P. Rinsland, M.A.H. Smith, D. Chris, V. Benner, M. Devi, J.-M Flaud, C. Camy-Peyret, A. Perrin, A. Goldman, S.T. Massie, L.R. Brown, R.A. Toth, "The Hitran Molecular Database: Editions of 1991 and 1992", J. Quant. Spectrosc. Radiat. Transfer, Vol. 48, p. 469, (1992).
[2] G. Hertzberg, Infrared and Raman Spectra, Van Nostrand Rheinhold Co., New York, 1945.
[3] personal communication, Mark Allen, Physical Sciences, Inc.

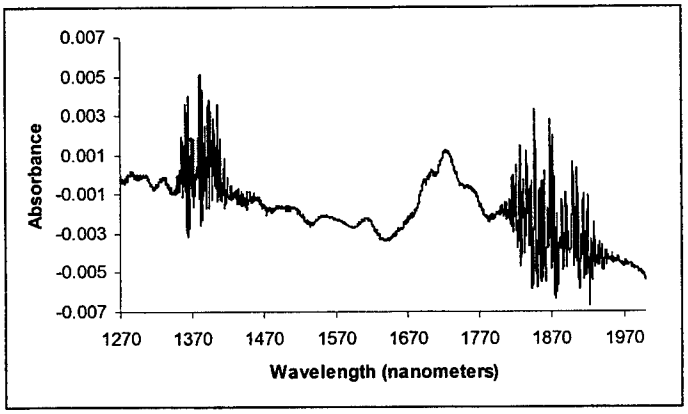

JP-8 vapor, 10 cm path length
355K, 4cm^{-1} resolution,
256 scans.

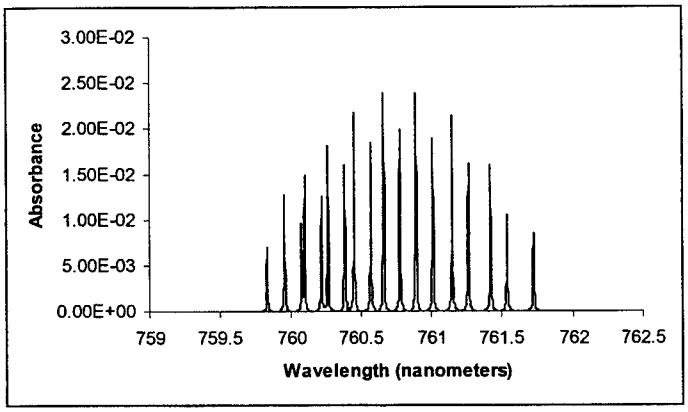

O_2, 1 m path length,
296K, calculated using
HITRAN database.

Figure 1: The measured near-infrared absorbance spectrum in the wavelength region near 1700 nanometers of JP-8 vapor at 355K, and the calculated absorbance spectrum in the wavelength region near 760 nanometers of O_2.

Measurement of NO, COF_2, and H_2O with a single mid-infrared laser

Patrick J. McCann, I-Na Chao, and Khosrow Namjou
School of Electrical and Computer Engineering, University of Oklahoma, 202 West Boyd Street, Room 219, Norman, OK 73019
pmccann@ou.edu

Abstract: A single IV-VI semiconductor mid-IR laser was used to measure NO, COF_2, and H_2O molecules. Potential applications for such measurements include medical diagnostics and plasma etching endpoint detection in semiconductor manufacturing.

OCIS codes: (120.6200) Spectrometers and spectroscopic instrumentation; (140.5960) Semiconductor lasers

1. Introduction

Mid-infrared lasers made from IV-VI semiconductors have the advantage of large tuning ranges due to the strong dependence of bandgap energy on temperature. This is in stark contrast to recently developed quantum cascade lasers which have only very limited tuning ranges. Consequently, individual IV-VI semiconductor lasers can be used to measure different molecules with widely separated absorption bands. We report here on the testing of a single IV-VI semiconductor mid-infrared laser using a Fourier transform infrared (FTIR) spectrometer. This laser exhibited several regions of strong single mode emission between 1848 cm^{-1} (5.41 μm) and 1989 cm^{-1} (5.03 μm) for heat sink temperatures between 90 K and 116 K. We also report on using this laser to measure nitric oxide (NO), carbonyl fluoride (COF_2), and water (H_2O). Applications for such measurements include medical diagnostics and plasma etching endpoint detection in semiconductor manufacturing.

2. Experimental Details

A PbEuSe IV-VI semiconductor laser (RMT Ltd.) mounted on a custom designed cold finger with an integrated heater, temperature sensor, and off-axis-parabolic mirror (OAPM) was cooled by a closed-cycle cryogenic refrigerator (CryoTiger, APD Cryogenics). The laser emission from this assembly passed through a CaF_2 window in the vacuum housing producing about a 10 mm diameter collimated beam. Before absorption spectroscopy experiments were performed, this laser was fully characterized over a range of heat sink temperatures, from 90 K to 116 K, and laser injection currents, from less than 400 mA to over 1000 mA, using a modular Fourier transform infrared (FTIR) spectrometer (MIR8000, Oriel) with a spectral resolution of 0.5 cm^{-1}. Several regions of repeatable single mode emission with tunable emission of over 3 cm^{-1} were observed. At least two of these regions overlapped with the absorption lines for nitric oxide (NO), carbonyl fluoride (COF_2), and water (H_2O), see Figures 1 and 2.

Molecular spectroscopy experiments were performed by focusing the collimated laser beam with an OAPM through a 10 cm long gas cell equipped with CaF_2 windows. The beam was then collected by a second OAPM and then focused with another OAPM onto a thermoelectrically-cooled HgCdZnTe infrared detector with a 6 μm cutoff wavelength (Boston Electronics). The laser was tuned by varying the above-threshold injection current with a 20 Hz saw tooth ramp. Second harmonic detection was employed by superimposing a 20 kHz AC current on the above-threshold injection current and the detector signal was sampled at 40 kHz by a lock-in amplifier (SRS). The output from the lock-in amplifier was fed into a computer through an analog-to-digital card and stored as a function of laser ramp time. This setup allowed collection of second harmonic absorption spectra every 100 msec. In addition, the use of a closed cycle refrigerator to cool the laser and a thermoelectrically-cooled detector enabled the assembly of a complete mid-infrared laser spectrometer that does not require cryostat refills with liquid nitrogen, a feature that allows this instrument to be used in non-laboratory settings.

Nitric oxide samples were prepared by introducing a 1 cm^3 volume of 10% NO from a gas cylinder into the 30 ml space of the 10 cm gas cell held at about 20 Torr. Very strong peaks in the measured second harmonic spectrum for NO were observed even though NO has a relatively weak electric dipole moment as reflected in line strengths in the low 10^{-21} range (see Figure 1). Based on the above numbers this gas sample had an NO concentration of 0.3%.

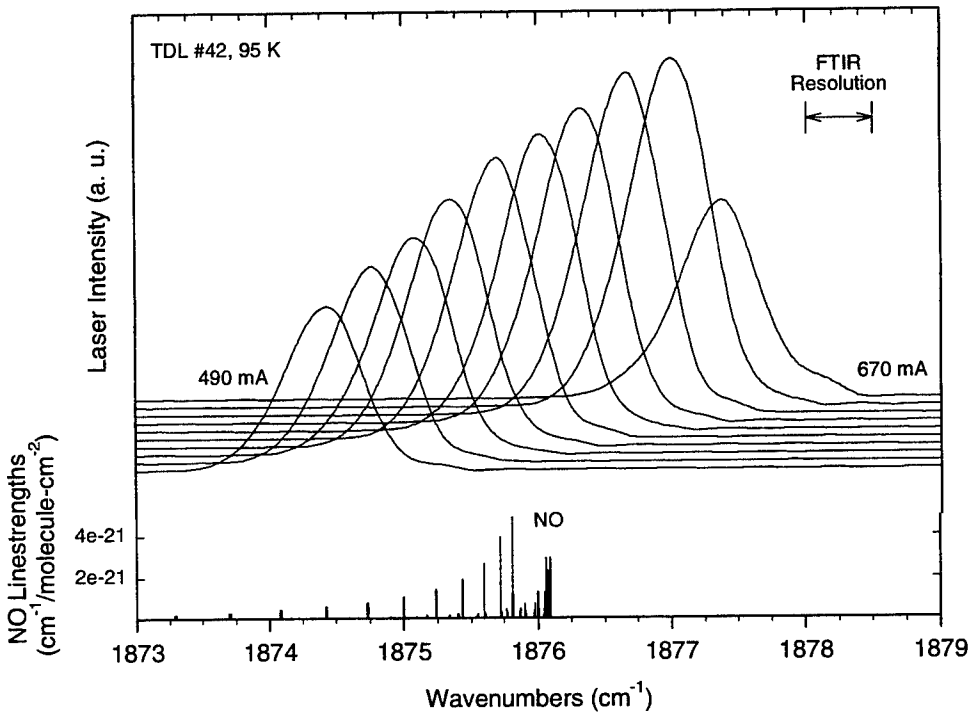

Figure 1: Mid-IR laser emission spectra at 95 K for injection currents of 490 mA to 670 mA in 20 mA increments as measured by a Fourier transform infrared (FTIR) spectrometer with a 0.5 cm^{-1} resolution. The laser line widths are actually much narrower that what are shown here. Absorption lines for NO molecules from the HITRAN96 database are shown at the bottom.

Using this value as a reference it is estimated that NO concentrations as low as 60 ppm can be measured in this 10 cm gas cell based upon signals obtained from the weaker NO absorption lines. Gas samples containing COF_2 were produced by burning polytetrafluoroethylene (Teflon) with a propane torch and collected into a 10 cm gas cell held at 200 Torr. Numerous peaks for COF_2 along with a peak for H_2O were observed in the second harmonic absorption spectrum. Distinct signals for closely spaced COF_2 absorption lines showed that this laser spectrometer had a spectral resolution of better than 0.005 cm^{-1}. Relative concentration values for both COF_2 and H_2O were also obtained from the second harmonic peak heights every 100 milliseconds over a 20 minute period following collection of the COF_2 gas sample. Exponential decreases in the concentrations of both molecules were observed, and fits to the data showed that both COF_2 and H_2O had lifetimes of about 12 minutes. These data suggest that COF_2 and H_2O react with each other and likely form HF and CO_2. This study has provided the first known experimental evidence that COF_2 is produced when Teflon is burned. Measured COF_2 concentration values were estimated to be as high as 200 ppm, well above the minimum threshold limit value of 2 ppm.

Potential applications for NO and COF_2 measurements include medical diagnostics and plasma etching endpoint detection in semiconductor manufacturing, respectively. Biological systems undergoing an inflammatory process can produce large amounts of NO as a result of the catalytic action of inducible nitric oxide synthase (iNOS) on the enzyme L-arginine. Measurement of NO in the exhaled breaths of patients can thus provide a diagnostic method for identifying a variety of pathologies. Such non-invasive breath testing can be used, for example, to provide early diagnosis of septic shock, a whole body inflammatory condition that afflicts an estimated 250,000 to 300,000 individuals in the USA alone and has a mortality rate of 50-60%. A common semiconductor manufacturing step involves plasma etching of silicon dioxide layers with fluorocarbon plasmas. COF_2 is known to be a reaction product during such etching and can be measured by simply passing a tunable mid-infrared laser beam through the plasma reaction chamber [1]. The ability to measure COF_2 with a time resolution of 0.1 seconds, as shown here, can make such measurements useful for monitoring the etching process. It is expected that *in situ* process monitoring

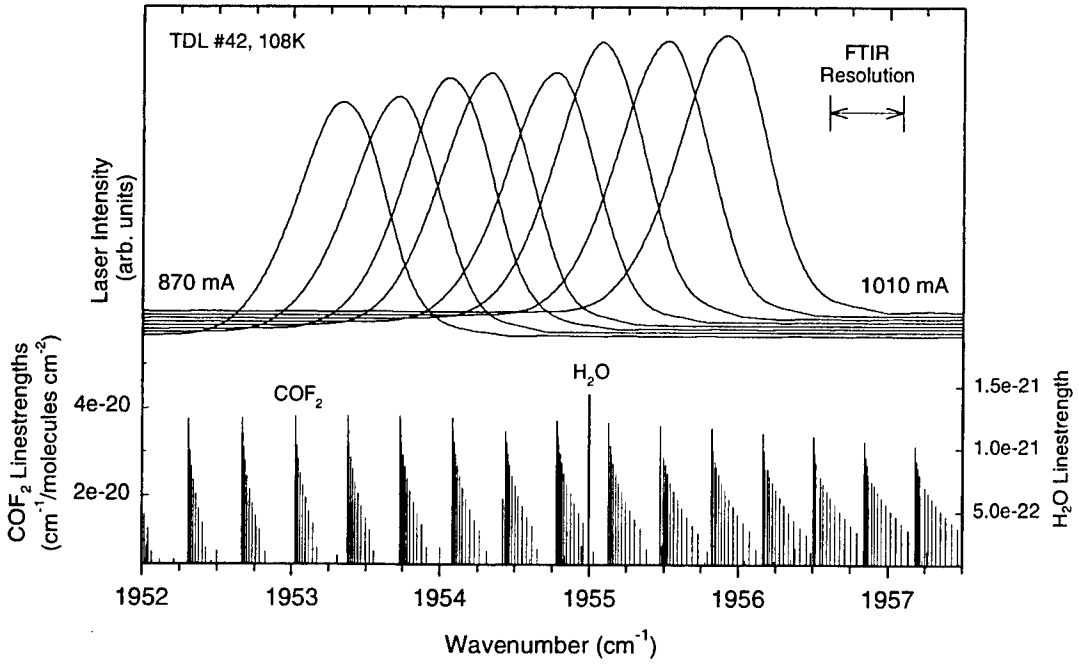

Figure 2: Mid-IR laser emission spectra at 108 K for injection currents of 870 mA to 1010 mA in 20 mA increments from the same laser that produced the spectra in Figure 1. Absorption lines for COF_2 and H_2O molecules from the HITRAN96 database are shown at the bottom.

measurements like these will provide critical information that can help increase chip yields. This will especially be true as dual damascene copper metallization techniques, which involve etching part way through thin SiO_2 layers, are adopted.

3. Summary

In summary, a IV-VI semiconductor laser was characterized using an FTIR spectrometer and then used to measure NO, COF_2 and H_2O. The wide temperature tuning range of this laser allowed measurement of these molecules even though they had widely separated absorption bands. Further advances in IV-VI laser technology such as the use of multiple quantum wells [2] and/or new packaging techniques [3] that can increase operating temperatures should make these widely tunable lasers attractive for a variety of molecular spectroscopy applications.

4. References

[1] D. B. Oh, A. Stanton, H. M. Anderson, M. Splichal, "In Situ Diode Laser Absorption Measurements of Plasma Species in a Gaseous Electronics Conference Reference Cell", *J. Vac. Sci. Technol. B* **13**, 954-961 (1995).

[2] P. J. McCann, K. Namjou, and X. M. Fang, "Above-Room-Temperature Continuous Wave Mid-Infrared Photoluminescence from PbSe/PbSrSe Quantum Wells", submitted to *Applied Physics Letters* (Aug. 20, 1999).

[3] P. J. McCann, "New Fabrication Method Promises Higher Mid-IR Laser Operating Temperatures", *Compound Semiconductor* **5** (4), 57 (May 1999).

Laser Applications to Chemical and Environmental Analysis

Poster Session

Saturday, February 12, 2000

SaC
6:00pm–8:30pm
Sunset

IRMA: A Tunable Infrared Multi-Component Acquisition System for Plasma Diagnostics

J. Röpcke and L. Mechold
Institut f. Niedertemperatur-Plasmaphysik, 17489 Greifswald, Friedrich-Ludwig-Jahn-Str.19, Germany
roepcke@inp-greifswald.de, mechold@ inp-greifswald.de

J. Anders and F. G. Wienhold
FhG Inst. f. Physikalische Meßtechnik, 79110 Freiburg i. Br., Heidenhofstr. 8, Germany
anders@ipm.fhg.de, wienhold@ ipm.fhg.de

D. Nelson, M. Zahniser, and J. Wormhoudt
Aerodyne Research, Inc., 45 Manning Rd, Billerica MA 01821-3976, USA
mz@aerodyne.com, ddn@aerodyne.com , jody@aerodyne.com

Abstract: IRMA is an InfraRed Multi-component Acquisition system for plasma diagnostics and control. Four independent tunable diode lasers can be temporally multiplexed, and directed into plasma reactors or into a multipass cell for exhaust gas detection.

OCIS codes: (300.6260) Spectroscopy, tunable diode lasers; (300.6390) Spectroscopy, molecular

1. Introduction

The monitoring of transient or stable plasma reaction products, in particular the measurement of their ground state concentrations, is the key to an improved understanding of plasma chemistry and kinetics in molecular non-equilibrium plasmas, which are of increasing interest for plasma processing. Infrared tunable diode laser absorption spectroscopy (TDLAS) is a modern promising technique with specific capabilities for effective and reliable on-line process control in research and industry. For plasma diagnostics and control a compact and transportable tunable infrared multi-component acquisition system, "IRMA", has been developed. The IRMA system contains 4 independent laser stations which can be temporally multiplexed. A multipass cell is included for exhaust gas detection. Based on rapid scan software using direct absorption with sweep integration, the absolute concentrations of several molecular species can be measured simultaneously within milliseconds and used as digital output for process control. This paper gives a survey of the optical subsytem, the data processing and the analysis technique. The flexibility and versatility of IRMA is demonstrated with an example of time-dependent species density measurement.

2. Optical Subsystem

The narrowband infrared emission of four lead-salt diode lasers is used to monitor the infrared absorption features of the target species. The instrument is contained on a 110- by 60-cm optical table. The four diode lasers are mounted in individual cold stations which are thermally coupled to the cold finger of a closed cycle cryostat (Model RGD 12/45, Leybold GmbH, Köln) by a wire structure etched in a 0.1 mm copper sheet. The temperature of each laser is controlled at milli-Kelvin precision in the range between 30 K and 100 K. A single cold station can be warmed to room temperature and decoupled from the main vacuum to allow laser replacement in typically 90 minutes time with the other laser stations remaining operative.

For each optical channel, the divergent laser emission is brought to an intermediate focus by an off-axis ellipsoidal mirror (OAE) and then collimated by an off-axis parabolic mirror (OAP). A fiber-coupled HeNe laser, an ocular or a reference pin-hole can be placed at the location of the intermediate focus for alignment purposes. During operation, the entrance slit of a grating monochromator, that serves as mode filter, is situated in this position. The blazed grating (90 lines/mm) is used in Littrow configuration with a lateral

angle of 12^0 separating the incident and diffracted beam. The desired wavelength is selected by an adequate tilt of the grating towards the optical table.

Plane steering mirrors direct the light of the four lasers to two combiner plates, each combining two beams. The two dual laser beams are then combined to a single quadruple beam by a third combiner. The two light paths emerging from this element are used for measurement and reference purposes, respectively. The measurement path can either be directed through a measurement cell external to the optical table after traversing the monochromator's exit slit in a focus formed by two OAPs, or through an internal multipass astigmatic Herriot cell (New Focus, Inc., model 5611). The Herriot cell entrance f-number is matched by an OAP-OAE combination with an intermediate focus where the exit slit of the monochromator can be located. In the reference path, the spectral absorption from small optical cells containing the target gas at high concentration is monitored as input for a laser emission wavelength control loop (line-locking). In this path, too, a monochromator exit slit can be placed at the intermediate focus of an OAP-OAE mirror arrangement.

The two measurement beams and the reference beam are focused on photoconductive infrared detectors (Model FTIR-16, 1.0, Graseby Inc.) mounted in liquid nitrogen cooled dewars. The optical quality of the imaging elements is near the diffraction limit. To avoid unwanted etalon background structure, wedge beam combiners and cell windows are used.

3. Data Processing and Analysis Technique

The data acquisition system for the four-channel tunable diode system consists of two 200 MHz Pentium computers combined with two high speed (300 kHz) boards (Scientific Solutions Lab Master AD boards) and two dual diode laser controllers (Laser Photonics, Model L5831) housed in a single transportable rack.

The data acquisition method is an advanced form of sweep integration which is carried out by a software package developed at Aerodyne Research, Inc. The software sweeps the laser frequency over the full infrared transition or group of transitions, then integrates the area under the transitions using nonlinear least squares fitting to the known spectral line shapes and positions. Frequency modulation (FM) techniques are not used, because the clear connection between the direct absorption spectrum and the species' concentration is preferred.

There are several advantages to this sweep integration approach. First, absolute species concentrations are returned from the nonlinear least squares fits so that external calibration is not required. The species concentrations may be determined from the absolute spectroscopic data available from the HITRAN or GEISA data bases or from user supplied data. Second, the line shape functions are known from theory and can be precisely calculated. Finally, this detailed understanding of the expected line shapes and positions allows the operator to easily monitor complex and overlapping spectral features by "fingerprint fitting." This is important because monitoring several transitions for one species can enhance sensitivity and is sometimes necessary—— especially for larger molecules. In addition, fingerprint fitting allows one to monitor multiple species simultaneously, since overlapping lines can be used, and it even allows fitting unknown lines which overlap the spectrum of the desired species.

The basic functions of the program for controlling two laser diodes are as follows. The software creates a waveform which is used to modulate the frequency of the laser or lasers. The digital waveform is converted to an analog voltage at a rate of 300 kHz using a 12 bit digital to analog converter. Typically 150 points are used to represent the waveforms so that each frequency sweep is 500 μs in duration. The current is varied linearly for a given time period, which causes a variation of the frequency of the laser light that the diode emits. Then the current is lowered to a much lower value, below the threshold for laser emission. This provides a measurement of detector output in the absence of laser light. Each laser is below its light emission threshold while the other is swept. Both lasers are below threshold at the end of the scan.

The detector output voltage is sampled by an analog-to-digital converter using the same data acquisition board. The individual spectra are automatically transferred to the computer's extended memory using direct memory access. The program divides the data in extended memory into individual sweeps and averages the sweeps to produce one resultant spectrum for each laser. The spectra are coaveraged using assembly language averaging routines in order to maintain a 100% duty cycle. The resultant spectra are analyzed spectroscopically to determine the concentrations or column densities of any species which absorb in that spectral window. The column densities are displayed to the operator, saved to disk and analyzed.

An example spectrum measured in a H_2-CH_4 plasma excited in a GEC reactor [1] is shown in Fig. 1. In that specific case the signal intensity was too low to fully use the capabilities of time resolution, since we had to coaverage spectra for about two seconds to get reasonable results. Acetylene and methane were measured by recording the change in absorption of individual rotational-vibrational lines at a frequency of 1303 cm^{-1} (7.67 μm). The diode laser was scanned over a spectral region of 0.2 cm^{-1} by varying the laser current in order to obtain a baseline for the pair of spectral lines. The laser was turned off at the end of each scan to obtain the total laser intensity during the scan.

The spectra are analyzed in real-time using the Levenberg-Marquardt non-linear least-squares method to obtain the best fit to the Voigt line shape and a baseline polynomial. Nonlinearity in laser frequency as a function of laser current is described by the laser tuning rate $T = C_1 + C_2 \exp(-C_3 t)$, where t is time since the laser was turned on and the C_i are free parameters which are determined using a germanium etalon. The average CH_4 and C_2H_2 densities in the laser beam were calculated from the measured fractional absorption using the tabulated line strengths and pressure broadening coefficients from the HITRAN data base. The software will fit up to four species simultaneously using up to 45 individual spectral lines per species.

Figure 2 shows the result of a stream mode data acquisition, giving an example of online measurements especially useful for process control. In the graph one can see how the change of a methane admixture to hydrogen and switching the plasma on and off influences the species densities of CH_4 and C_2H_2 (which were calculated using the lines shown in Fig. 1) in the laser beam path.

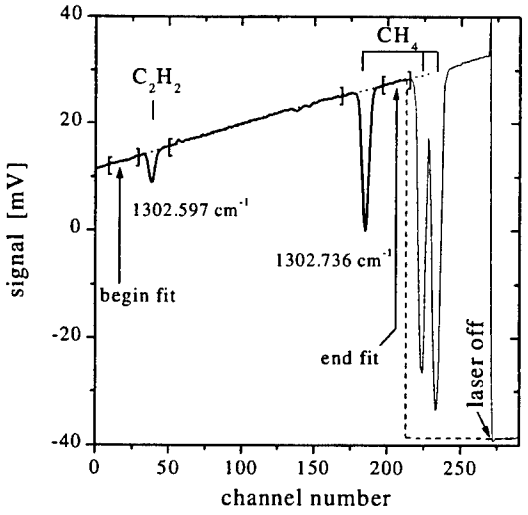

Fig. 1: Measured and fitted absorption spectrum of methane and acetylene in a H_2-CH_4 plasma ($[H_2]$:$[CH_4]$ = 1:1, ϕ_{total} = 66 sccm, p = 100 Torr, P = 50 W) [1].

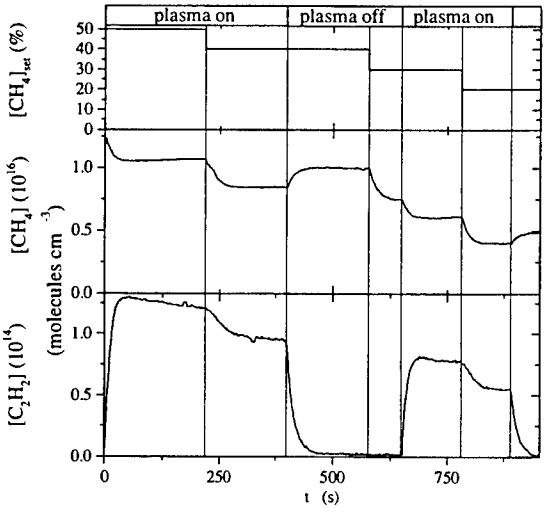

Fig. 2: Results of stream mode data acquisition of species densities with varying methane admixture using the absorption lines from Fig. 1 [1].

References

[1] J. Röpcke et al *Proc. Front. in Low Temp. Plasma Diagnostics III, Saillon,* (1999) p. 113.

Pseudo-random tone burst modulation for active remote sensing of gases using diode lasers

Chris Hovde
Southwest Sciences, Inc., Ohio Operations Office, 6837 Main Street, Cincinnati, OH 45244 USA
Tel. (513) 272-1323, Fax (513) 272-6053 dchovde@swsciences.com

Abstract: Applying bursts of wavelength modulation to a diode laser in a pseudo-random pattern measures the spectrally narrow, wavelength dependent part of the power absorption that can be used to compute range-resolved trace gas concentrations.

OCIS codes: (280.1910, 300.6380, 300.6360) remote sensing, DIAL, spectroscopy

1. Introduction

Remote measurement of trace gases is important in pollutant monitoring. Active techniques such as differential absorption lidar (DIAL) can provide range resolved gas concentrations at distances up to several kilometers. To achieve wider use and greater impact, DIAL instruments must use laser sources that are simple to operate and place in the field. Diode lasers are well suited to field operation due to their small size, low power requirements and ease of operation. However, diode lasers produce very low peak power levels. Special techniques are required to apply diode lasers to DIAL measurements.

Like lidar, the technique on which it is based, DIAL measures the light scattered back from the atmosphere. Whereas in lidar the back-scattering amplitude is itself the desired signal, in DIAL the wavelength dependent absorption is the desired signal. One is interested in the ratio of the power at a strongly absorbed wavelength (on the spectral line) to the power at some nearby reference wavelength (off-line) with otherwise similar propagation characteristics. Natural variations in the atmospheric scattering can appear as noise in the DIAL measurement. The laser power and the telescope alignment may also vary. These variations may not have a "white noise" spectrum. To minimize the effects of these sources of noise, the on line and off line measurements should be made as close together in time as possible. This paper describes a DIAL technique based on pseudo-random lidar for measuring the on-line and off-line signals over time scales of a few microseconds and some initial experiments to verify its operation.

2. Pseudo Random Lidar

The pseudo-random or pseudo-noise modulation method was first demonstrated for lidar by Takeuchi et al [1,2]. In their approach, the laser is modulated with a sequence of ones (laser on) and zeroes (laser off). They took advantage of the delta-function properties of certain pseudo-random patterns of length 2^n-1 [3]. The return signal was digitized once per clock cycle of the pseudo random code into a buffer. The range resolved return power is determined by cross-correlating the signal buffer with a pseudo-random pattern related to that used to modulate the laser, in which negative ones replace the zeroes.

The advantage of the pseudo-noise method is that the laser is operated at high duty cycle, helping to offset the low peak power that can be achieved with the diode laser. A significant disadvantage compared to pulsed lidar is that the shot noise from strong signals at close range will affect the recovery of signals from all ranges. Amplitude modulation suffers from higher laser noise, which can be an important noise source for strong return signals.

Abshire and Rall applied the pseudo-random modulation method to DIAL measurements of water vapor [4,5]. Their approach involved amplitude modulating the laser with a pseudo random code while accumulating data for up to a minute at an on-line wavelength, then shifting the laser wavelength to an off-line value and accumulating for another minute. This approach has the disadvantage that the on-line and off-line return signals are probed at different times. For typical wind speeds on the order of 1 to 10 m s^{-1} and beam profiles of about 1 m, the column of air probed by the beam is replaced in 0.1 to 1 s.

Varying its injection current modulates the wavelength as well as the amplitude of a diode laser. Instead of modulating the amplitude of the laser, one can modulate its wavelength or frequency. Wavelength modulation and frequency modulation techniques have been applied very successfully to *in situ* trace gas detection in both lab and field instruments, achieving detection limited by residual etalon fringes or by shot noise. Tone burst modulation is a variation of wavelength modulation in which the modulating waveform is periodically turned on and off. When the

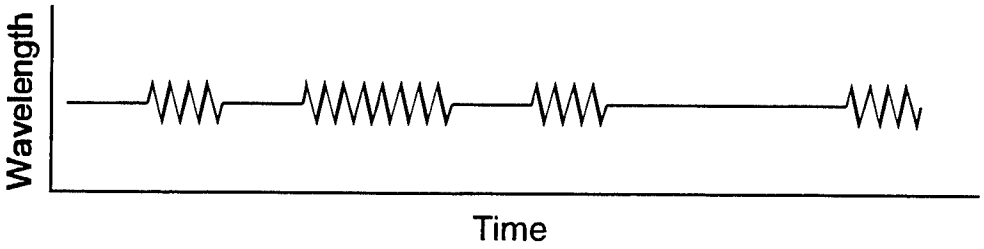

Fig. 1. Modulation of the diode laser current with a pseudo-random tone burst waveform results in modulation of the laser wavelength.

laser is tuned to line center and the modulation is off, the target gas absorbs some fraction of the laser power. When the modulation is turned on, the laser wavelength rapidly moves from one wing of the line to the other, spending most of its time where the absorption is weakest. As a result, more power is transmitted when the tone is on than when it is off. Lock-in detection at the on/off frequency recovers the absorption signal.

By applying the tone burst modulation using a pseudo-random code, the path-integrated absorbance from each range element results in a pseudo-random absorption (fig. 1) of the laser light with a delay corresponding to the round trip time. A simplified model of the return signal in the single scattering limit is

$$S(t) = \int P(t-\tau) \left(\frac{2}{c\tau}\right)^2 \beta\left(\frac{c\tau}{2}\right) \exp(-\alpha(\lambda(t-\tau))\, d\tau \qquad (1)$$

Here S is the signal amplitude, P is the laser power, t is time, τ is the round trip time, β is the atmospheric scattering amplitude, α is the wavelength dependent absorbance (and thus is proportional to the column density of the target gas), and λ is the instantaneous wavelength. In this model, the signal arises from light projected at an earlier time, t-τ, which travels a round trip distance $c\tau$. Each distance is weighted by a geometric factor for the incoherent return beam, the range dependent value of the scattering amplitude, and the attenuation due to atmospheric absorption at that projected wavelength.

Cross correlating the signal S(t) with the pseudo-random code yields range-resolved values of the product $\beta\exp(\alpha)$. In order to extract gas concentrations, it is still necessary to measure separately the unknown atmospheric scattering β. One possible method is to use the amplitude modulation that accompanies the current modulation of the laser. By demodulating the return signal at the tone burst frequency, it should be possible to recover the high frequency components of Eq. 1. However, because the demodulation phase varies with distance as well, this approach may work best only in cases where a single range dominates the scattering, for example, when using topographic targets such as the sides of buildings to check for a gas located along the line of site.

3. Experiments

The wavelength modulation approach was tested using a 1760 nm diode laser to probe an overtone transition of hydrogen chloride, HCl. A 40 cm long sample cell was evacuated, then filled with HCl to a pressure of 1.3 kPa, producing an absorbance of nearly 100% at line center. The laser current was modulated with a tone burst waveform as shown in Fig. 1. The tone burst waveform was generated using a programmable digital function generator; the modulation frequency was 10 MHz and the pseudo-random clock rate was 5 MHz. Thus, during an single "on" cycle, there are exactly 2 periods of the modulation waveform. After passing through the HCl sample, the laser light was directed onto a white card. An f#/2 lens imaged the spot onto an extended wavelength range InGaAs photodetector, which was also exposed to ambient lighting. The resulting photocurrent was converted to a voltage using a 100 Ω resistor, and digitized without further amplification at 10 Msample/s with a fast transient digitizer with a 3.6 MHz anti-aliasing filter to attenuate high frequency noise.

The resulting signal is shown in Fig. 2. The signal at each point is proportional to the power transmitted by the HCl sample, averaged over the measurement bandwidth. The data were collected in just a single shot. The transmitted power clearly follows the applied modulation waveform.

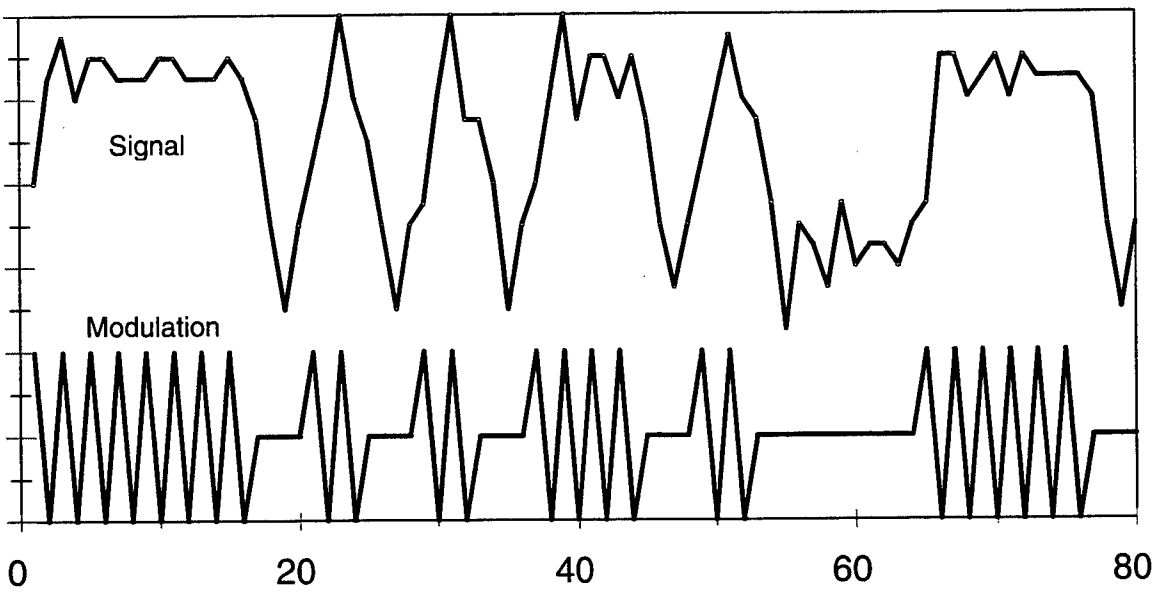

Fig. 2. First eighty points of a pseudo-random tone burst signal obtained through 1.3 kPa HCl sample 40 cm long to give about 100% absorbance at line center. Bottom trace shows the applied modulation. Note that signal power is lowest when modulation is off

4. Conclusions

The pseudo-random tone burst modulation method makes a very rapid comparison between the on-line and off-line transmission of the atmosphere and thus can suppress noise due to atmospheric turbulence, wind, power variations of the laser, or changes in the optical alignment. However, the method must be combined with a method for measuring the atmospheric back scattering amplitude in order to get quantitative, range resolved gas concentrations. Pseudo-random tone burst DIAL may find its greatest usefulness when the return signal is dominated by scattering from a single range, or when fluctuations in the back scattering amplitude are very large.

This work was supported by the Air Force through the SBIR program under contract F-19628-98-C-0055.

5. References

1. N. Takeuchi, N. Sugimoto, H. Baba and K. Sakurai, "Random Modulation CW Lidar," Appl. Opt. **22**, 1382-1386 (1983).
2. N. Takeuchi, H. Baba, K. Sakurai and T. Ueno, "Diode laser random modulation cw lidar," Appl. Opt. **25**, 63-67 (1986).
3. C. Nagasawa, M. Abo, H. Yamamoto, and O. Uchino, "Random modulation cw lidar using new random sequence," App. Opt. **29**, 1466-1470 (1990).
4. J. B. Abshire and J. A. R. Rall, presented at "Semiconductor Lasers: Advanced Devices and Applications," paper TuB1-1, Optical Society of America, Keystone CO, August 1995.
5. J. A. R. Rall, Ph. D. Thesis, NASA Technical Memorandum 104610, 1994.

Development of a real-time continuous emissions monitor for polychlorinated dioxins and furans

Harald Oser, Michael J. Coggiola, Gregory W. Faris, and David R. Crosley
Molecular Physics Laboratory, SRI International, Menlo Park, CA
Ph: 650-859-3311, Fax: 650-859-6196, harald.oser@sri.com

Abstract: The need for a continuous emissions monitor for the determination of dioxins and furans at realistic (ppt or sub-ppt) concentrations in real time (minutes) is widely recognized in the waste combustion community. The key issues are overall sensitivity, and selectivity among the many congeners found in real applications. At SRI International we have begun a project designed to meet these needs. Our instrument is based on supersonic jet expansion and cooling, followed by resonantly enhanced multiphoton ionization (REMPI) into a mass spectrometer. This furnishes the dual selectivity of tuned laser absorption and mass analysis. We have made direct measurements of several polychlorinated dioxins and furans using a one-color REMPI scheme, and we have demonstrated a two-color excitation scheme.

OCIS codes: (010.1120) Air pollution monitoring; (120.1740) Combustion diagnostics

1. Introduction

Emission control strategies must ultimately rely upon a careful assessment of the link between health effects and ambient, human exposure levels to hazardous air pollutants (HAPs). Because polychlorinated organic compounds in general, and dioxins and furans in particular, are among the most toxic of HAPs, SRI International is developing a continuous emission monitor (CEM) for these species using the jet-REMPI technique under support from the U.S. Department of Energy (DOE). The unique capability for real-time detection and identification of these and other toxic HAPs directly in incinerator emissions using a CEM instrument is an essential component of emissions modeling, dispersion modeling, source apportionment, and ultimately, of human exposure modeling. Jet-REMPI is the only instrumental technique that can provide the speed, breadth, and sensitivity of measurement capabilities that are required in support of the development of a comprehensive strategy to monitor and control emissions of dioxins and furans from waste incinerators.

Our technique will provide real-time dioxin and furan concentrations rather than the multi-hour or multi-day averages as in the case for existing, conventional sampling and analysis methods. This capability will allow a detailed investigation of the relationship between dioxin emissions and the incinerator operating parameters and waste feed characteristics. Such a study may reveal that "puffs" (transient pollutant emission events) account for a majority of the dioxin emissions, and hence only short-term control methods would be required to meet time-averaged regulatory emission limits. Such control strategies may be much more cost effective than full-time emission control approaches. Tailoring the emission control strategy in response to minute-by-minute changes in the emission of hazardous pollutants can only be accomplished if a suitable CEM is available, such as our jet-REMPI based instrument.

2. Materials and methods

Our approach to acquiring the data on dioxin and furan levels is to perform direct measurement of specific congeners using the jet-REMPI method. Jet-REMPI is an ultra-sensitive analytical technique that can selectively identify and quantify vapor-phase constituents present at ppt levels in incinerator emissions without preconcentration or sample collection.

In recent years, many significant improvements have been made in the detection of hazardous, vapor-phase, organic compounds of environmental importance. Several research groups, including SRI, [1-3], DLR, [4], and The Technical University of Munich, Germany, [5], have demonstrated instruments or components of instruments based on REMPI and mass spectrometry.

Ions produced by resonance enhanced multiphoton ionization (REMPI) are typically detected using a time-of-flight mass spectrometer (TOF-MS) that takes advantage of the pulsed nature and well-defined temporal character of laser ionization. The simultaneous detection by mass and wavelength yields extremely high chemical selectivity crucial to identifying one trace compound in the midst of many other similar ones. Typical sensitivities of conventional REMPI TOF-MS systems that do not use sample molecule cooling are in the mg/dscm range and

higher, which is totally insufficient either for a laboratory system or for regulatory monitoring of chlorinated aromatics in a waste treatment process such as an incinerator.

A major improvement in sensitivity without loss in selectivity can be achieved using a pulsed gas valve that produces a supersonic expansion. Pulsed gas valves provide a number of advantages over continuous gas inlets, including reduced gas flow and hence smaller vacuum pumps, higher local gas densities, well-defined spatial distribution, significantly reduced translational energy distribution orthogonal to the propagation direction, and reduced internal (vibrational and rotational) temperatures leading to greatly enhanced spectroscopic resolution.

REMPI is a highly sensitive, highly species-selective, gas-phase analysis technique that has been applied to numerous problems in molecular spectroscopy and combustion research. For REMPI of complex molecules, such as dioxins, the spectra can be simplified greatly by expansion through a nozzle. Adiabatic expansion results in low sample temperatures, which increases the electronic ground state population and narrows the resonance line widths through reduction in molecule velocities (reduced Doppler or temperature broadening) and through reduction in transition-perturbing collisions (reduced pressure broadening). These reduced linewidths lessen the ionization of other molecular species (interferences – leading to improved selectivity – and make the peak absorption larger—leading to improved sensitivity. One or more wavelengths are used to ionize the cooled gas molecules by absorption of two or more photons, one of which must be resonant with an electronic transition in the target molecule.

Because different isomers of a given chemical composition may have very different toxicities, it is essential that a measurement instrument be capable of distinguishing among isomers. Our instrument is able to do this without any sample pre-separation, such as by gas chromatography, for example, because of the inherent ability of optical spectroscopy (REMPI in this case) to readily distinguish among isomers. The selectivity of the optical spectroscopy is vastly improved through the pulsed nozzle cooling effects, as discussed above.

The mass spectrometric capabilities of our reflectron-type TOF mass analyzer include an upper mass range typically up to 500 amu, limited only by the size of the mass spectral data files, and mass resolution ($m/\Delta m$) greater than 500.

3. Results and discussion

The laser system used in our preliminary experiments described below consists of a Continuum Powerlite Precision 9010 Nd:YAG and Sunlite EX OPO with a nominal tuning range in the visible between 445 and 710 nm, a 5 ns pulse width, and a repetition rate of 10 Hz. Frequency doubling is achieved using an Inrad autotracker II. The optical linewidth of the system is approximately 0.1 cm^{-1}.

The pulsed valve is an unmodified General Valve series 9 unit, with an orifice diameter of 0.5 mm. The nominal opening time was 150 μs, with a 2.5 cm separation between the exit of the valve and the ionization region. With the sample reservoir at atmospheric pressure, the two 250 l/s turbomolecular pumps (Varian Turbo V-250) maintain pressures in the ionization chamber and mass spectrometer regions of 10^{-5} Torr, and 5×10^{-7} Torr, respectively.

The ionization conditions used to acquire the data included a pulse energy of approximately 1mJ in a 1.5 mm diameter laser beam. Ion signals from the R. M. Jordan reflectron TOF-MS were amplified by a Ortec 9306 preamplifier with a gain of 85 and a 1 GHz bandwidth, and recorded by a 500 MHz, Signatec DA500A digitizer.

A sample consisting of a mixture of equal amounts of 2,7-dichlorodibenzodiozxin (DCDD) and 2,8-DCDD was used to demonstrate isomer selectivity. To simplify these tests, a small quantity of the liquid mixture was injected into a stainless steel sample flask on the upstream side of the pulsed valve, and room air was used as a carrier gas. All components in the sample stream were heated to prevent condensation. Figure 1 shows the ion signal recorded at m/z 252, corresponding to the parent ion of both isomers. Several individual absorption features are labeled to show which isomer gave rise to the signal. Assignment of these absorption features was made by measuring the jet-REMPI spectra for each isomer separately.

For many molecules of interest, particularly tetrachlorinated and higher dioxins and furans, the one-color, two-photon REMPI excitation and ionization scheme is not possible as the first excited state lies less than half to the ionization limit. For those molecules, a two-color REMPI scheme must be used where a tunable wavelength is used to excite the first excited state resonantly, and a second, fixed wavelength is used to achieve ionization. To demonstrate the two-color approach, we have examined the jet-REMPI wavelength dependence for 1,2-dichlorobenzene. Figure 2 shows the m/z 146 ion signal measured using a combination of tunable uv from the OPO, and 266 nm produced by quadrupling the Nd:YAG fundamental. Since 1,2-dichlorobenzene can be ionized by the one-color, two-photon scheme, we have shown that ion signal in Figure 2 as well. Note that the large absorption peak at 272.61 nm appears using both ionization schemes. However, the absorption peak at 273.58 nm appears only in the two-color signal. This feature arises from the absorption of one photon that is resonant with vibrationally excited ground state molecules, followed by absorption of a 266 nm photon to produce ionization.

Because the absorption of a second photon at 273.58 nm cannot ionize 1,2-dichlorobenzene, this feature does not appear in the one-color REMPI spectrum. As shown in Figure 2, the threshold for the one-color, two-photon process is approximately 273 nm.

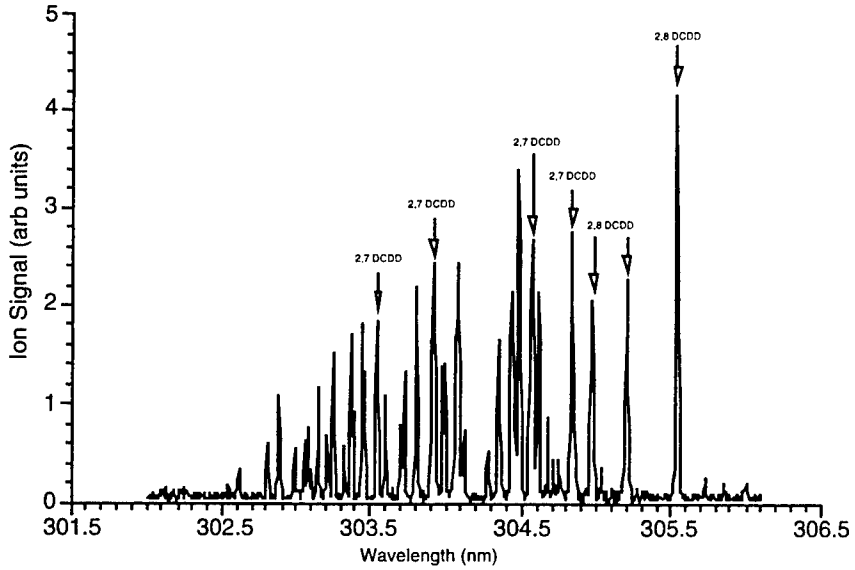

Fig. 1. Jet-REMPI wavelength dependence for a equimolar mixture of 2,7-DCDD and 2,8-DCDD measured at m/z 252.

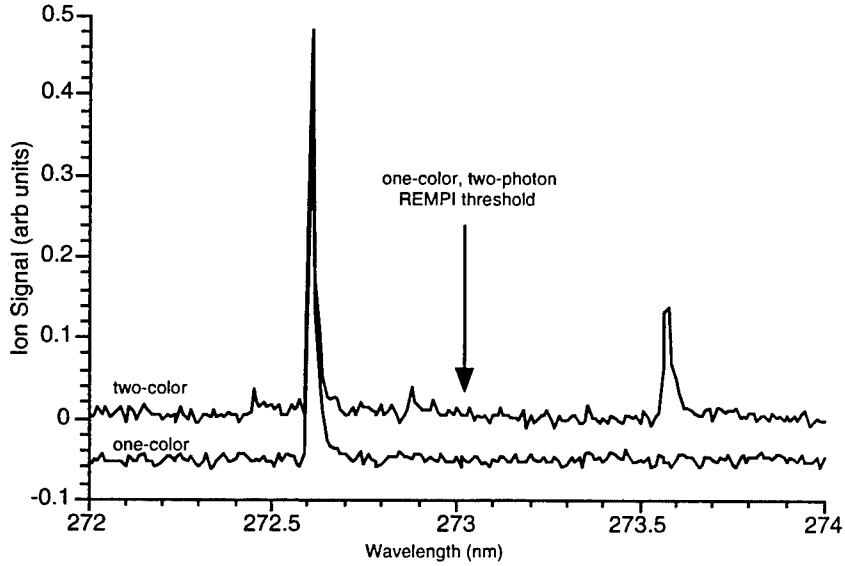

Fig. 2. Wavelength dependence of the m/z 146 ion signal for 1,2-dichlorobenzene recorded using both a one-color, two-photon excitation/ionization scheme, and a two-color, two-photon REMPI scheme.

4. References

1. E. Y. Xu, T. Tsuboi, R. Kachru, and H. Helm, "Four-photon dissociation and ionization of H_2," Phys Rev. **A36**, 5645-5653 (1987).
2. M. Rossi and D. J. Eckstrom, "Quantitative aspects of benzene photoionization at 248 nm," Chem. Phys. Lett. **120**, 118-123 (1985).
3. M. Rossi and H. Helm, "Multiphoton ionization of vinylchloride, trifluoroethylene, and benzene at 193 nm," J. Chem. Phys. **87**, 902-909 (1987).
4. H. Oser, R. Thanner, H. H. Grotheer, "Jet-REMPI for the detection of trace gas compounds in complex gas mixtures, a tool for kinetic research and incinerator process control," Comb. Sci. and Tech. **116**, 567-572 (1996).
5. R. Zimmermann, U. Boesl, D. Lenoir, A. Kettrup, Th. L. Grebner, and H. J. Neusser, "The ionization energies of polychlorinated dibenzo-p-dioxins: new experimental results and theoretical studies," Int. J. Mass Spectr. and Ion Phys. **145**, 97-108 (1995).

Robust external cavity diode laser (ECDL) and their application in water vapor and saturated-absorption rubidium spectroscopy

F. Schael
Institut für Physikalische und Theoretische Chemie, Universität Erlangen-Nürnberg, Egerlangstr. 3, D-91058 Erlangen, Germany
Phone: +49 9131 852 7317, FAX: +49 9131 852 8696,
schael@pctc.chemie.uni-erlangen.de

L. Hildebrandt, R. Knispel, J. Sacher
Sacher Lasertechnik, Hannah-Ahrendt-Str. 3-7, D-35037 Marburg,Germany
Phone: +49 6421 305 290, FAX: +49 6421 305 299, email: Lars@sacher.de

Abstract: External cavity diode laser (ECDL) in Littman and Littrow configuration are optimized for optical sensor applications in industrial environments. The performance of the ECDL are demonstrated by water vapor absorption spectroscopy and rubidium saturated-absorption spectroscopy.

OCIS codes: (020.0020) Atomic and molecular physics; (140.2020) Diode laser; (300.6260) Diode laser spectroscopy

Recent improvements of room temperature diode laser technology for communications and data storage applications have given rise to enhanced availabilty of semiconductor lasers with wavelengths in the near infrared spectral region. However, wavelength tuning characteristics of commercially available standard laser diodes are far from ideal, and thus many applications in the near infrared are limited to the use of relatively expensive distributed feedback (DFB) laser diodes. External cavity diode lasers (ECDL), in which antireflection coated Fabry Perot laser diodes can be utilized, can provide a cost-effective alternative with wavelength tuning ranges of up to 100 nm (depending on the center laser wavelength) and linewidths of several hundred kHz. They are small-sized and amenable to electronic high frequency modulation which makes these light sources desirable for sensor applications. However, ECDL are often too sensitive to vibrations and often require extensive alignment prior to use.

The objective of the current work is to optimize the optical design of ECDL for robust optical sensor applications. The performance of the laser systems is demonstrated (i) in a diode laser spectrometer for monitoring and spectroscopic studies of water vapor and (ii) in a saturated-absorption spectrometer for spectroscopic studies of rubidium vapor.

Common ECDL designs use gratings as wavelength-selective elements with external optics either in Littrow configuration, where the laser output beam is coupled out of the resonator via the grating and the wavelength tuning is achieved by turning the grating, or in Littman configuration, in which the resonator length and thus the wavelength tuning is achieved by moving an additional reflecting element (e. g. a mirror or prism) inside the laser resonator.

In the current work, ECDL in both Littman and Littrow configurations were compared and optimized for applications in industrial environments and sensor technology. Wavelength regions that are currently covered by our lasers with various laser diodes include the regions 625 - 700, 730 -1090, and 1250 - 1660 nm, limited at this point by the avalability of the laser diodes. Spectral linewidths of typically 1 MHz are achieved, which make the laser suitable for atomic and gas phase molecular spectroscopy. The mode-hop free tuning range obtained was at least 50 GHz and at least 4 GHz for the Littman and for the Littrow ECDL, repectively, and was dependent on the central wavelength and the piezoelectric tuning range.

For the (patented) Littman configuration, a prism was employed as reflecting element in the external laser resonator, which leads to a considerable simplification of alignment procedures and enhancement of robustness of the laser system. The Littman ECDL was optimized for wavelength scanning applications and

spectroscopy. The Littrow ECDL is more suited for applications where high output power is needed and change of wavelength is rarely required. For example, output power of 70 mW at 780 nm from a Littrow ECDL was obtained in this work, which is to our knowledge the highest output power described in the literature for an ECDL at this wavelength.

Simple and cost-effective active wavelength stabilization of the ECDL is performed using a line-locking procedure on either water or rubidium vapor absorption lines.

The optimized ECDL in Littman configuration was utilized in a spectrometer for atmospheric monitoring and spectroscopic studies of water vapor. Direct absorption and wavelength modulation schemes were applied to determine concentration of water vapor and linewidths of several water absorption lines at around 1387 nm.

A Littrow ECDL was employed in a saturated-absorption spectrometer to study Doppler-free linewidths of rubidium vapour absorption lines at 781.5 and 795 nm.

The relevance of the achieved progress in ECDL technology for construction of ECDL-based sensor systems for in-situ analysis is discussed.

Acknowledgement

Financial support by the Bundesministerium für Bildung, Forschung und Technologie is gratefully acknowledged (Förderprogramm Laser 2000, Forschungsverbund "Grundlegende Untersuchungen zur Gasanalyse mit Diodenlasern"; FKZ 13N7164, 13N7157).

The effect of laser pulse shape on the saturation of the forward degenerate four-wave mixing signal

Dai-Hyuk Yu, Jai-Hyung Lee, and Joon Sung Chang
Department of Physics, Seoul National University, 151-742, Korea

Jae-Seok Ryu and Jae Won Hahn*
Optical High Temperature Measurement Group, Korea Research Institute of Standards and Science
P.O. Box 102, Yusong, Taejon 305-600, Korea
Phone: 82-42-868-5221, Fax: 82-42-868-5118, E-mail: jwhahn@kriss.re.kr

Paul M. Danehy
Department of Physics, The Australian National University, Canberra, ACT 0200, Australia

Abstract

We investigate the effect of laser pulse shape on the forward degenerate four-wave mixing(DFWM) in two-level media. Saturation behavior of the DFWM signal generated with the square top and Gaussian pulses are analyzed.

OCIS codes: (190.4380) nonlinear optics, four-wave mixing; (280.1740) combustion diagnostics

1. Introduction

Degenerate four wave mixing (DFWM) is now a well-known technique in nonlinear optics and is widely used to study the process occurring in the hostile environment, e.g. combustion and plasma[1]. In the simple description, DFWM signal generation process can be understood as the scattering of the one of the pump beams off the grating made by the combinations of the probe and the other pump beam.

Since the works of Abrams and Lind in 1980, many of the research have been performed on the better understanding of the DFWM process. Most of them deal with the phase-conjugate DFWM (PC-DFWM), in which the pump beams are counter-propagating and the signal beam is generated and propagates backward with a conjugate phase along the same path of the probe beam (Fig. 1(a)). An analytical model of PC-DFWM in stationary two-level saturable absorbers was presented by Abrams and Lind[2]. Extension of the Abrams and Lind model was made to handle arbitrary-intensity input beams for both orthogonal and parallel polarizations of pump beams[3,4]. Studies to consider Doppler broadening in the gas phase as well as the saturation have also been made analytically and numerically[5].

Recently forward DFWM (FDFWM), that adopts the laser beams propagating from the same side and arranged in a three-dimensional box-type geometry and that generates signal beam propagating in the direction determined by the phase-matching condition, is also frequently used (Fig. 1(b)). Theories for the forward DFWM have been developed by several authors. Attal-Trétout, *et al.* dealt with a Λ type three-level model with orthogonal polarization of pump beams which had arbitrary intensities[6]. Reichardt, *et al.* used direct numerical integration method as it was used in the PC-DFWM signal calculation[7]. Bratfalean, *et al.* calculated the signal analytically in two-level absorbing sample [8]. And more recently, we reported the calculation for arbitrary absorption and input intensities [9]. In the calculation, assuming intensity being constant in time domain, we calculated the steady-state signals. However, we found that the laser pulse shape makes notable effects on saturation behavior of DFWM signal giving differences in both of the magnitude and the spectral lineshape of the DFWM signal.

In this paper, we investigate the effect of laser pulse shape on the saturation of the FDFWM signal in two-level saturable absorbers.

2. Principle of FDFM signal calculation with the arbitrary laser pulse input

The calculation procedure is as follows. We divide the given laser pulse into a number of square pulses in the time-domain. The signal is calculated at each time point with the given intensity assuming the steady state is reached at each time. Therefore, the resulting signal intensity is obtained by simple summation of the contribution at each time component, and the electric field for the total input is given by

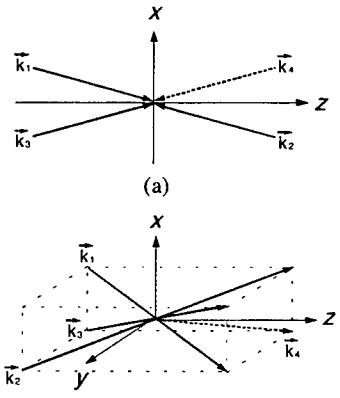

Fig. 1. Phase matching configurations for DFWM: (a) PC-DFWM geometry, (b) FDFWM geometry

$$E(\mathbf{r},t) = E_0(\mathbf{r},t)\exp(-i\omega t) + c.c. = \sum_{n=1}^{3}\frac{1}{2}A_n(t)\exp[i(\mathbf{k}_n\cdot\mathbf{r}-\omega t)] + c.c., \tag{1}$$

where, $A_n(t)$ and $\mathbf{k}_n$ is the electric field amplitude and wave vector of beam n respectively, ω is the frequency.

For optically thin media under the slowly varying amplitude approximation, the amplitude of the FDFWM signal is given by

$$A_4(t) = \frac{c}{2\omega}L\,\hat{P}_4(t), \tag{2}$$

where L is the interaction length between the lasers and the nonlinear medium. We also assume that the intensity of the input laser pulse varies slowly enough compared to the response of the medium in the time-domain and the signal reaches the steady-state value at each time. With these assumptions, $\hat{P}_4(t)$ is the nonlinear polarization component contributing the FDFWM signal generation and is equal to

$$\hat{P}_4(t) = -\frac{4\pi k^2}{l_1 l_2}\int_{-l_1/2}^{l_1/2}dx'\int_{-2_1/2}^{l_2/2}dy'\exp(-ik_4\cdot r')\frac{2\varepsilon_0\alpha_0}{k}\frac{i(1-i\delta)}{1+\delta^2}\frac{E_0(\mathbf{r},t)}{1+|E_0(\mathbf{r},t)|^2/E_S^2(\delta)}, \tag{3}$$

In Eq. (3), l_1 and l_2 are grating periods along the directions of the gratings (x-axes and y-axes in Fig. 1). And ε_0 is the permittivity of vacuum, α_0 is the linear field absorption coefficient at line center. δ is the normalized detuning parameter defined as $(\omega_0-\omega)T_2$, where ω_0 is the resonance frequency and T_2 is the transverse relaxation time. $E_S(\delta)$ is the saturation electric field defined by

$$E_S^2(\delta) = \frac{\hbar^2(1+\delta^2)}{T_1T_2\mu^2}, \tag{4}$$

where T_1 is the longitudinal relaxation time and μ is the dipole moment. Already we reported the calculation of the steady-state nonlinear polarization of Eq. (3) in the general case and detailed derivation will not be given here. The experimentally measured signal is given by the time integration of the intensity [9].

$$I_4 \propto \int_0^T |A_4(t)|^2 dt \tag{5}$$

3. Results and discussions

With the forward geometry, the measured FDFWM signal dependent on interacting laser-pulse intensity is plotted in Fig. 2. The laser source was a Nd:YAG (532nm) pumped OPO laser to probe 4s-4p transition of Ar atom (751.465nm) in RF discharge plasma. The laser pulse had an 8-ns duration and a FWHM linewidth of 0.08cm^{-1}. Three beams have the same input intensity. Each data point is the averaged value of several tens of laser pulses, while the dashed and solid lines are the calculated results with the square pulse and the Gaussian pulse input, respectively.

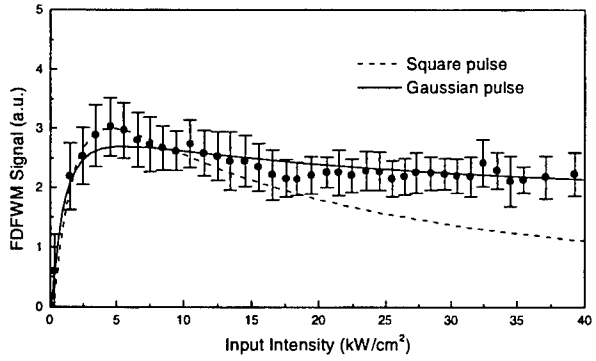

Fig. 2. FDFWM signal versus input beam intensity. Experiment shows the decrease in signal intensity and calculational results by square pulse and Gaussian pulse input are also plotted.

As shown in the figure, the signal intensity decreases as the input intensity increases. In the previous work, we already predicted the decrease of DFWM signal after saturation because of the saturation of medium by the strong probe beam. This is first experimental demonstration that

shows the decrease of DFWM signal. However, another interesting feature in Fig. 2 is the difference in the signal behavior in large intensity region between the square and Gaussian pulse. Square pulse causes the stronger saturation than the Gaussian pulse. This is due to the different intensity distribution of the input pulse in the time domain. In case of Gaussian laser input, the weak intensity in leading part of the pulse can generate signal effectively even at the strong peak intensity. However, in case of square pulse there is no such weal intensity part, so that the generated signal shows strong signal decrease.

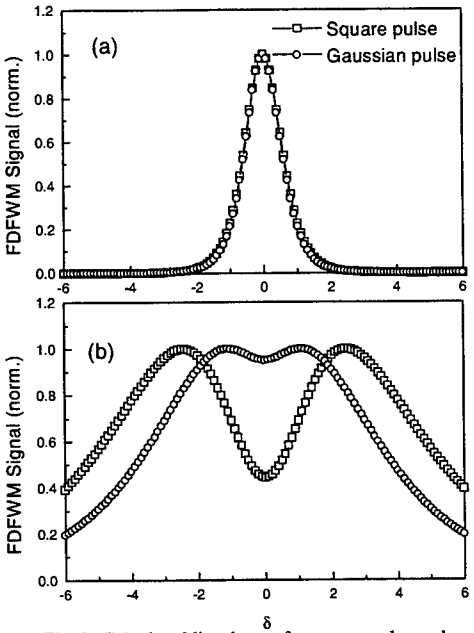

Fig. 3. Calculated lineshapes for square pulse and Gaussian pulse input. (a) I_I=0.1 I_S (b) I_I=10 I_S.

Similar tendency is also observed in the lineshape. Fig. 3. shows the calculated lineshapes for the square pulse and Gaussian pulse inputs. All three beams have the same intensity. In Fig. 3(a). the laser intensity is set to the one tenth of the saturation intensity given by Eq. (4). In this case, two lineshapes are of the same form. This means that at low input intensity, the lineshape for any kind of pulse input should have the same form as obtained by the perturbation theory. However, in the strong laser input case, where the perturbation theory cannot work, remarkable difference in lineshape is observed as shown in Fig. 3(b). As already discussed above in explaining the Fig. 2. The lineshape for square pulse input shows the far stronger saturation dip at the line-center.

From the results so far discussed, the existence and the distribution of the weak intensity part of the pulse have an important role in the signal intensity and lineshape, especially in the saturation region.

5. Conclusion

We have demonstrated and discussed the effect of laser pulse shape on the FDFWM signal in two-level saturable absorbers. Experiment showed that the decrease in the signal intensity for the strong input intensity fits well with the results calculated with Gaussian pulse. In all conditions, the signal intensity and the lineshape produced with the square pulse input show stronger saturation than those produced with the Gaussian pulse input. Especially, the difference in spectral lineshape is enormous in the strongly saturation region. This means that we need to implement the shape of the input pulse in the calculation of the FDFWM signal to understand the real experimental conditions.

References

[1] R. L. Farrow and D. J. Rakestraw, "Detection of trace molecular species using degenerate four-wave mixing," Science **257**, 1894-1900 (1992).
[2] See, for example, R. A. Fisher, ed., Optical Phase Conjugation (Academic, New York, 1983).
[3] W. P. Brown, "Absorption and depletion effects on degenerate four-wave mixing in homogeneously broadened absorbers," J. Opt. Soc. Am. **73**, 629-634 (1983).
[4] B. Ai and R. J. Knize, "Degenerate four-wave mixing in two-level saturable absorbers," J. Opt. Soc. Am. B **13**, 2408-2419 (1996).
[5] R. P. Lucht, R. L. Farrow, and D. J. Rakestraw, "Saturation effects in gas-phase degenerate four-wave mixing spectroscopy: nonperturbative calculations", J. Opt. Soc. Am. B, **19**, 1508-1520 (1993).
[6] B. Attal-Tretout, H. Bervas, J. P. Taran, S. LeBoiteux, P. Kelley, and T. K. Gustafson, "Saturated FDFWM lineshapes and intensities: theory and application to quantitative measurements in flames," J. Phys. B: At. Mol. Opt. Phys. **30**, 497-522 (1997).
[7] T. A. Reichardt, R. P. Lucht, P. M. Danehy, and R. L. Farrow, "Theoretical investigation of the forward phase-matched geometry for degenerate four-wave mixing spectroscopy," J. Opt. Soc. Am. B **15**, 2566-2572 (1998).
[8] R. T. Bratfalean, G. M. Lloyd, and P. Ewart, "Degenerate four-wave mixing for arbitrary pump and probe intensities," J. Opt. Soc. Am. B **16**, 952-960 (1999).
[9] D. H. Yu, J. W. Hahn, J. H. Lee, and J. S. Chang, "Theory of forward degenerate four-wave mixing in two-level saturable absorbers," J. Opt. Soc. Am. B **16**, 1261-1268 (1999).

MIR-Evanescent-Field Spectroscopy for Environmental Analysis

Ulrike Willer, Torsten Blanke, Wolfgang Schade

Physikalisches Institut, Technische Universität Clausthal
Leibnizstrasse 4, D-38678 Clausthal-Zellerfeld, Germany
e-mail: ulrike.willer@tu-clausthal.de

Abstract: Evanescent-field spectroscopy in the mid-infrared (MIR) spectral range is applied for online and in-situ gas detection. Tunable MIR laser radiation is generated by difference frequency generation of two single mode diode lasers in $AgGaS_2$.

OCIS Codes: 060.2370, 300.6340

Laser absorption spectroscopy is a very suitable technique for measuring gaseous environmental pollutants because of its high sensitivity and selectivity and the capabilities for online and in-situ applications. In this context the mid-infrared (MIR) spectral region between 4 and 10 microns is of special interest because nearly all molecules have characteristic absorption bands within this „fingerprint" region. Recent developments in compact MIR laser sources make this spectral region even more interesting for analytical applications because single-mode diode lasers and difference frequency generation (DFG) with conventional „off-the-shelf" diode lasers allow to engineer MIR-laser spectrometers that operate under room temperature conditions [1,2]. Recently quantum cascade lasers are discussed as new and miniaturized cw-laser sources for spectroscopic applications in the MIR even though they are still not applicable at room-temperature [3,4].

In general laser absorption spectroscopy requires an open optical path or a one- or multi-pass absorption cell that contains the gas under investigation and a laser source and a detector at each side. This technique requires optical thin media, scattering processes have to be negligible, and only optical accessible paths or places can be used. This limits the possibilities of this method for a lot of in-situ applications. However, most of these problems can be solved by using the so-called evanescent-field spectroscopy [5] in the MIR.

The basic experimental setup of this method is shown in fig. 1. MIR laser light is coupled into an optical fiber that only consists of the core material and has sufficient transmission within the spectral region of interest. At the other end of the fiber a MIR detector is used to record the laser light intensity that is transmitted through the fiber. If the index of refraction of the fiber material is higher than the one of the surrounding medium the MIR laser light is guided through the fiber due to total reflection at the interface between fiber core and surrounding medium. Essentially, there are two loss mechanisms responsible for the attenuation of the MIR laser intensity in the fiber: (1) The frustrated total reflection (FTR) and (2) the attenuated total reflection (ATR). The FTR is related to a change of the index of refraction while the ATR is related to a change of the absorption coefficient.

In evanescent-field spectroscopy the wavelength of the MIR laser radiation that is transmitted through the fiber is tuned over an absorption line of molecular species that surround the fiber. In the vicinity of an atomic or molecular resonance simultaneously a wavelength dispersion of the index of refraction and of the absorption coefficient is observed and results in a change of the FTR and the ATR, respectively. When measuring the MIR laser intensity at the end of the fiber while tuning the MIR laser over an absorption line, both effects contribute to the measured spectral line profile. Similar to the direct laser absorption spectroscopy the recorded line profiles in the case of evanescent-field spectroscopy can be used for analytical applications, e.g. measuring the concentrations of environmental pollutants.

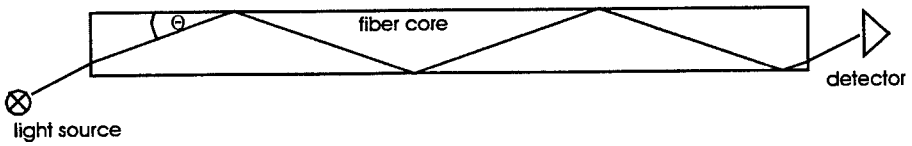

Fig. 1: Schematic of the experimental setup for a MIR-evanescent-field laser sensor

In order to optimize this effect, the number of reflections at the interface of fiber and surrounding medium should be as large as possible. This is achieved by increasing the length z of the fiber and decreasing the radius r of the fiber. Because of the given numerical aperture (NA≈ n sinΘ) of the fiber in use there is not only one fixed angle Θ when coupling laser light into the fiber. Therefore, the laser power P which is measured by the MIR detector at the end of the fiber is an integral over all possible angles Θ and is proportional to the incident laser intensity I and to the reflectivity R raised to the power of m which is the number of reflections [6]:

$$P(z,\lambda) = \int 2\pi\, I(z=0,\Theta,\lambda)\, R(\lambda,\Theta)^{m(\Theta,z)} \sin\Theta\, d\Theta \qquad (1)$$

Since the reflectivity $R(\lambda,\Theta) = [1 - \alpha(\lambda) \cdot d_{eff}(\lambda,\Theta)]$ contains the absorption coefficient $\alpha(\lambda) = \sigma_{ik} \cdot \Delta N$ the number density N_0 of molecules in the ground state can be determined by measuring $P(z,\lambda)$ with $\Delta N = N_0 - N_1$ and $N_1 << N_0$. d_{eff} gives the penetration depth of the evanescent-field into the surrounding medium and depends on the MIR laser polarization, the index of refraction, and the wavelength λ. The number of total reflections can be calculated from $m(z,\Theta) = (z \tan\Theta)/r$.

In the present experiment a silverhalide fiber ($AgCl_xBr_{1-x}$) with about 90% transmission between 4 and 18 µm, a core diameter of 500 µm, and a length z = 50 cm is used. This fiber material has the advantage that it is commercially available without a cladding. The MIR laser radiation was generated by difference frequency generation of two standard single-mode diode lasers in $AgGaS_2$ [1]. Either an InSb or a thermo-electrically cooled IR detector (DoroTEC PCI-2TE) was used for recording the MIR laser light. As an example, such a system was used to detect water vapor in ambient air at λ = 5.083 µm. The evanescent-field signal is shown in fig. 2 as the DFG laser wavelength is tuned over the water absorption line.

Evanescent-field spectroscopy is also applied to measure H_2S concentrations online and in-situ in volcano gases at λ = 1.57 µm. Evanescent-field spectroscopy is very advantageous in these experiments since scattering of the laser light by the high concentration of water vapor which is typical in volcano gas streams will dramatically limit the laser absorption method for any analytical application. First results from field measurements at the volcano Galeras in Columbia will be shown and discussed at the meeting.

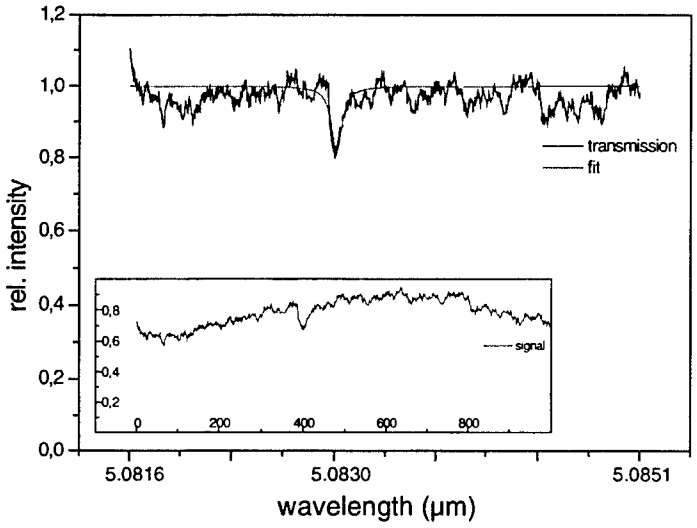

Fig.2: Detection of water vapor in ambient air at λ = 5.083 µm by MIR evanescent-field laser spectroscopy.

This work was supported by the BMBF under contract 13N6883A.

References

[1] W. Schade, T. Blanke, U. Willer, C. Rempel; Appl. Phys. B **63**, 99 (1996).

[2] V. Petrov, C. Rempel, K.-P. Stollberg, W. Schade; Appl. Opt. **37**, 4925 (1998).

[3] J. Faist, F. Capasso, A. Y. Cho; Appl. Phys. Lett. **67**, n 21, 3057 (1995)

[4] C. Gmachl, F. Capasso, A. Y. Cho; Appl. Phys. Lett. **72**, n 12, 1430 (1998)

[5] D. Bunomovich et al.; Journal of Molecular Structure **292**, 125 (1993).

[6] N.J. Harrick; Internal Reflection Spectroscopy, John Wiley & Sons, New York (1967).

Quantitative minor species concentration measurements in atmospheric pressure flames with time-resolved LIF

A. Brockhinke, A. Bülter and U. Rahmann
Physikalische Chemie I, Universität Bielefeld, Universitätsst. 25, D-33615 Bielefeld, Germany
Fax: +49-521-106-6027, e-mail: brockhinke@pc1.uni-bielefeld.de

Abstract: Energy transfer and quenching processes are studied with simultaneous wavelength, temporal and polarization resolution. A method to obtain quench-free data is devised. Quantitative OH and H concentration profiles in a counterflow burner interacting with a vortex are presented.

OCIS codes: (280.1740) Combustion diagnostics; (300.6500) Spectroscopy, time-resolved

1. Introduction

Counterflow diffusion flames sustained by two opposing jet nozzles are widely used. They can operate with different fuels and over a wide range of mixtures and flow velocities. The resulting flame may be treated as one-dimensional and is easily probed with diagnostic techniques. The relatively simple geometry of this type of flame facilitates model calculations [1]. Recently, Rolon et al. described an experimental configuration which allows the reproducible generation of a vortex ring in a counterflow flame [2] and thus the study of the interaction of an isolated vortex with a flame front. Since flame/vortex interactions are of great importance in turbulent combustion and extinction processes, several experimental and numerical studies have been performed on this type of flame including PIV and planar LIF [2, 3].

However, for a meaningful comparison between experiment and model, accurate measurements of radical concentrations are necessary. The hydroxyl radical plays a key role in the reaction kinetics. Additionally, simulations indicate that quantitative hydrogen atom measurements provide a crucial test for flame models. Since LIF signals are affected by quenching and energy transfer processes [4], quantitative measurements require either a detailed knowledge of these processes, or experiments with a sufficiently-fast time resolution to avoid these problems.

In the present work, a picosecond laser is used in conjunction with an intensified streak camera to study energy transfer processes in OH. A method is presented to obtain quench-free results from the time-resolved spectra. Quantitative concentration profiles for OH and H are presented in a counterflow burner interacting with a vortex.

2. Experimental

A novel laser system based on a regeneratively amplified Ti:sapphire laser which produces tunable, Fourier-limited pulses of 80 ps duration is used as light source. Pulse energies of up to 3 mJ are obtained for the third harmonic radiation with wavelengths between 250 and 300 nm. LIF signals are collected by a spherical mirror in the usual 90 degrees excitation-detection geometry. After passing a Glan-Thompson polarizer, they are spectrally dispersed by a 275 mm focal length monochromator and then detected by a streak camera. The overall temporal resolution of the complete system (including trigger jitter and broadening effects in the detection optics) is about 120 ps and thus is very well matched to the typical time between collisions in atmospheric pressure flames ($\tau_c \approx 100$ ps).

3. Energy transfer in OH

For these measurements, only moderate pulse energies (in the order of 100 μJ) and mild focussing of the radiation are employed to avoid saturation effects. Several rotational lines in the OH A-X (1-0) transition are probed. Entrance slits of monochromator and streak camera are oriented perpendicular to each other. This detection geometry yields two-dimensional spectra; temporal resolution corresponds to the vertical axis and the spectral dispersion corresponds to the horizontal axis.

A sample spectrum is shown in Fig. 1. In this case, the $R_2(10)$ line is excited and fluorescence in the 0-0 and 1-1 band is detected. The spectrum is dominated by the three strong lines originating from the directly populated level. However, a multitude of additional lines appears as time progresses. These lines generally reach their maximum intensity several 100 ps after the initial laser pulse and are due to energy transfer processes.

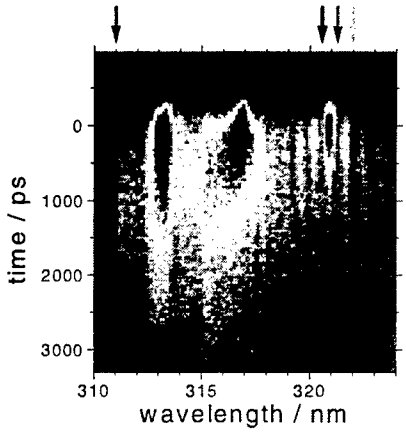

Fig. 1. Raw data after excitation of the OH $R_2(10)$ line. Intensities are color-coded.

For a more detailed analysis, Fig. 2 shows vertical cuts (which correspond to time-resolved spectra) through this raw image at the positions indicated by the arrows. The intensity development follows the expected pattern: Fluorescence from the directly populated level decreases rapidly with a decay time of $\tau_d \approx 300$ ps. Both, quenching and energy transfer processes contribute to this decay. Rotational energy transfer (RET) is relatively fast, whereas lines originating from levels populated by vibrational energy transfer (VET) reach their maximum intensity roughly 1 ns after the initial laser pulse.

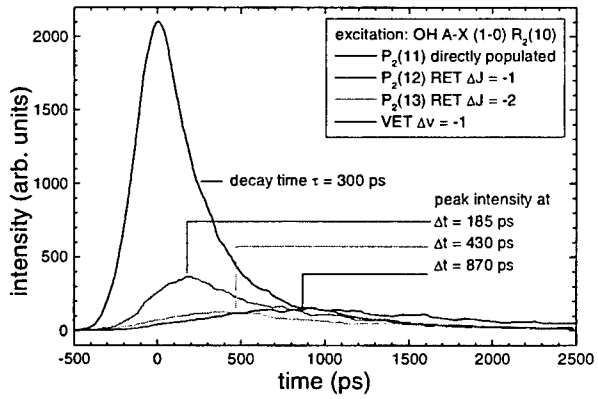

Fig. 2. Fluorescence decay curves for different levels; extracted from the raw data presented in Fig.1.

Furthermore, polarization effects in LIF spectra affected by energy transfer are studied [5]. Surprisingly, it is found that reorientation of the OH radicals is slow in all cases investigated. Orientation is preserved over several collisions, even for radicals undergoing RET or VET. Comparisons with energy transfer models [6, 7] show a reasonably good agreement.

4. Concentration measurements

For concentration measurements, parallel orientation of monochromator and streak camera entrance slit is used. This yields spatially and temporally resolved images. From the time-resolved fluorescence spectra, quench-free results are obtained by extrapolating the observed decay curves backwards to t=0. Besides determining the OH concentration by probing different rotational lines, hydrogen atom mole fractions are determined. For this, we have excited the n=4 level by a three-photon step and detected the fluorescence to the n=2 level at 486 nm [8]. The high energy density (50 GW/cm^2) obtained in the focus region of the laser beam allows the one-dimensional, time-resolved detection of the fluorescence. Calibration measurements show that no additional H-atoms are generated by photolytic processes and that the detection is not affected by flame luminosity.

Figure 3 shows experimentally determined hydrogen atom concentrations and comparisions with model calculations in a stable counterflow diffusion flame. Additional spatially resolved (in height and radial direction) profiles have been obtained in the counterflow flame interacting with a vortex.

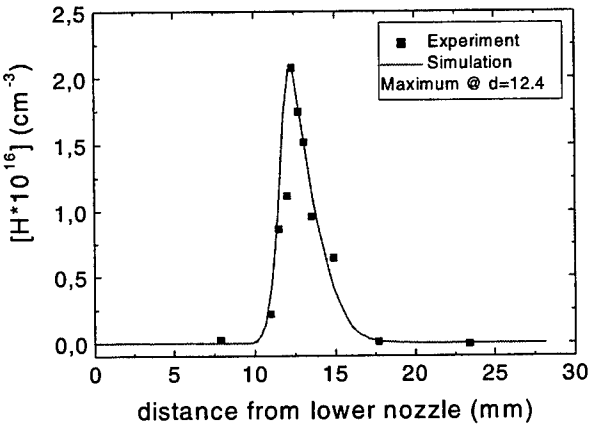

Fig. 3. Hydrogen concentration in a stable counterflow flame in comparison with a CHEMKIN simulation.

5. Summary

In this contribution, results obtained with a novel laser system based on a regeneratively amplified Ti:sapphire laser which produces tunable, Fourier-limited pulses of 80 ps duration are presented. Pulse energies of up to 5 mJ are obtained for the third harmonic radiation with wavelengths between 250 and 300 nm. LIF signals are spectrally dispersed and then detected by a streak camera. Energy transfer processes in OH are studied for several rotational lines in the A-X (1-0) band. Comparisons with model calculations show a reasonably good agreement. Reorientation of OH during collisions is found to be slow. From the time-resolved fluorescence spectra, quench-free results are obtained by extrapolating the observed decay curves backwards to the time of the laser excitation. In a counterflow diffusion flame interacting with a vortex, quantitative OH and H concentration profiles are obtained.

6. References

[1] N. Darabiha, and S. Candel, "The influence of the temperature on extinction and ignition limits of strained hydrogen-air diffusion flames," Combust. Sci. and Tech. **86**, 67-85 (1992)

[2] J. C. Rolon, F. Aguerre, and S. Candel, "Experiments on the interaction between a vortex and a strained diffusion flame," Combust. Flame **100**, 422-429 (1995)

[3] P-H. Renard, J.C. Rolon, D. Thévenin, S.Candel, "Investigations of heat release, extinction, and time evolution of the flame surface, for a nonpremixed flame interacting with a vortex," Combust. Flame **117**, 189-205 (1999)

[4] K. Kohse-Höinghaus, "Laser techniques for the quantitative detection of reactive intermediates in combustion systems," Prog. Energy Combust. Sci., **20**, 203-279 (1994)

[5] A. Brockhinke, W. Kreutner, U. Rahmann, K. Kohse-Höinghaus, T. B. Settersten, M. A. Linne, „Time-, wavelength- and polarization-resolved measurements of OH ($A^2\Sigma^+$) picosecond laser induced fluorescence in atmospheric pressure flames," accepted for publication, App. Phys. B, June 1999

[6] U. Rahmann, W. Kreutner, K. Kohse-Höinghaus, "Rate equation modeling of single- and multiple-quantum vibrational energy transfer of OH ($A^2\Sigma^+$, v'=0 to 3)," Appl. Phys. B **69**, 61-70 (1999)

[7] R. Kienle, M. P.Lee, K. Kohse-Höinghaus, "A detailed rate equation model for the simulation of energy transfer in OH laser-induced fluorescence," Appl. Phys. B **62**, 583-599 (1996)

[8] M. Aldén, A. L. Schawlow, S. Svanberg, W. Wendt, and P.-L. Zhang, "Three-photon-excited fluorescence detection of atomic hydrogen in an atmospheric-pressure flame," Opt. Lett. **9**, 211-213 (1984)

Spherical cavity ringdown spectroscopy experiments

R. W. Shaw, W. B. Whitten, M. D. Barnes, and J. M. Ramsey
Chemical and Analytical Sciences Division
Oak Ridge National Laboratory
P.O. Box 2008, MS-6142
Oak Ridge, TN 37831-6142
Tel. 423/574-4920 FAX 423/574-8363
email shawrw@ornl.gov

L. J. Wang
Department of Physics, Geology, and Astronomy
University of Tennessee at Chattanooga
Chattanooga, TN 37403
Tel. 423-755-5248
email lingjun-wang@utc.edu

Introduction

We recently reported the time-domain observation of whispering gallery mode (WGM) propagation for picosecond optical pulses and macroscopic glass spheres.[1,2] By analogy to the well-known acoustic phenomenon, optical WGMs propagate along the surface of spheres with high quality factors (Q) allowing optical path lengths many times the sphere diameter. The optical pulse duration (2 ps) was short relative to the equatorial round trip time and the detector response; thus, resolution of a series of individual output pulses was achieved, each corresponding to a single traverse of the sphere circumference. These results are complementary to optical frequency domain measurements wherein continuous wave excitation is used and WGMs are observed as sphere scattering resonances as the excitation laser wavelength is scanned. An unexpected build-up of the oscillation intensity was observed in our experiments that was approximately constant in the number of sphere round trips, independent of the sphere diameter; this phenomenon was explained using a mode evolution argument invoking a coupling of a family of efficiently excited modes to different modes better coupled to the detector geometry.

We speculated that these robust spherical cavities could find use for cavity ringdown spectroscopy,[3] as a replacement for the more common linear cavities. The evanescent wave penetrating the sphere surface should interact with the external environment. Optical absorption by species at the interface would create loss during each round trip, yielding a shorter cavity

decay time, indicative of the absorption. Absorbing gases, adsorbed surface species, and liquid solutions would be sample candidates. The results of experiments designed to test this concept are reported here.

Experimental

Two-picosecond duration pulses near 795 nm at 76 MHz were generated using a Kerr lens mode-locked titanium:sapphire laser with an average power of approximately 1 watt. Two different experimental configurations were used to probe time-domain absorption by WGM ringdown. The first configuration was similar to that previously reported where laser pulses were focused at the contact point of a 26.25 mm-diameter glass sphere (BK-7, n= 1.51) and an equilateral prism (SF-18, n= 1.722). The sphere was mounted so that a petri dish containing an aqueous solution of $NdCl_3$ (which exhibits a narrow absorption feature at the laser wavelength) could be raised to wet a portion of the sphere circumference. Part of laser pulse circulating around the sphere was coupled out through the prism and imaged onto a fast photodiode (14 ps risetime) and processed with digital oscilloscope. In this mode, the light interacts with material external to the sphere through the weak evanescent portion of the circulating pulse.

In the second mode, we probed time-domain absorption of material within a sphere using a locally-fabricated vessel with a spherical shape and a 18-mm inner diameter. The wall of this vessel was carefully ground just to the point of breakthrough, leaving a flat surface centered about a 1-2 mm orifice. It was glued to the high index prism at the hole location so that a contained sample fluid was in contact with the prism. This allowed for optical pulse coupling into liquid samples while maintaining minimal distortion of the circular geometry of the vessel inner circumference, i.e., the creation of a liquid sphere. The samples used were infrared dyes in carbon disulfide.

Results and Discussion

Waveforms were recorded for the glass sphere in air, the sphere partially immersed (ca. 30% of the circumference covered) in distilled water, and the sphere similarly immersed in a $NdCl_3$ solution. Surprisingly, the time waveform of the WGM propagation around the 26-mm glass sphere was immune to the cavity surface environment. Only slight modulation of the individual oscillations was observed, as evidenced by the Figure; the overall ringdown constant of the progression was unaffected. A few possible explanations exist for this insensitivity. First, the light intensity in the evanescent wave may be dwarfed by the circulating intensity that corresponds to the detected signal and constitutes an invariant background. Second, the WGMs detected efficiently by the photodiode (see above) may be of high order and thus propagate more deeply within the sphere bulk than lower order surface modes. Finally, the Q of the spherical cavity may be such that the intrinsic loss is substantially greater than our absorptive loss. Further studies are in progress to determine the lack of an effect due to surface absorption.

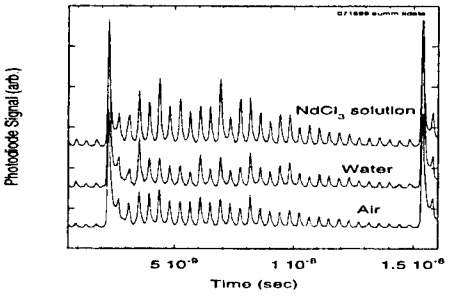

Figure 1. WGM waveforms for a 26-mm glass sphere exposed to air, distilled water, and an aqueous $NdCl_3$ solution.

For the liquid sphere experiments, there is no dependence on loss induced by absorption of an evanescent wave; most of the laser energy propagates within the sample itself. However, to achieve a long path length, total internal reflection at the liquid/glass interface is required. Thus, the material indices must satisfy the constraint: $n_{prism} > n_{liquid} > n_{glass}$. This limits the choice of a common solvent to carbon disulfide or aniline. We examined IR-125 laser dye in CS_2. An oscillating waveform with a 310 ps cycle time was recorded for pure CS_2 and a distinct equatorial ring could be observed in the vessel with the aid of an infrared viewer. When the vessel was filled with air, methanol, or water, only the unaltered laser pulse shape was recorded. The oscillating waveform decayed rapidly (3 rings) due to the imperfect shape of the vessel inner wall that yielded a helical light path; the round trip path quickly walked off the orifice coupling spot. When the absorbing dye/CS_2 solution was placed in the vessel, the oscillating signal was extinguished after a single round trip. Armed with this encouraging preliminary data, attempts are currently in progress to fabricate spherical vessels with improved geometry that will allow extended time domain data and possibly cavity ringdown absorption measurements.

Acknowledgement

This research was sponsored by the Division of Chemical Sciences, Office of Energy Research, U.S. Department of Energy, under Contract DE-AC05-96OR22464 with Oak Ridge National Laboratory, managed by Lockheed Martin Energy Research Corporation. LJW acknowledges an appointment to the U. S Department of Energy Faculty Research Participation Program at the Oak Ridge National Laboratory. This program is administered by the Oak Ridge Institute for Science and Education under a contract between the U.S. Department of Energy and Oak Ridge Associated Universities.

References:

1. W. B. Whitten, R. W. Shaw, M. D. Barnes, and J. M. Ramsey, Technical Digest, 7th Laser Applications to Chemical and Environmental Analysis; Orlando, FL; March 9-11, 1998, p. 55.

2. R. W. Shaw, W. B. Whitten, M. D. Barnes, and J. M. Ramsey, Opt. Lett. **23**, 1301 (1998).

3. J. B. Paul and R. J. Saykally, Anal. Chem. **69**, 287A (1997).

Diode-Laser-Based In-situ-CH_4-Detection for the Surveillance of Ignition Processes in Gas-fired Power-Plants

H. Pitz, T. Fernholz, C. Giesemann, V. Ebert
Institute of Physical Chemistry ,University of Heidelberg
INF 253 - 69120 Heidelberg
volker.ebert@urz.uni-heidelberg.de

Abstract: We demonstrate the first simultaneous in-situ detection of methane and water in a full-scale 1 GW_{th} gas-fired power plant with an absorption resolution in the order of 10^{-4} OD corresponding to less than 5 ppmV at 400K.

OCIS codes: (120.0120)(140.0140)(120.1740)

1. Introduction

The combustion of natural gas in addition with combined-cycle processes will play an increasingly important role in the energy production due to the high conversion efficiency of the process and its very low pollutant emission and overall costs. To maintain the positive properties under all process conditions, i.e. under frequent and strong variations in total power, and to enable secure ignition - ignition failures have lead to severe power plant damages in the past- and precise active control of the multi-burner systems with up to 20 large-scale burners, it would be helpful to have a fast in-situ gas sensor, which is able to circumvent the problems associated with the local sampling character of extractive sampling probes. Species of interest for such a sensor are methane as an indicator of an ignition failure , water to perform an in-situ temperature measurement and oxygen to determine the mean fuel-to-air-ratio along the absorption path. Since the data are needed most right after the ignition of the first few burners it is unavoidable to perform a simultaneous optical temperature measurement to extract meaningful quantitative methane concentrations.

We have started with the development of such an in-situ absorption spectrometer based on near infrared diode lasers, which is able to determine simultaneously multiple species concentrations, namely CH_4, H_2O and O_2, and the temperature during the ignition cycle of a full-scale gas-fired power-plant with an inner diameter of 10 meters and a thermal gross power of 1 GW. We report about our first results regarding the optical characterization of the in-situ absorption path and about our in-situ-detection of methane and other gaseous species under ignition conditions. We can show that we are already able to detect an ignition failure and prevent dangerous process conditions.

2. Experimental details

Tunable diode lasers in the red to near infrared spectral range (630nm to 1700nm) are very promising tools for industrial in-situ species sensors [1-3]. They are inexpensive, rugged, extremely compact, can be operated at room temperature from relatively simple current sources without a need for additional cooling and offer a unique combination of spectroscopic properties like fast tunability, narrow spectral line width and high spectral brightness, which makes them near ideal candidates for in-situ sensors. For our application at a full-scale power plant we used the lasers indicated in table 1:

Table 1: Properties of NIR-Diode lasers used in our setup

Species	Transition	Laser type	Power mW	Current tuning nm/mA	Temp. tuning nm/K
CH_4	$2\nu_3$	DFB: 1653 nm	7	0.017	0.010
H_2O	000→211; 000→112	FP: 813 nm	35	0.007	0.067
O_2	$X^3\Sigma^-_g \rightarrow b^1\Sigma^+_g$	DFB: 760 nm	5	0.013	0.058

All lasers were coarse tuned by temperature to the transition of interest. Rapid wavelength tuning with repetition rate in the kHz range was initiated by current modulation to cover the rovibrationally resolved absorption lines. The laser beams were collimated and combined to form a single beam which was then directed through the combustion vessel via air cooled flanges and air purged windows under Brewsters angle.

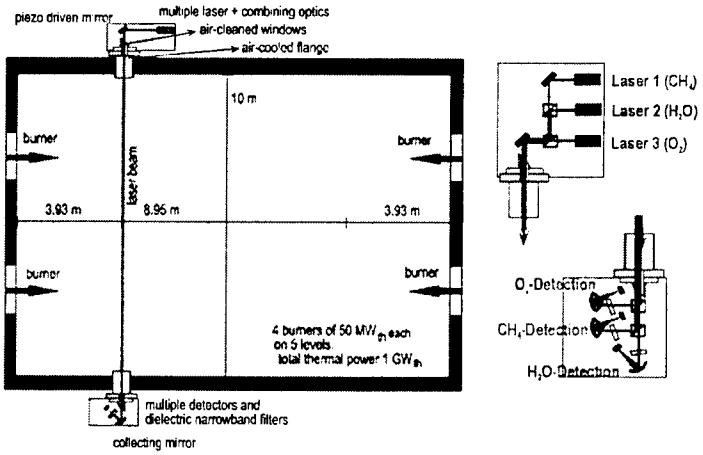

Fig. 1. Optical setup at gas-fired power plant

On the receiving side (figure1) the light was collected with a spherical mirror and separated into the individual wavelengths by dichroic beamsplitters. To further eliminate cross talk between the wavelength channels and to minimize disturbances by fluctuating thermal background emission each channel was further separated by narrow band dielectric interference filters. The absorption signals are evaluated by digitizing the dc-signals with a 12bit ADC with 8 simultaneous sampling channels, averaging up to 200 successive absorption profiles per species and finally extracting the line area by a fast fitting routine. One of the major problems which has to be solved to be able to allow continuos combustion monitoring during the entire startup process is correction for transmission fluctuations. In order to choose the laser scan frequency to be high enough to "freeze" the disturbances during a single scan we carefully studied the amplitude and frequency behavior of the transmission of the in-situ path and of the thermal background emission which is also collected by the receiving optics. The corner frequencies for emission were 50 Hz and for transmission 1khz. Emission suppression is important since part of the transmission correction is a division of the raw scan by the reconstructed baseline. Another additional major problem which was found rather unexpected was a severe thermally induced deformation of the combustor walls during the startup phase which lead to complete misalignment of the laser beam. To compensate these wall deformations we designed and lab-tested a robust closed loop beam stabilization system (based on a position sensitive photodiode and a piezo driven mirror mount) which is insensitive to the unavoidable strong amplitude fluctuations of the pilot beam and the background emission. An In-situ test under industrial conditions is planned in the near future.

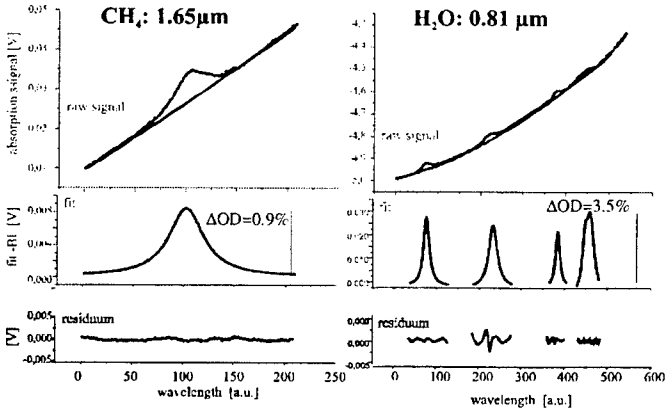

Fig. 2. In-situ signals of methane and water at the 1 GW$_{th}$- gas-fired power plant

3. Results

First results gained with the described setup at the full scale device during startup conditions are shown in figure 2. The depicted raw in-situ signals with peak absorptions below 1% for the R5-line methane and up to 3.5% for the line group of water were captured simultaneously and could be fitted with good accuracy to Lorentzian line shapes. Despite strong background emission and severe transmission fluctuations down to 5% transmission we estimate from the residuum of the fit an absorption resolution for the spectrometer in the order of 10^{-4} OD, which is equivalent to an improvement in signal to noise by the transmission correction of more than three orders of magnitude. The time resolution achievable depends obviously on averaging rate, with a 200 fold average a time resolution of two seconds could be achieved. A typical time evolution of the methane absorption signal during a startup event is shown in figure 3.

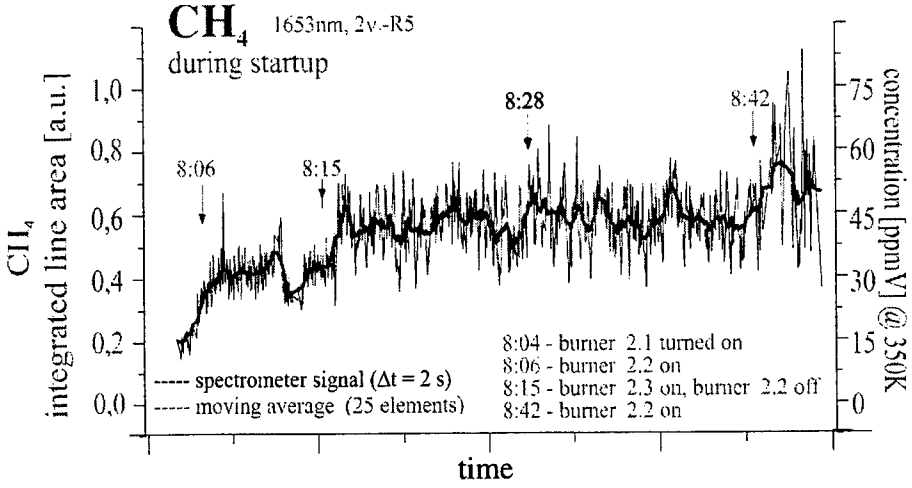

Fig. 3. Time evolution of the in-situ methane signal

Arrows indicate special events during the startup procedure like the ignition of an additional burner. As shown it is already possible to detect a weak increase in the signal during some ignition events, which has to be concentration rise since it cannot be explained by the increase in temperature.

To convert the absorption signal in concentration units it is necessary to perform a temperature correction which will be done in the near future. As a first preliminary step we used the shape of the methane line and HITRAN calculations to estimate the temperature of the gas to be about 400K and compared this temperature with the result of the line strength ratio of the water peaks which lead to a temperature of at least 700K. This surprising discrepancy seems to indicate that the temperature of the water and the methane molecules differs by some hundred degrees. If this discrepancy is caused by incomplete mixing and resulting temperature gradients or by other causes will be investigated during the following measurement campaigns by redundant temperature measurements with different educt and product molecules. Using the temperature estimated from the methane line shape to convert the absorption signal to a concentration we end up with an average methane concentration during startup of 50 ppmV which is in good agreement with the expected values under standard process conditions. From this we conclude that we are able to detect clearly any ignition failure with the in-situ spectrometer since the concentration would then rise to far more than 100ppmV.

[1] Ebert, V., Fitzer, J. ,Gerstenberg, I., Pleban, K.-U., Pitz, H., Wolfrum, J., Jochem, M., Martin, J., "Online monitoring of water vapor with a fiber coupled NIR-diode laser spectrometer", 5th Intern. Symposium on Gas Analysis by Tunable Diode Lasers, Freiburg, February 25-26 1998, 145-154, (VDI-Berichte 1366)

[2] Ebert, V., Pleban, K.-U., Wolfrum, J., "In-situ Oxygen-Monitoring using Near-Infrared Diode Lasers and Wavelength Modulation Spectroscopy", in *Laser Applications to Chemical and Environmental Analysis*, Technical Digest (Optical Society of America, Washington DC), pp 206-209, March 9-11, 1998, Orlando, Florida, USA, Paper No LWB3

[3] Ebert, V., Fitzer, J. ,Gerstenberg, I., Pleban, K.-U., Pitz, H., Wolfrum, J., Jochem, M., Martin, J., "Simultaneous Laser-based In-Situ-Detection of Oxygen and Water in a Waste Incinerator for Active Combustion Control Purposes", 27th Symposium (Int.) on Combustion, The Combustion Institute, Pittsburgh, pp. 1301-1308 (1998)

Laser spectroscopy of Magnesium Oxide in Magnesium metal combustion

Christopher B. Dreyer, John W. Daily, Angel Abbud-Madrid, and Melvyn C. Branch
Center for Combustion and Environmental Research, Department of Mechanical Engineering, CB 427, University of Colorado at Boulder, Boulder, CO 80309-0427
christopher.dreyer@colorado.edu, daily@spot.colorado.edu, abbudmad@colorado.edu, branch@spot.colorado.edu
Phone: (303)492-8920, Fax: (303)492-3498

1. Introduction

A study of the combustion of bulk samples of magnesium (Mg) in atmospheres of carbon dioxide (CO_2), carbon monoxide (CO), and oxygen (O_2) is currently being conducted at the Univeristy of Colorado. Although there has been much work on metal reaction kinetics, the combustion of bulk metals remains an incompletely understood phenomenon. This is due to the interaction of several complex processes, including low-temperature surface oxidation, heterogeneous reactions, product condensation, high-emissivity products, convective action, non-premixed combustion, and multi-phase thermodynamics. The motivation for this work is to examine the feasibility of Mg-CO_2 combustion as a rocket propulsion source for exploration of Mars and other planetary bodies. Our work focuses on fundamental aspects of bulk metal combustion. This work is supported by the NASA Micogravity Combustion Program (grant NAG3-2220).

This paper presents a spectroscopic investigation of magnesium oxide (MgO) which is carried out in support of Planar Laser Induced Fluorescence (PLIF) imaging planned for the metal combustion experiments. Excitation scans of MgO are done in a seeded acetylene-air flame. The flame is seeded with an aqueous magnesium chloride aerosol generated by a pneumatic nebulizer, and provides a steady source of MgO at high temperature. Excitation scan measurements in this flame precisely locate transition wavelengths in the complex MgO spectrum.

2. Experimental

The experimental apparatus consists of an acetylene-air flame stabilized on a Perkin-Elmer slot burner fitted to a mixing chamber and a pneumatic nebulizer. The flame was seeded at 0.37 cc per minute with an aqueous solution of magnesium chloride at a concentration of 50 g/l of $MgCl_2 \bullet 6H_2O$. The flame was set at 9.6 slpm Air and 0.9 slpm C_2H_2, to produce a slightly rich flame at 1.12 equivalence ratio.

The laser system consists of a Nd:YAG laser pumping a dye laser with the second harmonic. Dye laser linewidth is estimated to be 0.1 cm^{-1}. The dye laser used a Bethune cell amplifier which produced a beam profile of 1mm diameter. Laser wavelength is measured with a Fizeau wavelength meter. Energy per pulse is monitored and recorded by a computer data acquisition system along with a ramp signal from the dye laser to record wavelength position. Appropriate beam samplers are used to direct the beam to the wavemeter and energy per pulse meter. Cylindrical optics are used to form the beam into a vertical sheet. Fluorescence detection for the excitation scan experiments are accomplished with a photomultiplier fitted with short pass and bandpass filters to provide a bandpass of approximately 12 nm centered at 497 nm. The PMT signal is recorded by a computer data acquisition system after 3 pulse averaging with a Boxcar integrator.

3. Fluorescence Detection Scheme

An energy level diagram of MgO is shown in Fig 1. The structure of MgO was first characterized by Lagerqvist and Uhler in 1949[1]. Subsequent investigations have added details about the structure and improved upon the accuracy of the structure [2-4]. In these experiments excitation of the $B^1\Sigma^+$-$A^1\Pi$ transition near 600 nm and detection of the entire $B^1\Sigma^+$-$X^1\Sigma^+$ band near 500 nm fluorescence is chosen. Several reasons can be given for this arrangement; at the high temperatures of the experiment, there will be a relatively large population in the A state, 12% at 2500K. In addition, some studies have observed the A state population to be greater than the ground state, speculating the cause to be due to direct chemical formation of the A state or by a collision induced transition with a preference for the A state [5]. MgO particle formation is observed in both the seeded flame and the bulk Mg combustion, the excitation-detection scheme used eliminates Mie scattering as a possible contributor to the signal.

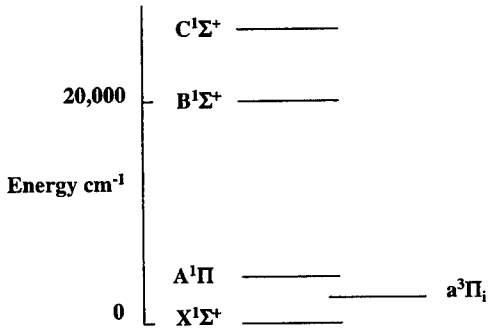

Fig. 1. Energy Level Diagram of MgO

4. Excitation Scan Results

Laser induced excitation spectra recorded by excitation of the $B^1\Sigma^+$-$A^1\Pi$ transition and fluorescence detection of the $B^1\Sigma^+$-$X^1\Sigma^+$ transition in the magnesium chloride seeded acetylene-air flame are presented in Fig. 2. Several dyes are needed to complete the excitation scans over the full spectrum. Laser pump energy density is maintained at 0.85 J/cm^2; this fluence is experimentally determined to minimize background and maximize signal. The sample region is centered at 15 mm above the burner surface and extends 8 mm horizontally, and it is 1 mm in height and, approximately 0.7 mm thick. The dye laser is run in burst scan mode at 0.001 nm stepping. Dye laser hold is set at 3.2 seconds per step. The signal is collected by a boxcar integrator with 3 pulse averaging, a >10 Hz input filter, and 20 ns gate.

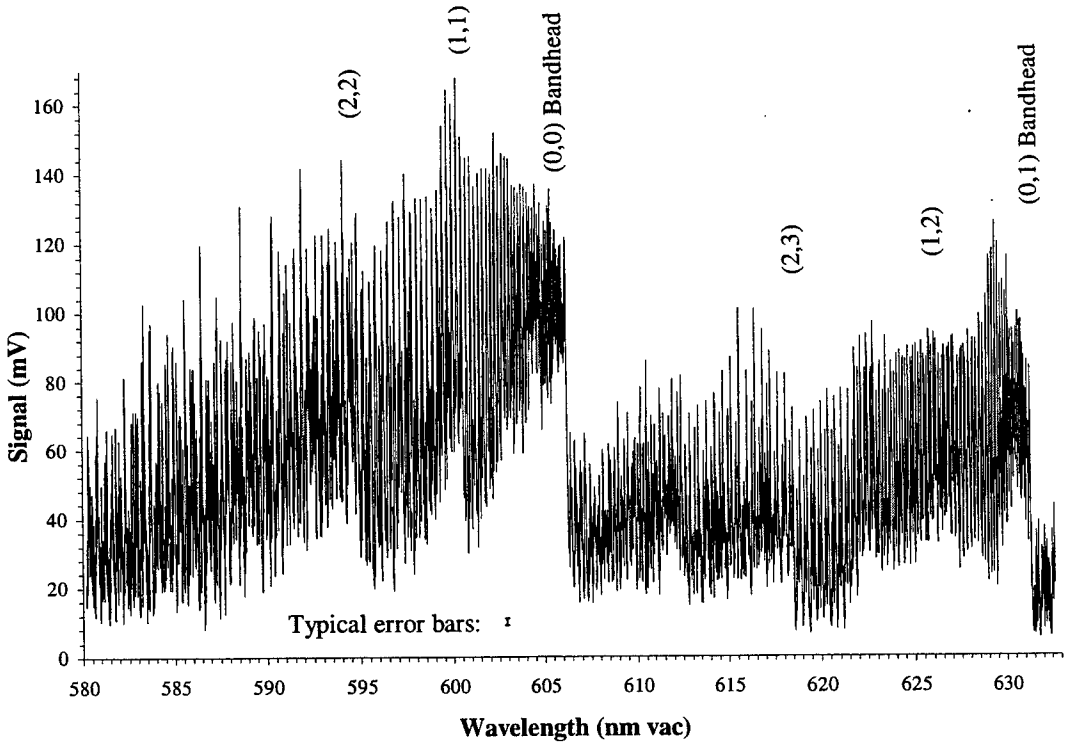

Fig. 2. Laser induced fluorescence excitation spectrum of MgO $B^1\Sigma^+$-$A^1\Pi$ transition.

5. Conclusions

The excitation spectrum of MgO reveals a dense and complex structure with many active states. The most dominant feature of the spectrum is the (0,0) bandhead at 606 nm. The R, P, and Q branches trail to the blue, overlapping with (1,1) transitions at 601 nm and the (2,2) band at 594 nm. The Δv=-1 vibrational bands, (0,1), (1,2), and (2,3) were also present due to the high temperature in the flame. The probable beginning of another set of lines, most likely from Δv=-2 vibrational transitions, appear at the far right in Fig. 2.

This work is an improvement over the only previous seeded flame study of MgO [5]. Pasternack et al.[5], seeded an acetylene flame with magnesium chloride and performed excitation scans of the $B^1\Sigma^+$-$A^1\Pi$ transition with a 0.25 cm^{-1} bandwidth laser. In their work [5], individual transitions were not well resolved, with distinct lines not emerging until 3 nm from the (0,0) bandhead, in this work, the comparable dimension is less than 0.5 nm. Pasternack et al. [5], also failed to observe the Δv=-1 vibrational bands, this may have been a simple oversight in that they did not probe to the red of the (0,0) bandhead.

The excitation scans are of sufficient quality, high signal-to-noise ratio and resolution, to accurately locate a large number of line positions. These data have been used to derive spectroscopic constants of the MgO $A^1\Pi$ state.

6. References

1. Lagerqvist, A., and U. Uhler, "The red and green bands of magnesium oxide", Ark. Fys **1**, 459-475 (1949).

2. Civis, A., Hedderich, H., Blom, C., "The infrared spectrum of magnesium oxide: a diode laser study using the discharge-enhanced reaction between hot magnesium vapor and N_2O", Chem. Phys. Lett. **176**, 489-494 (1991).

3. P.C.F. Ip, Ph.D. thesis, "Laser spectroscopy and dynamics of magnesium + nitrous oxide flame systems", Department of Chemistry, Massachusetts Institute of Technology, USA (1983).

4. Azuma, Y, Dyke, T.R., Gerke, G.K., Steimle, T., "Laser-Induced Fluorescence and Microwave-Optical Double-Resonance Study of the $B^1\Sigma^+$-$X^1\Sigma^+$ System of Magnesium Monoxide", J. Mol. Spec. **108**, 137-142 (1984).

5. Pasternack, L., A. P. Baronavski, and J. R. McDonald, "Application of saturation spectroscopy for measurement of atomic Na and MgO in acetylene flames", J. Chem. Phys. **69**, 4830-4837 (1978).

NO Detection by Cavity Ringdown Laser Spectroscopy

Alexandre D. Usachev,[1] Tracy S. Miller, Jagdish P. Singh,[✉] Fang-Yu Yueh,
Ping-Rey Jang and David L. Monts.

Diagnostic Instrumentation and Analysis Laboratory,
Mississippi State University,
Research and Technology Park, 205 Research Boulevard,
Starkville, Mississippi 39759-9734

Introduction

Rapid detection and precise analysis of explosives in the environment is playing an increasingly important role in the modern world:[1] for example, in criminal investigations of bombings, in detection of explosive materials concealed in mail or in airline baggage, in detection of soils and/or groundwater polluted by explosive materials. Spectroscopic methods can provide high selectivity and sensitivity for explosive detection.[2] Because of their low vapor pressure,[3] very sensitive detection is needed. Cavity Ringdown Laser Spectroscopy (CRDLS) is the most suitable technique for this purpose. The basic principles of CRDLS are presented in Reference 4.

The absorption spectra of most nitro explosives dissolved in ethanol lie in the UV spectral region (210-260 nm),[5] due to an $n \rightarrow \pi^*$ electronic transition primarily associated with the nitro group. Unfortunately, the mirrors available for this region have relatively poor reflectivities (Fig.1), limiting the detection sensitivity (Table 1). In spite of relatively low of UV-CRDLS detection sensi-

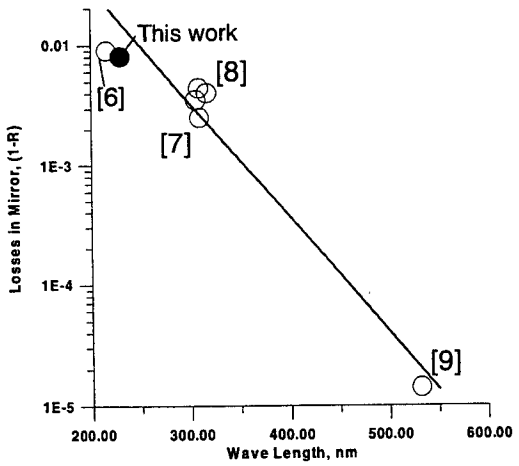

Figure 1. Losses (1-R) for Mirrors used in Different Works

Table 1.
CRDLS Sensitivity (Absorption/pass) for Different Mirror Reflectivities R with decay time precision $\delta\tau/\tau$=2%.[3]

R	Absorption/pass
0.995	102 ppm
0.999	20 ppm
0.9999	2 ppm
0.99999	0.2 ppm

tivity, a few works have appeared in the last five years.[5-7] Recent rapid progress in mirror coating technology permits hope for further decreasing mirror losses.

As an initial step in our effort to measure gas-phase 2,4,6-trinitrotoluene (TNT) by means of UV-CRDLS, we have investigated UV-CRDLS detection of NO. Nitric oxide was chosen for study because (1) it has a well-known absorption spectrum in the appropriate spectral region for testing and optimizing the experimental setup and (2) since UV-detection of TNT usually involves photo-fragmentation of TNT and subsequent production of NO,[10,11] the effect NO on the UV-CRDLS signal of TNT will need to be taken into account in our future investigations.

(Visiting scientist, July-December 1999, from Russian Academy of Sciences,
HEDRS-IVTAN, Izhorskaya, 13/19, Moscow, Russia 127412.
✉ Corresponding author phone: (662) 325-7375; fax: (662) 325-8465; E-mail: singh@dial.msstate.edu

Experimental

Figure 2 illustrates the experimental arrangement. A dye laser (Continuum ND60) was pumped by the third harmonic (355 nm) of a pulsed Nd:YAG laser (Continuum NY82S-10) with 10 Hz repeti-tion rate. The pulse duration was about 7-8 nsec. The dye laser was operated with Coumarin 460

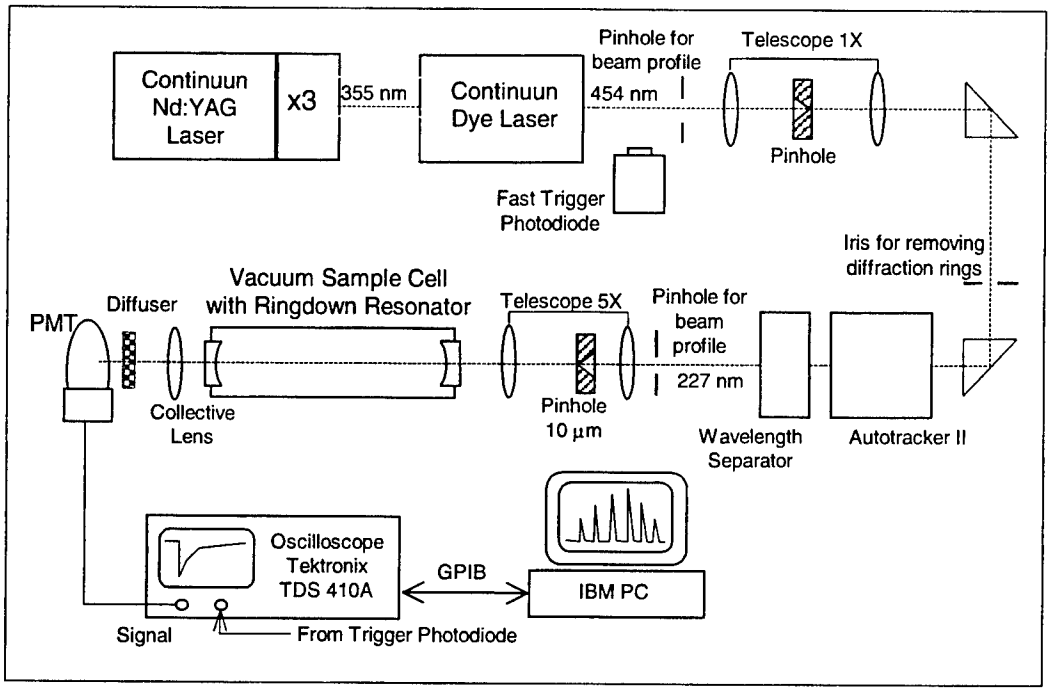

Figure 2. Schematic of UV-CRDLS apparatus.

dye and generated 5 mJ pulses with 0.04 cm^{-1} spectral width in the 445-485 nm spectral range. To achieve a proper spatial quality, 1X-Galilean telescope with two 200 mm focal length lenses, a 100 μm pinhole was used together with two iris apertures. The dye laser was doubled by an Inrad AT-II Autotracker II and filtered by an Inrad 752-104 four-prism filter. Mode matching was achieved with the help of a 5X-Galilean telescope with two quartz lenses with 20 and 100 mm focal lengths and a 10 μm pinhole. The 227-nm laser beam entering the ringdown cavity has 3-mm diameter and 0.75 m^{-1} beam convergence. The vacuum sample chamber was built from ultrahigh vacuum components and has 59 cm length. The mirrors are from MLD Technologies Corporation with 0.91-0.93 reflection coefficient (in spectral range under consideration) and 6-m radius of curvature. The Hamamatsu R166UH photomultiplier tube is used for registration of the decay waveform. Special attention was paid to the acquisition mode of the PMT to avoid signal saturation. As was experimentally verified, the signal amplitude with 50 ohm impedance does not exceed 20 mV. To make the receiver system less sensitive to the ringdown resonator alignment, a converging lens and quartz diffuser plate before PMT are used. Signals are digitized by a Tektronix TDS 410A digital oscilloscope and transmitted to a PC through a GPIB interface.

Results and Discussion

The goals of the experiment were to estimate noise equivalent sensitivity (NES) of the setup and to receive an absorption spectrum of a trace amount of NO. A typical decay curve is presented in Fig. 3. The scope averaged together 10 waveforms. The gate for the exponential fitting was chosen between 0.1 and 0.6 μs. Under this conditions decay time τ at 227 nm was equal 244 ns which corresponds for mirror reflectivity R of 0.992. The decay time deviation $\delta\tau/\tau$ did not exceed 1.5%.

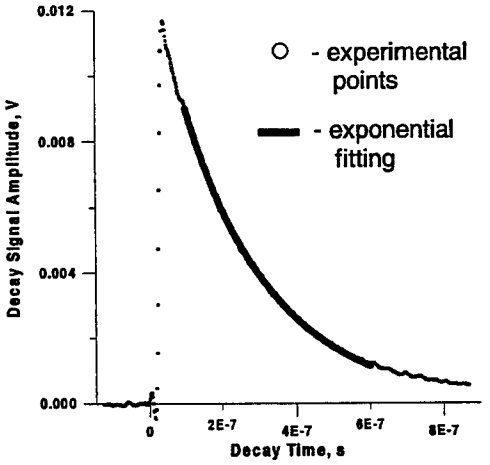

Figure 3. UV-CRDLS Ringdown curve for NO.

The measured NO UV-CRDLS absorp-tion spectrum is presented in Fig.4 together with a calculated spectrum. In this experiment the NO pressure was around 1 mtorr which is the detection limit of the pressure sensor used. As one can see, there is a good correlation between measured and calculated spectra. NES consisted of 100 ppm/pass or 2×10^{-6} cm^{-1}.

The data presented here is our initial work. Future investigations include the TNT absorption spectra in gas-phase.

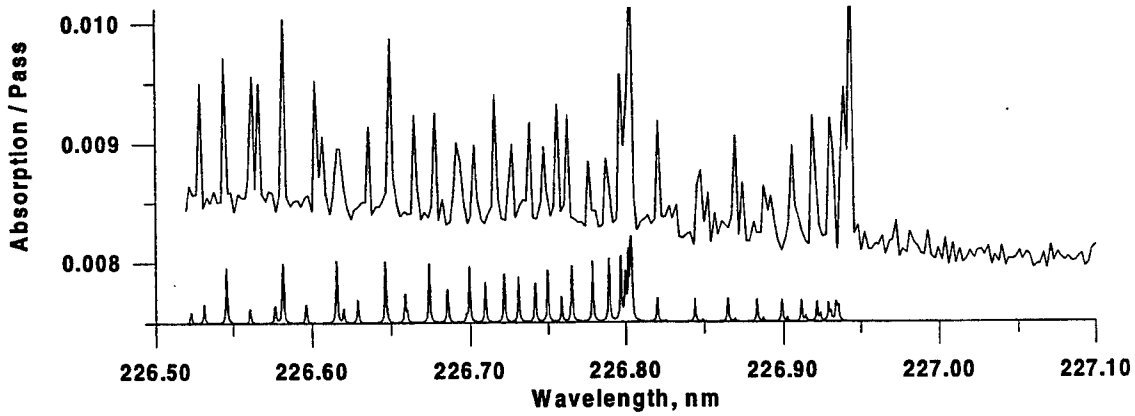

Figure 4. UV-CRDLS absorption spectra of NO recorded as a function of dye laser wavelength. T = 300 K and NO pressure 1±0.5 mtorr.
The lower is a calculated spectrum, the upper is the measured spectrum.

Acknowledgments

The work is supported by US Department of Energy, contract number DE-FG02-93CH-10575. The authors wish to thank Dr. Ch. B. Winstead for help and useful discussions.

References

1. J.I.Steinfeld and J.Wormhoudt, "Explosives Detection: A Challenge for Physical Chemistry", *Annu. Rev. Phys. Chem.* **49**, 203-232 (1998).
2. D.L.Monts et al, Laser- and Optical-Based Techniques for the Detection of Explosives", Encyclopedia of Analytical Chemistry: Instrumentation and Applications, Wiley, Chichester, UK, 2000. In Press.
3. B.C.Dionne *et al, J. Energ. Materials.* **4**, 447-472 (1986).
4. J.J.Scherer *et al, Chem. Rev.* **97**, 25-51 (1997).
5. W.A.Schroeder *et al, Anal. Chem.* **23**, 1740-1747 (1951).
6. P.Zalicki *at al, Chem. Phys. Lett* **234**, 269-274 (1995).
7. X.Mercier *et al, Chem. Phys. Lett* **305**, 334-342 (1999).
8. S.Cheskis *et al, Appl. Phys.* **B 66**, 377-381 (1998)
9. J.J.Scherer and D.J.Rakestraw, *Chem. Phys. Lett* **265**, 169-176 (1997).
10. Dongdong Wu *et al, Appl. Opt.* **35**, 3998-4003 (1996).
11. G.M.Boudreaux *et al, Appl. Opt.* **38**, 1411-1417 (1999).

Pressure Dependence of Polarization Spectroscopy Signals

J. Walewski, C. Kaminski, and M. Aldén
Lund Institute of Technology, Division of Combustion Physics, Box 118
SE-22100 Lund (Sweden)
+46-46-2229858, +46-46-2224542, clemens.kaminski@forbrf.lth.se

Abstract: In this work investigations on the dependence of polarization spectroscopy signal on gas pressure and species concentration are presented and compared with results from laser-induced fluorescence.

OCIS codes: (300.0300) Spectroscopy; (300.6290) Spectroscopy, four-wave mixing

1 Introduction

Polarization spectroscopy (PS) is a fairly new resonant laser-spectroscopic method in the field of combustion diagnostics, combining interesting features. It was first demonstrated in flames by Zizak et.al. [1] and later for flame radicals by Nyholm et.al. [2]. In contrast to laser-induced fluorescence spectroscopy (LIF) PS has the advantage of being a coherent technique, which means the signal propagates as a laser like beam which is easily discriminated against incoherent background radiation. Unlike other parametric non-linear spectroscopic methods no critical phase-matching condition has to be fulfilled when using this technique. This makes the overall setup fairly easy. Moreover PS has very interesting characteristics for combustion diagnostics, like scattering-free detection [3] and detection of species with weak or no fluorescence signal.
Today one of the main drawbacks of PS is the lack of a general theory describing the dependence between obtained PS signal and relevant flame parameters like species concentration and temperature.
New theoretical approaches are under development (see for example [4]), but these have to be compared with experimental results.

Extensive studies on the pressure dependence of PS signal in low pressure flames have been carried out. To make a comparison possible with theoretical models, the work was focused on two issues: pressure dependence of the saturation intensity and dependence of the PS signal on species concentration.

2 Experimental

For this investigation the OH radical was chosen because of well separated absorption lines and its well understood spectrum.
The excitation source was an optical parametrical oscillator (OPO) pumped by a Nd:YAG laser. The frequency doubled output of the OPO was approx. 6 mJ at 309 nm, and the linewidth approx. 0.3 cm^{-1}. The total energy of the beam was controlled by a beam attenuator. Approximately 0.1 % of the beam was split of to serve as the probe beam. The remaining beam served as pump beam and was linearly polarized using a Glan-Taylor type polarizer. Both beams were focused using a single 500 mm lens into a gas cell containing a low pressure burner. The probe beam passed through a polarizer within the gas cell, resulting in a linear polarization with 45° angle relatively to the pump beam polarization. The focused pump and probe beam were crossed in the center of the low pressure flame. The PS signal was generated in this crossing point. The excited line was $Q_2(8)$ in the $A^2\Sigma \quad X^2\Pi(0,0)$ band. The variation of the probe beam polarization was analyzed in the cell with a crossed polarizer after the flame. Then the probe beam was imaged on a photomultiplier outside the cell. LIF from the crossing point was collected at 90° and imaged on another photomultiplier. Fluorescence from other transitions than the $A^2\Sigma \rightarrow X^2\Pi(0,0)$ band was attenuated with glass filters in front of the photomultipliers.
The McKenna type burner in the middle of the low pressure cell was mounted on a height translator with a step motor making it possible to probe the flame at different heights above the burner.
The gas pressure in the cell was adjusted by varying the pump speed and a bypass nitrogen flow, which was

used to keep the polarizers free from condensation.

3 Results and Discussion

The dependence of the PS signal on the pump intensity I_p was recorded for fixed height above the burner and for different gas pressures. The relation between I_{PS} and I_p can be described by

$$I_{PS} \sim (I_p)^a \tag{1}$$

with $a = const.$ In our experiments both the pump and the probe beam intensity were varied simultaneously. The exponent a was attained through fitting equation 1 to the experimental data. For moderate spectral pump intensities ($I_p < 2 \cdot 10^7$ W/(cm^{2}cm^{-1})) the parameter a was found to be slightly below 3 and did not depend on the gas pressure p.
For higher pump intensities ($I_p \leq 6 \cdot 10^7$ W/(cm^{2}cm^{-1})) a was found to be much smaller (see table 1). This may be explained with saturation of the strong pump beam. Therefore the following model was used for fitting:

$$I_{PS} \sim I_{probe} \cdot \left\{ \frac{I_p}{(1 + I_p/I_{sat})} \right\}^2 \sim \frac{I_p^3}{(1 + I_p/I_{sat})^2} \tag{2}$$

The results of this fits are also shown in table 1, and an example for p = 700 mbar is seen in figure 1. The fits reveal a dependence of I_{sat} on p. One possible explanation for this is the faster dephasing of the induced birefrigency at higher pressures, leading to higher saturation intensities for I_{PS}.

Table 1. Fitted parameters for different gas pressures using equation 1 and 2.

p/mbar	a	$I_{sat}/10^7$W(cm^{2}cm^{-1})
30	1.8	2.4
700	1.8	3.8
900	2.2	5.3

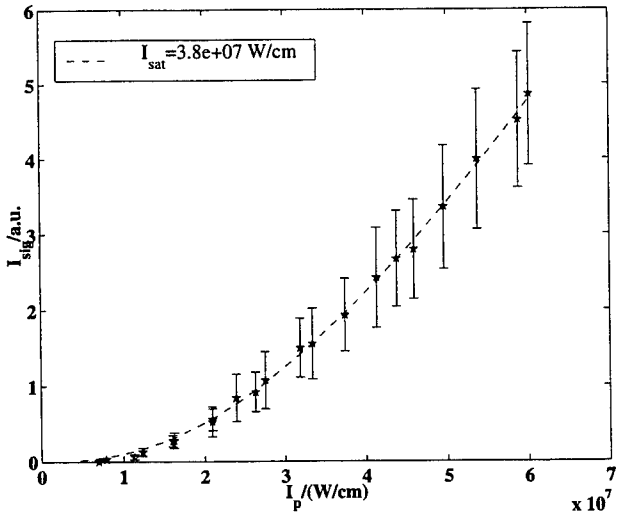

Fig. 1. Dependence of the signal strength I_{PS} on the pump intensity I_p at p = 700 mbar.

To investigate the dependence of I_{PS} on species concentration, heightscans were performed for different pressures. Both I_{PS} and I_{LIF} were recorded. The laser intensities were kept constant at $1.5 \cdot 10^7$ W/(cm^{2}cm^{-1}) (PS) and $5 \cdot 10^6$ W/(cm^{2}cm^{-1}) (LIF) respectively. The results for 30 and 700 mbar gas pressure are shown

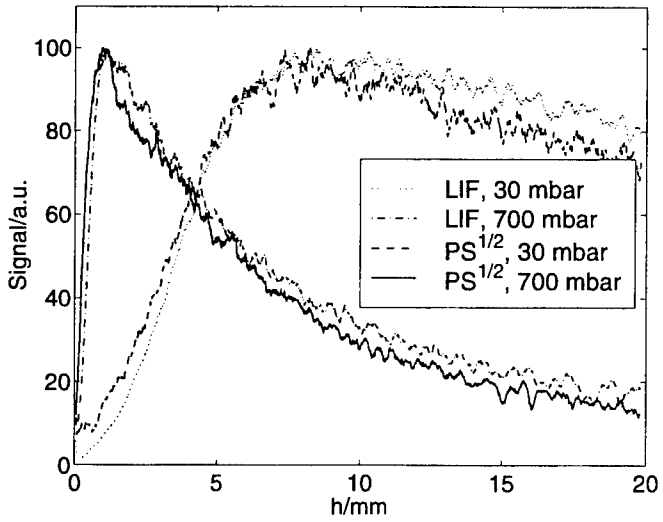

Fig. 2. Heightscans through center of the flame. h: Height above the burner. The signals are scaled on their maxima.

in figure 2. The LIF and PS signals were scaled on their maxima. In the figure $\sqrt{I_{PS}}$ is shown, accounting for the fact that I_{PS} depends on the number density squared. The overall trends of I_{LIF} and $\sqrt{I_{PS}}$ follow each other quite well. But for both 30 and 700 mbar I_{LIF} tends to be higher in the after burn zone of the flame. On the other hand, I_{LIF} is lower than $\sqrt{I_{PS}}$ in the reaction zone. A possible explanation for this small effect may be, that the LIF signal only is quenched by electronic collisions while the PS signal is quenched by both dephasing and electronic collisions. Depending on the flame composition at different heights the collision cross sections for these collisions may also vary compared to each other, leading to different collision rates for I_{LIF} and I_{PS}.

References

1. G. Zizak, J. Lanauze, and J. D. Winefordner. Cross-beam polarization in flames with a pulsed dye laser. *Appl. Opt.*, 25:3342–3346, 1986.
2. K. Nyholm, R. Maier, C.G. Aminoff, and M. Kaivola. Detection of OH in flames by using polarization spectroscopy. *Appl. Opt.*, 32(8):919–924, 1993.
3. J. Walewski, K. Nyholm, B. Löfstedt, R. Fritzon, A. Dreizler, and M. Aldén. Polarisation spectroscopy for combustion diagnostics. In *Survey of Combustion Research in Sweden*, pages 298–300, Gothenburg, Sweden, October 21-22 1998. The Swedish Section for Detonics and Combustion, The Combustion Institute.
4. T.A. Reichardt and R. Lucht. Theoretical calculation of line shapes and saturation effects in polarization spectroscopy. *J. Chem. Phys.*, 109(14):5830–5843, 1998.

An IR imaging system for remote sensing of chemicals

S. Kalem, O. Yavuzcetin, Tubitak Inst. of Tech., Turkey.

An IR active imaging system with separate optical pathways is constructed and tested for remote sensing of chemicals. The technique, which is based on laser light selective heating and its application to the detection of chemicals are discussed.

Laser Applications to Chemical and Environmental Analysis

Combustion Diagnostics 1

Sunday, February 13, 2000

Douglas S. Baer, Stanford Univ., USA
Presider

SuA
8:00am–9:50am
Anasazi North

Diode laser-based tunable ultraviolet sources for combustion diagnostics

Kristen A. Peterson and Daniel B. Oh*

Southwest Sciences, Inc.,1570 Pacheco St., Suite E-11,Santa Fe, New Mexico 87505

Phone:(505)984-1322; Fax (505)988-9230; peterson@swsciences.com; dboh@swsciences.com

Abstract: Tunable, wavelength modulated ultraviolet sources have been developed based on nonlinear conversion of high power diode laser outputs and were used to probe key combustion radicals by high sensitivity absorption and phase-sensitive fluorescence methods.

OCIS Codes: (120.1740) Combustion diagnostics; (300.6260) Spectroscopy, diode lasers

Quantitative mapping of combustion species with good spatial resolution is essential for improved understanding of flame chemical kinetics and fluid dynamics. Laser induced fluorescence (LIF) spectroscopy has been a main staple of combustion diagnostics due to its high detection sensitivity, selectivity, and excellent spatial resolution. However, extracting quantitative species densities from LIF measurements requires careful calibration of geometric factors and laser intensity, as well as modeling of fluorescence quenching by collision partners. This has been challenging even under the most favorable conditions.

Wavelength modulation absorption spectroscopy (WMS) provides quantitative, high sensitivity detection of trace species and is used in a diverse range of applications including combustion studies. Minimum detectable absorbance of 10^{-6} have been demonstrated with current-modulated diode lasers. However, this provides the integrated absorbance along a line-of-sight optical path and does not characterize the distribution along this line-of-sight.

LIF detection perpendicular to the laser beam can be used to map relative species densities along the line-of-sight while the integrated absorption available through WMS provides a mathematical constraint on the extraction of quantitative information from the LIF data. Combining line-of-sight absorption with LIF – especially if the measurements are made simultaneously with the same excitation beam – can yield quantitative, spatially-resolved combustion diagnostics of key intermediates under the reactive flow field. In order to demonstrate the viability of simultaneous WMS and LIF detection of flame species, we have been developing tunable, wavelength modulated UV sources based on nonlinear upconversion of tunable, wavelength modulated high power near-IR diode lasers. The generated light sources have been utilized to detect combustion radicals in laboratory flames. In this presentation, generation of tunable, wavelength modulated UV sources and the flame measurements of key combustion radicals including CH^1 and OH will described along with improvements in progress to achieve the quantitative, spatially-resolved combustion diagnostics.

References

1. Kristen A. Peterson and Daniel B. Oh, "High-sensitivity detection of CH radicals in flames by use of a diode-laser-based near-ultraviolet light source" Opt. Lett. **24**, 667-669 (1999).

Measurement of SO_2 and SO_3 in Aircraft Engine Exhausts Using a Tunable Diode Laser System

J. Wormhoudt, T.A. Berkoff, and R.C. Miake-Lye
Center for Aero-Thermodynamics, Aerodyne Research, 45 Manning Road, Billerica, MA 01821-3976
jody@aerodyne.com, rick@aerodyne.com

Abstract: We used a mid-infrared (lead-salt) diode laser and multipass cell to measure few ppm_v SO_2 concentrations in an aircraft engine exhaust in an altitude test chamber, and demonstrated the possibility of similar sensitivity for SO_3.

OCIS codes: (300.6260) Spectroscopy, diode lasers; (280.1740) Combustion diagnostics

1. Introduction

At Aerodyne Research, multipass TDL systems using signal processing based on the sweep-integration method have been developed and applied to the real-time analysis of multiple gas species concentrations, both within a single laser spectrum and in time-multiplexed spectra from two laser diodes [1,2]. In this paper, we report on a recent demonstration of a TDL system that provided in-situ measurements in the exhaust plume of an aircraft engine mounted in an altitude test chamber. The primary focus of this effort was to quantify the gaseous sulfur emissions, SO_2 and SO_3, in a representative exhaust under different altitudes, power conditions, and fuel sulfur loadings. This work was part of a NASA program with the overall objective of the development of scientific bases for assessing the atmospheric impacts of the exhaust emissions of aircraft. Our system had been applied to a number of other molecular species in several other tests. The work described here is unique in that an open-path multipass cell was used inside the engine test chamber to increase signal responsivity, and in-situ exhaust measurements of SO_2 and SO_3 had not previously been conducted using a TDL spectrometer.

2. Lead-salt tunable diode laser system

The TDL system used consisted of an optical table that includes a liquid nitrogen dewar housing the laser diodes and photodetectors. Light from the two diodes at opposite sides of the dewar (each side has four diodes which can be accessed by translation of collection optics) is collected and combined to form a pair of co-axial collimated beams that can be directed off the table using a steering mirror. Optical beam aiming and alignment are facilitated using a visible trace beam from a HeNe laser. A reference path is also included that incorporates a monochromator and reference gas cells to monitor the diode outputs for mode purity, correct operating wavelength range, and measurement of wavelength tuning rate parameters.

The temperature and current of the laser diodes are controlled by software running on an IBM compatible computer that is interfaced with a laser diode controller manufactured by Laser Photonics. With this system, spectral information for two different wavelength regions is obtained by alternating the current sweep signal applied to the two diodes. For the measurements reported here, a laser diode sweep rate of ~600 Hz was used and averaged spectra were written to disk at prescribed time intervals for later analysis. Laser diode tuning rate parameters are determined from the reference cell spectra and are entered into the TDL analysis software to provide the absolute frequency scale required for quantitative analysis. The TDL software includes a sophisticated collection of fitting routines that enable the concentration levels for multiple constituents to be calculated and displayed in real-time or during post-test analysis. This is accomplished by using molecular line parameters and fitting to a set of Voigt line profiles using a weighted non-linear least squares method to obtain fit parameters inluding the constituent mixing ratios of interest.

3. NASA PSL-4 test chamber set-up

The aircraft engine exhaust measurements took place at the Propulsion Systems Laboratory (PSL) at NASA Lewis (now Glenn) Research Center. This facility houses two different chambers 38 feet in length and 24 feet in diameter capable of providing true flight simulations for altitudes up to 70,000 feet for testing of aircraft engines. The engine used in this test was a Pratt & Whitney F100-200E turbofan engine. Test

conditions ranged from idle to military power settings over a range of altitudes from sea level up to 55,000 ft. The simulated Mach number was 0.8 for all conditions except at sea level when the Mach number was nominally zero. Four different fuels were used that ranged in sulfur content from ~18 to 1113 ppm by weight. The engine test program took place over the course of a month, with measurements obtained for engine test runs on 13 different days from 8 August to 6 September 1997. The TDL optical table was mounted outside the test chamber. It was oriented so that the steering mirror could send the IR and visible HeNe beams through a CaF_2 window (with a 1° wedge) in the chamber wall to a pair of multipass mirrors mounted on either side of the engine exhaust. The multipass mirrors were 15 cm in diameter with a 91.4-cm focal length and were configured in an open path multipass cell of the Herriot type which yielded 14 passes through the engine exhaust before returning to the TDL table. The multipass mirrors were mounted inside protective aluminum boxes with stainless-steel tubes 15 cm in diameter and 30 cm in length that provided a purged beam cover extending towards the edge of engine exhaust flow, leaving a 122 cm gap between the tubes. In the center of this gap was the exhaust flow, exiting from the engine nozzle approximately 65 cm in diameter. A probe rake mounted downstream of the IR laser beams included thermocouples to measure temperature at various locations within the exhaust flow as well as probes for gas sampling and pressure measurements. The mirror boxes, optical path, and optical table were purged with nitrogen to prevent recirculating exhaust affecting the mirrors and to reduce effects from atmospheric water vapor and methane. Figure 1 shows a schematic of the engine test-cell setup.

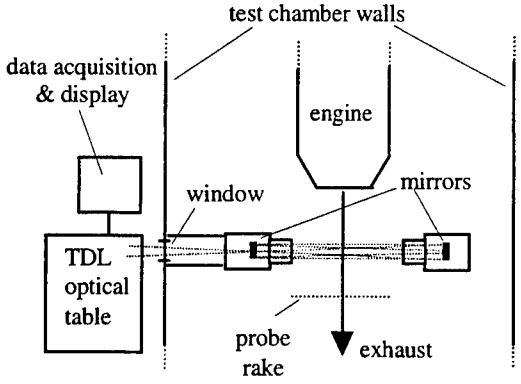

Fig. 1. Schematic of the engine test chamber set-up

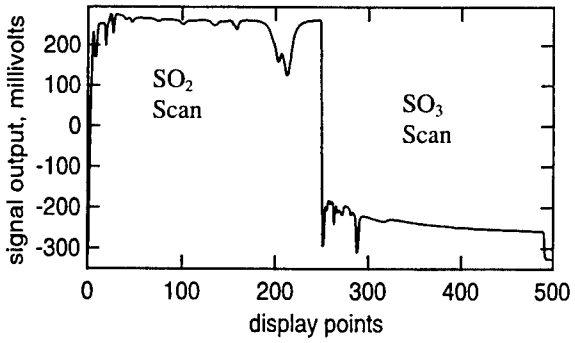

Fig. 2. Raw signal output from photodetector

4. Aircraft engine measurements

Figure 2 shows a typical raw diode intensity spectrum observed during engine exhaust measurements. The left side of the scan is the diode intensity sweep for the SO_2 region and the second half of the trace is the intensity sweep for the SO_3 region. The strongest absorption feature seen in the SO_2 (left) scan corresponds to the water absorption line at 1332.757 cm^{-1}. Since water lines are present in both the SO_2 and SO_3 scans, water vapor concentration was also available from recorded spectra. Baseline variations due to interference fringes, diode laser intensity fluctuations or other broad spectral features unrelated to absorption species of interest, were represented by a fourth order polynomial incorporated into the fitting routine. For the results reported here, spectra recorded during engine tests were evaluated for SO_2 and SO_3 concentrations after the test when average exhaust temperature and pressure values, derived from the probe rake sensors, could be used in the analysis. Fig. 3 shows examples of spectra recorded during engine tests for SO_2 and SO_3 along with the corresponding least-squares fits used to calculate concentration levels. Line parameters used in the least squares fits are taken from the HITRAN compilation or from more recent measurements. An analysis of the noise present in recorded spectra indicated that the minimum detectable concentration for SO_2 was less than 1 ppm_v and for SO_3 less than 2 ppm_v for spectra averaged for 1 minute. An analysis comparing spectra for the highest and lowest fuel sulfur loadings indicated that SO_3 levels were below the detection limit.

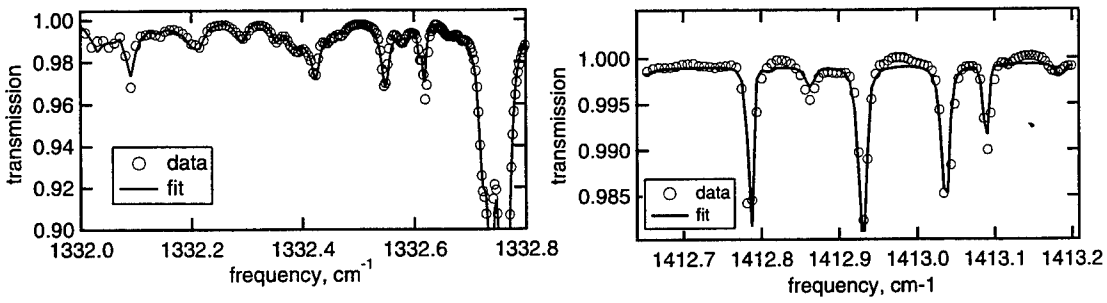

Fig. 3. Example spectra showing data (circles) and fit (line) for SO_2 (left) and SO_3 (right) spectral regions

The primary focus of this effort was to quantify, for a variety of engine operating conditions, the engine emission indices for SO_2 where emission index (EI) is defined as the weight in grams of an exhaust component per kilogram of fuel burned. Since water lines were available in the SO_2 spectra, and the emission index for H_2O is known for a given fuel, relative column densities were used to yield a direct measurement of SO_2 EI. Of particular interest was the calculated SO_2 EI obtained from TDL measurements to the theoretical EI derived from separately measured fuel sulfur content and assuming 100% conversion of fuel sulfur to SO_2. A value of this quantity greater than 1 clearly indicates a measurement error, while a value differing from 1 by more than our estimated error limits indicated currently unknown plume chemistry forming other sulfur oxide species. Our measurements for three different fuel sulfur contents (152, 336, & 1113 ppm_m) and a variety of simulated altitudes, each averaged over all engine conditions, comprise 14 cases. In all but one case, our value for fraction of sulfur in the fuel converted to SO_2 is in the range of 70–90%, with error estimates typically around 20%. The one exception (in which the sulfur conversion fraction was 110% ±19%) was the lowest sulfur loading at the next to lowest altitude. This case is difficult both because of the low SO_2 concentration and because the higher pressure broadens lines into each other and makes accurate baseline determination more difficult. The low upper limit for SO_3 concentration (~10% conversion for some high sulfur cases) is consistent with the measured high level of sulfur emitted as SO_2. Furthermore, at chemical equilibrium, H_2SO_4 will not be a major species at this point in the exhaust.

5. Conclusions

We have successfully demonstrated operation of a lead-salt tunable diode laser system to measure SO_2 and SO_3 in the exhaust plume of an aircraft engine mounted in an altitude test chamber. Signal responsivity was enhanced using a pair of mirrors, mounted inside the test chamber, to form an open-path multipass cell that allowed 14 passes of the infrared diode laser beams through the engine exhaust. System noise for a 1 minute average during engine measurements corresponded to less than 1 ppm_v for SO_2 and less than 2 ppm_v for SO_3. Results obtained during a series of engine tests defined an upper bound for SO_3 and quantified SO_2 levels for a variety of test chamber altitudes, engine power conditions, and fuel sulfur loadings. Approximately 80% of the sulfur in the fuel is converted to SO_2, with our error limits allowing the possibility that SO_3 and H_2SO_4 emissions are very small or negligible. The TDL system performed reliably in a demanding environment, and could be considered for a variety of applications involving from non-intrusive detection of multiple gas species, such as fence line monitoring or measurement of stack emissions.

1. D.D. Nelson, M.S. Zahniser, J. B. McManus, J.H. Shorter, J.C. Wormhoudt, and C. Kolb, "Recent improvements in atmospheric trace gas monitoring using mid-infrared tunable diode lasers" in Application of Tunable Diode and Other Infrared Sources for Atmospheric Studies and Industrial Process Monitoring, A. Fried, ed., Proc. SPIE 2834, 148–159 (1996).

2. J. Wormhoudt, M.S. Zahniser, D.D. Nelson, J.B. McManus, R.C. Miake-Lye, and C.E. Kolb, "Infrared Tunable Diode Laser Diagnostics for Aircraft Exhaust Emissions Characterization", in Optical Techniques in Fluid, Thermal, and Combustion Flows, S. S. Cha and J. D. Trolinger, eds., Proc. SPIE 2546, 552–561 (1995).

Real-time 2-D imaging of water vapor in diffusion flames

Jeffrey S. Goldmeer and Daniel J. Kane
Southwest Sciences, Inc., 1570 Pacheco Street, Santa Fe, NM 87505
goldmeer@swsciences.com, djkane@swsciences.com

Abstract: An *imaging* Wavelength Modulation Spectroscopy system was developed for measuring combustion species concentrations in flames. Images taken at 23 Hz by a diode laser are used to generate "movies" of strong absorbers within the flame.

OCIS codes: (120.1740) Combustion diagnostics; (300.6260) Spectroscopy, diode lasers; (300.6340) Spectroscopy, infrared

Introduction

Ideally, to bridge the gap between chemistry and fluid mechanics in combustion, species concentrations and temperature profiles are needed throughout the flame. However, many techniques, invasive and non-invasive, are limited to point or line-of-sight measurements that cannot provide quantitative data over a larger physical domain. Other systems are not compatible with experiment environments that limit the size, weight, and/or power requirements of the diagnostic. This paper reports on a innovative *imaging* Wavelength Modulation Spectroscopy (WMS) system that can measure full field flame temperatures and species concentrations. This system is capable of taking images at near video frame rates to generate "movies" of strong absorbers in flames. This paper presents water vapor images of a two-dimensional diffusion flame using WMS and a near-infrared diode laser.

Wavelength Modulation Spectroscopy

WMS is a technique used to measure weak absorption signals slowly or, alternatively, strong absorption signals at high bandwidth. WMS has been applied to sensitive absorption measurements using visible or near-infrared GaAlAs or InGaAsP diode lasers [1]. This technique has the advantage over other laser-based methods as being simple and inexpensive to implement, provides signals which are directly linear in concentration, and is easily calibrated to provide accurate quantitative results. Unlike direct absorption, the detection sensitivity is limited by detector quantum noise and not by laser $1/f$ noise. This can improve the detection sensitivity by 3-4 orders of magnitude. This technique has been described in considerable detail elsewhere, including comparisons with other high frequency diode laser detection methods (e.g. one- and two-tone frequency modulation spectroscopy) [2]. In addition, these methods were previously applied to the measurement of water vapor in microgravity diffusion jet flames [3].

Briefly, this method, which is an extension of diode laser "derivative spectroscopy" techniques widely used at kHz frequencies, involves a superposition of a small sinusoidal modulation at frequency f on the diode laser injection current. In the small modulation limit, the WMS lineshape is the n^{th} derivative of the original molecular absorption lineshape. In practice, the modulation depth is set at a value to maximize the signal level and, in this regime, lineshapes only approximate derivatives, but can be readily calculated. The high sensitivity of WMS permits the *in situ* detection of chemical species of interest such as water, methane, O_2, CO, CO_2, OH, *etc.* at bandwidths approaching MHz ranges. The strong absorption line strengths of water make detection by optical means attractive and allows 2-D absorption images to be obtained in real time.

Detection bandwidths of ~ 100-200 kHz are required to obtain images in real time. To support this bandwidth, frequency modulations of 5 MHz and 364 kHz are superimposed, allowing the detection band to be moved down to frequencies compatible with digitizing electronics while maintaining the increased sensitivity of WMS. This is because the signal is demodulated at 10 MHz before digitization. The lower frequency modulation allows multiple sampling of the peak-to-trough amplitude of the high frequency $2f$ signal, nulling baseline effects [4].

Experimental Hardware

The optical layout is fairly simple, as shown in Fig. 1. A wavelength modulated laser beam is collimated by an anti-reflection coated aspheric lens to a diameter of ~1 mm and is pointed onto an X-Y optical scanner placed at the focus of an off-axis paraboloid (OAP). The laser beam then passes through the flame and reflects off a second off-axis paraboloid, which focuses the beam onto a photo-diode (PD). The raw AC signal is demodulated at 10 MHz before

being read via a fast A/D and recorded on the host computer. This system has an acquisition rate of approximately 238,000 pixels per second allowing a 100×100 array of pixels to be obtained at a rate of 23.8 Hz (42 ms per frame). This high data rate is attainable because of the large signal-to noise obtained when using WMS. The system uses a near-infrared 1.4 μm laser diode tuned to a water vapor absorption line whose line strength is optimal at 1800 K. Initial tests indicate a signal-to-noise of 60 with a bandwidth of 184 kHz for absorbances of ~2-3% due to this (7,6,2)←(7,6,1) transition at 7179.75 cm^{-1} of the v_1+v_3 combination band.

Experiments are performed using a two-dimensional methane/air diffusion flame produced with a Wolfhard-Parker slot burner shown in Figs. 2 and 3. The laser raster scan configuration used for these experiments provides a 2.5 c x 2.5 cm scan area nearly centered on the fuel slot, as shown in Fig. 3. The base of the scan is positioned just abo the surface of the burner. All experiments were conducted in ambient air, with a nominal ambient pressure of 0. Atm.

Experimental Results

This experiment generates four channels of data: AC & DC absorption data, and X-Y scanner positions. Since t laser beam is focused onto a single location on the detector, the absorbance data must be mapped to the correct locati within the scan area using the X-Y position data. Once re-mapped, the absorbance data and the XY position data c be used to create images of the water vapor absorbance within a steady flame (Fig. 4) or a transient flame (Fig. 5

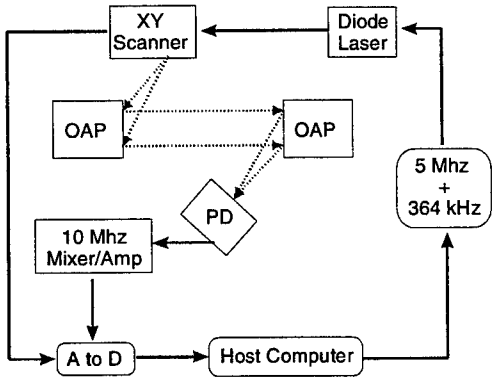

Figure 1 - Schematic diagram of the imaging system. (The flame is located between the OAPs.)

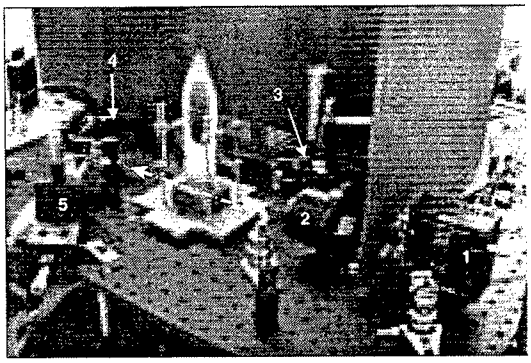

Figure 2 - Two-dimensional imaging system. The dotted arrow indicated the direction on the beam. Numbered components in the figure are: 1. diode-laser; 2. OAP; 3. X-Y scanner; 4. OAP; and 5. detector assembly.

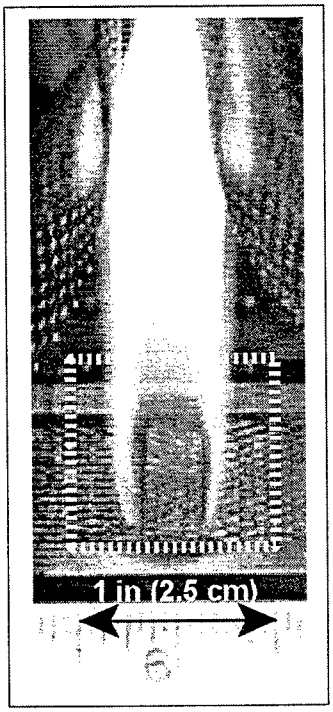

Figure 3 - Two-dimensional diffusion flame produced using a Wolfhard-Parker slot burner. The laser beam path is orthogonal to the ruler in the image. (Scale in inches.) The scan region is indicated by the dotted outline near the burner surface.

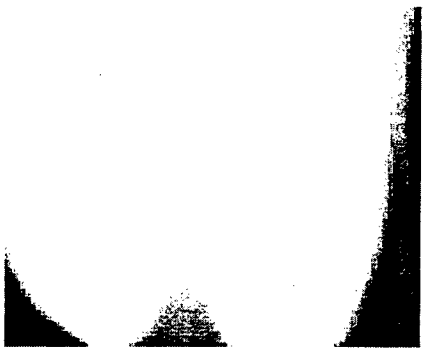

Figure 4 - Normalized water vapor absorbance image from a methane/air diffusion flame in a Wolfhard-Parker slot burner. White (bright) regions contain the highest absorption, dark regions the lowest.

In these images, gaseous fuel (methane) enters upward from the bottom, just left of center, with a co-flow of air on either side. White (bright) regions contain the highest absorption, dark regions the lowest. The flame in Fig. 5 is perturbed by a force flow (or wind), from left to right in the images, which are at 42 millisecond intervals. Images similar to these can be animated using numerous computer packages to generate a "movie" of water vapor absorbance in a flame.

Future Work

One of the goals of this project is to create "movies" of flame temperature and water vapor concentration within a flame. Flame temperatures can be measured using the ratio of absorbance measurements at two different wavelengths. These tasks require a parametric study to examine of the effect of temperature and number density on the absorption behavior. This study will be performed numerically using data from the Hitran database. An expected result of this study will be the creation of a three-dimensional absorption surface that is a function of temperature and number density. The absorption map along with a calibration measurement of the system will allow the relative absorption data, shown in Figs. 4 and 5, to be converted into an absolute measurement of water vapor concentration within a flame.

References

1. D.B. Oh, A.C. Stanton and J.A. Silver, Journal of Physical Chemistry **97**, 2246 (1993).
2. J.A. Silver, Applied Optics **31**, 707 (1992); D.S. Bomse, A. C. Stanton and J. A. Silver, Applied Optics **31**, 718 (1992).
3. J.A. Silver, D.J. Kane and P.J. Greenberg, Applied Optics **34**, 2787 (1995).
4. D.S. Bomse, Applied Optics **30**, 2922 (1991).

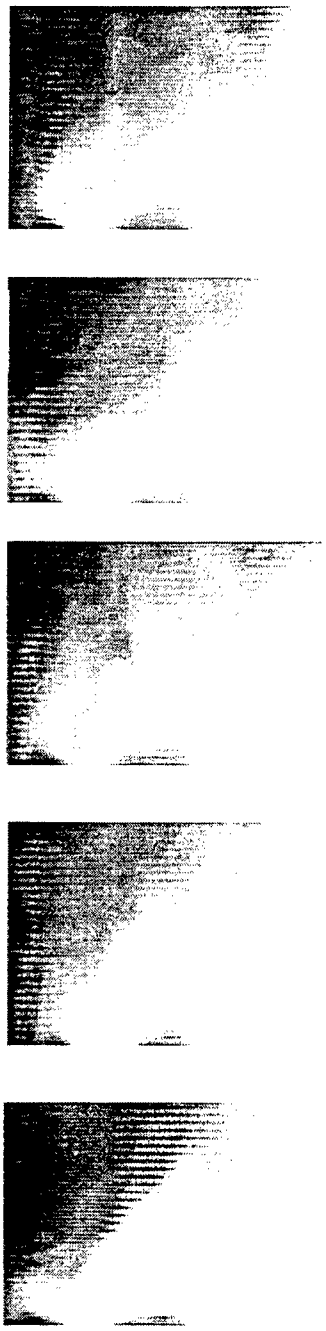

Figure 5 - Normalized water vapor absorbance images from a methane/air diffusion flame with a forced air flow from left to right. Images are 42 milliseconds apart.

Application of RF Frequency-Division Multiplexing for Multiple Species Measurements in Large Pool Fires

P.J. Santangelo, P.D. Ludowise, C.R. Shaddix,
S.W. Allendorf, D.K. Ottesen and G.L. Hubbard

Combustion Research Facility
Sandia National Laboratories
7011 East Avenue
Livermore, CA 94550
pjsanta@sandia.gov

Introduction

Researchers at Sandia have been experimentally and numerically investigating large-scale pool fires for several years, because of the risk that these fires pose to critical engineered systems during transport accident scenarios. Due to the difficulty of fielding optical measurement techniques in this turbulent, optically thick, high-temperature environment, experimental measurements in large fire research have traditionally been limited to thermocouples, heat-flux gauges, and bidirectional velocity probes. Recently, Sandia developed and successfully implemented an insulated, water-cooled fiber optic probe (see Figure 1) that utilized a combined HeNe-laser-absorption and a 2-color emission technique to determine soot volume fraction distributions and soot temperatures over a 2-cm sampling distance in a 6-meter diameter JP-8 pool fire [1]. With the collection and analysis of soot property data, attention has turned to the measurement of gas-phase species concentrations (together with soot properties), in order to evaluate mixing phenomena, gas-phase radiation interactions, and soot formation and oxidation chemistry in these large fires.

In principle, *in situ* tunable diode laser absorption spectroscopy (TDLAS), utilizing distributed feedback (DFB) lasers, allows for a fast (1 kHz) frequency response and reasonable spatial resolution can be achieved by physically constraining the probe volume. In addition, standard telecommunications grade fibers can be used to transmit light to and from an *in situ* probe. In spite of these favorable features of near-IR TDLs, performing quantitative species measurements in fires remains a formidable challenge. This is due to the very weak overtone and combination band rovibrational transitions in the near-IR in addition to the highly transient flowfield and the time-dependent beam steering, optical attenuation, and thermal emission effects from the sampled flame volume. These considerations, coupled with our desire to measure four different chemical species simultaneously, have necessitated a laboratory-based research program to elucidate the optimal design choices in fabricating a TDL system for applications to the fire environment. This paper will focus on our selection of radio-frequency (RF) frequency-division multiplexing as a viable option for spectroscopic applications and specifically on design considerations for the simultaneous measurement of multiple species.

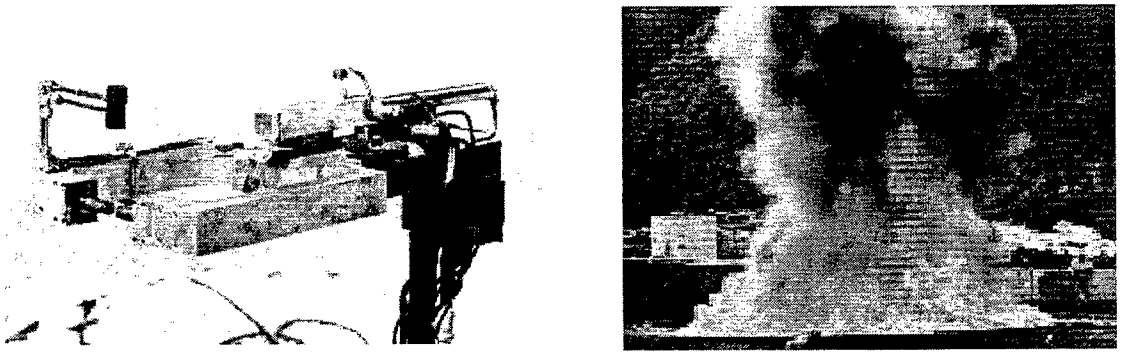

Figure 1. The photograph on the left shows a fiber-optic probe design for local optical measurements in large fires. A typical experimental flame system is a 5-m diameter pool fire of JP-8, shown here in the photo on the right.

RF WMS/Frequency-Division Multiplexing

The two most common techniques to sensitively perform TDL absorption spectroscopy are to use wavelength modulation spectroscopy (WMS) or to apply balanced ratiometric detection (BRD). However, the BRD approach does not respond well to transient variations in the measured light intensity and therefore is not well suited for measurements in the pool fire environment. In order to properly interpret the 2nd harmonic (2f) signal from a wavelength-modulated TDL spectral scan, the characteristic scan time across the absorption feature of interest must be less than any of the time scales characterizing the flowfield across the probe volume. Experimental measurements show that these time scales can be less than 1 ms. Therefore, in order to apply WMS to kHz frequency spectral scans, modulation frequencies > 1 MHz must be used. Such frequencies are easily achieved, but commercial diode controllers are limited to 2 MHz modulation and commercial RF lock-in amplifiers are expensive and have time constants on the order of 100 μs, which are insufficient to suitably resolve kHz-level spectral scans. Consequently, we have evaluated the relative merits of utilizing 2f detection via the use of custom RF lock-in amplifiers.

Several options exist for a multiplexed TDL system, including "temporal stagger", "grating separation", and "frequency-division" approaches. For this application, with the incumbent need for RF WMS, the "frequency-division" approach appears to be most favorable, although there are important considerations such as saturation of the detector and 2f crosstalk.

Frequency-division multiplexing has been demonstrated by Oh et al. [2] for two lasers modulated by sine waves at 40 and 50 kHz, respectively and a low frequency (LF) "saw tooth" or "ramp" function of 39 Hz. In order to extend the frequency-division approach to RF multiplexing and to determine the minimum high frequency spacing (ΔHF) necessary, we performed experiments in two separate combustion environments. First, two TDLs operating at 1.55 μm and 1.57 μm, respectively, were used to simultaneously detect H_2O and CO_2 in a 1-atmosphere optical furnace. In a separate experiment, two separate H_2O lines and one C_2H_2 line were detected in a buoyant, turbulent diffusion flame.

For the ambient pressure, optical furnace (see Figure 2), the injection-current of each laser is modulated by a different high frequency (HF ~ 1 MHz) sine wave and a low frequency (LF~1 kHz) ramp. The LF ramp varies the current linearly thereby tuning the laser across a specific wavelength range. The laser light is combined via a fiber coupler, traverses the probe volume and is focused on one detector. To separate the information from each laser, the detector signal is then split and directed to custom RF lock-in amplifiers locked to the HF frequency or a multiple (harmonics) of the HF frequency of each of the lasers. The goal is to ensure that the output of each lock-in amplifier is independent and represent the information from *only* one laser. Information from one laser may leak into the signal of the other if the two modulation frequencies are too close. Experiments were performed to determine the minimum modulation frequency separation (ΔHF) to prevent crosstalk (see Figure 3) and adequately resolve the shape of the absorption features.

Crosstalk was evaluated at frequency separations of 100 to 20 kHz. No significant leakage occurred until ΔHF was less than 60 kHz using our own custom lock-in amplifiers. Therefore, as long as ΔHF > 60 kHz, the two molecular species can be measured simultaneously, over the same probe volume, without crosstalk. Crosstalk was also evaluated for 3 multiplexed laser measurements made in a buoyant, turbulent natural gas diffusion flame with similar results. Therefore, with kHz slow ramps and modulations in the MHz, simultaneous measurements of multiple species can be made.

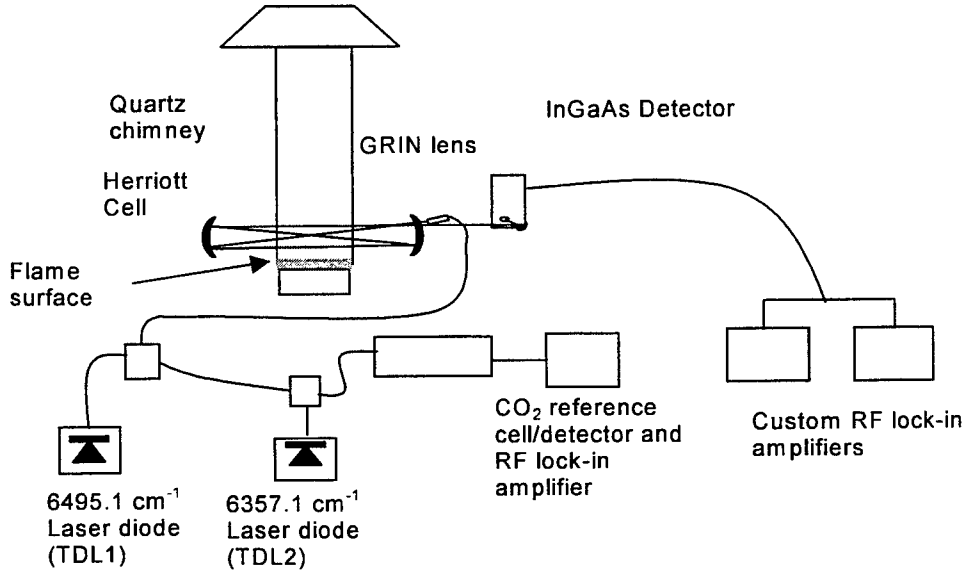

Figure 2. Schematic of 1 atmosphere optical furnace used for one multiplexing experiment.

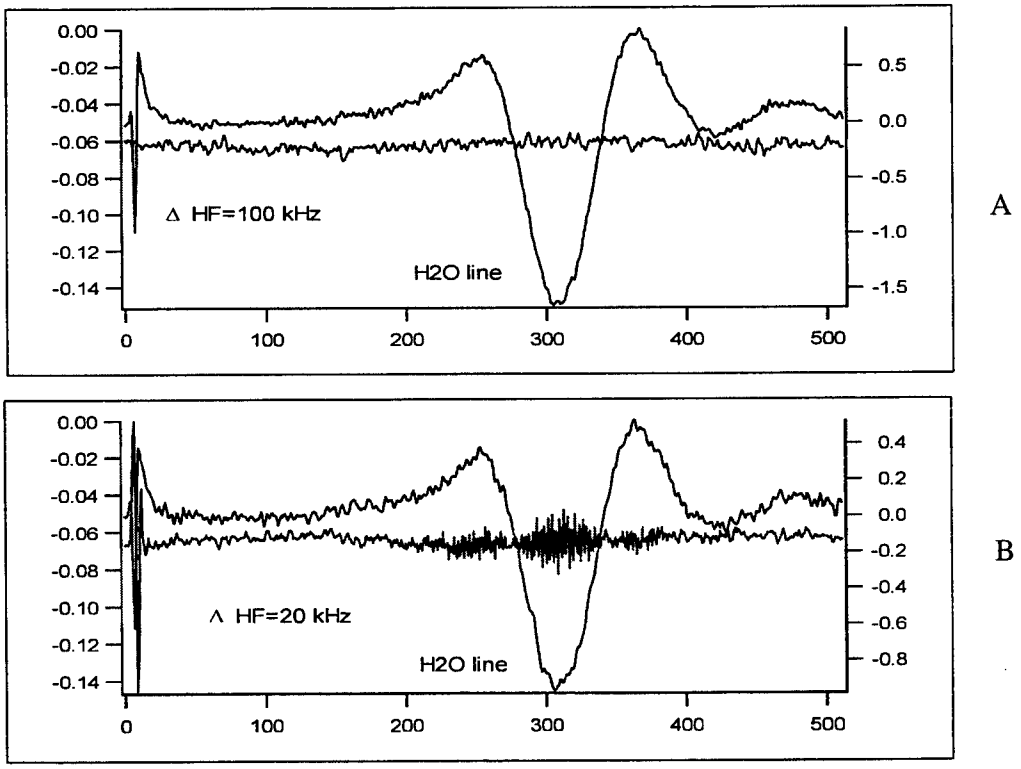

Figure 3. *A.* Trace of H_2O line and TDL2 lock-in signal with TDL2 off (measure of leakage) with $\Delta HF = 100$ kHz. *B* Trace of H_2O line and TDL2 lock-in signal with TDL2 off (measure of leakage) with $\Delta HF = 20$ kHz.

References

1. Gritzo, L.A., Sivathanu, Y.R., and Gill, W., "Transient measurements of radiative properties, soot volume fraction and soot temperature in a large pool fire", *Combust. Sci. Technol.,* 139:113, 1998.
2. Oh, D.B., Paige, M.E., Bomse, D.E., "Frequency modulation multiplexing for simultaneous detection of multiple gases by use of wavelength modulation spectroscopy with diode lasers", *Appl. Opt.* 37:2499, 1998.

In-situ Combustion Diagnostics Using Diode Laser Absorption Sensors

M.E. Webber, S. Kim, D.S. Baer and R.K. Hanson
High Temperature Gasdynamics Laboratory, Mechanical Engineering Department, Stanford University, Stanford, CA, 94305-3032
Phone: 650/723-0941, Fax: 650/723-1748, E-mail: webber@navier.stanford.edu

Abstract: The availability of extended wavelength DFB diode lasers makes *in-situ* flame measurements of important combustion species such as CO_2 possible. This work presents recent measurements near 2 μm of CO_2 concentration above flat-flame burners.

OCIS codes: (120.1740) Combustion Diagnostics; (300.6260) Spectrosocopy, Diode Lasers

In the past, multiplexed diode laser sensor systems have been applied for *in-situ* measurements of important combustion parameters such as gas temperature and water concentration [1, 2]. These *in-situ* measurements traditionally have been restricted to the near-infrared (NIR), where single-mode distributed feedback (DFB) diode lasers have been available. Conveniently, major combustion products H_2O and CO_2 both have absorption bands in the NIR at 1.4 and 1.5 μm respectively (See Figure 1). However, the large population (10–18%) of hot H_2O in the products of premixed natural gas combustion combined with H_2O's strong absorption band at 1.4 μm introduces significant spectral interference with the much weaker CO_2 band at 1.5 μm and inhibits accurate *in-situ* measurements of CO_2 at that wavelength. Previous work with this CO_2 band used fast extractive sampling techniques to make combustion measurements of CO_2 populations in order to eliminate the water interference and increase sensitivity [3]. The availability of new fiber-coupled DFB lasers at longer wavelengths, including 2.0 μm, enables interference-free *in-situ* flame measurements of CO_2. The 2.0 μm band of CO_2 is advantageous because its relative band strength is much greater than at 1.5 μm (see Figure 1) and because isolated CO_2 lines are available for *in-situ* monitoring (see Figure 2).

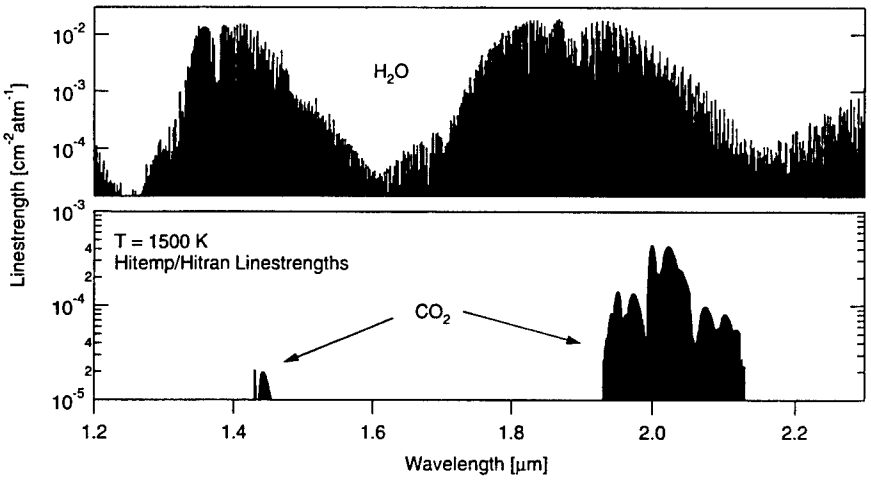

Fig. 1. Linestrengths of CO_2 and H_2O at $T = 1500K$ in the near-infrared.

Previous measurements of CO_2 at 2.0 μm employed external-cavity diode lasers (ECDL) whose convoluted power curves and low-bandwidth wavelength-tuning (less than 50 Hz) made the combustion sensors susceptible to baseline fitting errors and beam-steering related noise [4]. New DFB lasers can be tuned up to 10 kHz, thereby lessening beam-steering related noise, and have smooth power curves that can be estimated with polynomial fits for approximating zero-absorption baselines. Thus, the new work presented here offers improved results for fundamental spectroscopic measurements and *in-situ* flame measurements of CO_2.

The fundamental theory governing absorption spectroscopy is embodied in the Beer-Lambert law, Equation 1. The ratio of the transmitted intensity I_t and initial (reference) intensity I_o of laser radiation through

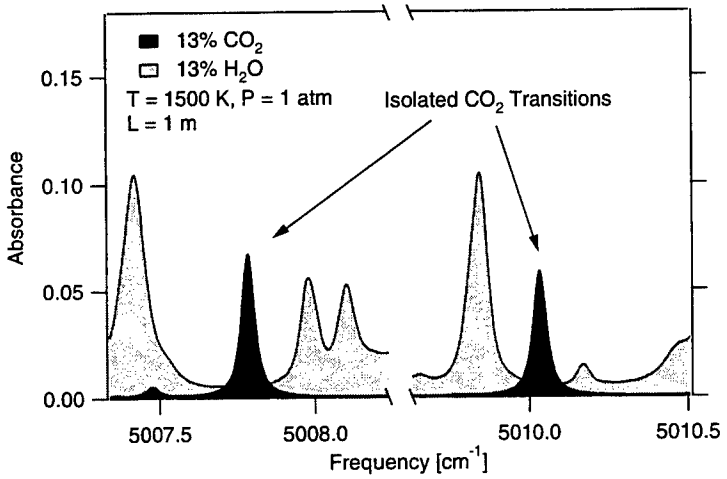

Fig. 2. Two isolated CO_2 transitions suitable for *in-situ* combustion monitoring based on HITRAN96 and HITEMP calculated spectra.

an absorbing medium at a particular frequency is exponentially related to the transition linestrength S_i [$cm^{-2}atm^{-1}$], lineshape function ϕ [cm], total pressure P [atm], molefraction of the absorbing species x_j, and the pathlength L [cm].

$$\frac{I_t}{I_o} = exp(-S_i \phi P x_j L) \tag{1}$$

The linestrength for an absorption transition can be measured using controlled partial pressures of pure CO_2 gas in a static cell that has a known pathlength. For premixed combustion environments, adiabatic temperatures are often greater than 1500 K. Thus, CO_2's absorption linestrengths at these elevated temperatures must be understood. The linestrength as a function of temperature for a particular CO_2 transition i is governed by its linestrength S_i at a reference temperature T_o; CO_2's partition function $Q(T)$; the frequency of the transition, $\nu_{o,i}$; and the lower-state energy of the transition, E_i''. This relationship is given by

$$\begin{aligned} S_i(T) &= S_i(T_o)\frac{Q(T_o)}{Q(T)}\left(\frac{T_o}{T}\right) exp\left[-\frac{hcE_i''}{k}\left(\frac{1}{T}-\frac{1}{T_o}\right)\right] \\ &\times \left[1-exp\left(\frac{-hc\nu_{o,i}}{kT}\right)\right]\left[1-exp\left(\frac{-hc\nu_{o,i}}{kT_o}\right)\right]^{-1} \end{aligned} \tag{2}$$

The measured variation of linestrength as a function of temperature for a particular transition and Equation 2 can be used to determine the lower-state energy of the transition. Once the temperature-dependent linestrength is known, laser absorption can be used to monitor the molefraction x_j of the target species.

Experimental room-temperature linestrength measurements for the two isolated transitions in Figure 2 are listed in Table 1. The linestrength measurements over a range of elevated temperatures are plotted in Figure 3 and overlaid with HITRAN96 predictions for CO_2. The measured lower-state energies for both transitions are also listed in Table 1, along with values from HITRAN96 for comparison.

	HITRAN96		Measured	
Position [cm^{-1}]	S_o [$cm^{-2}atm^{-1}$]	E'' [cm^{-1}]	S_o [$cm^{-2}atm^{-1}$]	E'' [cm^{-1}]
5007.787	0.00129	994.2	0.00143	983
5010.035	0.000424	1244.2	0.000427	1224

Table 1. Measured room-temperature linestrengths and lower-state energies compared with values from HITRAN96 for the two isolated CO_2 transitions shown in Figure 2.

The measured room-temperature linestrengths disagree with HITRAN96 by 11% for the transition at 5007.787

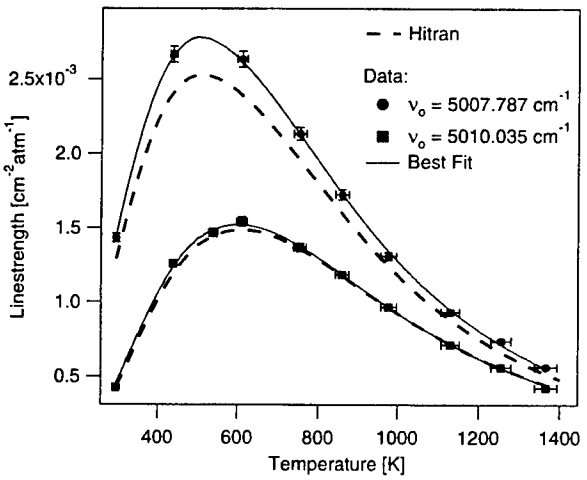

Fig. 3. Linestrengths vs. temperature for two isolated CO_2 lines.

cm^{-1} and agree within 1% for the transition at 5010.035 cm^{-1}. The measured lower-state energies for both transitions agree within 2% with HITRAN96.

With the development of real-time *in-situ* CO_2 sensors, diagnostics are now available that offer a more complete sensing capacity for combustion environments. Future multiplexing opportunities of CO_2 with H_2O and temperature diagnostics along with novel extended-wavelength room-temperature lasers at 2.3 μm for *in-situ* CO monitoring will be discussed.

References

1. D.S. Baer, R.K. Hanson, M.E. Newfield and N.K.J.M. Gopaul, "Multiplexed diode-laser sensor system for simultaneous H_2O, O_2 and temperature measurements", Optics Letters **19**, 22: 1900–1902 (1994).
2. E.R. Furlong, D.S. Baer and R.K. Hanson, *Twenty-Sixth Symposium (Inernational) on Combustion*, The Combustion Institute, Pittsburgh, pp. 2851–2858 (1996).
3. R.M. Mihalcea, D.S. Baer and R.K. Hanson, "Diode-Laser Sensor for Measurements of CO, CO_2, and CH_4 in Combustion Flows", Appl. Opt. **36**, p. 8745 (1997).
4. R.M. Mihalcea, D.S. Baer and R.K. Hanson, "Advanced Diode Laser Absorption Sensor for *In-Situ* Combustion Measurements of CO_2, H_2O, and Gas Temperature", *Twenty-Seventh Symposium (Inernational) on Combustion*,The Combustion Institute, Pittsburgh (1998).

Laser Applications to Chemical and Environmental Analysis

Combustion Diagnostics 2

Sunday, February 13, 2000

Volker Sick, Univ. of Michigan, USA
Presider

SuB
10:20am–NOON
Anasazi North

Atmospheric pressure laser induced fluorescence measurements of CH in flames using $B^2\Sigma^-$ levels near predissociation

Robert J. H. Klein-Douwel, Jorge Luque, Jay B. Jeffries, Gregory P. Smith, and David R. Crosley
Molecular Physics Laboratory
SRI International
333 Ravenswood Ave.
Menlo Park, California 94025
Jay.Jeffries@SRI.com

Abstract: Laser-induced fluorescence of CH $B^2\Sigma^-v'=1$ is excited in flames using rotational levels above and below the predissociation limit. At atmospheric pressure rotational energy transfer produces a variation in the fluorescence quantum yield with rotational level and gas temperature.

OCIS codes: (280.1740) Combustion Diagnostics, (300.2530)Spectroscopy, Laser-Induced Fluorescence

1. Introduction

A variety of strategies have been proposed for quantitative laser-induced fluorescence measurements of reactive intermediate radicals in atmospheric pressure flames attempting to minimize collisional quenching corrections using predissociative levels of the excited radical.[1] If the predissociative level has a lifetime short compared to the time for quenching collisions, then fluorescence from the predissociated state itself is free from the influence of collisional quenching. However, the collisional energy transfer of even a small population to non-predissociative levels complicates this simple picture because the fluorescence quantum yield is much larger for the non-predissociative states. In a related previous work,[2] we found a rotational level dependent quantum yield when non-predissociative levels below the predissociation limit in CH B v'=0 are excited. A non-negligible fraction of the excited molecules are transferred by collisions beyond the predissociation limit and this fraction becomes larger when the level pumped is closer to the onset of predissociation. If this rotational level variation in the quantum yield is ignored temperature errors of 10% are found in atmospheric pressure flames.

2. Experiment

In the work reported here, we measure excitation and dispersed laser induced fluorescence spectra of predissociative and non-predissociative levels of CH B v'=1 in atmospheric pressure, Bunsen-type partially premixed, methane/air flames. Rotational levels with N'>6 are predissociated, and the fluorescence lifetime decreases from 400 ns for N'≤6 to 5 ns for N'=7, 0.4 ns for N'=8, and less than 0.07 ns for N'>8.[3] The existence of non-predissociative and highly predissociative rotational levels in the same vibrational state provides a unique scenario to test the effects of rotational relaxation in laser-induced fluorescence measurements.

3. Results

When a level beyond the predissociation limit is excited in the atmospheric pressure flame, much of the resulting fluorescence originates from non-predissociating levels populated by rotational energy transfer. This is illustrated in the wavelength resolved fluorescence spectrum in Figure 1. Here the Q_1 (8) line is excited, but only 40% of the fluorescence originates from the N'=8 level (solid line). The rotational relaxation rates are modeled with a statistical power gap law whose parameters are fit to the observed spectrum.[4] The resulting simulated spectrum is shown as a dashed line. The relative time-integrated rotational populations are shown in the inset, and we see that all of the levels below the predissociation limit are populated.

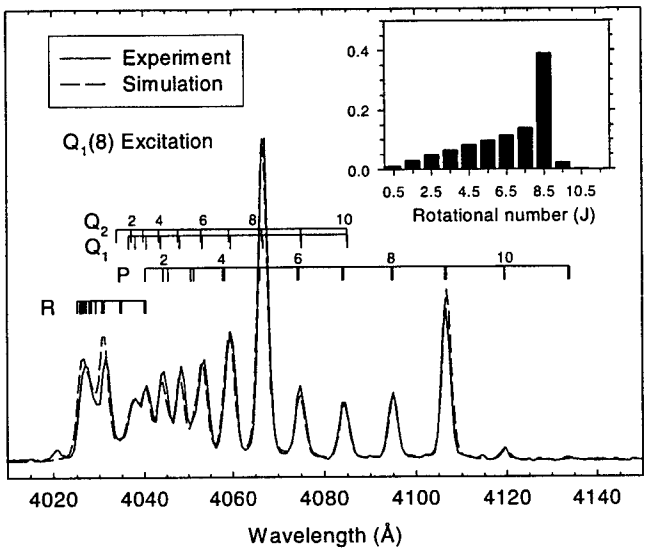

Fig. 1 Dispersed fluorescence (0.25 nm resolution and total time integrated) in an atmospheric pressure methane/air Bunsen flame

We next estimate the fluorescence quantum yield as a function of rotational level, using quenching data from low-pressure flames,[5] our rotational energy transfer model,[4] and theoretical predissociative lifetimes.[3] The results are shown in Figure 2. Note that RET to levels above the predissociation limit reduces the quantum yield for levels below predissociation. Conversely, levels above the predissociation limit have a larger quantum yield because of RET to levels that do not predissociate. The amount of transfer is rotational level dependent, producing a rotationally dependent quantum yield.

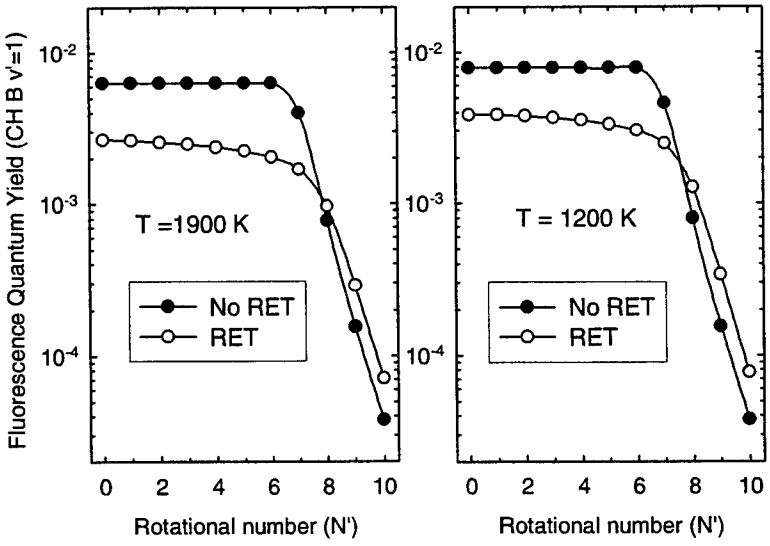

Fig. 2 Fluorescence quantum yield in atmospheric pressure methane/air flame at two different temperatures modeled with and without RET versus initially excited rotational level.

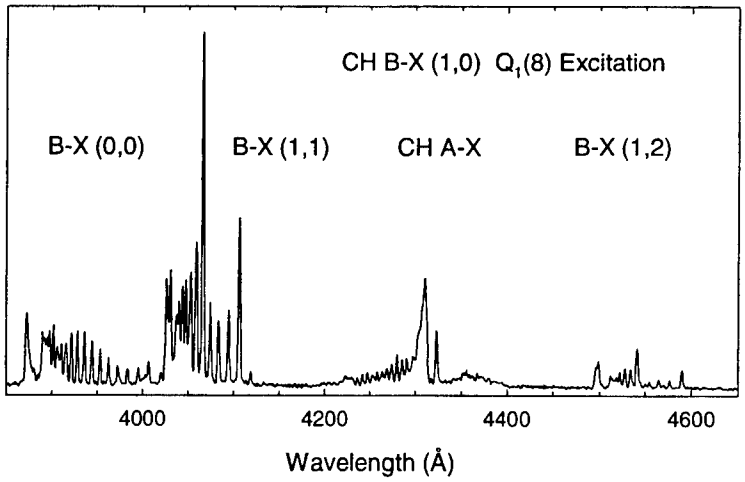

Fig. 3 Dispersed Fluorescence with 0.25 nm resolution and total time integration from atmospheric pressure methane/air flame

Vibrational and electronic energy transfer (VET and EET) are also important collisional removal pathways even for levels above the predissociation limit. Energy transfer from predissociating to non-predissociating levels of only a small fraction of the population can account for a large fraction of the total fluorescence, and result in a substantially larger effective quantum yield. The data in Figure 3 show that EET and VET together account for nearly half of the total fluorescence observed after exciting the predissociative N'=8 level of v'=1 of the B-state.

4. Conclusions

Quantitative LIF using an electronic state with some predissociative rotational levels (e.g. measurements of CH using the B-state) must account for energy transfer in the determination of the quantum yield. If the observed fluorescence is not limited light from the initially excited vibrational band, then VET and EET also must be considered as well.

5. Acknowledgements

This work was funded by the Basic Research Group of the Gas Research Institute.

6. References

1. E. W. Rothe and P. Andresen, "Application of tunable excimer lasers to combustion diagnostics: a review," Appl. Opt. **36** 3971-4033 (1997).
2. J. Luque and D. R. Crosley, "Radiative, collisional, and predissociative effects in CH laser-induced fluorescence flame thermometry," Appl. Opt. **38** 1423-1433 (1999).
3. N. Elander, M. Henenberger, and P. R. Bunker, "Theoretical studies related to time resolved spectroscopy: the iterative Rydberg-Klein-Dunham method and Weyl theory applied to the predissociation in the B state of CH," Phys. Scripta, **20** 631-646 (1979).
4. J. Luque, R. J. H. Klein-Douwel, J. B. Jeffries, and D. R. Crosley, "Collisional Processes Near the CH $B^2\Sigma^-$ v'=0,1 Predissociation Limit in Laser-Induced Fluorescence Flame Diagnostics," Applied Phys. B., submitted, September, 1999.
5. M. Tamura, P. A. Berg, J. E. Harrington, J. Luque, J. B. Jeffries, G. P. Smith, and D. R. Crosley, "Collisional Quenching of OH, CH, and NO in Low-Pressure Flames," Combustion and Flame, **114** 502-514 (1998).

Simultaneous Laser-induced Fluorescence Visualization of Acetone and OH for a Study on a Crevice Flow in an SI Engine

M. Tamura, T. Sakurai and H. Tai
Corporate R&D Department, Tokyo Gas Co., Ltd., 1-16-25, Shibaura, Minato-ku, Tokyo 105-0023, Japan
Tel. +81-3-5484-4810 Fax. +81-3-3453-7583 e-mail. m-tamura@tokyo-gas.co.jp

Abstract: A crevice flow in a spark ignition gas engine was visualized by LIF of OH and acetone. Oxidation of crevice flow was found to be stopped at timing of exhaust valve opening.

OCIS codes: (120.1740) Combustion diagnostics, (280.1740) Combustion diagnostics, (280.2470) Flames

1. Introduction

Visualization of flame structure is generally important for research and development of combustion systems. Several studies on simultaneous visualization technique of fuel and reacting zones in flames using combination of LIF of acetone and OH have been reported previously[1][2]. Acetone is seeded into fuel as a tracer, and it vanishes when the fuel burns. Namely, acetone acts as a marker of unburned zones. On the other hand, OH exists naturally in high-temperature zones in flames, and its presence stands for reacting zones. Because excitation wavelengths of these two species overlap, simultaneous excitation by single laser light is possible, and it makes the visualization technique free from a complex experimental set-up. We apply this method to a study on a crevice flow in an engine cylinder.

Around a combustion chamber of an engine, there are narrow crevices into which flame cannot propagate[3]. One of the largest crevices is a space between a cylinder wall and a piston. A fuel/air mixture is introduced into the combustion chamber through an intake valve during an intake stroke. During a compression stroke, a part of the mixture is compressed into crevices around the combustion chamber, and the mixture becomes residual fuel in exhaust gas. From a viewpoint of environmental pollution or energy saving, this unburned fuel from the crevice has to be reduced.

In this work, we visualized blow-off process and oxidation process of the crevice flow. Effects of back pressure, i.e., pressure in exhaust port, on flame extinction phenomenon is investigated.

2. Experimental set-up

Our experimental set-up is shown in Fig. 1. Frequency doubled output of a dye laser (12mJ/pulse, 283.92nm: corresponding to OH $A^2\Sigma^+ \leftarrow X^2\Pi$ (1,0) $Q_{11}(9.5)$ and $Q_{22}(7.5)$) was shaped into a laser sheet by cylindrical lenses. The dimension of the laser sheet was 30 mm (width) and 1 mm (thickness). The laser sheet passes through the center of a transparent engine cylinder, made of fused silica, in order to take a tomogram of a vertical section of the combustion chamber. The engine is a 2-valve spark ignition gas engine whose bore size and stroke are 85 mm and 90 mm, respectively. The combustion chamber is simple disk shape without a cavity on the top of the piston. The fuel is mixture of methane (90%) and acetone (10%), and it was premixed with air before intake. An excess air ratio was set to 1.33. A speed of engine operation was set to 1200 rpm, and ignition timing was 23 deg. BTDC (before top dead center) in crank angle.

LIF signals from OH and acetone were imaged on two intensified CCD cameras (LaVision: FlameStar 2 / 286×384 pixels, 12bit, UV Nikkor 105mm F/4.5 for OH, Micro Nikkor 105mm F/2.8 for acetone) through wavelength filters which transmit each signals. The wavelength filters used were a band-pass filter (center wavelength: 307 nm, bandwidth: 25 nm (FWHM)) for OH, and a long-pass color glass filter ($T>50\%$ at $\lambda>355$ nm) for acetone. Gate lengths for image intensifiers were 100 nsec. in order to suppress self-luminescence signal from a flame.

3. Results

Figure 2 shows LIF images of OH and acetone with a pressure trace in an engine cylinder. Vertical bars which locate from 65 to 302 deg. ATDC (after top dead center) in the pressure trace indicate imaging timings, and points A to C correspond to those shown beside of LIF images. Because the maximum repetition rate of our laser pulse was

10 Hz, sequences of images in Fig. 2 are not real sequential images in one cycle of combustion, but they were taken in different cycles with various detection timings. Each data was taken with one laser pulse.

According to Fig. 2, OH radical disappears around the timing B, and no more OH is observed later. This means that chemical reaction in the engine cylinder was stopped around the timing B. After the timing B, unburned crevice flow from the bottom of the imaging area was clearly observed. This flow appeared along a cylinder wall, and it is naturally understood that the flow is unburned fuel which had been compressed into a crevice between a piston and a cylinder wall. This result shows that the simultaneous LIF visualization of OH and acetone was successfully applied to a visualization of a phenomenon in an engine.

In order to avoid scraping the glass cylinder, piston rings for this engine are located at lower positions than typical commercial engines. We calculated the crevice volume of this test engine, and the amount of crevice flow in typical engines is estimated a fifth of our engine.

For error estimation of Fig. 2, we evaluated characteristics of quantum yield of OH LIF under various pressure and temperature conditions. Among all elements which affect LIF characteristics, effect of collisional broadening of OH absorption line is the most significant on signal intensity in the pressure range of 0.1 to 0.9 MPa and temperature range from 300 to 2000 K. LIF signal of OH decreases down to a third in this pressure range (in case of 1600K). Whereas, temperature-dependence of signal yields ± 7 % error at 0.1 MPa. The error increases up to ± 20 % at 0.9 MPa. We multiplied only correction factors to each OH images in order to cancel the pressure dependence of LIF signal. Therefore, images still contain errors yielded from temperature-dependence. We also conducted an experiment on characteristics of acetone LIF under various pressure and temperature. We observed a large temperature-dependence of quantum yield. We estimate the maximum error which is caused by temperature variation to be ± 17 %.

The pressure trace Fig. 2 implies a reason of flame extinction around the timing B. A remarkable drop of the cylinder pressure was observed around timing B. This is caused by a lift of an exhaust valve. In our engine, the exhaust valve starts to lift at 125 deg. ATDC, and opens completely at 240 deg. ATDC. When the valve lifts, burned gas in the cylinder blows off, and the density of species and temperature in the cylinder drop suddenly. We supposed that the flame extinction in the cylinder was caused mainly by this blow off of the hot gas to the exhaust port, and in order to confirm the inference, we conducted an experiment described below.

We used a butterfly valve which was inserted into an exhaust pipe to regulate pressure in an exhaust port. Using the valve, we could obtain back pressure range from 0.1 MPa up to 0.2 MPa (absolute). Under the condition of 0.2 MPa, OH radical was observed even after the timing B as shown in Fig. 3. In this case, a part of crevice flow reacted and the amount of measured acetone is clearly reduced compared to the former case (Fig. 2). In fig. 3, a pressure trace is also plotted with that of the former case for reference (broken line). The reason why the oxidation of crevice flow continued even after the timing B is supposed that the higher back pressure made the blow-off of in-cylinder hot gas moderate.

4. Conclusion

Simultaneous visualization technique of reacting and unburned zones in an engine cylinder using LIF of OH and acetone was performed in order to investigate a crevice flow in an engine. Pressure- and temperature-dependence of LIF signal were evaluated on OH and acetone, respectively. We conducted visualization experiments in a transparent research gas engine, and proved the method to be an effective tool for crevice flow analysis. In this work, we showed that back pressure, or movement of exhaust valve, affects oxidation process of a crevice flow. To our knowledge, this is the first time that this phenomenon was clarified.

5. References

[1] B. Yip, M. F. Miller, A. Lozano and R.K. Hanson, "A combined OH/acetone laser-induced fluorescence imaging technique for visualizing combusting flows," Exp. Fluids **17** 330-336 (1994)

[2] M. Tamura, H. Tai and T. Sakurai, "Simultaneous LIF imaging of fuel and OH in constant volume combustion chamber with a prechamber." in "Proceedings of the fourth international symposium on diagnostics and modeling of combustion in internal combustion engines : COMODIA 98," (Japan Society of Mechanical Engineers, Kyoto, 1998)

[3] J.B. Heywood : *Internal Combustion Engine Fundamentals*, (McGraw Hill, New York, 1988)

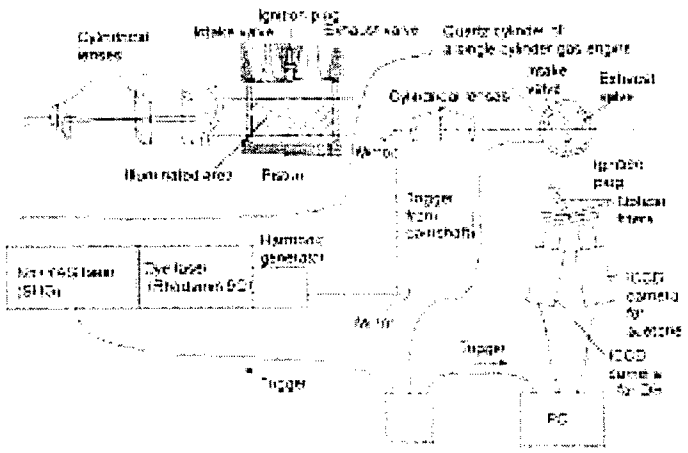

Fig. 1. Schematic of the experimental set-up

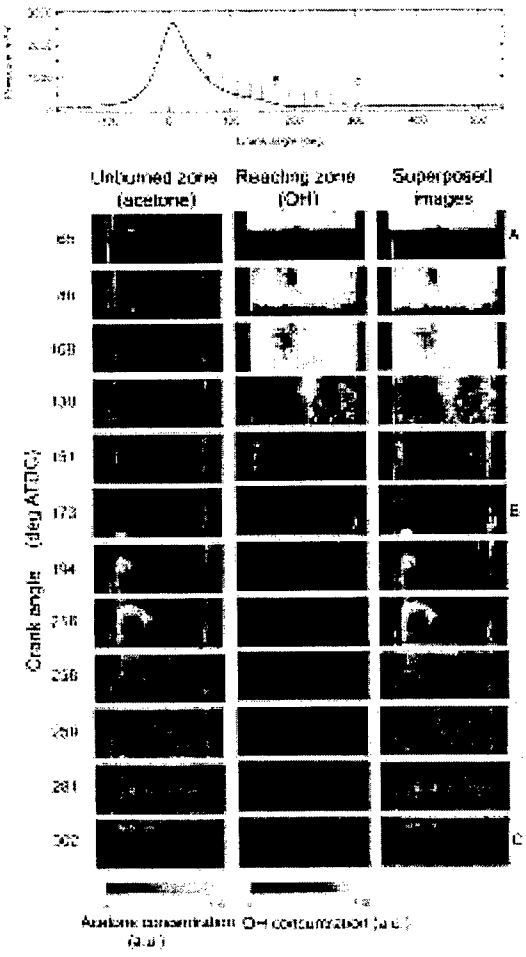

Fig. 2. Pressure trace in the engine cylinder and LIF distributions of OH and acetone (Back pressure: 0.1 MPa (absolute)).

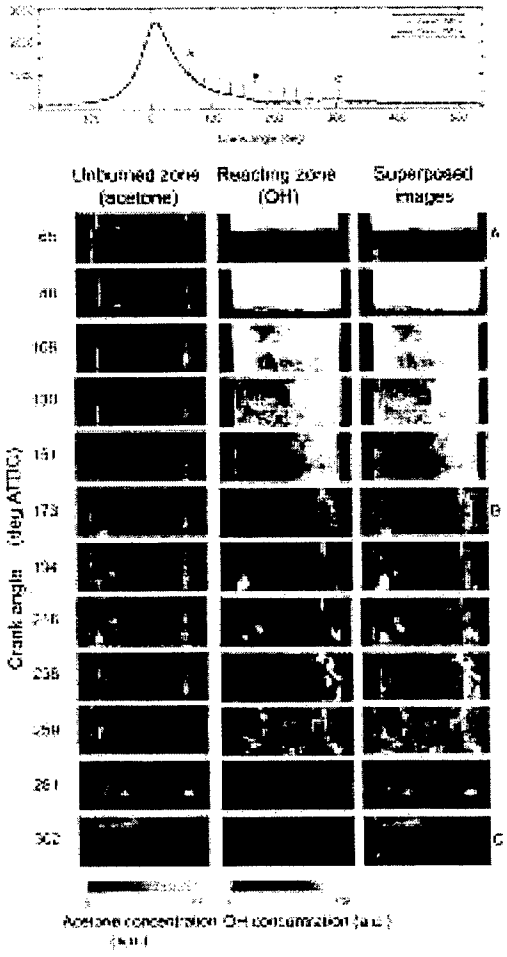

Fig. 3. Pressure trace in the engine cylinder and LIF distributions of OH and acetone (Back pressure: 0.2 MPa (absolute)).

Laser-Induced Incandescence Non-Intrusive Measurements of Particles in Exhausts

John D. Black
Strategic Research Centre, Rolls-Royce plc, P.O. Box 31, Derby, DE24 8BJ, U. K.
tel.: 44-1332-246142 fax: 44-1332-247129 e-mail: john.black@rolls-royce.com

Vartan Grigorian
School of Mechanical Engineering, Cranfield University, Bedford, MK43 0AL, U. K.
tel.: 44-1234-754657fax: 44-1234-750728 e-mail: v.grigorian@cranfield.ac.uk

Abstract: Laser-induced incandescence (LII) measurements of carbonaceous particle concentrations have been made in the exhaust of a current large civil aero-engine on a sea level test bed. Comparison of LII with conventional gas sampling is discussed.

OCIS codes: (010.1100) Aerosol detection; (010.1120) Air pollution monitoring; (120.1740) Combustion diagnostics

1. Introduction

The conventional method of particle measurement, which must be used in aero-engine certification tests, involves passing a prescribed volume of extracted exhaust gas through a filter paper and measuring the reflectance of the stained paper [1]. In addition to requiring a gas sampling rake to be placed in the engine exhaust, this technique is slow compared to gas analysis. Modern gas turbine engines generate very low concentrations of very small particles often referred to as 'smoke' or soot'. These consist almost entirely of carbon, but have a much lower specific gravity than bulk graphite. Recent extractive tests on aero-engine combustor test rigs [2] indicate that particle number densities of $<10^{12}$ m^{-3} with mean diameter ~ 50 nm, corresponding to mass concentration <0.2 mg m^{-3} (SAE smoke number ~2), are commonly encountered. Such levels are close to the limit of sensitivity of the filter paper based measurement technique.

Although the number of particles emitted by aircraft is very small, and very few of them will enter human or other biological systems, they may have a disproportionate effect on atmospheric chemistry and geophysics. This is due to their function as condensation nuclei, influencing the formation of contrails behind aircraft in the upper troposphere. Carbonaceous particles can have molecules emitted from the engine attached to their surface, for example SO_3 formed from sulphur in the fuel, making them much more effective as condensation nuclei [3]. There is also the possibility that particles will react as heterogeneous catalysis sites for chemical reactions in the exhaust plume.

Laser-induced incandescence (LII) is produced when a short pulsed laser, e.g. a Q-switched Nd/YAG laser with pulse length ~ 10 ns, is used to heat the surface of absorbing particles in a gas stream. Incandescent radiation from the heated particles is detected before their surface temperature returns to the equilibrium temperature of the surrounding gas. The LII signal is proportional to the particle volume fraction. LII, which was first observed as an interference in attempts to use spontaneous Raman spectroscopy as a temperature diagnostic in flames in the 1970s [4], is particularly suited to the study of small carbon particles which absorb light over the whole range from UV to mid-IR. Because of the very high vaporisation temperature of carbon (>3900K), radiation from laser heated carbon particles is very efficient with a large proportion of the radiation in the visible range (peak wavelength at 3900K is 743 nm). When CCD imaging detectors became available in the mid to late 1980s, LII became a useful technique for imaging soot distribution in flames. Nearly all reports of LII have been on its use in that application, for example [5,6], although there has been some use of imaging LII in Diesel engine exhausts [7] and the potential of LII for gas turbine exhaust measurements has been investigated in the laboratory [8].

2. Application of LII in Large Engine Exhausts

Usually LII is applied to small scale flames using a laser light sheet with the incandescent light collected at 90^0 to the laser propagation direction providing an image of the relative distribution of soot in the flame. However, in aero-engine exhausts this configuration is difficult to implement because of the scale of the system. Exhaust plume diameters may be up to 2.5 m. Also, the required measurement is an average over the whole exhaust. Thus, the quasi-backscatter configuration shown in Figure 1 was used.

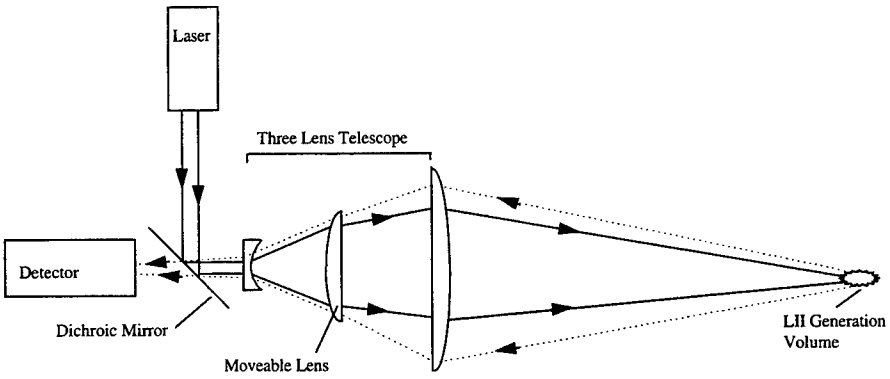

Fig. 1: Backscatter LII Configuration Used for Exhaust Measurements

The laser used was a Q-switched Nd/YAG operating at its fundamental wavelength (1064 nm) in the near infrared. and the detector was a gated, intensified CCD (Princeton Instruments) which was sensitive only in the visible region. In an aero-engine test cell there are often high concentrations of non-absorbing particles such as water and oil droplets in the air surrounding the exhaust plume. Hence, it is important to discriminate against scattered light at the laser wavelength.

Although LII has no physical threshold, there is a dependence on laser fluence. At very low fluences particles are not heated sufficiently to radiate detectable visible light. Above the level of detectability the LII intensity increases rapidly with laser fluence, then becomes almost constant, and finally decreases at very high fluence when particles begin to vaporise. Therefore, it is possible to change the spatial resolution of the LII measurement by varying the laser power.

3. Comparison with Conventional Measurements

The filter paper stain technique has become the accepted method for smoke measurement, although the physical significance of the quantity measured is not well defined. There are some empirical correlations between filter paper measured SAE smoke number and carbon mass loading measured using a tapered element microbalance at the end of the gas sampling line. An instrument has been developed which measures visible light absorption in a gas cell at the end of the gas sampling line. Absorption correlates fairly well with filter paper measured smoke number [9]. An assessment of the effect of varying the type and length of sampling line has been made [2], but it is impossible to determine the effect of the sampling rake using only extractive techniques. Particle size distribution and composition may change as a consequence of being sampled.

While conventional measurements can only provide a time-averaged measurement of particles as sampled, LII is capable of supplying spatially and temporally resolved information. Spatial resolved particle measurements using a single point sampling probe have been obtained in a few cases, but extended engine running with attendant high costs is required. LII data was obtained from single laser pulses on an older generation military turbofan and with 0.5 s (5 laser pulses) integration on a current large civil engine. This new capability for non-intrusive particle measurement opens the possibility for many non-traditional applications of emissions measurement. For example, particle emission during engine transients can be examined and this may be useful for engine diagnostics and condition monitoring.

4. Calibration

Engine tests to date show that the LII technique has the sensitivity required to detect the very low levels of particles emitted by present generation civil aircraft engines, and that the LII intensity scales with engine condition. A much larger database is required to determine the reliability and relative accuracy of the technique. There are many uncertainties in comparison with extractive measurements, and a method of direct calibration of LII is required. For this, an aerosol generator producing a suspension of commercial carbon black particles is being developed. Although it does not reproduce engine exhaust conditions, this device produces a localised aerosol of highly absorbing particles with a known size distribution in the same range and concentration as expected to be emitted by an engine. The carbon black aerosol can be translated within the field of view of the LII system to determine its spatial resolution and sensitivity. However, because carbon black particles may differ in their physical properties from in-situ exhaust soot, it may not be possible use the aerosol generator to provide an absolute calibration in terms of mass concentration.

References

1. Society of Automotive Engineers, "Aircraft Gas Turbine Engine Exhaust Smoke Measurement," ARP1179 Rev B 19/4/1991 (SAE International, 400 Commonwealth Drive, Warrendale PA 15096-0001, USA) (1991).

2. C. D. Hurley, "AEROTRACE - Measurement of Particulates from an Engine Combustor," proceedings ICAO International Colloquium, *Impact of Aircraft Emissions upon the Atmosphere*, Paris, France, October 14 - 18, 1996.

3. R. C. Brown, R. C. Miake-Lye, M. R. Anderson, and C. E. Kolb, "Aerosol dynamics in near-field aircraft plumes," J. Geophys. Res., **101**, 22,939-22,953 (1996).

4. A. C. Eckbreth, "Effects of Laser Modulated Particulate Incandescence on Raman Scattering Diagnostics," J. Appl. Phys. **48**, 4473 (1977).

5. B. Quay, T.-W. Lee, T. Ni, and R. J. Santoro, "Spatially Resolved Measurements of Soot Volume Fraction Using Laser-Induced Incandescence," Combust. Flame **97**, 384-392 (1994)

6. N. P. Tait and D. A. Greenhalgh, "PLIF imaging of fuel fraction in practical devices and LII imaging of soot," Ber. Bunsenges Phys. Chem. **97**, 1619-1625 (1993).

7. M. E. Case and D. L. Hofeldt, "Soot Mass Concentration Measurements in Diesel Engine Exhaust Using Laser-Induced Incandescence," Aerosol Science and Technology **25**, 46 -60 (1996).

8. R. T. Wainner, J. M. Seitzman, and S. R. Martin, "Soot Measurements in a Simulated Engine Exhaust Using Laser Induced Incandescence," AIAA Journal **37**, 738 - 743 (1999).

9. R. Burrows, "A report on the correlation between SAE smoke number and optical smokemeter reading," Rolls-Royce report number DNS38017 (1997).

Vibrational temperature imaging using two-line laser-induced fluorescence of seeded NO

Wolfgang Bessler, Frank Hildenbrand, Christof Schulz*
PCI, Universität Heidelberg, INF 253, 69120 Heidelberg, Germany
Phone: +49 6221 545008, fax: +49 6221 545050, christof.schulz@urz.uni-heidelberg.de

Introduction: Laser-based imaging techniques are frequently used to assess concentration and temperature information from reactive flow systems without perturbing the system under study. Planar laser-induced fluorescence has been used to assess local temperatures with high temporal and spatial resolution. Both, single-line [1,2] and two-line [3] excitation techniques have been used. With single line techniques measured fluorescence signals are a function of temperature which includes temperature-dependent local number densities and fluorescence cross-sections. However, local concentrations of the fluorescing or scattering species under investigation have to be known. Therefore this approach is prohibitive in systems where fluctuations in gas concentrations occur and where the tracer concentration is affected by chemical processes. Two-line techniques circumvent this problem by inferring temperature information from the ratio of two individual measurements.

Temperature measurements by laser-induced fluorescence (LIF) have been performed using NO [1,2], OH [3,4] vibrationally hot O_2 [5] and fuel-tracers like ketones [6]. The availability of these molecules differs in reactive systems. The presence of OH and hot O_2 is limited to the vicinity of the flame front in combustion processes whereas fuel tracers are only available in unburned gases and are therefore limited for temperature imaging of unburned mixtures. NO, seeded to reactive flow systems, however, is present in both, the unburned and the post-flame gases and provides relatively large fluorescence cross-sections. In contrast to OH, radiative lifetimes and fluorescence quenching in the NO $A^2\Sigma^+$, $v' = 0$ state are insensitive to rotational quantum number [7]. Therefore, it is not required that both transitions populate the same excited level. The techniques of NO thermometry shown to date used two-line excitation of different rotational lines within the $^2\Sigma^+A$–$^2\Pi X$ system.

Theoretical background: The dependencies of NO-LIF intensity I_{LIF} for weak, non-perturbing laser excitation is shown in equation 1. I_{LIF} depends on the number density of the excitable molecules (which is the number density N_{NO} of the species times the Boltzmann fraction f_B giving the population of the initial level i), the Einstein B_{ik} coefficient for absorption $i \rightarrow k$, the spectral overlap $g_\lambda(p,T)$ of laser profile and

$$I_{LIF} \propto I_{Laser}\, N_{NO}\, f_B\, B_{ik}\, g_\lambda(p,T) \sum_{k,j} \frac{A_{kj}}{\sum_l A_{kl} + Q_k(p,T)} \qquad (1)$$

NO absorption spectrum and the fluorescence quantum yield $A/(\Sigma A + Q)$, where A and Q are the rates of spontaneous emission and collisional quenching. Q depends on local temperature and gas composition. For NO at atmospheric pressure, the denominator is dominated by Q which for the NO $A^2\Sigma^+$, $v' = 0$ does not depend on rotational quantum number [7]. Therefore, with two-line excitation, the ratio R of the signal intensities is independent on depopulation processes and the local species concentration cancels out (eq. 2). Here the Boltzmann fractions f_B and the overlap coefficients g_λ are temperature dependent.

$$R_{12} = \frac{I_{Laser,1}\, f_{B,1}\, B_{ik,1}\, g_{\lambda,1} \sum A_{kj,1}}{I_{Laser,2}\, f_{B,2}\, B_{ik,2}\, g_{\lambda,2} \sum A_{kj,2}} \qquad (2)$$

With excitation of single rotational lines overlap coefficients cancel if the spectral profile of the excimer laser is broader than the width of the absorption lines of NO at atmospheric pressure. Therefore, the ratio

depends on the ground state energy difference $\Delta\varepsilon_{12}$ and a calibration constant C_{12} which has to be determined using known temperature data.

$$R_{12} = C_{12}\exp(-\Delta\varepsilon_{12}/kT) \quad (3)$$

With excitation of multiple lines like in the bandhead region, the temperature dependent overlap between spectral laser profile and absorption spectra have to be included using spectra simulations [8]. Choosing rotational transitions from different vibrational levels gives access to large ground state energy differences $\Delta\varepsilon_{12}$. In the present case excitation of the $R_1(21.5)$ line within the (0,0) band and the O_{12} bandhead of the (0,2) band ($O_{12}(8.5)$ to $O_{12}(10.5)$) were chosen. Both transitions have been extensively used for NO concentration imaging in previous work [8-10]. They allow for selective detection even in harsh environments like IC engines. The ground state energy difference is $\Delta\varepsilon_{12}$ = 3171 – 3238 cm^{-1} providing good temperature sensitivity for temperatures above 800 K. Figure 1 shows the variation of LIF ratios with temperature both, with and without correction for line overlap and multiple line excitation.

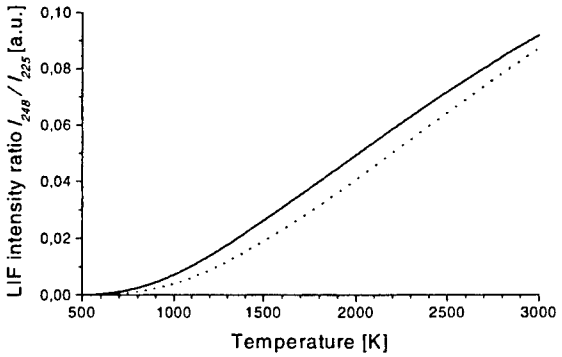

Fig. 1: Temperature dependence of the LIF intensity ratio according to equation 3 (dashed line) and including temperature dependent overlap and multiple line excitation (solid line).

Experiment: The beam from a tunable KrF excimer laser (*Lambda Physik*, EMG 150 TMSC, $\Delta\nu$ = 0.4 cm^{-1}) was formed into a vertical light sheet (0.2 mJ/pulse in a 10 x 0.5 mm cross section) and aligned through lean (equivalence ratio ϕ = 0.92) and sooting (ϕ = 2.0) Taran type ehtylene/air flames. The laser was tuned to 247.94 nm to excite the O_{12} bandhead in the NO A-X(0,2) band. Alternatively the laser was Raman-shifted to 225.25 nm (in H_2, 10 bar, 2.6mJ/pulse) to excite the $R_1(21.5)$ line within the NO A-X(0,0) band. Signals were acquired using an ICCD camera (*LaVision* Flamestar II) equipped with an achromatic lens (*Halle*, f = 100 mm, $f_\#$ = 2) and appropriate bandpass filters. The fluorescence intensities of 1500 laser shots were averaged and stored for further data evaluation. Due to the laminar nature of the flame, subsequently obtained images for both excitation wavelengths were used to facilitate the experimental setup.

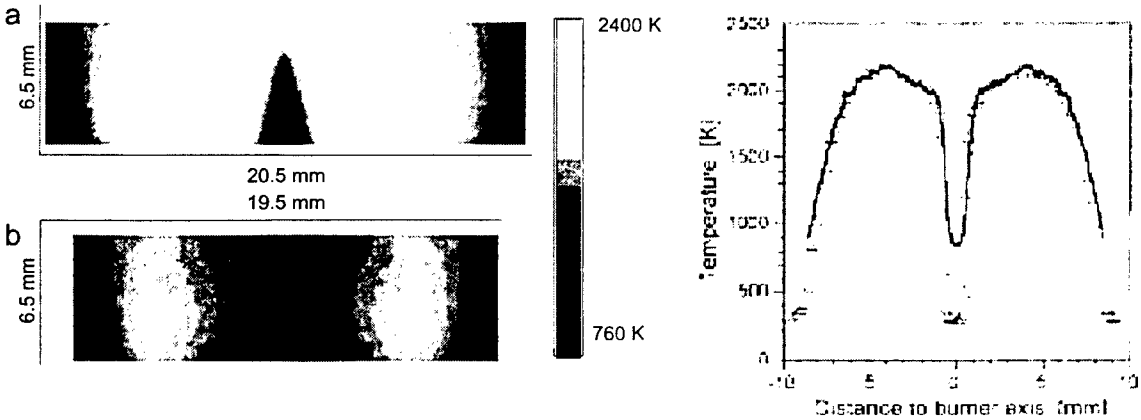

Fig. 2: Vibrational temperature fields in the lean (a) and sooting flame (b) obtained from NO two-line excitation from v" = 2 and v" = 0, resp. The profile at the right compares the temperature profiles at 14 mm above the burner exit in the lean flame obtained from 2-line LIF (solid line) and CARS measurements (symbols).

Results: From the ratio of the signal intensities obtained for the two different excitation wavelengths two-dimensional relative temperature maps are calculated according to fig. 1. C_{12} (eq. 3) was obtained from a calibration using temperature profiles obtained from CARS measurements in the lean flame [4]. Figure 2 shows the results of the temperature measurement for the lean and sooting flame. For the lean flame a profile 14 mm above the burner exit is compared with CARS measurements. For non-stationary flames it is necessary to simultaneously measure NO fluorescence distributions upon excitation with both wavelengths. It would be advantageous, however, if only one laser system was required for this purpose. The use of a Raman shifter for frequency conversion offers the opportunity to simultaneously generate 248 and 225 nm radiation. With optically delaying one of the beams quasi-simultaneous measurements using two ICCD cameras can be performed. Figure 3 shows possible transitions which could be excited simultaneously. The simulated spectra are superimposed using a frequency shift of the anti-Stokes line in H_2 of 4158 cm^{-1}.

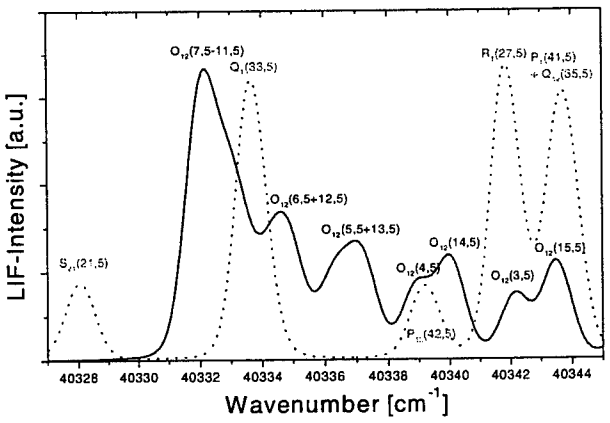

Fig. 3: Calculated fluorescence excitation spectra in the NO A-X (0,0) (dashed line) and (0,2) (solid line) band resp. assuming simultaneous excitation with the anti-Stokes and fundamental output of the H_2-Raman-Shifter (frequency shift: 4158 cm^{-1}).

Conclusions: The present experiment shows the possibility of measuring vibrational temperatures of NO upon excitation in the NO A-X(0,0) and (0,2) band. Measurements have been shown in lean and sooting ethylene/air flames. The LIF intensity ratios are calibrated in the lean flame using CARS temperature profiles. The possibility of single-shot temperature measurements using only one laser are discussed.

Acknowledgements: This work has been funded by the Bundesministerium für Bildung, Forschung und Technologie under contract No. 13N7184/3.

1 J.M. Seitzman, G. Kychakoff, R.K. Hanson, Opt. Lett. 10, 439 (1985).
2 M. Tamura, J. Luque, J.E. Harrington, P.A. Berg, G.P. Smith, J.B. Jeffries, D.R. Crosley, Appl. Phys. B 82, 2072 (1997).
3 R. Cattolica, Appl. Opt. 20, 1156 (1981).
4 A. Arnold, B. Lange, T. Bouché, T. Heitzmann, G. Schiff, W. Ketterle, P. Monkhouse, J. Wolfrum, Ber. Bunsenges. Phys. Chem. 96, 1388 (1992).
5 M.P. Lee, P.H. Paul, R.K. Hanson, Opt. Lett. 12, 75 (1987); A. Roller, A. Arnold, M. Decker, V. Sick, J. Wolfrum, W. Hentschel, K.-P. Schindler, SAE paper No. 952461 (1995)
6 S. Einecke, C. Schulz, V. Sick, A. Dreizler, R. Schießl, U. Maas, SAE Transactions, Paper No. 982468 (1998).
7 I.S. McDermid, J.B. Laudenslager, J. Quant. Spectrosc. Radiat. Transfer 27, 483 (1982); G.F. Nutt, S.C. Haydon, A.I. McIntosh, Chem. Phys. Lett. 62, 402 (1979); T.J. McGee, G.E. Miller, J. Burris, Jr., T.J. McIlrath, , J. Quant. Spectrosc. Radiat. Transfer 29, 333 (1983).
8 C. Schulz, V. Sick, J. Heinze, W. Stricker, Appl. Opt. 36, 3227 (1997).
9 C. Schulz, V. Sick, J. Wolfrum, V. Drewes, M. Zahn, R.R. Maly, 26th Symposium (Intl.) on Combustion, The Combustion Institute, Pittsburgh, 1996, p. 2597.
10 A. Bräumer, V. Sick, J. Wolfrum, V. Drewes, R.R. Maly and M. Zahn, SAE paper 952462 (1995).

Comparison of particle image velocimetry and optical flow velocimetry for turbulent flows and flames

J. Fielding and M.B. Long
Department of Mechanical Engineering, Yale University, New Haven, Connecticut, 06520-8284
(203) 432-4229, FAX: (203) 432-6775, marshall.long@yale.edu

1. Introduction

Particle image velocimetry (PIV) has become an accepted technique for measuring two components of the velocity field in a cross section of reacting and non-reacting flows. To implement PIV, particles are introduced into the flow to track the fluid velocities. It has been demonstrated that PIV can be combined with scalar measurements by using laser-induced fluorescence (LIF) [1], however, particle-based techniques complicate simultaneous laser-based measurements of many scalar quantities due to strong scattering interference from the seed particles. A number of "non-particle" velocimetry approaches have been applied in turbulent flows, though few have found broad applicability under reacting conditions. For instance, the Scalar Imaging Velocimetry approach of Dahm et al. [2] produces a velocity field by inverting the scalar transport equation. The Image Correlation Velocimetry (ICV) technique of Tokumaru and Dimotakis [3] provides a basis for measuring the displacement fields of gas-phase fluid motions. Extension of this approach to reacting flows appears feasible [4,5] provided appropriate scalars are selected for imaging and validation experiments are carried out. Recent work on dynamic programming algorithms has been reported to achieve results that in some cases are superior to conventional PIV [6].

These velocimetry techniques obviate the need for seeding by obtaining velocity vectors from the displacement fields of molecular flow tracers. Extracting velocity from a pair or sequence of images is a concept derived from the field of optical flow. Optical flow is the apparent motion of the brightness or intensity pattern in an image pair or sequence [7,8]. If the intensity **I** at a point (x, y) and time t is constant between frames

$$\mathbf{I}(x+\Delta x, y+\Delta y, t+\Delta t) = \mathbf{I}(x, y, t)$$

then the velocity is simply the displacement of that point over the interframe time. In general, further assumptions are required to solve the problem, employing constraints based on the smoothness of the velocity field or derived from the equations of fluid motion. In this work, we report experiments involving simultaneous measurements of Mie scattering from seed particles and LIF of acetone as a tracer in a turbulent isothermal air jet at two successive times. This arrangement allows for determination of velocity from cross-correlation PIV as well as by applying a region-based matching optical flow algorithm. The velocity fields obtained using the two different approaches can then be compared.

2. Experiment

The fourth harmonic (266 nm) of a double-pulsed Nd:YAG laser is used to illuminate the seed particles for PIV and excite acetone fluorescence for the scalar measurements. The beam is formed into a sheet ~5 mm high with a beam energy of ~2.5 mJ per pulse and a pulse separation of 57 μs. Submicron sugar particles are introduced into the air flow using an aerosol seeder, which provides a constant seeding density. A portion of the overall air flow is sent through a heated bubbler unit filled with acetone. The bubbler consists of a porous tube submerged in 500 mL of acetone at 20° C. The nozzle used in these experiments consists of a straight tube with a 4.57 mm inner diameter. The turbulent jet issues into an unconfined coflow of air (~2.6 m/s). The results presented here correspond to a *Re*=2810 jet with an exit velocity of 7.7 m/s.

Lorenz-Mie scattering from the particles is collected using an *f*/11 quartz camera objective coupled to a liquid-cooled UV-sensitive CCD camera. A mirror is mounted to a DC motor rotating at ~50 Hz to spatially separate the images from the two laser pulses, allowing for cross-correlation velocimetry to be performed. Timing of the experiment is controlled by reflecting a HeNe laser from the mirror onto a photodiode to synchronize the cycle.

Acetone fluorescence occurs between 350 and 550 nm, and the signal is sufficiently strong for unintensified imaging. Fluorescence from the two laser pulses is imaged using a progressive-scan interline-transfer CCD camera coupled with a large format *f*/1.4 camera objective. This equipment allows the acquisition of two images (temporally separated by at least 1 μs) which makes it well suited for either PIV or time-resolved scalar imaging. A clear glass filter (Schott WG305) is used to block any residual Mie-scattering.

3. Discussion

Figure 1 shows a scalar image pair from the turbulent jet, with velocity vectors derived from two different techniques. In frame (a), vectors have been determined by cross-correlation of the corresponding particle images within 64 × 64 pixel interrogation windows. The vectors in frame (b) are obtained by applying a region-based matching algorithm [8,9] to the fluorescence image pair. A number of optical flow methodologies exist, and here we have employed the approach of Anandan [9]. Briefly, the implementation depends on minimization of the sum-of-squared differences (a distance measure) within a window of size $n \times n$. A coarse-to-fine strategy is employed where displacements are determined first at the coarsest level (using smoothed and sub-sampled images), with subsequent refinement at each finer level. User inputs include window size, number of hierarchical refinement levels, and number of constraint iterations within each level.

This and other scalar velocimetry approaches can at best provide an approximation to the instantaneous two-dimensional fluid velocity given a planar scalar measurement. The approximation is valid when the velocity in the third, unmeasured direction is small, or the scalar gradient in that dimension is small [3]. (A similar requirement applies to two-dimensional PIV.) However, additional constraints exist when using scalar fields with optical flow algorithms for velocimetry applications. Large spatial regions lacking sufficient variation in intensity can cause problems because some optical flow algorithms will produce small or zero velocities in these regions. Generally, this condition of inhomogeneity should not pose a problem in sufficiently turbulent flows and can be overcome to some extent by adjusting a smoothness constraint. Consistency between frames presents an additional requirement. Large interframe times can be problematic for fast flows if the pixel displacements are too large.

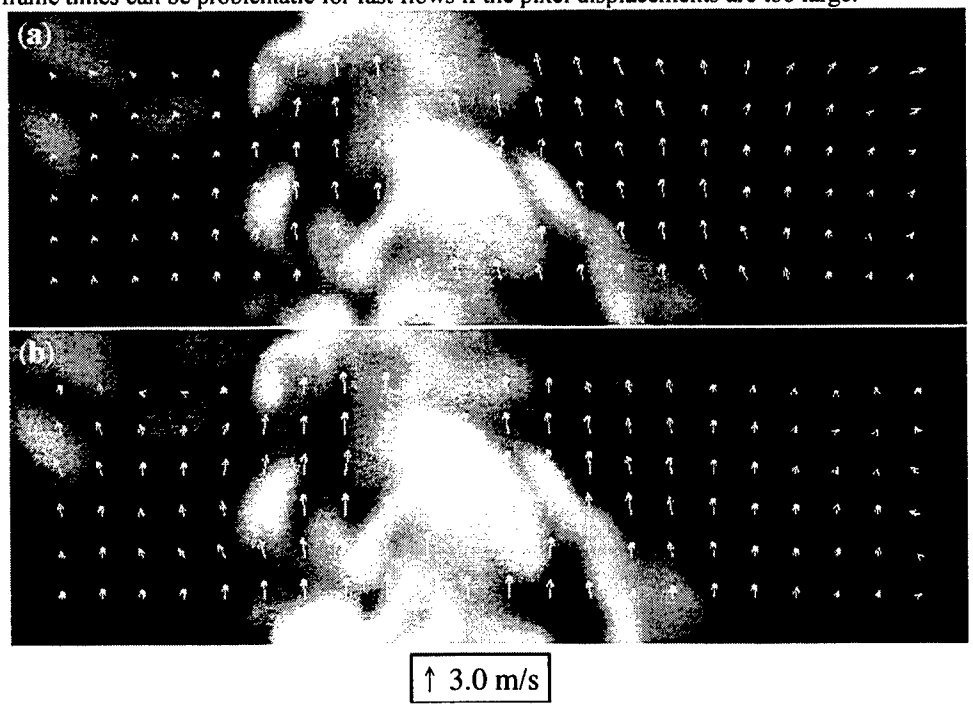

Fig. 1. Acetone fluorescence image pair with velocity vectors. (a) t_0; vectors obtained from cross-correlation PIV. (b) $t_0 + 57$ μs ; vectors obtained from region-based matching optical flow algorithm of Ref. [9].

As can be seen from Fig. 1(b), qualitative agreement between the velocity vectors from region-based matching and PIV in Fig.1(a) appears to be quite good for the particular shot considered here. A more stringent test involves statistical comparisons of an ensemble of velocity fields. To allow this comparison, a collection of 50 scalar/particle image pairs was recorded. Figure 2(a) shows a comparison of the average velocity magnitude obtained with both PIV and the optical flow algorithm (downstream location x/d= 14). While the agreement in overall magnitude is excellent, a calculation of the mean angular deviation of the PIV and optical flow vectors, shown in Fig. 2(b), demonstrates some systematic discrepancies between the two techniques. The average angular deviation of vectors is quite small near the jet centerline, and increases significantly toward the edges of the flow.

One limitation of the algorithm used here is that it does not include the equations of fluid motion as constraints to the problem. It is possible that other optical flow algorithms may provide better agreement, but it is clear from the results shown here that careful validation of various optical flow algorithms will be needed. The experimental data obtained from this work will provide a valuable test bed for developing and evaluating optical flow algorithms for velocimetry. The data used here are electronically available for others wishing to validate different algorithms [10].

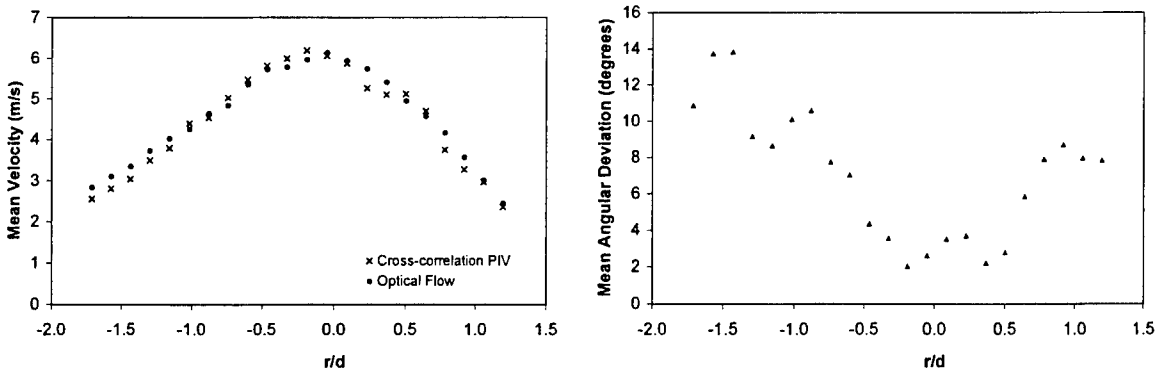

Fig. 2. (a) The magnitude of the mean velocity obtained with PIV and optical flow. (b) The mean angular deviation between velocity vectors from the two different techniques. Averages were calculated from a set of 50 images taken 14 nozzle diameters downstream.

4. Acknowledgment

The authors would like to thank Dr. Gabriel Fielding for his assistance in implementing the optical flow algorithm used in this work.

5. References

[1] J.H. Frank, K.M. Lyons, and M.B. Long, "Simultaneous Scalar/Velocity Field Measurements in Turbulent Gas-Phase Flows," *Combust. Flame*, **107**:1-12 (1996).

[2] W.J.A. Dahm, L.K. Su, and K.B. Southerland, "A Scalar Imaging Velocimetry Technique for Fully Resolved Four-Dimensional Vector Velocity Field Measurements in Turbulent Flows," *Phys. Fluids A*, **4**:2191-2206 (1992).

[3] P.T. Tokumaru and P.E. Dimotakis, "Image Correlation Velocimetry," *Exp. In Fluids*, **19**:1-15 (1995).

[4] M. Komiyama, A. Miyafuji, and T. Takagi, "Flamelet Behavior in a Turbulent Diffusion Flame Measured by Rayeligh Scattering Image Velocimetry," *Twenty-Sixth Symposium (International) on Combustion*, The Combustion Institute, Pittsburgh, PA, pp. 339-346 (1996).

[5] G. Grunefeld, A. Graber, A. Diekmann, S. Kruger, and P. Andresen, "Measurement System for Simultaneous Species Densities, Temperature, and Velocity Double-pulse Measurements in Turbulent Hydrogen Flames," *Combust. Sci. and Tech.*, **135**:135-152 (1998).

[6] Y. Levy, B. Golovanevsky, and T.A. Kowalewski, "Fluid Image Velocimetry for Unseeded Flow," *9th International Symposium on Applications of Laser Techniques to Fluid Mechanics*, Lisbon, Portugal, July 13-16 (1998).

[7] Horn, B.K.P. and Schunk, B.G., *MIT Artificial Intelligence Laboratory* , Memo No. 572 (1980).

[8] J.L. Barron, D.J. Fleet, and S.S. Beauchemin, "Performance of Optical Flow Techniques," *Int. J. Comp. Vision*, **12**:43-77 (1994).

[9] P. Anandan, "A Computational Framework and Algorithm for the Measurement of Visual Motion, " *Int. J. Comp. Vision*, **2**:283-310 (1989).

10 J. Fielding and M.B.Long. "Optical Flow Velocimetry@Yale," http://cld3.eng.yale.edu/fielding/

Laser Applications to Chemical and Environmental Analysis

Analytical Applications 1

Sunday, February 13, 2000

Jay B. Jeffries, SRI Intl., USA
Presider

SuC
1:30pm–3:10pm
Anasazi North

Industrial and Environmental Analysis by Diode Laser Atomic Absorption Spectrometry

Joachim Koch, Kay Niemax and Alexandr Zybin
Institute of Spectrochemistry and Applied Spectroscopy (ISAS)
Bunsen-Kirchhoff-Strasse 11, 44139 Dortmund, Germany
Phone: +49-231-1392-101, Fax: +49-231-1392-310, e-mail: niemax@isas-dortmund.de
Christoph Schnürer-Patschan
LaserSpec Analytik GmbH, Frankfurter Ring 193a, 80807 Munich, Germany

Introduction

The wavelength of commercially available semiconductor laser diodes of the AlGaAs (625-700 nm), InGaAsP (735-980 nm) and GaN type (385-420 nm), and the wavelength range obtained by second harmonic and sum frequency generation in non-linear media allow the measurements of almost all elements of the periodic table with good or excellent detection limits in absorption [1,2]. For example, shot noise limited absorption at mW laser power levels has been demonstrated recently [3]. It was shown that it is possible to measure an optical depth ( ) of about 2×10^{-7} at a band width of 1 Hz with 2 mW laser power in a two-beam arrangement with logarithmic processing of absorption and reference signal if the diode laser wavelength as well as the absorption are modulated by the frequencies f_1 and f_2, respectively, and the measurements are performed by lock-in technique at the frequency $2f_1\pm f_2$. The shot noise limited absorption measurement were made in plasmas which were turned on and off with frequencies in the kHz range.

Diode laser atomic absorption spectrometry (DLAAS) has been sucessfully used for element analysis in flames and graphite tube atomizers [4-6] and in plasmas [7], as well as in combinations with chromatographic techniques, such as gas chromatography (GC) [8-10] or high performance liquid chromatography (HPLC) [11-13].

2. Experiment

The experimental arrangement as it was applied for the analysis of chlorine in polymers is shown in Fig. 1. It consists of the basic arrangement for DLAAS with the wavelength modulated laser diode, the absorption and the reference beam, the logarithmic processing of the signals, and the detection of the sum- or difference frequency $2f_1\pm f_2$. The laser ablation cell and the microwave induced plasma used for atomization of the ablated material and the production of

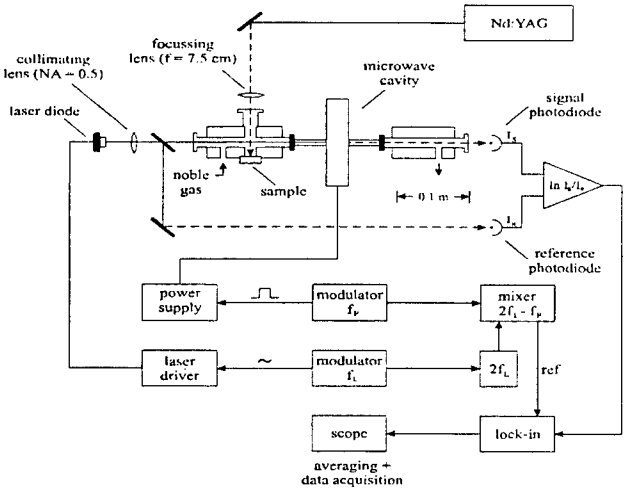

Fig. 1: Experimental arrangement for shot noise limited DLAAS in a MIP coupled with laser ablation.

Cl metastable atoms have to be replaced by a graphite tube atomizer, as known from classical hollow cathode AAS, or by a HPLC device with a flame atomizer for extreme trace analysis of ultrapure liquids or metal species analysis, respectively.

3. Results and Discussion

3.1 Measurement of light elements in ultra-pure liquids and on silicon wafers

Since about three years DLAAS in graphite tube atomizers is used in the semiconductor industry for the characterization of surface contaminants on silicon wafers. The total contamination level to be measured is very low (10^{10}-10^{11} atoms/cm^2). In a well controlled procedure the contaminants are etched by HF-droplets from the surface. While the heavy and medium heavy elements are analysed by Total Reflection X-Ray Fluorescence (TRXF) the light elements are measured by DLAAS in a graphite tube atomizer. The light elements of interest are, e.g., Na, K, and Al. The analytical power of DLAAS is demonstrated in Fig. 2 and 3 showing absorption signals of Al and a calibration graph for K, respectively. Note, the detection limit of K is in the fg/mL-range.

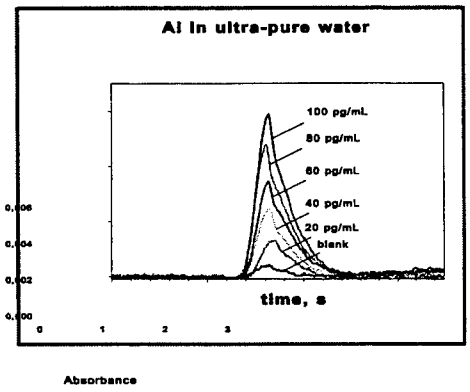

Fig. 2: DLAAS of Al in ultra-pure water.

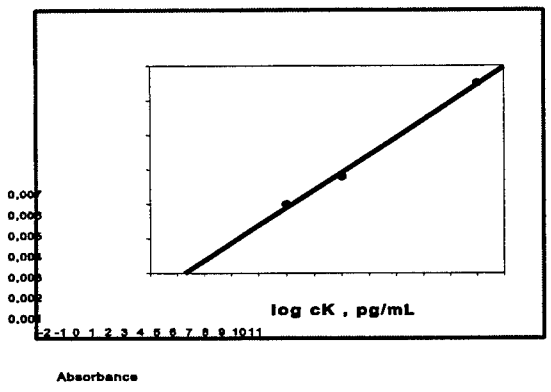

Fig. 3: Calibration of K in ultra-pure water.

3.2 Measurement of chlorine in polymers

The direct analysis of chlorine in solid samples is possible by laser ablation and DLAAS in a MIP, as shown in Fig. 1. The laser ablated sample plume is transported by a noble gas into a low pressure MIP where chlorine atoms are excited efficiently to highly exited metastable states. These metastable atoms can be measured conveniently with very low detection limits applying commercial laser diodes at 837.8 nm. The transient Cl absorption signals from a PVC and a LEXAN sample (0.1 %) are shown in Fig. 4. Cl detection limits of 10 pg/laser shot, or 85 µg/g

have been found [14]. It is obvious that this technique has microanalytical potential and can also been used for the analysis of other elements in polymers.

Fig. 4: Cl in PVC (50%) and LEXAN (0.1%) measured by laser ablation and DLAAS in a MIP.

3.3 Measurement of Metallic Species by HPLC and Diode Laser AAS

Metal species, such as Cr(III) and Cr(VI), have been analysed by WM-DLAAS in a flame coupled to HPLC [11,12]. For the detection of Cr at 425.4 nm the radiation of a near-IR laser diode was frequency doubled in an optical non-linear crystal. A detection limit of 30 pg/mL was found for Cr(VI). It has to be noted that this value is better than the detection limit of Cr(VI) applying HPLC-ICP-MS. Recently, the same technique has been applied for the measurement of methycyclopentadienyl maganese tricarbonyl (MMT) in different matrices, such as urine [13]. MMT is used as fuel additive in unleaded gasoline to increase the octane number, and there are a strong concerns about its toxicity in particular in the United States.

ACKNOWLEDGMENTS

Funding from the Deutsche Forschungsgemeinschaft (DFG), the Ministerium für Bildung und Forschung of the Federal Republic of Germany, and the Ministerium für Schule und Weiterbildung, Wissenschaft und Forschung of the state Northrhine-Westphalia is gratefully acknowledged.

REFERENCES

[1] K. Niemax, C. Schnürer-Patschan, A. Zybin, H. Groll, Anal.Chem. **68**, 351A-356A (1996).
[2] A. Zybin, C. Schnürer-Patschan, M.A. Bolshov, K. Niemax, Trends Anal.Chem. **17,** 513-520 (1998).
[3] V. Liger, A. Zybin, Y. Kuritsyn, K. Niemax, Spectrochim.Acta **52B**, 1125-1138 (1997).
[4] H. Groll, K. Niemax, Spectrochim.Acta **48B**, 633-641 (1993).
[5] C. Schnürer-Patschan, A. Zybin, H. Groll, K. Niemax, J.Anal.At.Spectrom. **8**, 1103-1107 (1993).
[6] H. Groll, C. Schnürer-Patschan, Yu. Kuritsyn, K. Niemax, Spectrochim.Acta **49B**, 1463-1472 (1994).
[7] A. Zybin, C. Schnürer-Patschan, K. Niemax, Spectrochim.Acta **48B**, 1713-1718 (1993).
[8] A. Zybin, C. Schnürer-Patschan, K. Niemax, J.Anal.At.Spectrom. **10**, 563-567 (1995).

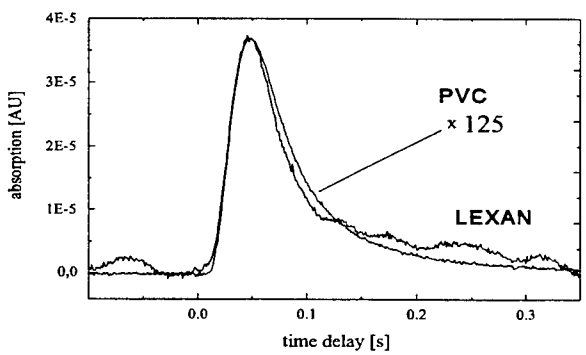

[9] A. Zybin, K. Niemax, Anal.Chem. **69**, 755-757 (1997).
[10] J. Koch, K. Niemax, Spectrochim.Acta **53B**, 71-79 (1995) .
[11] H. Groll, G. Schaldach, H. Berndt, K. Niemax, Spectrochim.Acta **50B**, 1293-1298, (1995).
[12] A. Zybin, G. Schaldach, H. Berndt, K. Niemax, Anal.Chem. **70**, 5093-5096 (1998).
[13] D.J. Butcher, A. Zybin, M.A. Bolshov, K. Niemax, Anal.Chem. **71** (1999) in press.
[14] J. Koch, M. Miclea, and K. Niemax, Spectrochim.Acta **54B** (1999) in press.

Photoacoustic Applications in Industrial and Atmospheric Measurement

J. S. Pilgrim, D. S. Bomse and J. A. Silver
Southwest Sciences, Inc., 1570 Pacheco Street, Suite E-11, Santa Fe, NM 87505
505.984.1322, FAX 505.988.9230, jpilgrim@swsciences.com

Abstract: Photoacoustic spectroscopy (PAS) is a well-known technique for trace gas detection. In its usual implementation PAS suffers several drawbacks that limit sensitivity. Southwest Sciences has developed techniques that recover the inherent sensitivity of photoacoustic spectroscopy.

OCIS codes: (130.6010) Sensors; (140.2020) Diode lasers

1. Summary

Photoacoustic spectroscopy (PAS) is a well-known technique for ultra-sensitive trace gas detection. However, in its usual implementation PAS suffers several drawbacks that limit sensitivity. Southwest Sciences has developed techniques that recover the inherent sensitivity of photoacoustic spectroscopy. Near microphone-noise limited detection limits are possible.

Work is currently underway to utilize photoacoustic spectroscopy for industrial (microelectronics) process gas contaminant measurements. The usual limiting noise source with photoacoustic detection is either ambient environmental noise or sample cell optical window noise. Window noise is a serious problem because in traditional PAS the *amplitude* of the laser is modulated to produce a synchronous acoustic wave *via* absorption and gaseous collisional transfer. In this implementation, absorption by either the sample or the sample cell windows, will create a synchronous acoustic wave. One can achieve some discrimination with detection phase, but the window noise will always contain some in-phase component.

Wavelength modulation (WM) can offer a solution to window noise. Because gaseous absorption line widths are orders-of-magnitude smaller than window absorption line widths, wavelength modulation can discriminate against the broadband window absorption. That is, since wavelength modulation signals appear as the derivative of the absorption line shape, for small modulation depths, the nearly flat absorption due to the windows is suppressed. Phase-sensitive detection at $1f$ is still problematic since the diode laser wavelength modulation is accompanied by a corresponding amplitude modulation. However, $2f$ detection is nearly immune to amplitude modulation and has a maximum at the absorption line center. We have achieved near microphone-noise limited sensitivity with this technique.

A second application we are pursuing is for airborne humidity measurements on weather balloons. Weight and power consumption are of paramount concern in this application. Infrared broadband LED's allow significant weight and power savings since they do not have to be temperature controlled. The broadband nature (50 nm FWHM) of these devices eliminates the pressure dependence of the absorption band cross section. This is of major benefit during a weather balloon ascent where drastic ambient pressure changes occur. While band absorption cross sections are much smaller than available single absorption line cross sections, the sensitivity of PAS can sufficiently overcome this deficiency for the moisture levels encountered on a typical balloon flight.

Because these infrared sources are broadband it is not practicable to utilize them with wavelength modulation. Nevertheless, near microphone-noise limited performance is achieved by using a windowless PAS cell. High frequency operation is necessary in the open cell in order to get out of the low frequency region where ambient noise is a problem. Unfortunately, PAS signals decrease with modulation frequency. This problem can be mitigated by the use of an acoustically resonant cell. Because of the geometry of the resonances and the frequency noise spectrum, a radially resonant cell is preferable. A radial resonance is not substantially affected by the removal of cell windows from the distal ends of a cylindrical cell.

The requirement for the radial resonance frequency to be within the sensitive response region of the microphone places minimum diameter restrictions on the PAS cell. This constraint typically dictates a cylindrical cell with a diameter of at least several centimeters. In a balloon-borne measurement this size facilitates ambient exchange in the windowless cell.

A laser-based system for chemical imaging

P.D. Ludowise, J.S. Robinson, D.K. Ottesen, T.J. Kulp,
U.B. Goers, K. Armstrong, and S.W. Allendorf
Sandia National Laboratories
Livermore, CA 94551

Introduction

We are currently developing a real-time, laser-based method to provide *in situ* qualitative and quantitative assessment of hydrocarbon contaminants on metallic surfaces for surface cleaning verification. Many manufacturing techniques require the use of hydrocarbon lubricants that are removed from finished and intermediate products by techniques such as vapor degreasing and solvent cleaning. Not only is the cleaning process laborious and time consuming, commonly used organic solvents are toxic and generate expensive hazardous waste. A rapid surface analysis technique that differentiates hydrocarbons will mitigate these problems by allowing accurate assessment of the type and amount of surface contaminants throughout the cleaning process. The development of an on-line technique will eliminate the need to send process parts out to a separate laboratory, thereby eliminating processing delays. Overall, this will lead to improved alternative cleaning products and processes, and reduction of hazardous materials usage and handling.

Currently, the detection of surface contaminants on reflective surfaces is most conveniently and rapidly done by Fourier transform infrared (FTIR) reflectance methods.[1, 2] These non-destructive, non-contacting optical techniques are sensitive to a wide range of organic and inorganic species, and can yield quantitative measurements with appropriate calibration. While an FTIR-based infrared reflectance analysis is able to characterize a very broad range of organic constituents and many inorganic species, a surface-probing FTIR instrument measures a spectrum at only a single small area on a sample, thus requiring broad area surveys to be done by sequentially probing many points. The rate of measurement by FTIR is constrained by the relatively low spectral brightness (compared to a laser) of the incandescent illumination sources used in an FTIR instrument, and makes it necessary to use relatively long integration times to achieve an acceptable signal-to-noise ratio. A position-sensitive FTIR technique also requires the computation of a Fourier transform at each point, further slowing the acquisition rate.

A highly desirable characteristic of a cleaning verification instrument is the ability to rapidly survey large surface areas and to determine the location and amount of contaminants during the cleaning process. The laser and imaging system for this application were adapted from a previously developed laser imaging device that was designed for gas leak detection.[3, 4] The present design performs real-time imaging of a broad surface area by infrared laser illumination. Measurements at multiple wavelengths are made by tuning the laser and repeating the image acquisition at each desired wavelength. While detailed spectral maps of a surface can be generated over the laser tuning range, the primary intent of the system is to provide rapid areal surveys at a few key wavelengths that correspond to absorptions by specific contaminants. The specular reflectance is detected by an InSb focal plane array camera (256 x 256 pixels), which allows ~65,000 surface points to be made on a timescale of 1/30th of a second.

Experimental design and discussion

The laser system is based on a previous design[5], and is only briefly discussed here. The idler output of a continuous-wave pumped optical parametric oscillator (OPO) is used to illuminate an aluminum panel that has been soiled by a mixture of two aliphatic hydrocarbon lubricants and two drawing agents. The OPO employs the quasi-phasematched material periodically poled lithium niobate (PPLN) as the active medium to generate high powers (0.5 Watts) in the frequency range of 2820 – 3150 cm^{-1}. The fan-out design of the PPLN crystal is used to achieve broad and complete spectral coverage without a change in temperature of the crystal. Rapid tuning of the laser is done by translating the crystal inside the cavity. The idler output is expanded to illuminate a 150 mm x 150 mm area of the panel. The specular component of the reflected

light is collected by an infrared imaging camera with an InSb focal plane array detector (Amber Engineering). The camera has a field-of-view 21 x 25 mm. Laser speckle noise is reduced by propagating the idler output through a rotating ZnSe diffuser. This acts to destroy the coherence of the laser beam and allows imaging of the aluminum panel with reduced spatial noise.

To emphasize the ability of the instrument to rapidly diagnose surface coverage, sequential spectra at two different wavelengths, on-resonance and off-resonance, are acquired. FTIR reflectance spectra of the panel were acquired by a commercial instrument (Biorad FTS-40) to determine the spectral characteristics of the hydrocarbon film and identify the optimal laser illumination frequencies for chemical imaging, as shown in figure 1. The band area near 2915 cm^{-1} is indicative of the $-CH_2$ asymmetric stretch of aliphatic hydrocarbons. The on-resonance laser frequency was chosen to correspond to the minimum FTIR reflectance, and an off-resonance laser frequency was tuned to the baseline reflectance, chosen to be 3050 cm^{-1}.

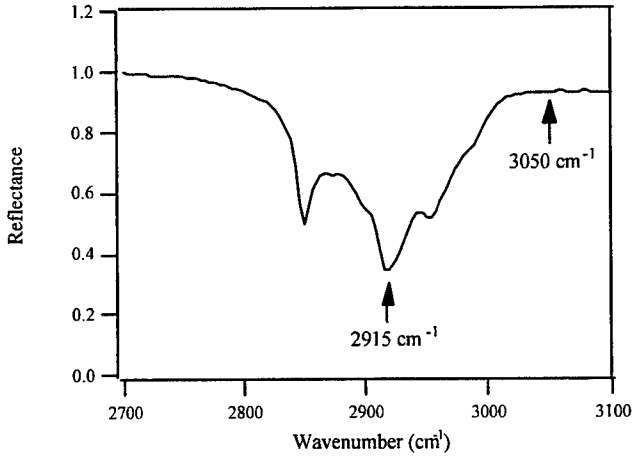

Figure 1. FTIR reflectance spectrum of an aluminum panel soiled with a mixture of four aliphatic hydrocarbon lubricants and drawing agents. The arrows correspond to the laser illumination frequencies.

Examples of the reflectance images acquired at the two different wavelengths are shown in Figure 2A and 2B. Each image has been normalized for differences in incident laser power. Note that the on-resonance image is much darker (Figure 2A), corresponding to significant attenuation of the specular reflectance due to absorption of the hydrocarbon residue. The thickness of the residue is not known, but is estimated to be several micrometers. The relative amount of surface coverage can be determined by the intensity ratio of the reflectance images, (on-resonance)/(off-resonance), which is shown in Figure 2C. The relatively dark areas of the image intentensity ratio correspond to thick coverages of the hydrocarbon residue.

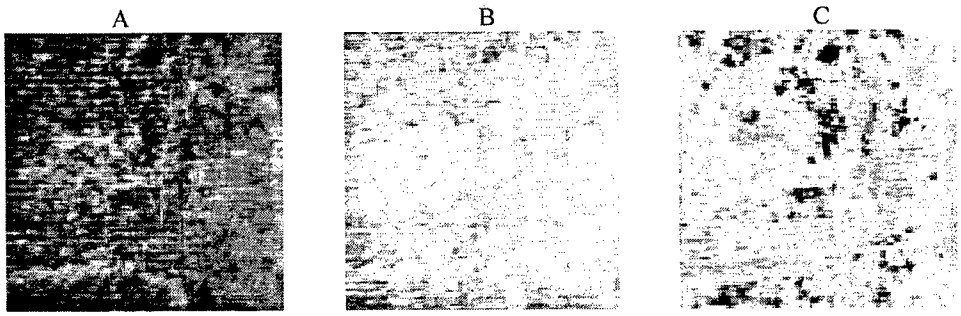

Figure 2. Reflectance images acquired at 2915 cm^{-1} (A) and 3050 cm^{-1} (B). Note that the darker image, (A), corresponds to significant attenuation of the specular reflectance due to absorption of the hydrocarbon residue. The image intensity ratio (on resonance)/(off resonance) is shown in C.

The sensitivity of this intensity ratio method to determine surface coverage is ultimately limited by the baseline noise level. This has been determined for a clean aluminum panel by measuring intensity ratio of two images acquired at the same laser illumination frequency. The observed noise level of a few percent is most likely dominated by residual laser speckle noise and by the limited dynamic range of the infrared camera resulting from a wide bandpass cold filter (3330 – 2220 cm^{-1}). Currently, improvements are being made to the instrument to minimize this baseline noise level. Improvements in the sensitivity of hydrocarbon detection will include the use of polarization reflectance techniques.[1, 2] Further investigations will include the determination of the ability of this instrument to analyze non-flat surfaces.

References

1. D. Ottesen, "Detection of contaminants in steel tubing using infrared reflection spectroscopy," *in Proceedings of SPIE, Optical Techniques for Industrial Inspection*, Vol. 665, G. Cielo, ed., (Society of Photo-Optical Instrumentation Engineers, Bellingham, WA, 1986), Quebec City, Canada, pp. 226-233.
2. D. Ottesen, "An experimental and theoretical study of the infrared reflectance of thin oxide films on metals," J. *Electrochem. Soc.*, **132** (9), pp. 2250-2257 (1985).
3. T.J. Kulp, P.E. Powers, R. Kennedy, and U.B. Goers, "The development of a pulsed backscatter absorption gas imaging (BAGI) system and its application to the visualization of natural gas leaks," *Applied Optics*, **37** (18), pp. 3912-3922 (1998).
4. T.J. Kulp, P.E. Powers, and R. Kennedy, "The development of a laser-illuminated infrared imager for natural gas leak detection," in *Proceedings of the U.S. Department of Energy Natural Gas Conference*, Houston TX, March 24-27, 1997, paper 2.7.
5. P.E. Powers, T.J. Kulp, and S.E. Bisson, "Continuous tuning of a continuous-wave periodically poled lithium niobate optical parametric oscillator by use of a fan-out grating design," *Optics Letters*, **23** (3), pp. 159-161 (1998).

A Systematic Approach To Characterize the Flame Structure of Partially Premixed Flames Based on Holographic Interferometry Measurements

Xudong Xiao and Ishwar K. Puri
University of Illinois at Chicago, Department of Mechanical Engineering (M/C251), 842 W. Taylor St., Chicago, IL 60607–7022
Phone: 312 413 7560, Fax 312 413 0447, Email ikpuri@uic.edu

Abstract: In order to describe the flame structure, a systematic approach is developed that is expressed in the form $\alpha = \alpha(\xi)$, where denotes any scalar for which a state relationship is pertinent.

OCIS codes: (090.2880) Holographic interferometry; (120.1740) Combustion diagnostics.

1. Introduction

Partially premixed flames (PPFs) represent a class of hybrid flames containing multiple reaction zones. A detailed understanding of the temperature distribution in PPFs is important from both practical and scientific considerations, since these flames occur in several applications. We have previously employed holographic interferometry (HI) to accurately determine the refractive index in double flames and triple flames established on a Wolfhard–Parker slot burner and to thereafter infer the temperature distribution [1]. The property that is directly measured by using HI is the refractive index (rather than the temperature or a species concentration). Therefore, in order to describe the flame structure, a systematic approach must be developed that relates the density, temperature, and composition to the refractive index.

2. Objective

Previous methods that relate various flow scalars to the refractive index have assumed that flames consist of an ideal gas of constant molecular weight. Those investigations disregarded flame structure effects on the inferred refractive index. We have simulated a variety of counterflow partially premixed methane–air flames using detailed descriptions for the species' thermophysical properties and the flame chemistry. We concluded that the constant molecular weight ideal gas assumption is satisfactory in case of premixed and partially premixed methane–air flames, but can lead to erroneous results in case of nonpremixed flames [1]. In this investigation we will discuss the effects of a realistically–varying composition (due to combustion) on the refractive index distribution in flames. Our objective is to develop a rational approach for determining the local mixture fraction, species distribution, and temperature in partially–premixed flames that is applicable to interferometric and deflectometric optical techniques. We will demonstrate that a conserved scalar ξ, that transforms the flame structure from a spatial to a generic distribution, can be inferred from the refractive index distribution. Thereafter, measurements of the density, temperature, and composition in two–dimensional PPFs becomes feasible. In the following sections we will provide the analytical details of the procedure, present the effect of strain rates on ξ and from the HI measurements infer the distribution of the modified mixture fraction, density, temperature, as well as species concentrations.

3. Procedure

Holographic Interferometry

We have previously reported on the utility of HI to obtain the local refractive index distribution in steady slot burner PPFs [1]. In that investigation we employed a modified off-axis double–exposure laser holographic technique. The "fringe equation" that describes the light interference has the form

$$\int(n_1 - n(x,y,z))ds = N\lambda, \qquad (1)$$

where n_1 is a constant that denotes the ambient refractive index at the time of the initial exposure of the holography plate, n(x,y,z) denotes the refractive index along the wave path through the flame during the second exposure, N the fringe number, and λ the wavelength. The phase recorded on a hologram represents the integration of the refractive

index along the relevant path, i.e., the hologram records a "projection" of the refractive index field. The path integration that occurs in Eq. (1) can be corrected for by applying the relation $n(x,y) = n_1 - N\lambda/L - n_1 L\,(n'/n_1)^2\,(L/3 - z_f/2)$, where L denotes the flame width in the cross stream direction, which is also referred to as the integration length, and $n'(x,y)$ denotes the local refractive index gradient. The coordinates x, y, and z, respectively, denote the transverse direction, the axial displacement, and the lateral (cross-stream) direction in the laboratory frame of reference. If an interferogram is formed by imaging a plane that lies at a distance $z_f = 2L/3$ that extends from the test entry plane to the image plane, Eq. (1) can be simplified into the form

$$n(x,y) = n_1 - N\lambda/L. \tag{2}$$

Therefore, in this investigation we do not neglect ray curvature, but eliminate its effects by a proper choice of z_f.

The refractive index and the temperature can be determined using a state equation and the Gladstone–Dale (G–D) relation. The ideal gas law for a mixture has the form $\rho(x,y,z) = (P/R)(W_{mix}(x,y,z))/T(x,y,z))$, where $\rho(x,y,z)$ denotes the mass density at position (x,y,z), T(x,y,z) the absolute temperature, P the pressure, R the gas constant, and W_{mix} the mixture molecular weight. The dependence of the refractive index on $\rho(x,y,z)$ is obtained from the G–D relation, i.e., $n(x,y,z) - 1 = \rho(x,y,z)\,K_{mix} = \rho(x,y,z)\,(\Sigma y_i(x,y,z)k_i)$, where n(x,y,z) denotes the refractive index and k_i the G–D constant for the i–th species. The temperature can be related to the refractive index, i.e., $T(x,y,z) = (n(x,y,z) - 1)^{-1}\,\beta(x,y,z)$, where $\beta(x,y,z) = (P/R)(\Sigma y_i(x,y,z)k_i)(\Sigma y_i(x,y,z)W_i^{-1})^{-1}$. If $\beta(x,y,z)$ is assumed to be constant throughout the flame, the temperature T(x,y,z) can be evaluated relative to some reference temperature T_0 at which the refractive index has a known value n_0. With this assumption,

$$T(x,y,z) = T_0\,(n_0 - 1)/(n(x,y,z) - 1). \tag{3}$$

Modified Mixture Fraction ξ

The modified mixture fraction transforms the system–specific spatial coordinates into a generic, universally–applicable coordinate so that the flame can be represented by a single parameter, $\xi(x,y,z)$. The temperature and species mass fractions in the PPFs can be inferred by using the conserved scalar approach as follows. Numerical simulations of strained methane–air partially premixed flames were performed using a previously developed computer code that employs a detailed model of both the molecular transport of chemical species and the chemical reaction schemes. We have considered seventeen species in the refractive index calculation for which values of the G–D constants are available in the literature. In terms of the modified conserved scalar, the refractive index in flame can be assumed the form

$$n(\xi) = 1 + \rho(\xi)\,(\Sigma y_i(\xi)k_i). \tag{4}$$

Since the structure of flames varies according to the flame stretch they experience, the counterflow calculations are performed for the same stoichiometry, but at different values of the strain rate in order to identify stretch–related effects. The results are expressed in the form $\alpha = \alpha(\xi)$, where α denotes any scalar for which a state relationship is pertinent, such as the refractive index or temperature. We will assume that if $\alpha_j = \alpha_j(\xi)$, this implies that $\xi = \xi(\alpha_j)$ and $\alpha_{k \neq j} = \alpha_k(\alpha_j)$, i.e., if the refractive index distribution n(x,y,z) can be determined in a flame, say, by using HI, then the temperature T(n), mixture fraction $\xi(n)$, or species mass fraction $y_i(n)$ distributions can also be inferred.

4. Results and Discussion

We have examined the effects of varying strain rates on the refractive index and scalar distributions in methane–air counterflow partially premixed flames. The flames were simulated at different stoichiometries and at three moderate–to–high strain rates a = 20, 50, and 150 s^{-1}. Direct measurements of n(x,y) are presented for the two flames in Fig. 1. The mixture fraction distribution ξ–field for the double flame and the triple flame that is inferred from the data presented in Figs. 1 is obtained in Fig. 2. Since we have divided the flame into two dichotomous regions, large gradients are inferred at the rich–lean interface. Consequently, the ξ–field in the vicinity of this interface cannot be spatially resolved. Once the mixture fraction distribution is known, state relationships for the temperature and species distributions of the form $\alpha = \alpha(\xi)$ can be applied. These relationships have been developed for counterflow flames established at a moderate strain rate of 50 s^{-1}. The temperature distribution T = T(n) is directly determined and by assuming that $T = T'(\xi)$. The local difference $\Delta T(x,y) = |T(n(x,y)) - T'(\xi(x,y))|$ due to the two approaches are presented in Fig. 3 for the double flame. In general, $\Delta T(x,y) < 40$ K.

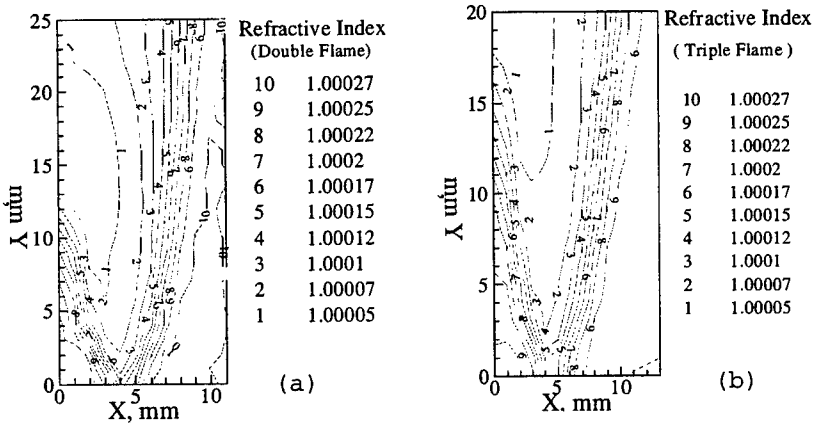

Fig. 1. The refractive index distribution for two PPFs: (a) a double flame and (b), a triple flame.

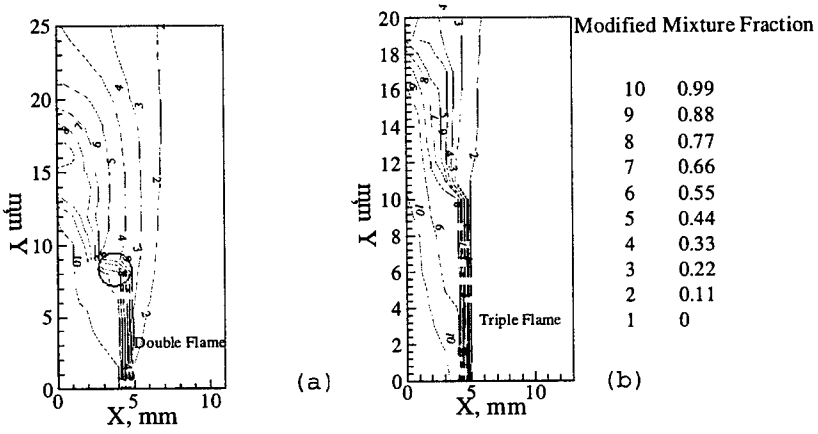

Fig. 2. The _ distribution for two PPFs: (a) a double flame and (b), a triple flame.

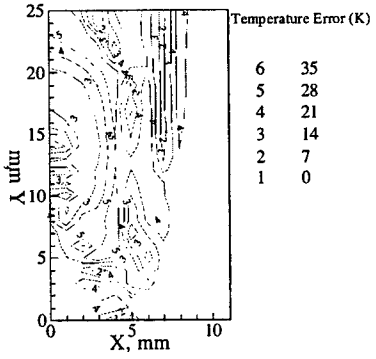

Fig. 3. Temperature difference distribution for the double flame.

5. References

1. Xiao, X., Choi, C. W., and Puri, I. K., "Temperature measurements in steady two–dimensional partially premixed flames using laser interferometric holography", to appear in *Combustion and Flame* (1999).

Gas Temperature Measurements by Spontaneous Raman Spectra of Carbon Dioxide

Hansheng Zhang, Fang-Yu Yueh, Jagdish P. Singh* and Robert L. Cook

Diagnostic Instrumentation and Analysis Laboratory
Mississippi State University
205 Research Boulevard, Research and Technology Park
Starkville, MS 39759-9734
Tel: 662-325-2105; Fax: 662-325-8465
e-mail: singh@dial.msstate.edu

Summary

Spontaneous Raman spectroscopy (SRS) has been used in combustion diagnostics to measure gas temperature and species concentration.[1-7] SRS is an inelastic process in which the scattered light undergoes a frequency change characteristic of the internal energy levels of the irradiated molecules. SRS is easy to implement as a fieldable system, because it is a relatively simple and inexpensive technique. The Raman signal can be collected in the backward direction which makes SRS suitable for industrial applications using only one optical port. However, it suffers from low collection efficiency due to its isotropy scattered signal. Recent Raman studies with pulsed lasers and gated detection have shown a great improvement in the sensitivity of SRS technique.[1,2]

The main goal of this work is to develop and build a rugged Raman instrument to measure gas temperatures in large oxygen-fed glass furnaces with clean gas streams using Raman spectra of carbon dioxide. Nitrogen Raman spectra have been well-characterized to infer gas temperature of air-fed combustion flames. In a CH_4/O_2 combustion facility, very little nitrogen is present. CO_2 is the major constituent in this combustion environment. Therefore, CO_2 was chosen to infer gas temperature. CO_2 is a linear triatomic molecule. It is characterized by vibrational quantum, v_1, v_2, v_3, of the fundamental vibrational mode and a vibration angular momentum quantum number ℓ_2. The simulation of CO_2 spectra is more difficult due to the accidental degeneracy, $v_1 \approx v_2$, which results in the Fermi resonant effect in which the vibrational states of these two modes mix together. The numerical simulation of the CO_2 Raman has been discussed in detail in Reference 8.

The optical design of the Raman system is shown in Figure 1. The second harmonic of a pulsed Nd:YAG laser is passed through a mirror with a 9-mm hole on the center and focused by a lens. The back scattered Raman signal is collected with the same focusing lens, and sent to the detection optics with the mirror. The detection optics includes a quartz lens, two notch filters and a quartz optical fiber bundle. The Mie and Rayleigh scattering at 532 nm is reduced by the two holographic notch filters placed in front of the optical fiber bundle. The optical fiber bundle delivers the Raman signal to a 0.5-m monochromator equipped with 1200 l/mm and 2400 l/mm gratings. The output of the fiber bundle has a slit shape (0.1x1.0 cm^2), and it is used as the entrance slit for the monochromator. The dispersed Raman signal is recorded with a gated, 256x1024, intensified charge-coupled device (ICCD) detector. Before a read-out, the pixels along the vertical axis of the detector are binned to improve the signal-to-noise ratio of the spectrum.

Experiments were performed in a commercial bench-top oven and a methane/air flame. The oven has a cylindrical heated volume (8-cm diameter and 50-cm length). A thermocouple placed near the focal volume was used to monitor the gas temperature. The CO_2 gas was flowed through the oven with a tube connected to the oven. The oven was used to record CO_2 anti-Stokes Raman spectra between 800 K and 1400 K. The methane/air flame was produced by a custom-made flat flame burner with a flame length of ~ 13 cm and flame width of ~ 1 cm.[5] The laser beam was aligned along the flame in order to increase the scattered photons. All experiments were performed at the maximum laser power (~ 160 mJ) and 10 Hz repetition rate to avoid the laser induced breakdown. Typically we use 510 ns delay and 70 ns gate width and 200 s averaging time in the flame measurement. Initial investigation shows the observed anti-Stokes

signal is stronger than the Stokes signal for temperature higher than 800 K. This is because one of the notch filters used has low transmission in the CO_2 Stokes signal region. The measurements were then performed with the anti-Stokes signal.

The performance of the CO_2 anti-Stokes Raman probe was first evaluated with temperature measurements in the bench-top oven. A 30 cm focal length lens was used to focus the laser beam ~ 5 cm before the center of the oven. Anti-Stokes Raman spectra recorded from 800 - 1400 K were analyzed by fitting with the theoretical model to extract gas temperature. The thermocouple readings were consistently higher than the temperatures inferred by fitting of the Raman spectra of CO_2. This discrepancy is caused by a temperature gradient near the end of the oven, so that the spectra are distorted by the Raman signal contribution from colder parts of the oven. The intensity ratios of the two CO_2 bands ($01^10 \rightarrow 11^10$ and $00^00 \rightarrow 10^00$) at various oven temperatures show a linear dependence, as shown in Figure 2. Therefore, this curve can be used as a calibration curve to inferred gas temperature under the same measurement condition. A shorter focal length lens would have solved some of this spatial averaging problem; however, the lens would then will have to place inside the oven.

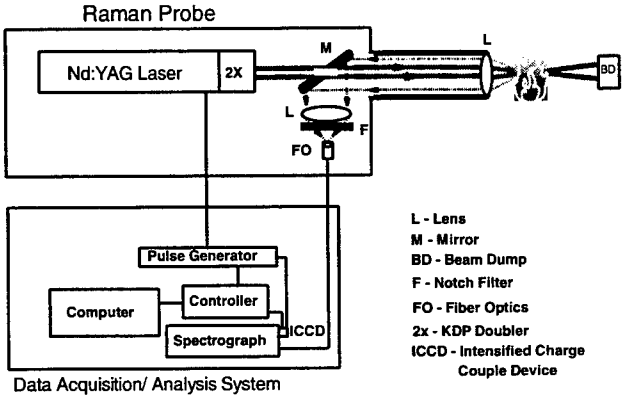

Figure 1. Experimental setup for Spontaneous Raman Spectroscopy.

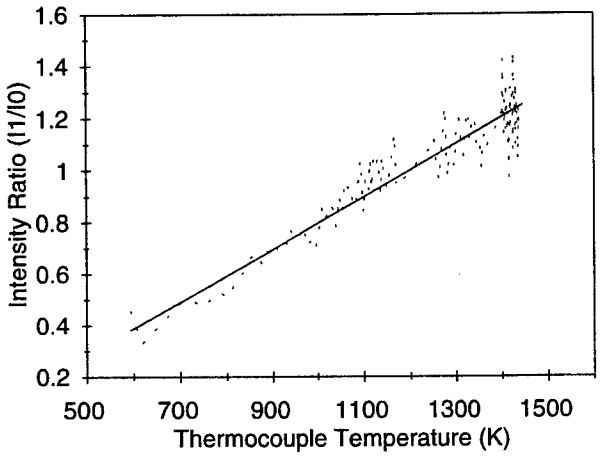

Figure 2. The intensity ratio of two CO_2 bands at different furnace temperatures.

In order to evaluate the CO_2 Raman technique in a higher temperature environment, CO_2 Raman spectra were recorded in a methane/air flame. The CH_4/air flame with stoichiometric mixtures give a maximum temperature of 2500 K and CO_2 concentration of 8.5%. The signal-to-noise ratio of the flame spectrum is poorer than the oven data due to its low CO_2 concentration. Figure 3 shows a fitting of experimental CO_2 anti-Stokes Raman flame spectrum with the calculated spectrum. During the flame experiments, we also recorded N_2 anti-Stokes spectra from the flame. The inferred gas temperature from N_2 Raman spectra were used to compare with that inferred from CO_2 Raman data. Figure 4 shows the inferred gas temperature from N_2 and CO_2 Raman spectra. Note that the CO_2 and N_2 data were recorded at different times under the same experimental condition. The inferred temperatures from N_2 and CO_2 are in reasonable agreement. However, the CO_2 data has poorer precision than the N_2 data. This is because the CO_2 data has poor S/N due to its low concentration.

The current design of the Raman probe using backscatter detection allows measurements in a large

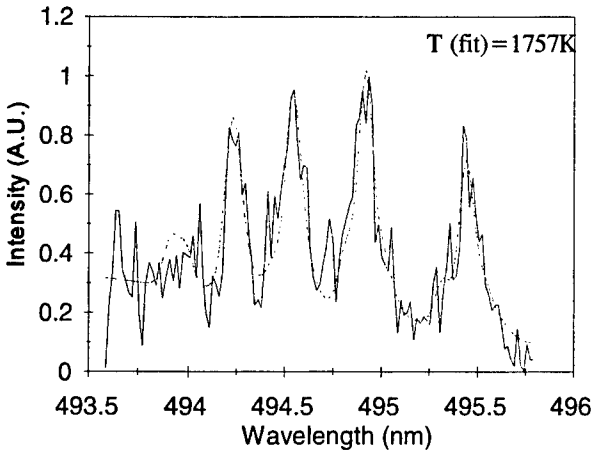

Figure 3. Fitting of a CO_2 spectrum from CH_4/air flame with the simulated CO_2 spectrum.

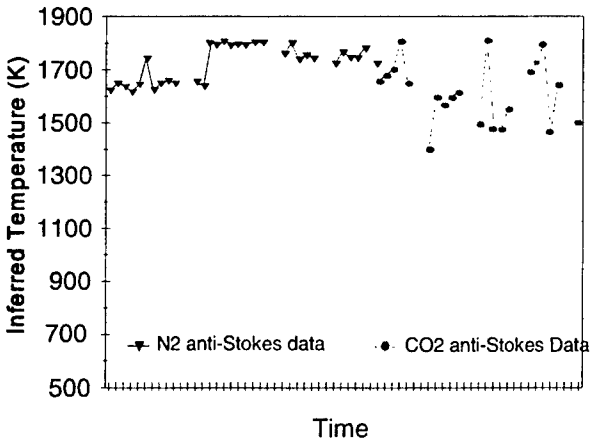

Figure 4. Comparison of the flame temperature inferred from CO_2 and N_2 Raman spectra.

industrial oven with one optical port. However, backscattering light collection introduces some spatial averaging problems. Any Raman signal generated along the laser beam between the dichroic mirror and the focusing lens and scattered in the backward direction is collected by the lens which focuses the collimated scattered light onto the optical fiber bundle input.[5] The spatial resolution of our current system along the beam axis is ~ 10 cm. This resolution is too coarse for most laboratory applications, but it is suitable for a large industrial oven.[5] Work to improve the detection sensitivity and accuracy of the technique will continue. This system will later be integrated with a water-cooled insertion probe to perform CO_2 Raman measurements in a large industrial combustion facility.

Reference

1. A.C. Eckbreth, "Laser Diagnostics for Combustion Temperature and Species", 2nd ed. (Gordon & Breach, Amsterdam, 1996), Chap. 5 and references therin, pp. 209-280.
2. *Non-intrusive Combustion Diagnostics* [Pap. Int. Symp. Spec. Top. Chem. Propul.], K. K. Kuo and T. P. Parr, eds. (Begell House, New York, 1994).
3. D. A. Long, *Raman Spectroscopy* (McGraw-Hill, Inc., New York, 1977).
4. N. M. Laurendeau, "Temperature measurements by light-scattering methods," Prog. Energy Combust. Sci. **14**, 147-170 (1988).
5. G. Zikratov, F.Y. Yueh, J.P. Singh, O. P. Norton, R. A. Kumar, and R.L. Cook, "Spontaneous anti-Stokes Raman probe for gas temperature measurement in industrial furnaces," Appl. Opt. **38**, 1467 (1999).
6. W. Reckers, L. Hüwel, G. Grünefeld, and P. Andersen, "Spatially resolved multispecies and temperature analysis in hydrogen flames," Appl. Opt. **32**, 907-918 (1993).
7. A.N. Karpetis and A. Gomez, "Temperature measurements in spray flames by spontaneous Raman scattering," Opt. Lett. **21**, 704-706 (1996).
8. R.J. Blint, J.H. Bechtel, and D. A. Stephenson "Carbon dioxide concentration and temperature in flames by Raman Spectroscopy," J. Quant. Spectrosc. Radiat. Transfer **23**, 89-94 (1980).

Laser Applications to Chemical and Environmental Analysis

Analytical Applications 2

Sunday, February 13, 2000

Kay Niemax, Inst. of Spectrochemistry and Applied Spectroscopy, Germany
Presider

SuD
3:40pm–5:20pm
Anasazi North

Laser-induced fluorescence detection of atmospheric NO_2 at parts per trillion mixing ratios

Ronald C. Cohen
Department of Chemistry, and Department of Geology and Geophysics, University of California, Berkeley, Berkeley, CA 94720-1460
Telephone: (510) 642-2735 Fax: (510) 642-6911 E-mail: cohen@cchem.berkeley.edu

Abstract: A laser-induced fluorescence instrument designed for continuous, autonomous, *in situ* observations of atmospheric NO_2. The instrument sensitivity is 10 parts per trillion (ppt) in 10 seconds of integration (S/N=2) with a detection limit below 1 ppt.

OCIS codes: (010.1120 Air pollution monitoring; 010.1280 Atmospheric composition)

Summary

Tropospheric NO_2 mixing ratios vary from 10's of parts per billion (ppb) in cities to below 10 parts per trillion (ppt) in remote regions of the atmosphere. We describe a laser-induced fluorescence (LIF) instrument designed for accurate (±5%, 1σ), continuous, autonomous, *in situ* observations of NO_2 in any of these environs. The technique is advantageous because it is direct, in that it does not require prior conversion of NO_2 into another species (e.g. NO) prior to detection, eliminating a class of potential interferences. It is also spectroscopically specific. The instrument we have developed is sensitive, capable of detecting 10 parts per trillion in 10 seconds of integration at a signal to noise ratio of 2 and with a detection limit below 1ppt. The instrument responds rapidly to changes in ambient NO_2 and it is capable of 10Hz time resolution for making flux measurements using the eddy correlation technique. It weighs about 300 lbs including all components necessary for operation (computers, calibration gases, ...) and consumes about 2.5kW of electrical power. Performance of the instrument is illustrated with in situ observations obtained in the summers of 1998 and 1999 at the University of California, Blodgett Forest field station located in the foothills of the Sierra Nevada and in Nashville, TN. Details are described by Thornton, Wooldridge and Cohen in a paper submitted to Analytical Chemistry [1].

Our instrument is described in Figure 1. The core is a YAG pumped dye laser and a multipass detection cell. The dye laser output (585nm, 0.06cm^{-1} 8kHz, 30ns, 200mW) makes 40 passes in the detection cell. Air, at 3 Torr, is continuously pumped through the cell at 1 slm. NO_2 fluorescence is collected at a right angle to the laser beam and detected using a cooled GaAs photomultiplier. The signal rate is ~60cts/ppb/sec (independent of pressure). Noise that survives the filtering is reduced by delaying the detection gate by 50ns. Long-lived NO_2 fluorescence is collected while more than 90% of the noise is eliminated. A series of optical filters are used to discriminate against Rayleigh and Raman scattering of the laser and against non-resonant scatter of the laser off of the mirrors and chamber walls.

Operation of the experiment begins by setting the laser on the line shown as point (a) in the scan in Figure 2. Once on the line, an automated algorithm maintains frequency lock indefinitely. Figure 2 shows a scan followed by tuning the laser on and off the molecular transition (dithering). The top trace shows transmittance through the NO_2 reference cell during this period. The bottom trace shows fluorescence from NO_2 in laboratory air at Berkeley. The arrows indicate the online (a) and offline (b) positions for the rovibronic feature at 17086 cm^{-1}. The NO_2 concentration in the laboratory was increasing during the dithering period.

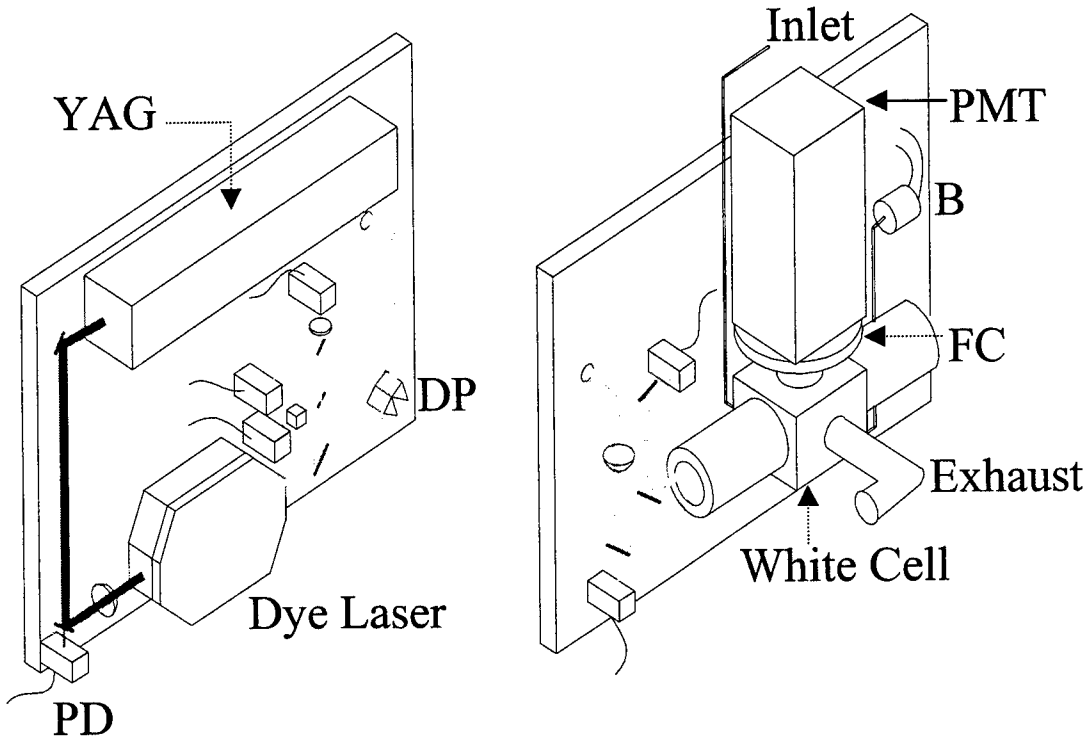
YAG
DP
Dye Laser
PD
Inlet
PMT
B
FC
Exhaust
White Cell

Fig. 1.

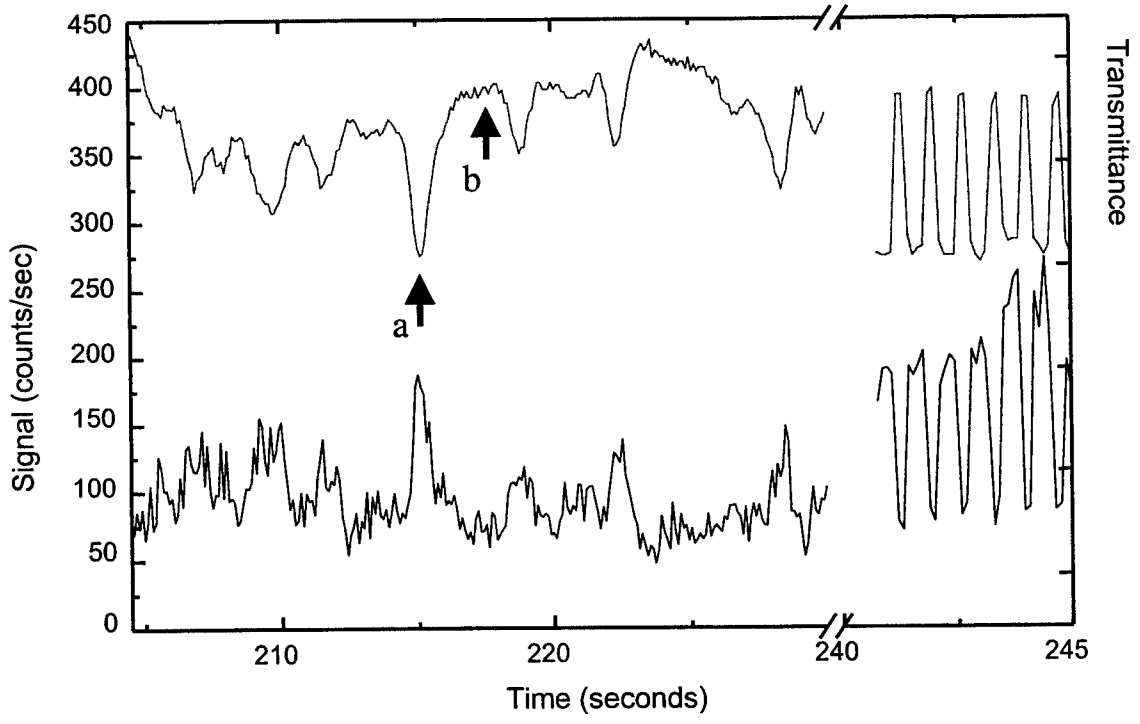
Signal (counts/sec)
Transmittance
Time (seconds)
a
b
0
50
100
150
200
250
300
350
400
450
210
220
240
245

Fig. 2.

The instrument is designed to be easily transported and to operate continuously from remote locations. Figure 3 shows NO_2 concentration plotted as 1-minute averages versus time at the UC Blodgett Forest Research Station. The site is 30 miles east of Sacramento in the foothills of the Sierra Nevada, and four miles beyond the end of the electrical grid. Points far from the mean are due to a nearby diesel generator used to provide power to the instrument.

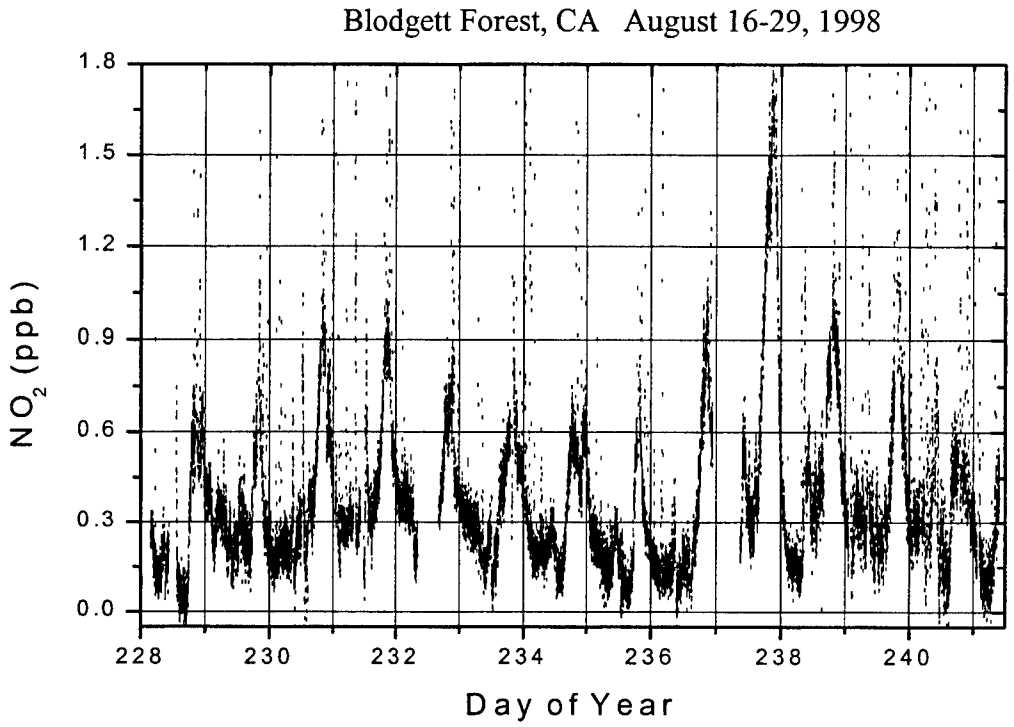

Fig. 3.

J. A. Thornton, P. J. Wooldridge, R. C. Cohen, "Atmospheric NO_2: *In situ* laser-induced fluorescence detection at parts per trillion mixing ratios," submitted to Analytical Chemistry, August, 1999.

Applications of Laser Multiphoton Ionization to Fast Analysis of Environmental Samples

Israel Schechter, Vladimir V. Gridin, Valery Bulatov, Salah Hasson, Takanori Inoue, Michal Fisher, Chanan Sluszny, Iris Litani-Barzilai, Alona Korol, Michal Kadosh

Department of Chemistry, Technion - Israel Institute of Technology, Haifa 32000, Israel
Tel/Fax:+972-4-9292579, E-mail:israel@tx.technion.ac.il

Abstract: Laser Multiphoton Ionization was applied for direct environmental analysis, under ambient conditions. In most applications, the fast-conductance detection system was used, where the laser induced photocharges are registered as a function of time. The studied environmental applications include contaminated soils, airborne contaminants and polycyclic aromatic hydrocarbons (PAH) in liquids. A modification of this technique, involving monitoring of the ion-induces mirror-charges, was applied of sensitive air analysis. The MPI techniques were successfully introduced for routine environmental analysis of organic contaminants such as PAHs.
OCIS codes: (040.0040) Detectors, (120.0120) Instrumentation, measurement, and metrology, (000.1570) Chemistry, (000.2170) Equipment and techniques, (010.1110) Aerosols, (010.1120) Air pollution monitoring, (020.4180) Multiphoton processes, (190.4180) Multiphoton processes, (280.3420) Laser sensors, (300.6280) Spectroscopy, fluorescence, (300.6410) Spectroscopy, multiphoton, (300.2530) Fluorescence, laser-induced, (260.3230) Ionization.

1. Introduction

Laser multiphoton ionization (MPI) is known as a very sensitive method of analysis, with high selectivity in its resonant mode. In this method a laser pulse in applied to a substrate for its ionization in a process that involves several photons. The MPI technique has been coupled to many ion detection systems: The most powerful tool is obtained with a full MS detection system, however, this setup is rather complicated and expensive. Simple and low-cost detection systems are required for possible application to chemical environmental sensors.

One of the simplest detection-system in the fast conductivity (FC) method, where the current resulting from the emitted electrons is monitored. This method has been successfully applied to a variety of systems of considerably analytical interest. Detection limits of this technique can be as low as sub-ppb or even the ppt range .

There are numerous useful applications of relatively low cost analytical techniques of this kind, especially when on-line and in-situ abilities of the method are considered. Of particular importance are environmental applications concerned with atmospheric, water resources and soil pollution analysis.

We report on the development of several new environmental applications of MPI – fast conductivity technique. These include:

(1) Direct soil analysis under ambient conditions,

(2) A renewable liquid droplet method for on-line pollution analysis by MPI,

(3) Simultaneous laser MPI and laser induced fluorescence for PAH analysis in solutions.

(4) Simultaneous MPI and LIF on-line screening of airborne PAH contamination.

(5) MPI-Fast-Conductivity applications to analysis of traffic contaminated soils.

Our achievements in these topics are briefly discussed in the following:

1. Laser Multiphoton Ionization of Pyrene on Contaminated Soils

The MPI process, coupled with a fast photocurrent detection system, has been applied for analysis pyrene contaminated soils. This method can handle contamination in a wide dynamic range (6 orders of magnitude), and a variety if initial soils. According to our estimate, pyrene detection limit is below 35 ng/g, which is adequate for environmental soil analysis. (Target PAH concentrations in contaminated soils are in the range of 0.85 to 125 μg/g.)

Although the ionization order (indicating the number of photons involved in the process) in soil samples varies between 2 and 4, the additional pyrene contamination could be monitored [1]. Moreover, by assuming a contamination model that separates geometrical effects from the pure MPI process, a remarkable compensation for

matrix effects was achieved. This model of an external contamination, where impurities are deposited onto the soil surface by contaminated solvents, suggests that the detection ability of the applied method could be influenced by the permeability of the soil surface with respect to the solvent. This result brings about several questions related to aerosol type depositions and analysis when the soil is heavily watered and neither the solvent nor the impurity are readily mixed or dissolved in the water table of the soil. Such questions are of current environmental interest. When the contamination is brought to the soil surface from below, by means of capillary effects, the method could help to relate, in a non-destructive manner, the surface concentrations with the internally present ones. Many of the involved effects (e.g. moisture dependence) were studied and understood [2]. Our main conclusion is that analysis of PAH in soil by laser multiphoton ionization is feasible.

2. A Renewable Liquid Droplet Method for On-line Pollution Analysis by Multiphoton Ionization

We address the potential of renewable sampling of gaseous / aerosol contamination by water droplets for the purpose of MPI-FC analysis. The MPI processes were induced on the sampling droplet by a pulsed N_2- laser, which is readily found in portable devices (Fig. 1). The principal action of this technique is based upon detecting short-lived photoionisation currents. The later are created when the pulsed laser flux is used to probe the organic traces in the droplet matrix. The detection system is both simple and low-cost, suggesting possible development of an in-situ instrumentation.

The environmentally important aerosols used for evaluation of the proposed method were those found in a typical motor vehicle exhaust gas and in cigarette smoke. Both of these complex pollutants contain PAHs, allowing for a two-photon ionization process. Since the 337.1 nm line of the N_2 laser is close to the resonant mode of MPI process in pyrene, the latter was especially examined in our set-up. In this case the calibration curve obtained for pyrene aerosol on a water droplet extends to about 1 pg levels [3]. Since the reported water solubility of pyrene under normal conditions is of the order of 0.1 ppm, we have contaminated our water droplets in a way that enables capturing of pyrene micro-particles by these droplets [4]. Our results suggest that UV absorbing particles sampled by renewable water droplets produce good quality signals in the MPI-FC detection method used.

It has been also shown that a universal calibration curve can be obtained for PAH, in the low contamination regime (where bulk droplet contamination is achieved). At higher concentrations, where surface deposition is relevant, a lower calibration curve slope is obtained. The feasibility of on-line analysis by micro-droplet sampling followed by MPI detection has been proven, although further research and engineering is still necessary.

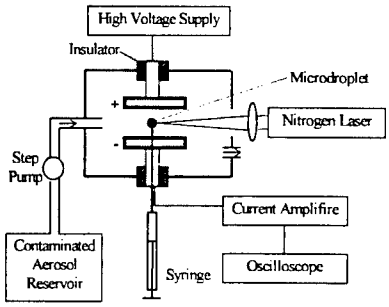

Fig. 1 Experimental setup for sampling and analysis of airborne pollution

3. Simultaneous laser MPI and laser induced fluorescence for PAH analysis in solutions

Laser multi-photon ionization and laser induced fluorescence (LIF) techniques were simultaneously applied to analysis of PAHs in apolar solutions. This combination of single photon (LIF) and multiphoton (MPI) processes provides unique information which is shown to be sufficient for both identification and quantification of PAH molecules in simple mixtures. We suggest 3-D calibration plots (concentration as a function of both MPI and LIF signals) where each PAH compound is represented by a unique vector in this space. The projections of such vectors onto the MPI-LIF plane are the basis of PAH analysis, where only two measurements (MPI and LIF signals) are required for speciation and quantification. A geometrical algorithm for decomposition of simple PAH mixtures is also addressed and it is shown that binary systems can be resolved as well [5].

As a result of these experiments, an analytical method based on simultaneous MPI and LIF signals was established and demonstrated for monocomponent PAH analysis in hexane solutions. This study presents and exemplifies the analytical principles, however, further investigation of the expected matrix effects is needed.

4. Simultaneous MPI and LIF On-line Screening of Airborne PAH Contamination

We have shown that LIF and MPI based detection methods compliment each other and can be applied to on-line screening of airborne PAH contamination [6]. For UV active organic compounds and adequate laser irradiation densities, the LODs offered by a single-color MPI-FC technique quite routinely fall within the sub-ppb range. In such case, the advantage of LIF is in a "finger print" type, PAH specific, fluorescence spectra. In turn, MPI processes might be initiated via short-lived, virtual states when essentially a single-photon LIF method fails.

We report a preliminary application of simultaneous LIF and MPI-FC techniques for continuous monitoring of sub-micron airborne PAH pollutants. The feasibility of this method was demonstrated. Both excellent LOD's and possible speciation may be obtained when the excitation wavelength is tuned to an MPI resonance. In such case, absolute cross-sections for the resonant state-to-continuum transitions seem to be obtainable too.

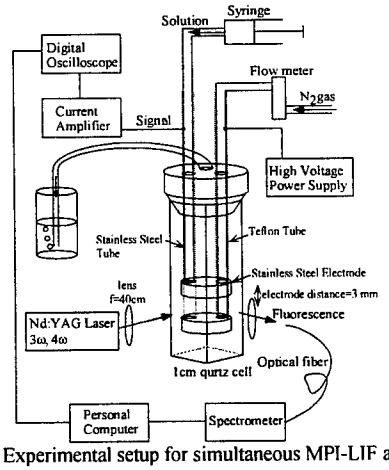

Fig. 2 Experimental setup for simultaneous MPI-LIF analysis.

5. Photoionization Fast-Conductivity Technique for Analysis of Traffic Contaminated Soils

The MPI process, coupled with a fast photocurrent detection system, was developed and used to study series of environmental soil samples in the vicinity of a busy traffic road [7]. An effective photoionization order of k=2 was found for these specimens. We observed that as long as environmental conditions during the fast conductivity characterization procedure stay similar, both the hexane extracts of organic traces and hexane wetted original soil probes have produced nearly identical results. This implies a gross simplification of sample preparation steps needed for such photo-conductivity analysis. Therefore, this method can be potentially applied for screening of soil contamination and for routine analyses of traffic contaminated soils.

Moreover, assuming a straightforward contamination model we have quite satisfactory accounted for the observed 1/R fall-off of the photo-conductivity signals detected from the readily collected soil probes [8]. The model did not involve any fitting parameters. On the contrary, it has been reasonably cross-referenced for by a close similarity between the model estimated half-road width and its actual size.

6. References

1. V.V. Gridin, A. Korol, V. Bulatov and I. Schechter, "Laser Two-Photon Ionization of Pyrene on Contaminated Soils", *Anal. Chem.*, **68**, 3359-3363, (1996).
2. V.V. Gridin, V. Bulatov A. Korol and I. Schechter, "Particulate Material Analysis by a Laser Ionization Fast-Conductivity Method – Water Content Effects", *Anal. Chem.*, **69**, 478-484, (1997).
3. V.V. Gridin, I. Litani-Barzilai, M. Kadosh and I. Schechter, "A Renewable Liquid Droplet Method for On-line Pollution Analysis by Multi-Photon Ionization", *Anal. Chem.*, **69**, 2098, (1997).
4. V.V. Gridin, I. Litani-Barzilai, M. Kadosh and I. Schechter, "Determination of Aqueous Solubility and Surface Adsorption of Polycyclic Aromatic Hydrocarbons by Laser Multiphoton Ionization", *Anal. Chem.*, **70**, 2685-2692, (1998).
5. T. Inoue, V.V. Gridin, T. Ogawa and I. Schechter, "Simultaneous Laser Induced Multiphoton Ionization and Fluorescence for Analysis of Polycyclic Aromatic Hydrocarbons", *Anal. Chem.*, **70**, 4333-4338, (1998).
6. V.V. Gridin, T. Inoue, T. Ogawa and I. Schechter, "On-line Screening of Airborne PAH Contamination by Simultaneous Multiphoton Ionization and Laser Induced Fluorescence", *Sci. Technol*, (in press, 1999).
7. V. Bulatov, V.V. Gridin, F. Polyak and I. Schechter, "Application of Pulsed Laser Methods to In-Situ Probing of Highway Originated Pollutants", *Anal. Chim. Acta*, **343**, 93-99, (1997)
8. V.V. Gridin, V. Bulatov A. Korol and I. Schechter, "Photoionization Fast-Conductivity Technique for Analysis of Traffic Contaminated Soils", *Instrum. Sci. Technol.*, **25**, 321-333, (1997).

Laser-Induced Breakdown Spectroscopy of Trace Metals

Dr. Randall L. Vander Wal
NCMR c/o NASA-Glenn
M.S. 110-3
21000 Brookpark Rd.
Cleveland, OH 44135
Ph. (216) 433-9065
FAX (216) 433-3793
Email: randy@rvander.grc.nasa.gov

Prof. Thomas M. Ticich;
Mr. Joseph R. West Jr.
Centenary College of Louisiana
Department of Chemistry
2911 Centenary Blvd.
Shreveport, LA 71134

Introduction

The detection and quantification of light elements and heavy metals within liquid samples and those produced by acid dissolution of solids are pertinent to industrial processing, environmental monitoring and waste treatment [1-5]. To-date, laser-induced breakdown spectroscopy (LIBS) has been tested with limited success. Dissolved gases, particulate material and nucleation-induced bubbles produced by prior laser pulses can lead to misfocusing of the laser beam and can also serve as breakdown sites prior to the laser beam focus [1-3,6,7]. Additionally, the high local density within the liquid leads to rapid quenching which prohibits temporally selective detection, high collision rates which broaden spectral transitions and confines the plasma emission spatially rendering spatially selective detection problematic. Given these inherent difficulties, in-situ LIBS analysis of liquids has not been widely sucessful with detection limits in the range of 1 - 100 ppm for light metals [1,3-6,8-11]. As a result, even fewer studies have investigated detection of heavy metals [1-3,6] with Hg being reported undetectable at 1000 ppm [3].

In contrast, solid surface analysis via LIBS exploits the strengths of the technique without the problems inherent to liquid analysis. Solid surfaces provide a uniform, well-defined sample surface. Additionally, the ambient background gas and pressure can be tailored to govern the plasma spatial and temporal evolution thereby optimizing detection conditions [12-16]. Finally, surface analysis of a reproducible uniform material avoids the inherent difficulties associated with varying sample matrices, particle grain size effects, analyte dispersion uniformity and varying moisture content [17,18]. In the work presented here, trace elemental identification within solutions is transformed into a solid surface analysis. Measurements for 15 metals (Mg, Al, Si, Ca, Ti, Cr, Fe, Co, Ni, Cu, Zn, As, Cd, Hg, Pb) are presented.

Experimental Approach

Our approach consisted of evaporation of the analyte solution upon an amorphous graphite substrate followed by LIBS analysis of the substrate surface. Using calibrated pipets, aliquots of environmental standard solutions (commercially available solutions of the metal as a nitrate or chloride salt in roughly 2 % HNO3 or HCl respectively) or diluted solutions prepared from these certified standards were deposited upon the carbon disks and then evaporated to dryness.

A pulsed Nd:YAG laser provided light at 1064 nm for the LIBS analysis withthe same single laser pulse serving to both atomize and electronically excite the elements. Using a 300 mm focal length fused silica lens, the beam focus was placed approximately 1 cm behind the sample surface. The beam diameter on the graphite planchet was determined to be roughly 750 microns, resulting in a laser fluence of roughly 35 J/cm^2 and an intensity of 4.4 GW/cm^2 for a nominal 8 nsec pulse width.

LIBS emission from the expanding plasma plume was directed into a 1-meter fused silica optical fiber using a collimating beam probe. A 1/4 meter spectrograph fitted with a cooled intensified array camera generated the spectra for subsequent analysis. For low resolution survey spectra, a 147 groove/mm grating blazed at 300 nm was used while a 1200 groove/mm grating blazed at 300 nm provided sufficient spectral resolution for detailed analysis of the atomic and ionic emission.

Results from previous LIBS investigations exploring the effects of focussing. laser excitation wavelength and laser repetition rate were used to select the conditions used here. Extensive testing of LIBs detection in different buffer gases and pressures confirmed results of prior LIBS investigations [12-16] and led to the choice of 75 Torr Ar.

Results

A. Substrate characterization

Figure 1 shows low resolution LIBS spectra from an undoped carbon disk. With the exception of the carbon atomic emission lines at 193.3 and 247.8 corresponding to C atom transitions from the $^1P_0$ level to the ^{1}D and ^{1}S levels respectively, the ultraviolet region is free of substrate spectral emissions.

B. Analyte spectral transition selection and identification

Table 1 lists the spectral transitions associated with LIBS in this study for all 15 metals tested under higher resolution. In some cases, such as for Hg, multiple spectral regions were investigated. at higher resolution. The spectral transitions chosen for analysis possess a strong oscillator strength, a moderately low excited-state energy level, and a minimal of overlap with spectral emissions from other elements. Figure 2 illustrates some representative spectra for selected elements.

C. Linearity and limits of detection

To assess the analytical capability of our technique, we explored the linearity with analyte concentration and determined limits of detection. Analytical working curves were developed over a range of concentrations for As, Cd, Hg, Pb and Cr. Figure 3 shows the results for As, Cr and Pb. Identical results were obtained using either the peak or spectrally-integrated intensities of elemental emissions.

Given limited success with developing analytical working curves, an empirical approach was undertaken to determine limits of detection (LOD). In our approach, the LOD was assigned to the concentration that resulted in recognizable elemental emission (S/N > 3) in greater than 75% of the spectra of a series of single laser pulse LIBS spectra. Table 1 also lists the detection limits of the elements determined in this manner.

Although the limit of detection is revealing, it does not convey the minute aliquots that could be analyzed by the technique in screening for trace elements. The laser pulse, with a spot size of 0.075 cm, samples 0.13% of the analyte in the 1.0 ml liquid volume initially deposited. This calculation assumes that the deposited liquid uniformly covers an area 3.5 cm^2 and that the evaporation resulted in uniform deposition over the carbon planchet. The liquid was not deposited to the edge of the planchet to avoid loss of material by runoff. For an initial liquid concentration of 0.1 ppm, this corresponds to 130 pg of trace metal sampled. For iron, this corresponds to approximately 2 picomoles of material. This calculated amount is competitive with those routinely reported using laser-induced fluorescence and graphite furnace atomic absorption spectroscopy. Another unique feature of the technique is the small volumes required. Taking the volume of the liquid cylinder with base equal to the laser spot size and height equal to the initially deposited liquid height, a single laser pulse samples a volume of 1.3 microliters. This calculated value is competitive with those routinely reported using laser-induced fluorescence and graphite furnace atomic absorption spectroscopy. Clearly, LIBS applied using our approach has potential for trace-element detection.

References

1. D. A. Cremers, L. J. Radziemski and T. R. Loree, Appl. Spectrosc. **38**:721 (1984).
2. J. R. Wachter and D. A. Cremers, Appl. Spectrosc. **41**:1042 (1987).
3. R. Knoop, F. J. Scherbaum and J. O. Kim, Fresenius J. Anal. Chem. **355**:16 (1996).
4. G. Arca, A. Ciucci, V. Palleschi, S. Rastelli and E. Tognoni, Appl. Spectrosc. **51**:1102 (1997).
5. L. M. Berman and P. J. Wolf, Appl. Spectrosc. **52**:438 (1998).
6. W. F. Ho, C. W. Ng and N. H. Cheung, Appl. Spectrosc. **51**:87 (1997).
7. A. V. Buntenin and B. Ya. Kogan, Kvantovaya Elektron. **1**:143 (1971). [Sov. J. Quantum Electron. **1**:561 (1972).
8. D. Yu. Tsipenyuk, D. V. Vlasov, A. M. Prokhorov and P. I. Ivashkin, Laser Physics **3**:910 (1993).
9. H. A. Archontaki and S. R. Crouch, Appl. Spectrosc. **42**:741 (1988).
10. K. C. Ng, N. L. Ayala, J. B. Simeonsson and J. D. Winefordner, Analytica Chim. Acta **269**:123 (1992).
11. D. E. Poulain, and D. R. Alexander, Appl. Spectrosc. **49**:569 (1995).
12. D. A. Rusak, B. C. Castle, B. W. Smith and J. D. Winefordner, Crit. Rev. Anal. Chem. **27**:257 (1997).
13. V. Majidi and M. R. Joseph, Crit. Rev. Anal. Chem. **23**:143 (1992).
14. Y. Iida, Appl. Spectrosc. **43**:229 (1989).
15. X. L. Mao, M. A. Shannon, A. J. Fernandez and R. E. Russo, Appl. Spectrosc. **49**:1054 (1995).
16. Y.-I. Lee, K. Song, H-K. Cha, J.-M. Lee, M.-C. Park, G.-H. Lee and J. Sneddon, Appl. Spectrosc. **51**:959 (1997).
17. R. Wisbrun, I. Schechter, R. Niessner, H. Schroder and K. L. Kompa, Anal. Chem. **66**:2964 (1994).
18. K. Y. Yamamoto, D. A. Cremers, M. J. Ferris and L. E. Foster, Appl. Spectrosc. **50**:222 (1996).

Improved Laser-Induced-Breakdown analysis of Environmental Samples by Plasma Imaging

Israel Schechter, Valery Bulatov, Liang Xu, Vladimir V. Gridin, Rievie Krasniker

Department of Chemistry, Technion - Israel Institute of Technology, Haifa 32000, Israel
Tel/Fax: +972-4-8292579, E-mail: israel@tx.technion.ac.il

Abstract: The introduction of spatial resolution to laser induced breakdown spectroscopy results in improved environmental analysis, such as aerosols and soils. Spatial resolution was introduced either as 2D chemical vision or as 1D information that maintains high quality spectral data. The additional information was used for matrix effect compensation and for exchanging the temporal gating by spatial resolution. A new data acquisition scheme, which overcomes known signal variations, was also suggested.

OCIS codes: (040.0040) Detectors, (120.0120) Instrumentation, measurement, and metrology, (000.1570) Chemistry, (000.2170) Equipment and techniques, (010.1110) Aerosols, (010.1120) Air pollution monitoring, (280.3420) Laser sensors, (170.0110) Imaging systems, (300.6500) Spectroscopy, time-resolved, (300.6210) Spectroscopy, atomic, (330.6130) Spatial resolution, (350.5400) Plasmas

1. Introduction

Imaging spectroscopy provides a new powerful tool for chemical imaging. It combines the analytical power of traditional spectroscopy with two-dimensional (2D) visualization. In this method one obtains a 2D image of an object with full spectrum at each of its pixels, providing information on chemical composition with spatial resolution. Our study was focused on the potential of chemical imaging in improving the analytical performance of the Laser Induced Breakdown Spectroscopy (LIBS) method.

Laser plasma imaging has been recognized as a powerful research tool. In most cases imaging has been achieved by fast framing photography, by steak cameras and by ICCD detectors. It has been applied for numerous basic studies of laser ablation processes, such as time-resolved spatial distribution [1]. These studies, however, were not both spectrally and spatially resolved simultaneously. In another study, full laser plume spectra have been obtained as a function of the distance from the ablated surface, by an optical setup that has focused a slice of the plume image into the spectrometer. The main observation obtained with this setup has been that as the distance from the surface is increased, the continuum fluorescence intensities of the emission spectra decrease with an increase in the relative intensities of the discrete lines which prominently merge. The main conclusion of that study has been that the plasma plume is highly non-homogeneous in its composition and temperature as a function of distance from the surface. This conclusion suggests that a 2D imaging with full spectral resolution at each pixel, is of considerable importance.

Concerning environmental monitoring, LIBS has several advantages over other traditional methods. The most important is the capability to perform direct solid analysis, without the need of chemical preparations. It can provide simultaneous analysis of many elements, and only optical access to the analyzed material is required. Actually, this method is especially suitable for environmental monitoring. In spite of the above advantages, the LIBS method has not reached yet the best sensitivity required in the most demanding environmental analyses. The current detection limits are in the range of 10 ppm (based on 95% confidence intervals) or 1 ppm (based on 3σ). The reason for this relatively poor performance is related to plasma instability, which depends on nonlinear ablation processes.

The instability of the plasma is an intrinsic property of the LIBS method, however, we can partially compensate for it, by a proper characterization of the plasma. For this purpose, and in order to optimize the optical measurements, we need detailed information of the plasma. Imaging spectroscopy provides this kind of information on the size of the plasma, on its spatial shape and on its temperature. These properties are closely related to matrix effects and to the actual ablation process. Moreover, imaging spectroscopy may provide information on the internal distribution of the elements within the plasma. Probably, each element or spectral line should be monitored at a preferred location in the plasma.

We have carried out such measurements and demonstrated the powerful information that is gained from chemical imaging of laser induced plasmas. We report the development and application of three imaging techniques in laser plasma analysis and a new data evaluation scheme:

1. Spectroscopic imaging of laser induced plasma by Fourier transform method.
2. Compensation for matrix effects in LIBS analysis by combined spatial and temporal resolutions.
3. Converting Spatial to Temporal Resolution in LIBS Analysis by Simultaneous Multifiber Spectroscopy.
4. New data acquisition scheme for absolute analysis by LIBS.

The above studied are briefly discussed in the following:

2. Spectroscopic imaging of laser induced plasma by Fourier transform method.

We present chemical imaging of laser produced plasmas (obtained by 2D full spectroscopy). An example is shown in Fig. 1. This powerful tool was proven to provide detailed information that can be used for experimental setup optimization and for improvement of analytical performance. Plasma imaging provided insight to effects of several factors that affect LIBS performance, such as the focusing conditions. Similarity and classification maps proved for the first time that each element is mainly present at a different location in the laser-induced plasma [2]. We also found the optimum location in the plasma that provides the best spectral signal to noise ratio.

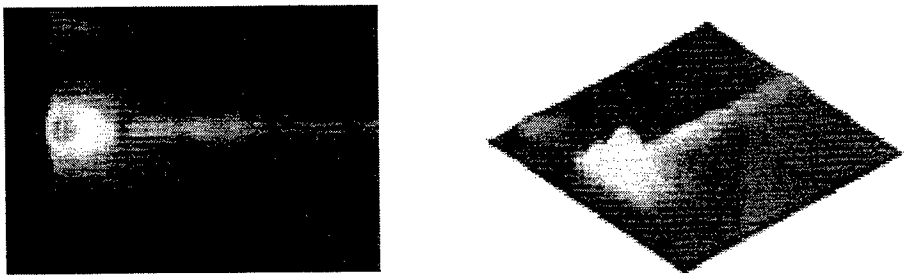

Fig.1 Chemical imaging of laser induced plasma (left) and its 3D representation (right).

3. Compensation for matrix effects in LIBS analysis by combined spatial and temporal resolutions.

A method for multipoint LIBS analysis with temporal resolution is suggested and applied for investigation of several matrix effects. It was found that the combination of spatial and temporal resolution is of considerable contribution to LIBS analysis [3]. We show that in this way the spectral signals can be optimized for better results. The proposed experimental setup was designed for simultaneous elemental analysis, since each element has its characteristic optimum conditions for data acquisition. Actually, this fiber optic setup is simpler than other devices that provide spatial resolution, and has no intrinsic limitations of the spectral resolution. Thus, this instrument, which combines spectral temporal and spatial resolutions, is advantageous for standard LIBS analysis.

The well-know matrix effect of sand/soil mixtures was investigated in terms of the spatial and temporal plasma profiles, as shown in Fig.2. It was found that the best sensitivity to trace elements (such as Pb) is obtained at a certain distance from the surface, and observation of the plasma at this distance is better than the integrated results [4]. The major matrix constituents were analyzed, regarding their spatial distribution within the plasma and examined as candidates for internal references. The signals from Si showed a different behavior than other matrix constituents, indicating that this element is not properly represented in the plasma. It should be emphasized that as far as the signal-to-background is considered, the matrix effects are mainly observed for the minor components.

Temperature maps as a function of time and matrix composition were calculated and shown to provide interesting information on plasma dynamics. Analysis of Pb calibration plots as a function of distance from surface revealed the existence of a plasma location of optimum sensitivity for this element. On the other hand, at a given analyte concentration, the optimum signals linearly change as a function of the distance from the surface. Finally, it was found that a clear measurement-optimum exists in time and space coordinates, supporting the need of these resolutions in LIBS analysis.

4. Converting Spatial to Temporal Resolution in LIBS Analysis by Simultaneous Multifiber Spectroscopy.
Traditional LIBS analysis requires time-gated detectors, in order to avoid the initial signal from the hot plasma. These detectors are expensive and often need to be cooled down and protected against vapor condensation. We suggest a low-cost setup that may replace these gated detectors, while maintaining acceptable analytical performance. The proposed setup is a result of investigation of plasma-front propagation in LIBS analysis. It is known that the plasma propagation is similar to the shock wave propagation after a strong explosion in the atmosphere. We found that the propagation of the plasma fits well the Sedov blast wave theory, providing a good agreement between the theoretical and experimental figures. A proper observation geometry, which is perpendicular to the plasma expansion vector, enables converting spatial to temporal resolution. We take advantage of the fact that the plasma reaches a given distance above the analyzed surface at a certain time delay. Therefore, a single optical fiber, positioned at a well-defined geometry, can provide spectral information corresponding to a certain time-delay. A multifiber imaging spectrometer provides information corresponding to a series of delay times, which is adequate for analysis of a variety of matrixes. It was found that the performance of the nongated detector is similar to that of a gated one.

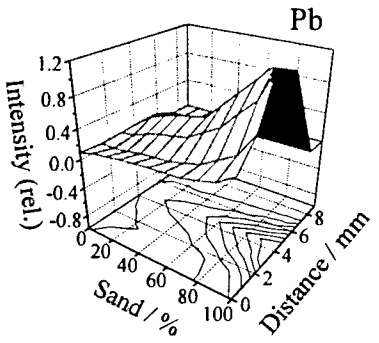

Fig. 2: Correlation between matrix effect and spatial resolution

5. New data acquisition scheme for absolute analysis by LIBS.

A method for compensating for shot to shot variations in LIBS analysis was established and evaluated. This method was based on the observation that a part of the average background undergoes the same pattern of variations as the spectral signals [5]. A model was developed, where the variations were assumed to be of multiplicative nature. This model leaded to the conclusion that a plot of the slope of the peak intensity - baseline (for a sequence of shots), against concentration, should be linear and thereof utilized for calibration purposes. The model was found to be valid for LIBS spectra.

The calibration plots obtained in this method are shown to be better than the traditional plots. Actually, LOD values obtained by this method are improved by an order of magnitude. Moreover, the proposed method provided *absolute* concentrations, while traditional LIBS provided relative values. The method did not require an internal standard element of known concentration, however, standard samples were still needed for obtaining calibration curves.

This method is especially valuable for particulate analysis, where signal fluctuations are severe. The most difficult case in this sense is aerosol analysis, where additional effects are introduced by the instability of the plasma location.

6. References

1. I. Schechter, "Laser Induced Plasma Spectroscopy. A Review of Recent Advances", *Rev. Anal. Chem.*, **16**, 173-298, (1997)
2. V. Bulatov L. Xu and I. Schechter, "Spectroscopic Imaging of Laser Induced Plasma", *Anal. Chem.*, **68**, 2966-2973, (1996).
3. V. Bulatov and I. Schechter, "A New Multifiber Spectrometer for Spatially and Time Resolved Laser Induced Breakdown Analysis", *Internet J. Chem.*, **1**, 8 (1998).
4. V. Bulatov, R. Krasniker and I. Schechter, "Study of Matrix Effects in Laser Plasma Spectroscopy by Combined Multifiber Spatial and Temporal Resolutions", *Anal. Chem.*, **70**, 5302-5311, (1998).
5. L. Xu, V. Bulatov, V.V. Gridin and I. Schechter, "Absolute Analysis of Particulate Materials by Laser Induced Breakdown Spectroscopy", *Anal. Chem.*, **69**, 2103-2108, (1997).

Laser Analysis and Cleaning of Nineteenth Century Daguerreotypes

Valerie V. Golovlev and John C. Miller*#, Life Sciences Division, Oak Ridge National Laboratory, P. O. Box 2008, Oak Ridge, TN 37831-6125

Grant Romer, International Museum of Photography and Film, George Eastman House, 900 East Ave., Rochester, NY 14607-2298

Paul Messier, Boston Art Conservation, 60 Oak Square Ave., Boston, MA 02135

Author for Correspondence: John C. Miller (423) 574-6239 – Tel.; (423) 576-4407 – Fax; jjm@ornl.gov

Summary

Laser desorption/ablation describes a process whereby an intense, pulsed laser beam interacts with a solid surface leading to the ejection of atoms, molecules, ions, clusters and macroscopic particles.[1,2] Electromagnetic energy is converted to electronic, thermal, chemical and mechanical energy. The process is extremely complex since different mechanisms operate at different values of laser wavelength, pulse duration and intensity. In general, the term laser desorption is used when particle emission occurs with no visible microscopic alteration of the surface composition or structure. In contrast, laser ablation is a much more energetic phenomenon accompanied by high temperatures, gas dynamic effects, plasma formation and surface cratering. In practice, these two processes are not completely distinct, but reflect a continuum of physical effects indexed to the laser power density and various material properties.

Shortly after the birth of the laser in 1960, a novel application was demonstrated by A. L. Shawlow, one of the pioneers of the early history of laser invention and development.[3] He showed that typewriter print could be selectively removed from paper by laser ablation. This "laser eraser" was based on the selective absorption of the laser energy by the black ink rather than the less-absorbing paper substrate. Although a somewhat whimsical demonstration at the time, the same principles have been applied to the use of laser ablation cleaning of a variety of substances. Of relevance to the present experiments, laser ablation cleaning has been applied to the restoration of various objects of artistic or historic value.[4,5] Although most well-developed for the cleaning of stone or

marble statues or building facades, laser ablation cleaning of such disparate art media as paintings, frescoes, parchment, leather, wood and stained glass has been demonstrated.[4-8]

Because of the fragile and unique nature of such national treasures, as well as their cultural and monetary value, extensive characterization of the object is prudent in order to guide the cleaning and restoration process.[9-14] Furthermore, laser ablation efficiency is strongly dependent on the composition and the optical and thermal properties of the material under study. Finally, in situ monitoring of the extent of the photoablation can be an important adjunct to effective restoration.[10-12]

In the present study, we have employed laser ablation mass spectroscopy in order to characterize the nature of pristine and degraded daguerreotypes in preparation for attempts at restoration by desorption/ablation of the surface contaminants. We have also demonstrated the use of daguerreotypes as a substrate for surface-enhanced Raman spectroscopy (SERS). Finally we have demonstrated the feasibility of laser ablation cleaning of daguerreotypes. Several successful examples of such cleaning will be shown and discussed.

Daguerreotypes were the first form of photographs and were popular between 1840 and 1860, after which they were superseded by more modern techniques. The daguerreotype image is composed of silver/mercury microcrystals of varying size and density on a silver-coated copper substrate. Nineteenth century daguerreotypes, over the intervening 140 years, have suffered degradation and oxidation, which has greatly reduced their historic and artistic value. More details of the present study may be found in a recent paper.[15] Related studies of image manipulation and optical properties of daguerreotypes[16] as well as the results of the laser cleaning[17] will be published elsewhere. Very recently, an independent study of laser cleaning of daguerreotypes has appeared in the conservation literature.[18]

REFERENCES

1. J. C. Miller, Ed., *Laser Ablation: Principles and Applications,* Springer Series in Material Science, Vol. 28 (Springer-Verlag, Berlin, 1994).

2. J. C. Miller and R. F. Haglund, Jr., Eds., *Laser Ablation and Desorption*, Experimental Methods in The Physical Sciences, Vol. 30 (Academic Press, New York, 1998).

3. A. L. Schawlow, Science, **149**,13 (1965).

4. J. F. Asmus, IEEE Circuits and Devices magazine, **2**, 6 (1986).

5. C. Fotakis, Opt. Photon. News, **6**, 30 (1995).

6. I. Gobernado-Mitre, J. Medina, B. Calvo, A. C. Prieto. L. A. Leal, B. Pérez, F. Marcos and A. M. Frutos, Appl. Surf. Sci. **96**, 474 (1996).

7. S. Georgiou, V. Zafiropulos, D. Anglos, C. Balas, V. Tornari, and C. Fotakis, Appl. Surf. Sci. **127**, 738 (1998).

8. W. Kautek, S. Pentzien, P. Rudolph, J. Krüger, and E. König, Appl. Surf. Sci. **127**, 746 (1998).

9. D. Anglos, M. Solomidou, I. Zergioti, V. Zafiropulos, T. G. Papazoglou, and C. Fotakis, Appl. Spectrosc. **50**, 1331 (1996).

10. P. V. Maravelaki, V. Zafiropolus, V. Kilikoglou, M. Kalaitzaki, and C. Fotakis, Spectrochem. Acta. **B 52**, 41 (1997).

11. D. Anglos, S. Couris, and C. Fotakis, Appl. Spectrosc. **51**, 1025 (1997).

12. I. Gobernado-Mitre, A. C. Prieto, V. Zafiropolus, Y. Spetsidou, and C. Fotakis, Appl. Spectrosc. **51**, 1125 (1997).

13. I. Borgia, R. Fantoni, C. Flamini, T. M. Di Palma, A. G. Guidoni, and A. Mele, Appl. Surf. Sci. **127**, 95 (1998).

14. P. Bocchini and P. Traldi, J. Mass. Spectrom. **33**, 1053 (1998).

15. D. L. Hogan, V. V. Golovlev, M. J. Gresalfi, J. A. Chaney, C. S. Feigerle, John C. Miller, G. Romer, and P. Messier, Appl. Spectrosc. **53**, 1161 (1999).

16. D. L. Hogan, V. V. Golovlev, and J. C. Miller, Submitted for publication (1999).

17. V. V. Golovlev, M. J. Gresalfi, John C. Miller, G. Romer, and P. Messier, J. Cultural Heritage, In Press (2000).

18. I. Turovets, M. Maggen, and A. Lewis, Studies In Conservation **43**, 89 (1998).

Key to Authors and Presiders

Abbud-Madrid, Angel ■ SaC10
Aldén, M. ■ SaC12
Allen, Mark G. ■ SaA, SaA4, SaB3
Allendorf, S.W. ■ SuA4, SuC3
Allerman, A.A. ■ FA2
Ambrose, William P. ■ FB
Amen, Jim L. ■ FA4
Anders, J. ■ SaC1
Aniolek, K. ■ FC4
Armstrong, Karla ■ FC4, SuC3
Arnold, D.W. ■ FA2
Asbill, R.E. ■ FA2

Baer, Douglas S. ■ SuA, SuA5
Bailey, C.G. ■ FA2
Baillargeon, James N. ■ SaA1, SaA2, SaA3, SaA4, SaA5, SaB2, SaB3
Bamford, Douglas J. ■ FC3
Barnes, M.D. ■ SaC8
Berger, S. ■ FB2
Berkoff, T.A. ■ SuA2
Bessler, Wolfgang ■ SuB4
Bewley, W.W. ■ FC1
Bisson, Scott E. ■ FC4
Black, John D. ■ SuB3
Blanke, Torsten ■ SaC6
Bolter, A. ■ SaC7
Bomse, David S. ■ SuC2
Bradshaw, J.L. ■ FC2
Branch, Melvyn C. ■ SaC10
Brockhinke, A. ■ SaC7
Bruno, J.D. ■ FC2
Bulatov, Valery ■ SuD2, SuD4
Bülter, A. ■ SaC7
Burde, Stefan ■ FB1
Buschmann, V. ■ FA3, FB3

Cai, Hong ■ FB1
Capasso, Federico ■ SaA1, SaA2, SaA3, SaA4, SaA5, SaB2, SaB3
Carter, T.R. ■ FA2
Chang, Joon-Sung ■ SaC5
Chao, I-Na ■ SaB6
Cho, Alfred Y. ■ SaA1, SaA2, SaA3, SaA4, SaA5, SaB2, SaB3
Coggiola, Michael J. ■ SaC3
Cohen, Ronald C. ■ SuD1
Connolly, J.C. ■ FC1
Cook, Robert L. ■ SuC5
Crosley, David R. ■ SaC3, SuB1
Curl, R.F. ■ SaA2

Daily, John W. ■ SaC10
Danehy, Paul M. ■ SaC5
Davis, Lloyd M. ■ FA4
Di Teodoro, Fabio ■ FD4
Draney, Dan L. ■ FA4
Dreyer, Christopher B. ■ SaC10

Ebert, V. ■ SaB4, SaC9
Eggeling, C. ■ FB2

Faris, Gregory W. ■ SaC3
Farrow, Roger L. ■ FD4
Felix, C.L. ■ FC1
Fernholz, T. ■ SaB4, SaC9
Fielding, J. ■ SuB5
Fisher, Michal ■ SuD2

Garbuzov, D.Z. ■ FC1
Giesemann, C. ■ SaC9
Gittins, C.M. ■ SaB3
Gmachl, Claire ■ SaA1, SaA2, SaA3, SaA4, SaA5, SaB2, SaB3
Göbel, F. ■ FB4
Goers, Uta-Barbara ■ FC4, SuC3
Goldmeer, Jeffrey S. ■ SuA3
Golovlev, Valerie V. ■ SuD5
Gomer, Grant ■ SuD5
Gridin, Vladimir V. ■ SuD2, SuD4
Grigorian, Vartan ■ SuB3

Hahn, Jae Won ■ FD1, SaC5
Hall, John L. ■ SaA5
Han, K.-T. ■ FB4
Hanson, R.K. ■ SuA5
Hartman, John S. ■ SaA3, SaA5, SaB2
Hasson, Salah ■ SuD2
Herten, D.-P. ■ FA3
Hildebrandt, L. ■ SaC4
Hildenbrand, Frank ■ SuB4
Hovde, Chris ■ SaC2
Hubbard, G.L. ■ SuA4
Hübner, T. ■ FB3
Hutchinson, Albert L. ■ SaA1, SaA2, SaA4, SaB3

Inoue, Takanori ■ SuD2

Jang, Ping-Rey ■ SaC11
Jeffries, Jay B. ■ SuB1, SuC
Jett, James H. ■ FB1
Jiao, Hong ■ FD2, FD3

Kadosh, Michal ■ SuD2
Kalem, S. ■ SaC13
Kaminski, C. ■ SaC12
Kane, Daniel J. ■ SuA3
Keller, Richard A. ■ FB1
Kelly, James F. ■ SaA3, SaA5, SaB2
Kemme, S.A. ■ FA2
Kim, Jae Wan ■ FD1
Kim, S. ■ SuA5
Klein-Douwel, Robert J.H. ■ SuB1
Knemeyer, J.-P. ■ FA3
Knispel, R. ■ SaC4
Koch, Joachim ■ SuC1
Köhler, Rüdeger ■ SaA1
Korol, Alona ■ SuD2
Kosterev, A.A. ■ SaA2
Krasniker, Rievie ■ SuD4
Kulp, Thomas J ■ FC4, SuC3

Larson, Erica J. ■ FB1
Lee, H. ■ FC1
Lee, Jai-Hyung ■ SaC5
Litani-Barzilai, Iris ■ SuD2
Long, M.B. ■ SuB5
Lucht, Robert P. ■ FD4
Ludowise, P.D. ■ SuA4, SuC3
Luque, Jorge ■ SuB1

Maiorov, M. ■ FC1
Marinelli, W.J. ■ SaB3
Marrone, Babetta L. ■ FB1
Martinelli, R.U. ■ FC1
Matzke, C.M. ■ FA2
McCann, Patrick J. ■ SaB6
McLaren, Ian A. ■ SaB5
McNesby, Kevin L. ■ SaB5
Mechold, L. ■ SaC1
Menna, R.J. ■ FC1
Messier, Paul ■ SuD5
Meyer, J.R. ■ FC1
Miake-Lye, R.C. ■ SuA2
Middendorf, Lyle R. ■ FA4
Miller, John C. ■ SuD5
Miller, M. ■ SaA4
Miller, Tracy S. ■ SaC11
Miziolek, Andrzej W. ■ SaB5
Monts, David L. ■ SaC11

Namjou, Khosrow ■ SaB6
Nelson, D. ■ SaC1
Neuweiler, H. ■ FB3
Niemax, Kay ■ SuC1, SuD

O'Keefe, Anthony ■ FD2, FD3
Oh, Daniel B. ■ SuA1
Olafsen, L.J. ■ FC1
Olsen, G.H. ■ FC1
Oser, Harald ■ SaC3
Ottesen, D.K. ■ SuA4, SuC3

Patterson, Thomas ■ FC3
Paul, Joshua B. ■ FD2, FD3
Penttila, Janetta R. ■ FB1
Peterson, Kristen A. ■ SuA1
Peterson, Rex A. ■ FA4
Petrov, Konstantin P. ■ FC3
Pham, J.T. ■ FC2
Pilgrim, Jeffrey S. ■ SuC2
Pitz, H. ■ SaB4, SaC9
Powers, Peter ■ FC4
Puri, Ishwar K. ■ SuC4

Rahmann, U. ■ SaC7
Rakestraw, David J. ■ FA
Ramsey, J. Michael ■ FA1, SaC8
Reichardt, Thomas A. ■ FD4
Richman, Bruce ■ FC4
Robinson, J.S. ■ SuC3
Romer, Grant ■ SuD5
Röpcke, J. ■ SaC1
Roth, Arti Prasad ■ FC3
Ryu, Jae-Seok ■ SaC5

Sacher, J. ■ SaC4
Sakurai, Teruhiro ■ SuB2
Samora, S. ■ FA2
Santangelo, P.J. ■ SuA4
Sauer, Markus ■ FA3, FB, FB3, FB4
Schade, Wolfgang ■ SaC6
Schael, F. ■ SaC4
Schaffer, J. ■ FB2

Schechter, Israel ■ SuD2, SuD4
Scherer, James J. ■ FD2, FD3
Schnürer-Patschan, Christoph ■ SuC1
Schulz, A. ■ FB3
Schulz, Christof ■ SuB4
Schweinberger, E. ■ FB2
Seidel, C.A.M. ■ FB2
Shaddix, C.R. ■ SuA4
Sharpe, Steven W. ■ SaA3, SaA5, SaB2
Shaw, R.W. ■ FD, SaC8
Shorter, J.H. ■ FC5
Sick, Volker ■ SuB
Silver, Joel A. ■ SuC2
Singh, Jagdish Prasad ■ SuC5, SaC11
Sivco, Deborah L. ■ SaA1, SaA2, SaA3, SaA4, SaA5, SaB2, SaB3
Sluzny, Chanan ■ SuD2
Smith, Gregory P. ■ SuB1
Sonnenfroh, D. ■ SaA4
Stanton, Alan C. ■ SaB
Stewart, Timothy L. ■ SaB2
Stokes, D.W. ■ FC1
Sugg, A.R. ■ FC1
Sweatt, W.C. ■ FA2

Tai, Hideo ■ SuB2
Tamura, Masayuki ■ SuB2
Taubman, Matthew S. ■ SaA5
Ticich, Thomas M. ■ SuD3
Tinnefeld, P. ■ FA3
Tittel, F.K. ■ SaA2
Tredicucci, Alessandro ■ SaA1

Usachev, Alexandre D. ■ SaC11

Vander Wal, Randall L. ■ SuD3
Volkmer, A. ■ FB2
Vurgaftman, I. ■ FC1

Walewski, J. ■ SaC12
Wang, L.J. ■ SaC8
Warren, M.E. ■ FA2
Webber, M.E. ■ SuA5
Wendt, J.R. ■ FA2
Werle, Peter W. ■ FC, SaB1
West Jr., Joseph R. ■ SuD3
Wetjen, Eric T. ■ SaA4, SaB3
Whittaker, Edward A. ■ SaA3
Whitten, W.B. ■ SaC8
Widengren, J. ■ FB2
Wienhold, F.G. ■ SaC1
Willer, Ulrike ■ SaC6
Williams, Richard M. ■ SaA3, SaA5, SaB2
Wolfrum, J. ■ FB3
Wormhoudt, J. ■ SuA2, FC5, SaC1
Wortman, D.E. ■ FC2

Xiao, Xudong ■ SuC4
Xu, Liang ■ SuD4

Yang, M.J. ■ FC1
Yang, R.Q. ■ FC2
Yavuzcetin, O. ■ SaC13
Yu, Dai-Hyuk ■ SaC5
Yueh, Fang-Yu ■ SaC11, SuC5

Zahniser, M. ■ SaC1
Zander, C. ■ FB4
Zayhowski, J.J. ■ FC5
Zhang, Hansheng ■ SuC5
Zybin, Alexandr ■ SuC1

Laser Applications to Chemical and Environmental Analysis Topical Meeting 2000

Postdeadline Papers

February 11, 2000 - February 14, 2000

Eldorado Hotel
Santa Fe, New Mexico

PD1 ■ A Fourier analysis approach to wavelength modulation diode laser abosrption spectrometry, Pawel Kluczynski, Asa M. Lindberg, Ove Axner, *Umeå Univ., Sweden.* A new theoretical formalism based on Fourier analysis for wavelength-modulated spectrometry, capable of handling both analytical and background signals under a variety of experimental situations, is presented. **(p. 189)**

PD2 ■ Collisional quenching of CO $B\,^1\Sigma^+$ (v' = 0) probed by two-photon laser-induced fluorescence with a picosecond laser, F. DiTeodoro, J.E. Rehm, R.L. Farrow, *Sandia Natl. Labs, USA.* Quenching cross sections for the $B\,^1\Sigma^+$ (v' = 0) state of CO in collisions with molecules present in combustion environments and noble gases were measured using time-resolved, two-photon laser-induced fluorescence with a picosecond laser. **(p. 193)**

PD3 ■ Carbon monoxide absorption spectroscopy using a diode-pumped continuous wave optical parametric oscillator, Angus Henderson, Pam Roper, Roy D. Mead, *Aculight Corp., USA,* James. R. Gord, Gregory J. Fiechtner, George E. Tietz, *Air Force Res. Lab, USA.* A compact mid-infrared diode-pumped optical parametric oscillator has been developed. Single longitudinal mode output tunable over 9GHz is produced with amplitude stability <1%. Use of the device in absorption spectroscopy has been demonstrated in carbon monoxide. **(p. 197)**

PD4 ■ A widely tunable cw Raman laser in H_2 pumped by an external cavity diode laser, L.S. Meng, P.A. Roos, K.S. Repasky, J.L. Carlsten, *Montana State Univ., USA* This paper reports the first ECDL-pumped cw Raman laser having μW level threshold and 40nm tuning range. This tunable source is suited for high-resolution spectroscopy in the NIR spectral region. **(p. 200)**

PD5 ■ Time-resolved optical heterodyne detected Raman-induced Kerr-effect spectroscopy of chemical analysis, Napoleon Thantu, *Idaho Natl. Eng. and Env. Lab., USA* A time-domain nonlinear optical method that may be of significant utility for chemical analysis is described. This technique which relies upon an ultrashort pulsed laser system is simple to implement, and is especially sensitive to weak low-frequency intermolecular modes in transparent liquids. **(p. 203)**

PD6 ■ Demonstration of a 200 cm^{-1} continuous scan in the mid-infrared with a PPLN-based OPG/OPA lightsource, Kenneth W. Aniolek, Thomas J. Kulp,* Serdar Yeralan, Scott E. Bisson, *Sandia Natl. Labs, USA.* Abstract not available. **(p. 206)**

PD7 ■ U.S. Army sponsored activities in LIBS research, applications, and commercialization, Andrzej W. Miziolek, Kevin L. McNesby, Richard T. Wainner, Robert G. Daniel, *US Army Res. Lab.*; Patrick D. French, Frank Sagan, *ADA Technol., Inc., USA*; Russell Harmon, *Army Res. Office, USA.* Laser-induced breakdown spectroscopy (LIBS) is a chemical analytical technique in the early stages of commercialization. The US Army has promoted the development of this technology through the Small Business Innovation Research (SBIR) program. This poster describes recent research activities, specific Army applications, and progress and challenges in the commercialization of LIBS technology. **(p. 209)**

A Fourier Analysis Approach to Wavelength Modulation Diode Laser Absorption Spectrometry

Pawel Kluczynski, Åsa M. Lindberg and Ove Axner
Department of Experimental Physics, Umeå University, SE-901 87 Umeå, Sweden.
(E-mail: pawel.kluczynski@physics.umu.se, asa.lindberg@physics.umu.se,
ove.axner@physics.umu.se)

Abstract

A new theoretical formalism based on Fourier analysis that is capable of handling both analytical and background wavelength modulated signals under a variety of experimental situations has been developed. The new formalism has several appealing features; it is not restricted to small modulation amplitudes, it is capable of correctly predicting the influence of the associated intensity modulation (so called residual amplitude modulation, RAM, signals), it can deal with wavelength dependent transmission effects (e.g. etalon effects), it provides expressions for the analytical and background signals separately, and it elucidates clearly how the associated intensity and wavelength dependent transmission combine with the analyte absorption to form the total *nf*-harmonic signal at the lock-in amplifier output. Experimental verifications of both analytical and background signals are presented.

Introduction

Wavelength-modulation diode laser absorption spectrometry (WM-DLAS) has become a powerful tool for sensitive and selective species detection under a variety of conditions during the last decades. A number of theoretical descriptions of the WM-technique have therefore appeared in the literature throughout the years. However, none of these descriptions has been able to give a proper and understandable description of WM-DLAS signals under the most commonly used conditions. Instead, their applicability has been limited to a few simple situations, e.g. small modulation amplitudes, because of various approximations used. There has therefore for a long time been a need for a new, more complete, description of the WM-DLAS technique. The present work presents such a new theoretical formalism based on Fourier analysis that is capable of handling both analytical and background harmonic signals under a variety of experimental situations (including the optimum and therefore most commonly used conditions).

Theory

In WM-DLAS, the wavelength of the laser light is modulated at a frequency f by its injection current before it is passed through a gaseous sample to be analyzed and detected by an ordinary detector whose signal is fed to a lock-in amplifier. By recognizing that the *nf*-harmonic output of the lock-in amplifier is analogous to the n:th Fourier component of the detector signal, a theoretical description of the WM technique has been constructed [1].

Analytical WM-signal

It was shown in Ref. [1] that the k:th even harmonics of the analytical signal can be written as

$$S_{AS,k}^{even}(\bar{v}_d,\bar{v}_a) = -\beta\frac{\alpha_0}{2}\left[\begin{array}{l}(1+\delta_{k0})\sum_{m=0}^{k}\bar{\chi}_{k-m}^{e}(\bar{v}_d,\bar{v}_a)I_m^e(v_c,v_a)+\\ \frac{1}{1+\delta_{k0}}\sum_{m=0}^{\infty}\bar{\chi}_m^{e}(\bar{v}_d,\bar{v}_a)I_{k+m}^e(v_c,v_a)+\\ \frac{1}{1+\delta_{k0}}\sum_{m=0}^{\infty}\bar{\chi}_{k+m}^{e}(\bar{v}_d,\bar{v}_a)I_m^e(v_c,v_a)\end{array}\right], \qquad [1]$$

where the various $\bar{\chi}_m^e$ and I_m^e are the m:th Fourier components of the analytical lineshape function and detected intensity (in the absence of absorbers), respectively.

As a part of this work, a new general non-complex formula for an arbitrary Fourier component of a modulation broadened Lorentzian absorption line shape function has been derived. It was shown in Ref. [2] that the n:th Fourier components of a Lorentzian function can be written succinctly as

$$L_n(\bar{v}_a,\bar{v}_d) = \frac{A_n}{(\bar{v}_a)^n}\left[B_n + \frac{C_nS_+ + D_nS_-}{\sqrt{2}R}\right], \qquad [2]$$

where $S_\pm = \sqrt{R \pm M}$, $R = \sqrt{M^2 + 4(\bar{v}_d)^2}$, $M = 1+(\bar{v}_a)^2 - (\bar{v}_d)^2$ and where the four parameters, A_n ... D_n, are general functions on the normalized frequency modulation amplitude $\bar{v}_a$ and normalized detuning $\bar{v}_d$ (given explicitly in Ref. 2).

Application of the expressions above has yielded good agreement with experiments. Figure 1a presents a comparison between experimental signals from measurements of the780 nm $5s\ ^2S_{1/2}$ - $5p\ ^2P_{3/2}$ transition of ^{85}Rb and ^{87}Rb in natural abundance in a room temperature glass cell (which consists of 6 hyperfine split transitions in each isotope) and calculated ones. As can be seen, the general agreement is good.

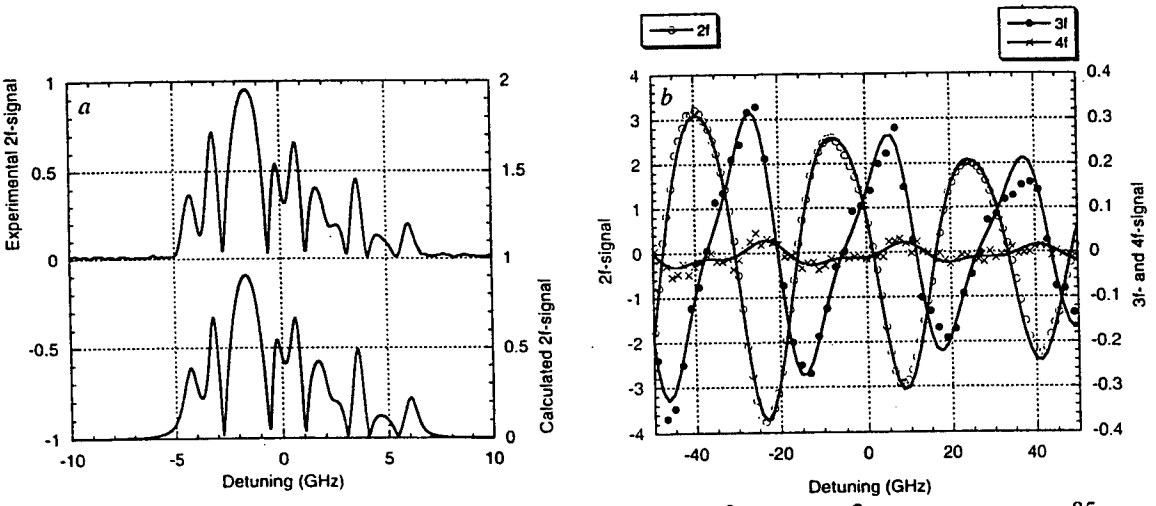

Figure 1a. Experimental signals from measurements on the $5s\ ^2S_{1/2}$ - $5p\ ^2P_{3/2}$ transition of ^{85}Rb and ^{87}Rb at 780 nm (upper panel) in a room temperature cell and calculated ones (lower panel). Figure 1b. Measured background signals (individual markers) and the corresponding theoretical curves, Eq. (4), (solid lines) as a function of laser frequency.

Background WM-signal

A general expression for the *nf*-harmonic of the WM background signal can be written [1,3]

$$S_{BG,k}^{even}(\bar{v}_d,\bar{v}_a) = -\beta\frac{1}{2}\left[\begin{array}{l}(1+\delta_{k0})\sum_{m=0}^{k} T_{k-m}^{e}(\bar{v}_d,\bar{v}_a)I_{L,m}^{e}(v_c,v_a)+\\ \frac{1}{1+\delta_{k0}}\sum_{m=0}^{\infty} T_{m}^{e}(\bar{v}_d,\bar{v}_a)I_{L,k+m}^{e}(v_c,v_a)+\\ \frac{1}{1+\delta_{k0}}\sum_{m=0}^{\infty} T_{k+m}^{e}(\bar{v}_d,\bar{v}_a)I_{L,m}^{e}(v_c,v_a)\end{array}\right], \qquad [3]$$

where T_m^e and $I_{L,m}^e$ are the m:th Fourier components of the transmission function and diode laser intensity, respectively.

The most common sources of background signals are those from the associated intensity modulation and reflection between two optical surfaces in the system. Proper evaluation of the Fourier components of the diode laser intensity and the transmission function of a weak Fabry-Perot etalon and inserting of those in the expression above have shown that a general expression for the n:th harmonics of the WM-background signal can be written as a function of the free-spectral-range-normalized laser center frequency in a rather compact and general form [3]. The expression consists of only three terms: one constant; one proportional to $cos(2\pi\tilde{v}_c^{FSR})$; and one proportional to $cos(4\pi\tilde{v}_c^{FSR})$, according to

$$S_n^{even} = \Gamma_n^e + A_n^e \cos(2\pi\tilde{\nu}_c^{FSR} + \alpha_n^e) + B_n^e \cos(4\pi\tilde{\nu}_c^{FSR} + \beta_n^e). \quad (4)$$

The coefficients Γ_n^e, A_n^e, α_n^e, B_n^e, and β_n^e consist of explicit expressions in terms of quantities such as frequency modulation amplitude, FP-free-spectral range, FP-finesse etc.

Figure 1b shows a comparison between some of the harmonic components of the background signals measured from a weak FP-etalon (individual markers) as a function of detuning of the laser and those predicted by the theory (solid lines). As can be seen from the figure, the agreement is good.

Conclusive Remarks

We have presented a new theoretical description based on Fourier analysis of the WM-spectroscopy technique. With a use of the formalism it is possible to determine both analytical and background harmonic signal strengths in various systems under a variety of experimental conditions. It takes into account various effects, like RAM and wavelength dependent transmission, which couple to analytical signals and give rises to background signals. It also predicts the existence of a non-zero out-of-phase signal component, a fact that could not be verified by "traditional" WM formalisms. Yet another advantage is its linearity, which implies that it can rather easily be generalized to more complex situations (e.g. multi-peak absorption as in Fig. 1a or multi-etalon transmission). The theory also shows clearly that a linear intensity modulation is not sufficient to cause any *2f*-background signals (so called residual amplitude modulation, RAM, signals). *2f*-background signals can only exist in systems with either wavelength-dependent transmission effects or with lasers with a nonlinear intensity modulation. We have shown, both theoretically and experimentally, the advantage of the *4f*-detection with respect to the *2f*-detection when short etalons dominate - *4f*-detection is subject to much smaller background and drifts.

References

1. Kluczynski P, Axner O. *"Theoretical description based on Fourier analysis of wavelength-modulation spectrometry in terms of analytical and background signals"*, Applied Optics 1999;38:5803-5815.

2. Axner O, Kluczynski P, and Lindberg Å.M. *"A general non-complex analytical expression for the n:th Fourier component of a wavelength-modulated Lorentzian lineshape function"*, submitted to Journal of Quantitative Spectroscopy and Radiation Transfer 1999.

3. Kluczynski P, Lindberg Å.M., and Axner O. *"Characterization of background signals in wavelength-modulation spectrometric techniques using Fourier analysis"*, in manuscript.

Collisional quenching of CO $B\ ^1\Sigma^+$ (v' = 0) probed by two-photon laser-induced fluorescence with a picosecond laser

F. Di Teodoro
(fditeod@ca.sandia.gov)
Ph: 925-294-4816

J. E. Rehm
(jerehm@ca.sandia.gov)
Ph: 925-294-1540

R. L. Farrow
(farrow@ca.sandia.gov)
Ph: 925-294-3259

Combustion Research Facility, Sandia National Laboratories, P. O. Box 969, Livermore, CA 94551-0969, Fax: 925-294-2276

Abstract: Quenching cross sections for the $B\ ^1\Sigma^+$ state of CO in collisions with molecules present in combustion environments and noble gases were measured using time-resolved, two-photon laser-induced fluorescence with a picosecond laser.

OCIS Codes: (300.2530) Fluorescence, laser-induced; (300.6500) Spectroscopy, time-resolved; (280.1740) Combustion diagnostics.

Two-photon laser-induced fluorescence (TPLIF) is an effective spectroscopic technique for sensitive and spatially precise detection of species such as CO, which would otherwise require vacuum-ultraviolet excitation and would fluoresce in a wavelength range where most practical environments (such as flames and plasmas) are opaque [1]. The CO molecule is the subject of intense study in combustion diagnostics for its significance as a combustion intermediate [2, 3] and for two-dimensional imaging of turbulent flames [4, 5, 6]. Imaging and other common diagnostic applications, however, demand the accurate determination of species concentrations and mole fractions. Laser-induced fluorescence techniques have a well-known potential for quantitative concentration measurements, but, in most cases, a detailed knowledge of the electronic quenching for the probed excited states is necessary [7, 8]. Quenching cross-sections can be measured in a direct and accurate way by time-resolving the fluorescence signal following short-pulse laser excitation of the species of interest in a controlled environment. In this paper, we report the use of picosecond TPLIF to measure room-temperature quenching cross-sections for the $B\ ^1\Sigma^+$ state of CO in collisions with 12 different species including molecules typically present in combustion environments (H_2O, C_3H_8, CO_2, CH_4, O_2, H_2, and N_2) and most noble gases (He, Ne, Ar, Kr, and Xe). CO and its collision partners were purified using gas-chromatography filters, mixed, and probed in a stainless steel cell pre-evacuated by a turbo-molecular pump. UV light at ~230 nm necessary for the 2-photon excitation of the $B\ ^1\Sigma^+$, v' = 0 state was obtained by frequency-tripling the output of narrow-band filtered ASE dye laser featuring pulses of ~85-ps duration and ~0.8-cm^{-1} bandwidth. Blue-to-green CO fluorescence in the Angström band $B\ ^1\Sigma^+ \rightarrow A\ ^1\Pi$ was spectrally selected using a band-pass color filter, detected with a microchannel plate phototube (response time ~0.2 ns) and recorded on a 1-GHz-band digital oscilloscope. Figure 1 shows a typical fluorescence signal (4 mTorr of CO diluted in about 2 Torr of water vapor) along with the total instrumental function characterizing our recording apparatus.

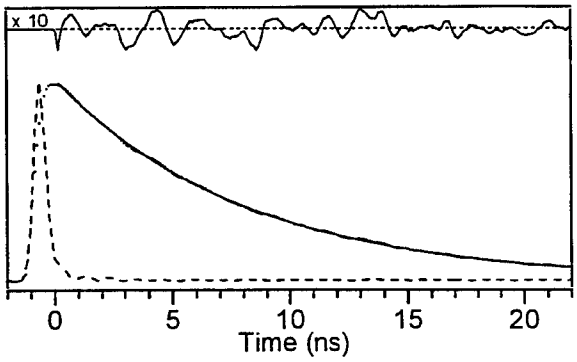

Figure 1. Dots: TPLIF from a CO/H_2O mixture (see text); solid line: single-exponential fit; dashed line: instrumental function (Rayleigh scattering from ~500 Torr of Argon); upper trace: fit residual.

As can be seen in Fig. 1, after an initial ~1-ns time interval corresponding to the temporal response of our instrumentation, the fluorescence signal is very well reproduced by a single-exponential decay function with a lifetime much longer than the laser pulse duration. In this regime, the signal is completely independent of the characteristics of the laser pulse and simply proportional to the population of the excited $B\ ^1\Sigma^+$ state which, in turn, decays with an effective lifetime, τ, given by

$$\tau = \tau_0 + \frac{1}{Q}. \tag{1}$$

Here, τ_0 and Q are the "apparent" radiative lifetime and quenching rate of the $B\ ^1\Sigma^+$ state. While Q is expected to be proportional to the pressure of the collision partner, τ_0 is a function only of the CO partial pressure because of the radiation trapping that affects the $B\ ^1\Sigma^+ \rightarrow X\ ^1\Sigma^+$ fluorescence channel. Figure 2 shows the observed pressure dependence of Q for the various collision partners utilized in our experiment.

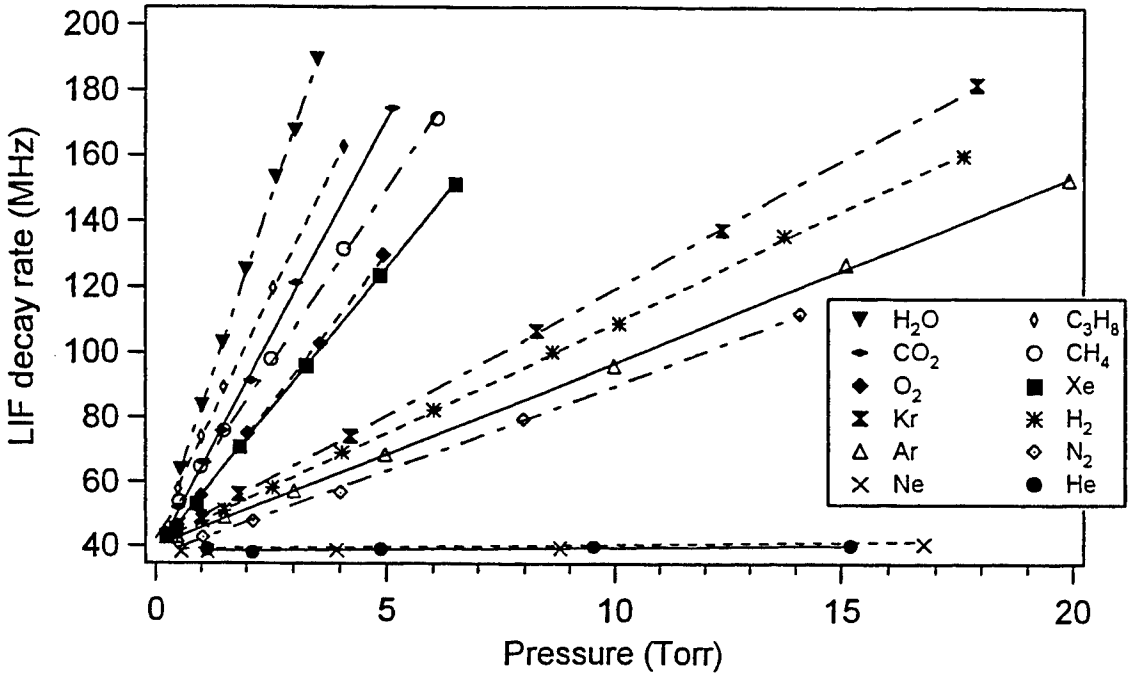

Figure 2. Fluorescence decay rates as a function of the total pressure of the CO-quencher mixture. The lines passing through the data points represent linear fits.

The species-specific values of Q have been directly extracted by fitting the fluorescence signal decays to a single-exponential function keeping constant the partial pressure of CO (and, therefore, τ_0) while varying the total pressure of the CO-buffer gas mixture. The slopes, q, of the Q-vs.-pressure curves were obtained from linear fits and are listed in Table I, along with the corresponding quenching cross-sections, σ, which, in the ideal-gas conditions of our experiment, are given by

$$\sigma = \frac{q}{2}\sqrt{\frac{\pi\mu k_B T}{2}}. \tag{2}$$

Here, μ is the reduced mass of the CO-collision partner system, k_B is the Boltzmann constant, and T is the temperature ($T = 294 \pm 1$ K).

Table I: Quenching rates and corresponding cross-sections for collisions between CO molecules and the investigated quenching species. The maximum relative uncertainty of the q values is $\approx \pm 10\%$.

Quencher	q (s^{-1} $Torr^{-1}$)	σ(Å^2)
Water	4.1×10^7	169
Propane	2.7×10^7	144
Carbon dioxide	2.5×10^7	134
Methane	2.3×10^7	90
Oxygen	1.8×10^7	72
Xenon	1.7×10^7	102
Krypton	7.8×10^6	44
Hydrogen	6.8×10^6	11
Argon	5.6×10^6	28
Nitrogen	5.5×10^6	25
Neon	1.4×10^5	0.6
Helium	1.2×10^5	0.3

The self-collision quenching cross-section and spontaneous-emission lifetime of the $B\ ^1\Sigma^+$ state can be obtained, instead, by modeling the pressure dependence of τ_0. Figure 3 shows the effective lifetime of the fluorescence from pure CO as a function of the CO pressure, P. The curve has been fitted to an analytic model obtained by interpolating the numerical solution of the Holstein equation for radiation trapping, modified to include quenching and branching of the emitted fluorescence [9]. The resulting expression for τ is

$$\tau = \left[\frac{1}{\tau_{rad}} + Q_{CO} - \frac{\beta}{\tau_{rad}} \left(1 - \frac{1}{g_0(k)} \right) \right]^{-1}, \tag{3}$$

where τ_{rad} is the spontaneous-emission lifetime of the $B\ ^1\Sigma^+$ state, $Q_{CO} = q_{CO} \times P$ is the self-collision quenching rate, β is the branching ratio for the $B\ ^1\Sigma^+ \rightarrow X\ ^1\Sigma^+$ fluorescence channel, and g_0 is a known function of the peak CO opacity, k, at the center of the spectral distribution of the trapped fluorescence. In the Doppler limit characterizing our experiment over the entire pressure range of Fig. 3, k is simply proportional to the CO pressure.

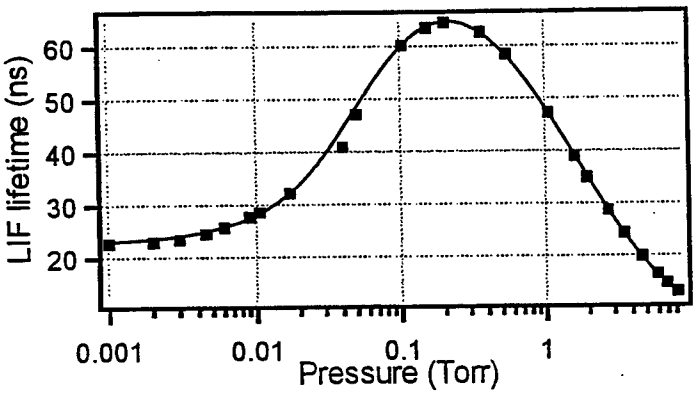

Figure 3. Lifetime of the fluorescence emitted by pure CO as a function of the CO pressure. Solid line: fit obtained by using Eq. (3).

From the fit, the following values were obtained (the uncertainties are indicated in parentheses): τ_{rad} = 22.3(0.8) ns, q_{CO} = 8.1(0.5)×10^6 s^{-1} $Torr^{-1}$, and β = 0.7(0.1). From the values of the branching ratio and spontaneous emission lifetime, we can also derive the Einstein coefficients for the $B\ ^1\Sigma^+ \rightarrow X\ ^1\Sigma^+$ and $B\ ^1\Sigma^+ \rightarrow A\ ^1\Pi$ fluorescence channels, namely $A_{B\rightarrow X} = \beta/\tau_{rad}$ = 3.2(0.5) ×10^7 s^{-1} and $A_{B\rightarrow A}$ = (1-β) /τ_{rad} = 1.3(0.2) × 10^7 s^{-1}.

In conclusion, we used picosecond time-resolved TPLIF to obtain quenching cross-sections for the $B^1\Sigma^+$ state of CO in collisions with several molecules and noble gases. By performing the measurements in the controlled environment of a pre-evacuated cell rather than in flames, errors that may arise from the presence of unknown contaminants in the burner and fuel lines are minimized. In addition, the experiment was conducted in a low-pressure regime where the fluorescence decay time is much longer than the laser pulse duration, which leads to a simple and direct interpretation of the observed signal. The reported values are of interest for both combustion diagnostic applications and mechanistic studies of collision dynamics.

Acknowledgements

This work was supported by the U.S. Department of Energy, Office of Basic Energy Sciences, Chemical Sciences Division.

References

1. K. Kohse-Höinghaus, "Laser techniques for the quantitative detection of reactive intermediates in combustion systems", Prog. Energy Combust. Sci., **20**, 203-279 (1994) and references therein.
2. M. Aldén, S. Wallin, and W. Wendt, "Applications of two-photon absorption for detection of CO in combustion gases", Appl. Phys. B **33**, 205-8 (1984).
3. A. V. Mokhov, H. B. Levinsky, C. E. van der Meij, and R. A. A. M. Jacobs, "Analysis of laser-induced fluorescence carbon monoxide measurements in turbulent nonpremixed flames", Appl. Opt. **34**, 7074-82 (1995) and references therein.
4. J. Haumann, J. M. Seitzman, and R. K. Hanson, "Two-photon digital imaging of CO in combustion flows using planar laser-induced fuorescence", Opt. Lett. **11**, 776-8 (1986).
5. J. M. Seitzman, J. Haumann, and R. K. Hanson, "Quantitative two-photon LIF imaging of carbon monoxide in combustion gases", Appl. Opt. **26**, 2892-9 (1987).
6. N. Georgiev and M. Aldén, "Two-dimensional imaging of flame species using two-photon laser-induced fluorescence", Appl. Spectr. **51**, 1229-37 (1997).
7. S. Agrup and M. Aldén, "Measurement of the collision-quenched lifetime of CO molecules in a flame at atmospheric pressure", Chem. Phys. Lett. **189**, 211-6 (1992).
8. S. Agrup and M. Aldén, "Measurement of the collision-quenched lifetime of CO in hydrocarbon flames", Appl. Spectr. **48**, 1118-24 (1994).
9. A. F. Mölisch and B. P. Ohery, *Radiation Trapping in Atomic Vapors* (Clarendon Press, Oxford, 1999).

Carbon Monoxide absorption spectroscopy using a diode-pumped continuous wave optical parametric oscillator

Angus Henderson, Pam Roper and Roy D. Mead,

Aculight Corporation
11805 N Creek Parkway S
Suite 113
Bothell
WA 98011
Tel. : 425 482 1100, fax : 425 482 1101
e-mail : angus@aculight.com

James R. Gord, Gregory J. Fiechtner, and George E. Tietz

Air Force Research Laboratory
Wright-Patterson Air Force Base
OH 45433

Summary

We have demonstrated for the first time long-term stable operation of a continuous wave optical parametric oscillator (CW OPO) pumped by a distributed bragg reflector (DBR) diode laser. We have also demonstrated the first use of a diode-pumped OPO in spectroscopic measurements. Continuous frequency scans through absorption features of Carbon Monoxide have been performed using the 2.3-μm OPO output. The OPO operates on a single longitudinal mode, with a bandwidth of 5MHz and an output power over 1mW in both signal and idler wavelengths. Continuous frequency scans of 9GHz have been demonstrated. Extension of the operating range of the OPO throughout the 1.1 to 3.6μm range will make such devices highly promising as room-temperature, low-cost, compact mid-infrared sources for numerous detection and spectroscopic applications.

The OPO uses an inexpensive, low-power (150-mW) DBR diode laser as a pump source. This source has several characteristics which make it suitable as a pump for a CW OPO. First, it operates stably on a single longitudinal mode with a measured bandwidth of less than 5MHz. Second, the diode frequency can be continuously tuned by as much as 50GHz without a mode hop, enabling continuous tuning of the OPO. Finally, the diode frequency can be rapidly modulated, allowing modulation of the OPO frequency and locking of the OPO frequency to absorption features. The diode output beam is focused through a Faraday isolator into a linear cavity OPO using periodically-poled lithium niobate (PPLN) as the nonlinear material. The OPO cavity is resonant at both signal and idler wavelengths, and the pump wave is double passed through the nonlinear crystal.

Output coupling of ~1% at signal and idler allows total OPO output of 18 mW to be obtained for 89 mW input power. OPO oscillation threshold is around 17mW. The PPLN is poled at 23.1-μm period to allow operation centered at 1.3 and 2.3 μm. Stable OPO operation requires precise control of OPO cavity length to maintain oscillation on the same signal and idler mode pair. This is achieved by implementing a dither-lock scheme, such that the diode current is modulated at up to 500kHz, and feedback is applied both to diode current and OPO cavity piezoelectric transducer (PZT). The high frequency component is fed back to the current and the low frequency component to the PZT. In this way the diode frequency is the frequency reference in the system. The diode frequency is significantly more passively stable than the frequency determined by the OPO cavity. Single-frequency operation has been observed without mode-hops for periods over one hour. OPO amplitude has been measured (at 1.3 μm) over a period of 15 minutes with a calculated standard deviation in amplitude <0.3% (figure 1). The linewidth of the OPO has been shown to be less than 60MHz using a confocal interferometer. According to previous investigations [1] , it is expected that the linewidth should match that of the pump source (<5MHz).

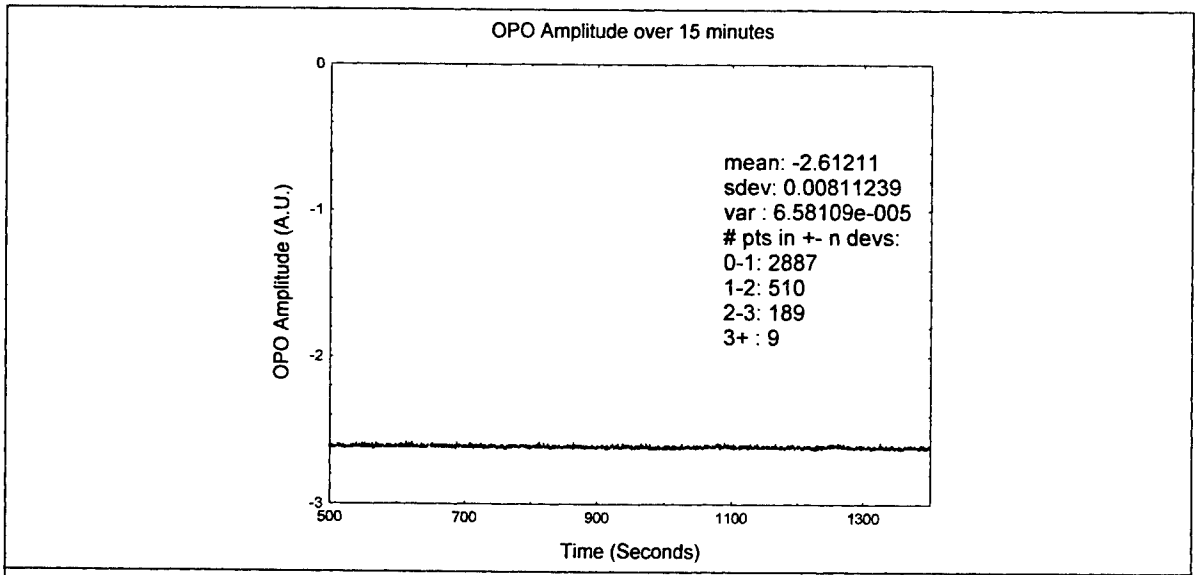

Figure 1 : OPO amplitude(negative) over a 15 minute period under 125kHz current dither / cavity stabilization. Standard deviation in amplitude is < 0.3%.

Continuous tuning of the OPO is obtained by applying an additional ramp voltage to the external input of the diode current supply while maintaining OPO cavity servo-lock. For a diode frequency scan of 14GHz, OPO signal frequency scanning of 9GHz and idler frequency scanning of 5GHz has been demonstrated. The OPO frequency has been scanned through carbon monoxide absorption features at 2.3 μm in a simple single-pass spectroscopy experiment (figure 2). OPO frequency scanning of up to 30GHz should be achievable using a cavity PZT with a greater travel range. We have also investigated rapid modulation of the OPO frequency. Frequency modulation is achieved by applying a rapid modulation of the diode current, while the cavity servo-control maintains locking of the OPO to the same cavity mode. Modulation at frequencies up to 800Hz with a range of 300MHz at the idler frequency has been demonstrated. Greater frequency range can be

obtained at lower modulation frequency. This capability will allow frequency modulation spectroscopy and locking of the OPO frequency to absorption lines to be performed. We intend to extend both modulation frequency and range.

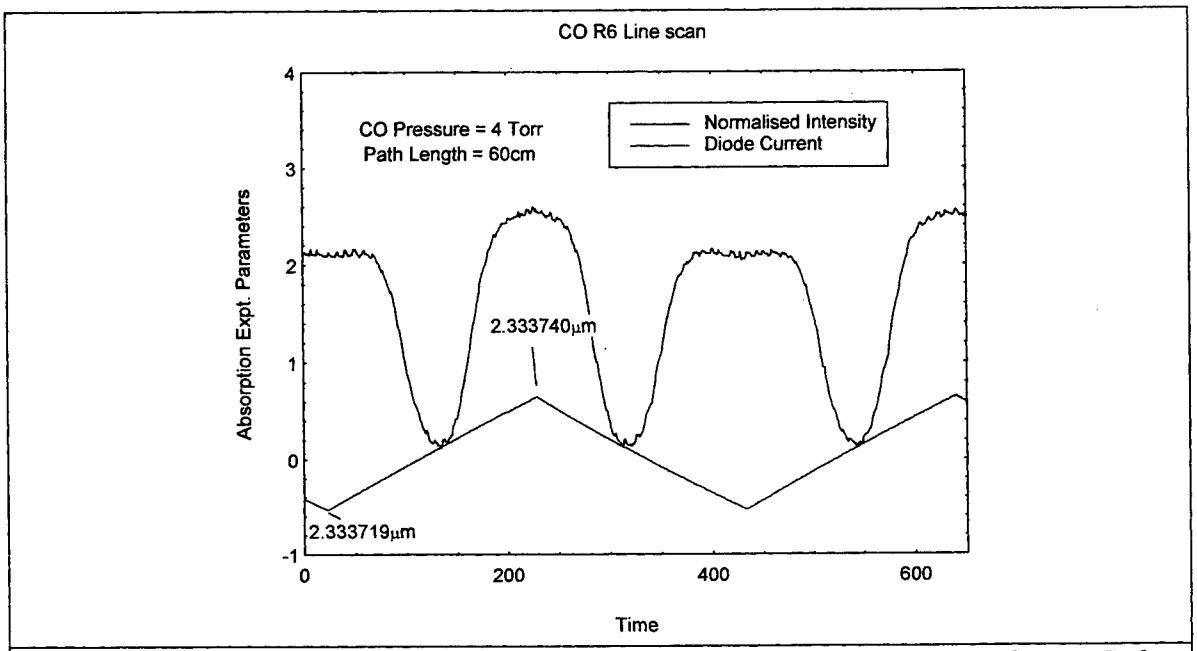

Figure 2 : 20pm wavelength scan of OPO idler wavelength through R6 absorption line in Carbon Monoxide, showing normalized transmitted amplitude through cell.

We are currently developing further OPO systems with idler wavelengths of 2.8μm, 3.2μm and 3.6μm. Such wavelength coverage will allow the OPO to be used in spectroscopic investigations of numerous species including N_2O, NO, CO and CO_2. These devices are compact, versatile, single-frequency sources, potentially tunable anywhere between 1.1 and 3.6 μm. Operating at room temperature or above, they offer significant advantages over current mid-infrared sources such as lead-salt diode lasers.

[1] C.D. Nabors, S.T. Yang, T. Day, and R.L. Byer, "Coherence properties of a doubly resonant monolithic optical parametric oscillator", J. Opt. Soc. Am. B. 7, 815-820 (1990).

A widely tunable cw Raman laser in H_2 pumped by an external cavity diode laser

L. S. Meng, P. A. Roos, K. S. Repasky, and J. L. Carlsten
Department of Physics, Montana State University, Bozeman, MT 59715
Phone: (406)994-6176, Fax: (406)994-4452, Email: carlsten@physics.montana.edu

Stimulated Raman scattering is conventionally studied in high-power and pulsed laser regimes. Continuous-wave (cw) Raman lasers have been realized but they have to operate near a molecular/atomic resonance utilizing the high Raman gain. The first non-resonant cw Raman laser was demonstrated by Brasseur, et al. in 1998 [1]. In this system, a frequency doubled cw Nd:YAG laser at 532nm was used as the pump source. The extremely low Raman gain far off resonance was compensated by placing the Raman gas between the mirrors of a high-finesse cavity (HFC). By high-reflective (HR) coating the HFC mirrors for both the pump and Stokes wavelengths, a threshold on the order of ~1mW was achieved. This indicated the possibility of pumping the cw Raman laser with conventional diode lasers. Roos et al. then demonstrated the first diode-pumped cw Raman laser [2]. A free-running laser diode was optically locked to an HFC and a threshold of 240μW was achieved.

Both of these cw Raman laser systems exhibited difficulty in wavelength tuning and the tuning ranges were limited. In this paper we choose an external-cavity diode laser (ECDL) as the Raman pump. Owing to the wide tuning range and wavelength selectivity of the ECDL, we obtain tunable cw Raman-shifted output in the NIR spectral region from 1174 to 1214nm. A 1.5GHz mode-hop-free continuous tuning is currently observed. Combined with its high spectral purity [3], this ECDL-pumped cw Raman laser becomes an attractive new laser source for high-resolution spectroscopy in the NIR spectral region.

Figure 1 shows the experimental setup. The ECDL pump source uses a 100mW laser diode with a center wavelength of 792nm in a Littman-style external cavity. The output beam has a 50dB side-mode suppression ratio and an 18nm tuning range from 789 to 807nm. The HFC consists of two curved mirrors of radii 50cm, spaced by 3 inches and HR coated for both the pump and Stokes wavelengths (finesse is about 60,000). The mirrors are enclosed within a hermetically sealed container filled with about 10atm H_2 gas. The ECDL and the HFC are frequency/phase locked together via the Pound-Drever-Hall locking technique [4].

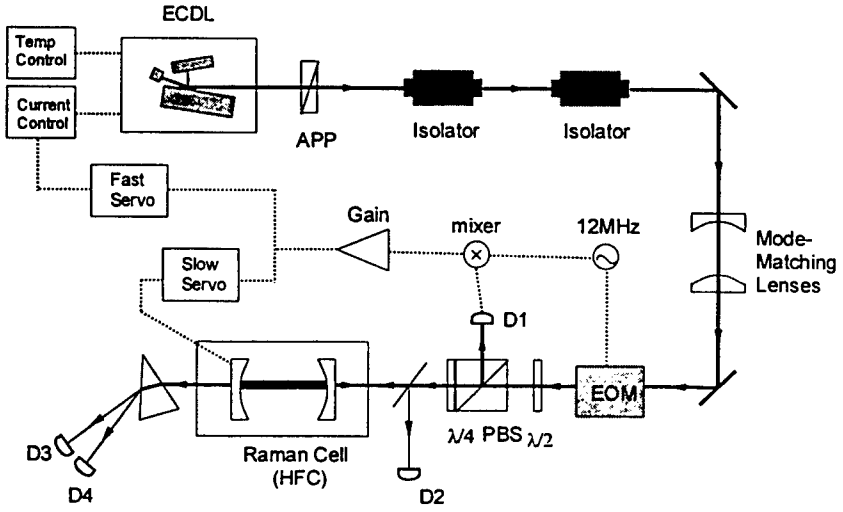

Figure 1: Experimental setup. APP = Anamorphic Prism Pair, EOM = Electro-optical Modulator, PBS = Polarizing Beam Splitter. Detector D1 receives the cavity reflected field to produce an error

signal for locking. Detectors D2, D3 and D4 are used to monitor the optical powers of the input pump, transmitted Stokes and pump respectively.

Figure 2(a) shows the measured Stokes and transmitted pump powers as functions of input pump power. The Stokes lasing threshold is observed to be 400 ± 30μW of coupled input pump power, (there is about 70% coupling efficiency from the incident pump beam into the fundamental HFC mode). The solid lines represent the theory given by Ref. 3 or 5, with the following parameters: λ_p = 795nm, λ_s = 1187nm, R_p = 0.99996, R_s = 0.99993, T_p = 33 parts in 10^6 (ppm), T_s = 20ppm, and α_g = 0.82×10^{-9} cm/W. Figure 2(b) shows the photon conversion efficiency as a function of the input pump power. The maximum photon conversion efficiency is 12 ± 1% occurring at 1.6mW coupled input pump power.

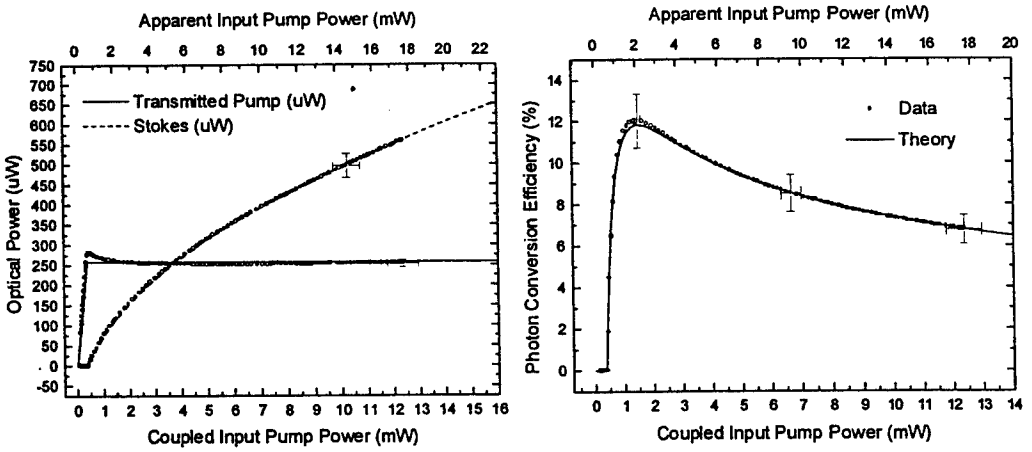

Figure 2: (a) Measured power (circles) of the Stokes and transmitted pump as a function of the input pump power. Lines represent the theory. (b) The photon conversion efficiency as a function of the input pump power.

This cw non-resonant Raman laser exhibits wide discrete tunability in the NIR region. The ECDL we use as the pump laser emits a single longitudinal-mode when tuned from 789nm to 807nm, resulting in cw Stokes form 1174nm to 1214nm (the Raman shift in H_2 is 4155cm^{-1}). Figure 3 shows the extremes of range for the pump and Stokes beams as measured by an optical spectrum analyzer.

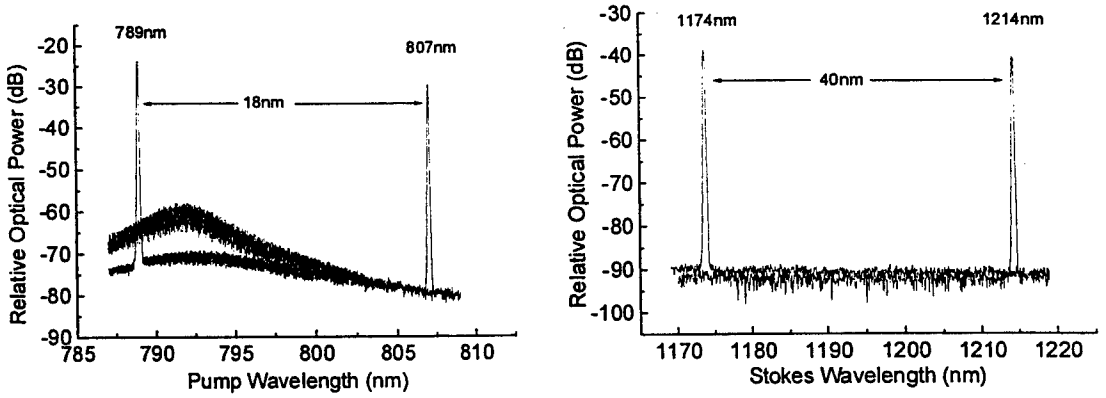

Figure 3: Tunability of the ECDL-pumped cw Raman laser. 18nm wavelength range of the pump (left) results in 40nm tunable Stokes (right). The wavelength measurements are taken by a HP optical spectrum analyzer.

Due to the limited Raman gain linewidth (about 500MHz FWHM in 10atm H_2 [6]) and therefore a double cavity resonance requirement for the pump and Stokes, a full-range continuous tuning of the

Stokes is not possible under the current configuration. As shown in figure 4 we observe ~1.5GHz continuous tuning with a fundamental Gaussian spatial mode of the Stokes emission. At various input pump power, the Stokes output power is measured when the frequency of the ECDL pump laser is tuned. Note that at high pump levels (>8 times threshold) the output Stokes power increases as it is tuned away form the Raman gain line center. This is due to the fact that Stokes conversion efficiency reaches a maximum at four times threshold while tuning away from the Raman gain line-center raises the threshold. Due to this effect, at pumping levels between 4 and 8 times of threshold, the output Stokes power remains relatively constant when its frequency is tuned. The continuous tuning of Stokes laser is expected to have broader range for higher H_2 pressure and different HFC parameters.

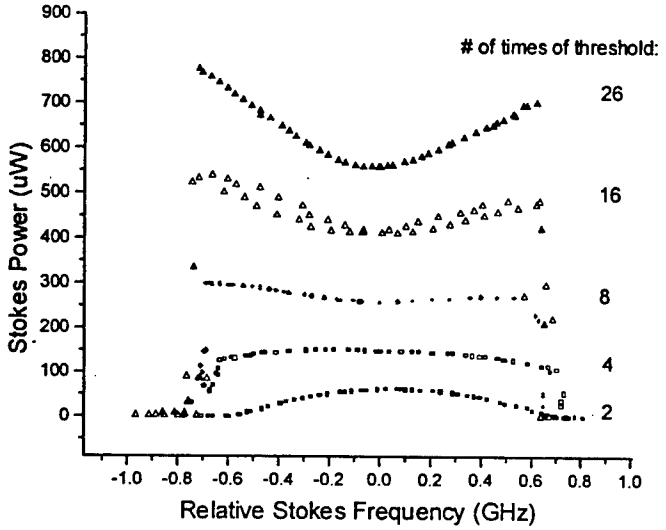

Figure 4: Continuous tuning characteristics of the Stokes output. Stokes power vs. frequency tuning is measured at different pumping level: 2, 4, 8, 16, and 26 times of threshold respectively. The optical frequency is measured by a Berleigh wavemeter.

Such an ECDL-pumped cw Raman laser is able to cover from visible to 4μm spectral region by use of the existing laser diodes and different Raman media [5]. Together with its tunability and spectral purity [3], it becomes a new promising laser source for atomic physics study and high-resolution laser spectroscopy. This work is supported by National Science Foundation grant 9731602.

References:

[1] J. K. Brasseur, K. S. Repasky, and J. L. Carlsten, "Continuous-wave Raman laser in H_2", Opt. Lett. **23**, 367 (1998)

[2] P. A. Roos, J. K. Brasseur, and J. L. Carlsten, "Diode-pumped nonresonant continuous-wave Raman laser in H_2 with resonant optical feedback stabilization", Opt. Lett. **24**, 1180 (1999)

[3] J. K. Brasseur, P. A. Roos, K. S. Repasky, and J. L. Carlsten, "Characterization of a continuous-wave Raman laser in H_2", J. Opt. Soc. Am. B **16**, 1305 (1999)

[4] R. W. P. Drever, J. L. Hall, F. V. Kowalski, J. Hough, G. M. Ford, A. J. Munley, and H. Ward, "Laser phase and frequency stabilization using an optical resonator", Appl. Phys. B **31**, 97 (1983)

[5] K. S. Repasky, J. K. Brasseur, L. Meng, and J. L. Carlsten, "Performance and design of an off-resonant continuous wave Raman laser". J. Opt. soc. Am. B **15**, 1667 (1998)

[6] W. K. Bischel and M. J. Dyer, "Temperature dependence of the Raman linewidth and line shift for the Q(1) and Q(0) transitions in normal and para-H_2", Phys. Rev. A, **33**, 3113 (1986)

Time-Resolved Optical Heterodyne Detected Raman Induced Kerr Effect Spectroscopy for Chemical Analysis

Napoleon Thantu (MS 2211)
Physics Department
Idaho National Engineering and Environmental Laboratory
2525 North Fremont Avenue
Idaho Falls, ID 83415
(208) 526-5065

Coherent light scattering techniques such as CARS (coherent anti-Stokes Raman scattering) are especially useful in probing adverse environments such as flames and plasmas.[1] Phase matching requirements lead to a coherent signal output that is highly directional, permitting spatial filtering of the signal from background radiation. Use of single frequency lasers requires a second laser to scan the Raman-active vibrational frequency spectrum of the material of interest, and can lead to a complex and spatially non-compact instrumentation for field work. On the other hand, a complete Raman spectrum can be potentially obtained in a single laser shot by use of a broad band laser source. In this paper, we describe a time-domain approach that relies upon a broad band, femtosecond laser source that is sensitive to weak depolarized intermolecular and intramolecular Raman modes that can be used as signatures to distinguish chemical species. This so-called femtosecond optical heterodyne detected Raman induced Kerr effect spectroscopy (OHD-RIKES) in one form or another has been employed by many ultrafast laser laboratories in their studies on ultrafast dynamics in condensed phases. Although femtosecond OHD-RIKES and traditional frequency-domain depolarized light scattering experiments extract the same information, OHD-RIKES more reliably reveal the very low frequency information of the intermolecular Raman spectrum. This low frequency region is sensitive to inhomogeneities of the intermolecular environment, temperature, and molecular symmetery. We demonstrate this technique by employing aniline (benzene with one of its hydrogen atoms substituted with a NH_2 amino group) as the chemical species.

For the sake of completeness we briefly describe the experimental apparatus, although it has been accounted for in detail elsewhere, and the Fourier transform procedure for extracting the intermolecular and intramolecular frequency spectrum.[2] Figure 1 is a schematic of the experimental apparatus.

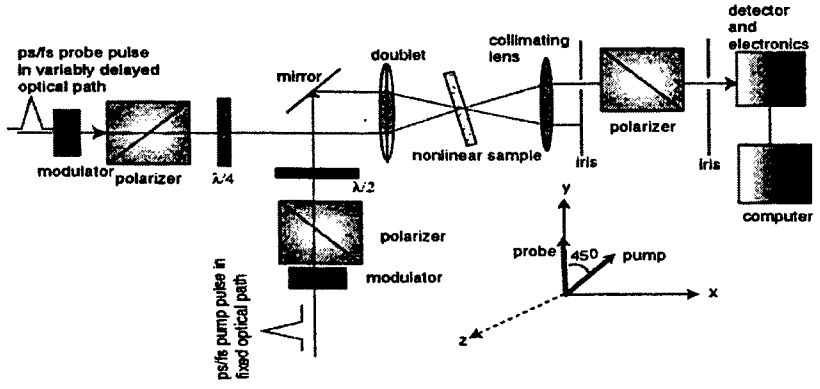

Figure 1. Femtosecond OHD-RIKES apparatus and the pump and probe polarizations.

40 fs optical pulses centered near 800 nm that originate in a Kerr-lens modelocked Ti:Al_2O_3 laser is spilt into pump and probe pulses. The strong pump pulse traverses a fixed optical path while the much weaker probe pulse traverses a computer-controlled, variably delayed optical path. The axis of the polarizer in the probe path before the sample is normally aligned with the probe polarization. In absence of the pump pulse, the probe pulse is blocked by the polarizer (analyzer) behind the sample. The pump pulse induces a third-order nonlinear optical Kerr

response in the material. Interaction between the probe pulse and the induced nonlinear optical response leads to rotation of the probe polarization in the x-y plane, and therefore leakage of the probe intensity through the analyzer. Variably delaying the probe pulse with respect to the pump pulse permits temporal mapping of the evolution of the material nonlinear optical response induced by the strong pump pulse. The coherent local oscillator in the heterodyned measurement is introduced through the rotation of the probe polarizer by ~ 1° while keeping the fast axis of the quarter-wave plate aligned with the probe polarization direction. This local oscillator is out of phase with respect to the probe polarization in the y-direction by 90° and is a small fraction of the probe field. The effect of the local oscillator is the mixing of the signal field and the local oscillator field. This heterodyned signal, proportional to $\mathrm{Re}(E_s^* E_{LO} + E_s E_{LO}^*)$ where E_s is the signal field and E_{LO} the local oscillator field, is phase-detected by a lock-in amplifier and chopping the pump beam. The transmitted signal through the analyzer is given by

$$E_s \propto i\chi_{eff}^{(3)} I_{pump} E_{probe}\,, \tag{1}$$

where $\chi_{eff}^{(3)}$ is the third-order effective nonlinear susceptibility. For the pump and probe configuration as defined in Figure 1,

$$\chi_{eff}^{(3)}(t) = \chi_{xxyy}^{(3)}(t) + \chi_{xyxy}^{(3)}(t)\,. \tag{2}$$

Depending on the direction of rotation of the probe polarizer, the local oscillator field is given by $E_{LO} = \pm i\varepsilon E_{probe}$, where ε is a small number such that $\sin\varepsilon \approx \varepsilon$. The heterodyned intensity is then proportional to

$$I_H \propto \pm \mathrm{Re}\left[i\chi_{eff}^{(3)} I_{pump} I_{probe}\right]. \tag{3}$$

The heterodyned signal is rigorously separated from the non-heterodyned intensity $|E_s|^2$ by performing measurements with both clockwise and counter clockwise directions of rotation and constructing the difference between the two measurements. The heterodyned transmission function of the nonlinear optical Kerr cell in Figure 1 follows from (3) and is given by

$$\begin{aligned} T(\tau) &= \int_{-\infty}^{\infty} \mathrm{Re}\,\chi_{eff}^{(3)}(t) < I_{pump}(t) I_{probe}(\tau - t) > dt \\ &= G_0^{(2)}(\tau) * R_{eff}(\tau)\,, \end{aligned} \tag{4}$$

where the bracketed term is the zero-background second order intensity autocorrelation function of the pump and probe pulses (denoted by $G_0^{(2)}(\tau)$ in the second line) and $R_{eff}(t) \propto \chi_{eff}^{(3)}(t)$ is the material impulse response function in the time domain. The intensity autocorrelation function is easily measured by replacing the aniline sample cell with a KDP crystal and measuring the second harmonic intensity as a function of the probe delay. The intensity autocorrelation function is indeed the instrument function of the apparatus. Fourier transformation of $T(\tau)$ gives a product of the Fourier transform of $G_0^{(2)}(\tau)$ and the Fourier transform of $R_{eff}(\tau)$. The frequency response spectrum of the material is given by

$$\chi_{eff}^{(3)}(\Delta\omega) = FT\left\{R_{eff}(\tau)\right\} = \frac{FT\left\{T(\tau)\right\}}{FT\left\{G_0^{(2)}(\tau)\right\}}, \tag{5}$$

where FT indicates Fourier transform operation and $\Delta\omega$ is the difference between various Fourier components of the pump pulse. The energy conservation diagram is the same as that of CARS except that the Raman excitation frequency, $\Delta\omega$, is supplied by a single pulse, instead of by two different laser fields. All of the information on the material nuclear response is contained in $\mathrm{Im}\,\chi_{eff}^{(3)}(\Delta\omega)$.

Measured transients for $T(\tau)$ contain contributions associated with electronic and nuclear degrees of freedom. The contribution stemming from diffusive reorientation of oscillators

that leads to relaxation of optically induced anisotropy is removed by a tail-matching procedure described in reference 2b. The electronic contribution is instantaneous and is removed from the frequency response spectrum through the deconvolution procedure in (5). Figure 2 shows measured femtosecond OHD-RIKES transients for aniline. Figure 3 is the

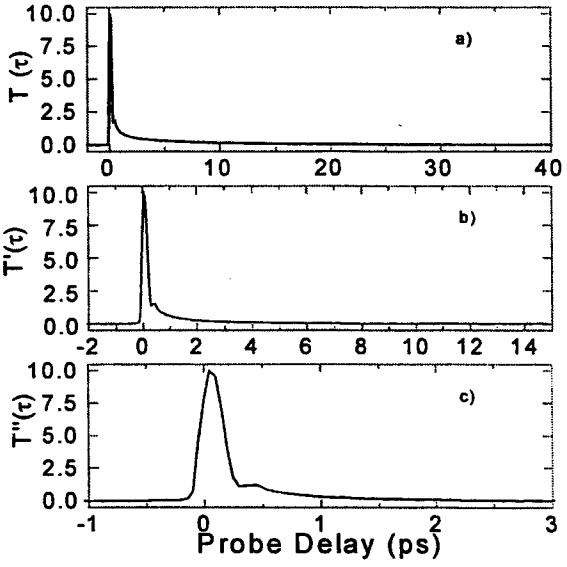

Figure 2. a) Raw data; b) slower diffusive reorientation component substracted; and c) faster diffusive reorientation component subtracted.

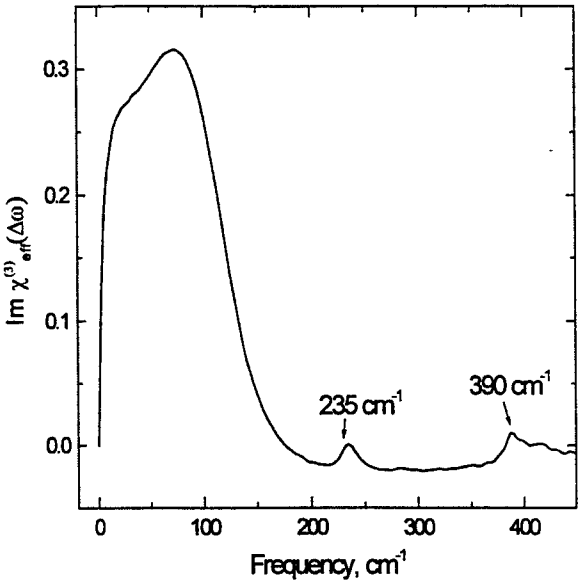

Figure 3. Frequency response spectrum.

resultant $\mathrm{Im}\,\chi^{(3)}_{eff}(\Delta\omega)$ after performing the tail-matching procedure and the deconvolution procedure. The low frequency (0-150 cm^{-1}) portion is identified as the intermolecular modes associated with collective librational motions and intermolecular interactions that lead to the distortion of molecular polarizabilities. This spectral region has a distinct shape (i.e., bimodal for aniline) and width that depend on the molecular symmetry, the environmental conditions (temperature, pressure, etc.) and inhomogeneities, and the intermolecular potential. In light scattering measurements, this low frequency portion is weighted by the Bose-Einstein prefactor $\left[1-\exp(-\hbar\Delta\omega/kT)\right]^{-1}$, which distorts the lineshape.[2a] Two high frequency bands at 235 cm^{-2} and 390 cm^{-1} are, respectively, intramolecular Raman-active modes 10b and 15 that correspond to out-of-plane and in-plane motions involving the NH_2 substituent. All of the depolarized intramolecular modes that lie within the laser bandwidth can be excited. In summary, the time-domain technique such as femtosecond OHD-RIKES may be used to perform spectroscopic analysis of chemical species. Its potentially simple and compact instrumentation and high S/N may find utility in chemical species analysis in adverse environments.

References

1) J. P. Singh and F. Y. Yueh, Combustion and Flames **89**, 77 (1992).
2) a) W. T. Lotshaw, D. McMorrow, N. Thantu, J. S. Melinger and R. Kitchenham, J. Raman Spectroscopy **26**, 571 (1995); b) C. Kalpouzos, D. McMorrow, W. T. Lotshaw and G. Kenney Wallace, J. Phys. Chem. **91**, 2028 (1987); c) N. Thantu, J. S. Melinger, D. McMorrow, and B. L. Justus, Nonlinear Optics **23**, (1999).

Demonstration of a 200 cm^{-1} Continuous Scan in the Mid-Infrared With a PPLN-Based OPG/OPA Lightsource

Kenneth W. Aniolek, Thomas J. Kulp*, Serdar Yeralan, and Scott E. Bisson

Combustion Research Facility, Sandia National Laboratories, Livermore, CA 94550
**tjkulp@sandia.gov*

In this paper, results are presented that demonstrate an infrared cavity ringdown spectrometer capable of rapid, uninterrupted tuning over a spectral range of over 200 cm^{-1}. This work addresses the need for a fieldable infrared sensor that can fully exploit the high sensitivity and specificity offered by laser-based IR spectroscopy when conducted in the fundamental absorption regions. To achieve maximum specificity, such a device would tune over significant fractions the fundamental absorption regions near 8-14 μm and 3-5 μm. This would allow measurement of multiple vibrational band systems of larger molecules in addition to resolving individual rovibrational lines of smaller species. The system described here is shown to tune continuously over 200 cm^{-1} segments in the latter spectral window. By combining more than one continuous scan, it is possible to cover the full CH-stretching range (3.1-3.7 μm). Ultimately, tuning is limited only by the spectral bandwidth (600 cm^{-1}) of the ringdown mirrors that are used. Future systems can extend this technique to the 8-14 μm window.

The cavity ringdown spectrometer is enabled by the combination of three new technologies: a single-frequency diode-pumped Nd:YAG microlaser, the quasi-phasematched nonlinear material periodically-poled lithium niobate (PPLN), and a high-finesse fiber-optic microetalon developed for telecommunication applications. Details of the system using a less capable free-space etalon are described elsewhere.[1-3] A system diagram is shown in Figure 1. It consists of a PPLN-based optical parametric generator (OPG) - optical parametric amplifier (OPA) cascade that is pumped by the Nd:YAG microlaser (120 Hz). The OPG crystal generates broad (~10-15 cm^{-1} FWHM) parametric fluorescence centered at signal and idler frequencies determined by the phasematching condition of the PPLN crystal. The signal beam is coupled into the fiber etalon where it is spectrally-filtered to a narrow bandwidth. The OPA amplifies the signal and idler beams at energies (1-10 μJ) that are useable for cavity ringdown spectroscopy.

Frequency tuning of the OPG/OPA output is performed by simultaneously varying the PPLN poling periods (center frequency of the gain curve) and microetalon transmission frequency. The poling period varies continuously along the transverse dimension of the PPLN crystal (called a "fan-out" structure); therefore, translation of the crystals tunes the PPLN gain frequency in a smooth and seamless manner. The poling periods vary continuously from 29.7 to 30.1 μm, allowing complete coverage of the 2800-3100 cm^{-1} idler region. Both crystals are mounted on translation stages driven by stepper motors. The single-mode microetalon (Micron Optics, 1 x 1 x 6 cm exterior dimensions) contains a small air-gap between the mirror surfaces for continuous variation of its transmission frequency, the length of which is adjusted by a 0-10 V piezoelectric

transducer. The current microetalon has a finesse of 730 and a free-spectral-range of 240 cm^{-1}, resulting in a transmission bandwidth (laser resolution) of 0.33 cm^{-1} (fwhm). This is not a limiting factor, however, as we are currently testing another microetalon with a bandwidth of 0.05 cm^{-1}. It should be pointed out that the pulsed damage threshold for these etalons is unknown. Experimental determination of this value is currently underway with a test etalon provided by the manufacturer.

Frequency scanning and data collection is automated remotely via a PC running LabVIEW. A GaGe compuscope card is used for ringdown signal acquisition. Two other PCI cards send out voltage ramps to the stepper motors (NI Motion Control card) and microetalon (NI E-Series DAQ card). The stepper motor position and etalon voltage is adjusted prior to ringdown signal acquisition and shot averaging. The LabVIEW program calculates the absorption intensity and displays it real-time.

Figure 2 shows a continuous 200 cm^{-1} scan taken with the 0.33 cm^{-1} bandwidth microetalon. For better sensitivity, 100 shots were averaged per data point, resulting in a total data acquisition time of 15 minutes, or 0.2 cm^{-1}/second. For an even faster data acquisition time, shot averaging can be turned off at the expense of detection sensitivity. In this manner, the scan in Figure 2 could, in principle, be acquired in under 10 seconds. The idler energy was 0.3 μJ, although energies as large as 5 μJ have been obtained with the microetalon. It should be pointed out that the data in Figure 2 contain a significant amount of saturation due to the low-bandwidth detector used and is unsuitable for quantification; the intention of this figure is to merely demonstrate the scanning capabilities of the system. We are currently testing the system with a 0.05 cm^{-1} etalon and faster ringdown detector, which will minimize any spectral broadening effects due to a large laser spectral-bandwidth and long detector rise-time.

Figure 3 shows a method of scanning when using a bulky commercially-available air-spaced etalon employing free-space optics. Continuous scanning was limited to shorter segments (~ 15 cm^{-1}) by the high-voltage piezo-driver that ramped the air-space length. Although the continuous short scans could be combined together to form longer scans (350 cm^{-1} in Figure 3), the etalon and crystals had to be manually synchronized prior to each scan, resulting in a rather lengthy (several hours) and laborious process.

In summary, we have demonstrated a narrow band infrared spectrometer capable of rapid and uninterrupted tuning over 200 cm^{-1}. To our knowledge, there is no compact pulsed laser source available with similar capabilities. The availability of other high-finesse microetalons make possible the construction of a spectrometer with a similar scanning capability (> 100 cm^{-1}) at a higher resolution (≥ 0.05 cm^{-1}).

References

[1] Aniolek, K. W., Powers, P. E., Kulp, T. J., Richman, B. A., and Bisson, S. E., *Chem. Phys. Lett.* **302,** 555 (1999).

[2] Aniolek, K. W., Kulp, T. J., Richman, B. A., Bisson, S. E., Schmitt, R. L., and Powers, P. E., *Proc. 44th Annual Meeting SPIE* **3758-08,** 62 (1999).

[3] Aniolek, K. W., Schmitt, R. L., Kulp, T. J., Richman, B. A., and Bisson, S. E., *Opt. Lett.* in press.

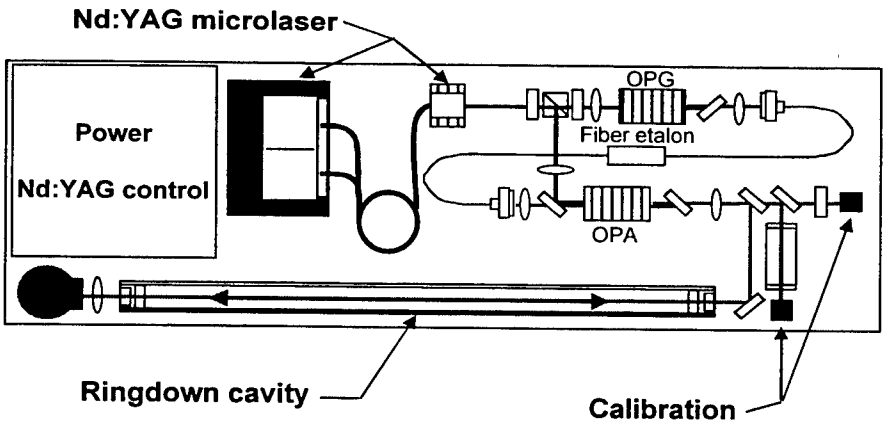

Figure 1. Block schematic of the infrared cavity ringdown spectrometer.

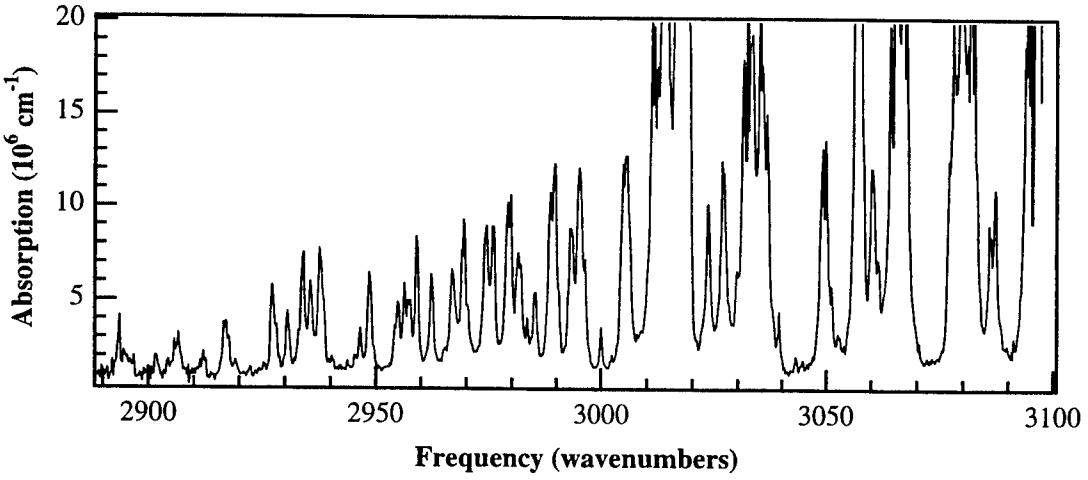

Figure 2. Demonstration of a continuous 200 cm^{-1} scan comprised of a single etalon sweep.

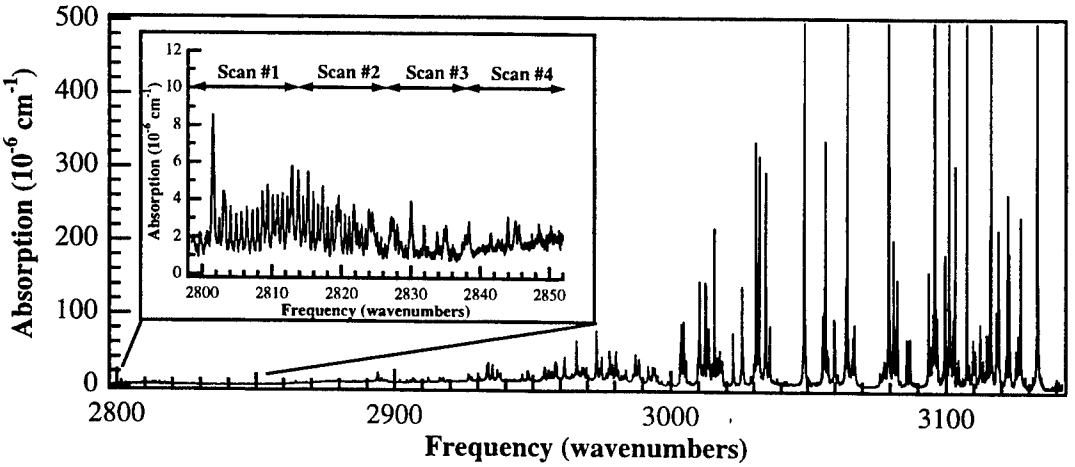

Figure 3. Demonstration of a 350 cm^{-1} scan comprised of 27 individual etalon scans.

Laser Applications to Chemical and Environmental Analysis VII

Title: US Army Sponsored Activities in LIBS Research, Applications, and Commercialization

Authors: Andrzej W. Miziolek, Kevin L. McNesby, Richard T. Wainner,
and Robert G. Daniel

Army Research Laboratory
AMSRL-WM-BD
Aberdeen Proving Ground, MD 21005-5069
Miziolek@arl.mil

Patrick D. French and Frank Sagan
ADA Technologies, Inc.
Littleton, CO 80127-4107

Russell Harmon
Army Research Office
Research Triangle Park, NC 27709-2211

Short Abstract

Laser Induced Breakdown Spectroscopy (LIBS) is a chemical analytical technique in the early stages of commercialization. The US Army has promoted the development of this technology through the Small Business Innovation Research (SBIR) program. This poster describes recent research activities, specific Army applications, and progress and challenges in the commercialization of LIBS technology.

US Army Sponsored Activities in LIBS Research, Applications, and Commercialization

Summary

ADA Technologies, Inc. has recently developed two prototype portable LIBS instruments under the sponsorship of the US Army's Small Business Innovation Research (SBIR) Phase I and Phase II programs, coordinated through the Army Research Office and Weapons and Materials Research Directorate of the Army Research Laboratory. Army interests in LIBS technology derive from a variety of military and environmental quality needs related to the detection of hazardous chemicals. For example, the detection of explosives or chemical warfare agents is an area of particular military interest, whereas the detection of toxic metals in soil is a high-priority environmental quality requirement (1).

On the environmental quality side, the Army has a need to detect, without recourse to conventional drilling or to conventional laboratory analysis, the chemical character of soil in areas that may have been contaminated by Army manufacturing, testing, operational, or maintenance activities. Of particular interest are new approaches or techniques (such as LIBS) for in-situ, non-intrusive, and point-source chemical characterization of surface materials and the spatial distribution of chemical constituents. Methods of real-time data integration and visualization are needed to support this requirement.

A rigorous program of field testing is an important component of the Phase II project. During 2000, the capability of the prototype LIBS system to detect Pb in painted surfaces will be field tested on WWII-age buildings at Ft Carson, CO. Also, attempts to semi-quantitatively measure Pb in soils will be made in an area of Pb-contaminated soil at the Sierra Army Depot, CA.

The goal at the inception of the SBIR project was to develop a field portable instrument suitable for mapping multi-metals contamination in soils at DOD facilities. During the Phase II program several additional applications were identified where it would be useful to measure contamination on surfaces and/or swipes. To address the various user needs, two different LIBS instruments were developed under the Phase II program along with the necessary support equipment. Externally both instruments look virtually identical. The figure below shows the overall LIBS instrument on the left and a close-up of the sampling wand with the optional borescope attachment on the right.

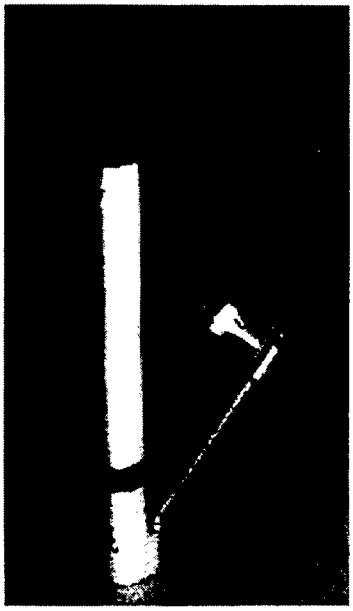

The sampling wand houses the laser head, the focusing optics, and a fiber optic pick-up. The sampling wand also has a pressure switch on the bottom to insure that the laser will not fire unless the wand is against a surface. The borescope allows the user to point the laser at specific particles on a surface. There are three modes of potential operation of the instrument. The first mode of operation is to point the sample wand using the borescope at a specific particle on a surface to obtain an elemental analysis of that particle. This mode of operation will be especially useful for forensics applications. The second mode of operation is to perform a field survey of a site (soil or surfaces) by moving the sample wand over the surface of interest and measuring hundreds of samples at various locations. This mode is particularly useful for getting a general map of contamination (concentration and location) at a site in real-time. This information can be used to define any additional sampling that might be required for regulatory purposes. By performing this quick survey, the user can save a significant amount of time and money sending samples out for ICP analysis. The problem with this mode of operation is that the variability in the sample surfaces (moisture, base material, surface irregularities, etc.) can introduce large errors into the readings that may or may not be important for the particular application. For situations where the sampling errors need to be minimized, a set of ancillary equipment has been developed to reduce or eliminate the variability in the samples. This third mode of operation requires the user to collect and prepare a sample before analysis. For soils this means that a soil sample is collected and compressed in a small aluminum pan. If the soil sample has a high moisture content, it may be necessary to dry it prior to LIBS analysis. The apparatus for preparing the soils samples is shown in the following figure.

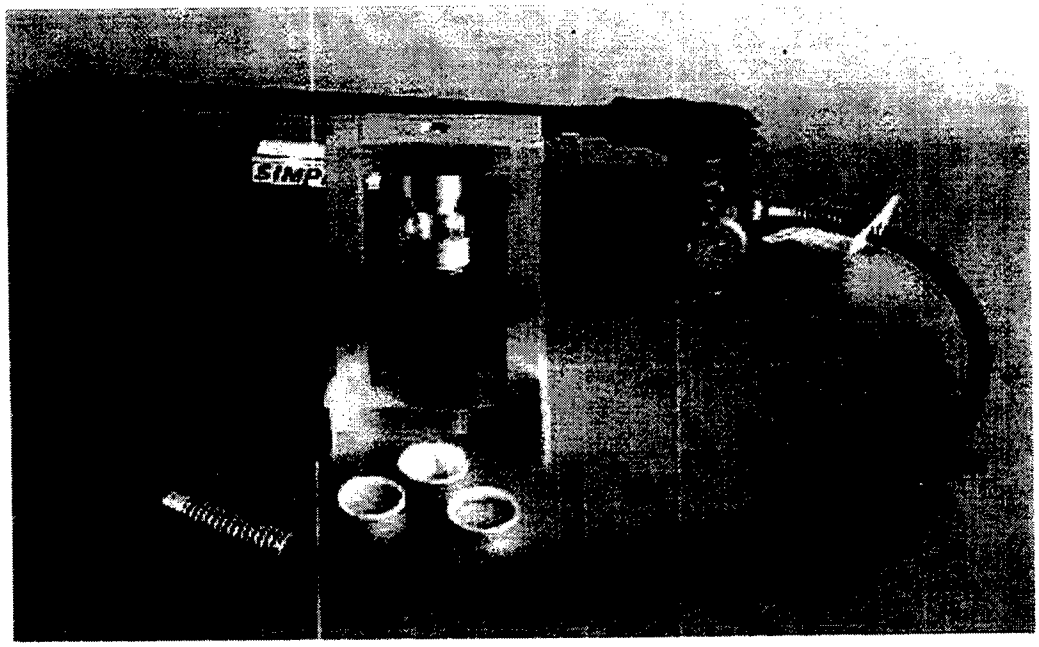

For surfaces, a swipe sample can be taken. A swipe sample is simply a piece of filter paper that has been rubbed across a surface. Both the filter size and the size of the area over which it is rubbed must be kept uniform to obtain comparable results. At this point, the swipe sample or the soil sample is placed into a sampling carousel that moves the sample under the laser head. The sampling carousel has been designed to insure that each sample point represents an equal area of the sample.

The difference in the two LIBS instruments developed by ADA under this Phase II contract becomes apparent at the time of data analysis. The first instrument developed is a multi-spectral unit capable of capturing the entire spectrum from 300nm to 800nm. This unit uses four fixed-wavelength spectrograph/detectors to collect this range. The modular nature of the design allows ADA to use any number of spectrograph/detectors to capture the spectral regions of interest. For the multi-spectral unit, photodiode array detectors are used. The large spectral range means the instrument can be used to fingerprint compounds. By identifying a series of peaks from a single microplasma event, various compounds should be identifiable. For applications where high spectral resolution and very low detection limits are necessary, ADA's second LIBS instrument is appropriate. The second LIBS instrument has a single wavelength-adjustable spectrograph (25nm range) with a backside thinned CCD. This instrument is capable of separating peaks that might overlap and the high sensitivity CCD is capable of detecting very low light levels down to 200nm. The software is similar for both instruments with the exception of the overall spectral range.

The Army Research Laboratory has been active in LIBS research for over a decade (2-7). Recently we have concentrated on the application of LIBS for detection of hazardous chemicals of military interest such as explosives and chemical warfare agents. The use of LIBS for molecular detection is rather novel, since the bulk of previous LIBS research has been concentrated on the detection of metals, usually at trace concentration. Traditionally, the metals have been detected by analyzing a rather small wavelength region where the metals emit. Our approach to molecular detection is based on capturing the full emission spectrum from each individual microplasma event which contains spectral information from nearly all constituent elements from the analyzed compound(s). Sensitivity of the LIBS technique is greatly enhanced when the sample size matches the beam waist at the focal point (micron range). In this case, when the laser beam hits a small particle or droplet, then the produced plasma consists of the chemical information for only the sample. Since the single shot plasma emission can be captured by the detector and spectrally analyzed, then the sensitivity can be especially high (nanograms). Examples of single-shot spectra of hazardous compounds are provided.

References-

1) D.A. Cremers, J.E. Barefield, and A.C. Koskelo, "Remote Elemental Analysis by Laser-Induced Breakdown Spectroscopy Using a Fiber Optic Cable", Appl. Spectrosc., Vol. 49, p. 857, 1995.

2) J.B. Morris, B.E. Forch, and A.W. Miziolek, "A Novel Detector for Gas Chromatography Based on UV Laser-Produced Microplasmas", Appl. Spectrosc., Vol. 44, p. 1040, 1990.

3) R.J. Locke, J.B. Morris, B.E. Forch, and A.W. Miziolek, "A UV Laser Microplasma-Gas Chromatography Detector: Detection of Species-Specific Fragment Emission", Appl. Opt., Vol. 29, p. 4987, 1990.

4) J.B. Simeonsson and A.W. Miziolek, "Time-Resolved Emission Studies of ArF Laser Produced Microplasmas", Appl. Opt., Vol. 32, p. 939, 1993.

5) J.B. Simeonsson and A.W. Miziolek, "Spectroscopic Studies of Laser-Produced Plasmas Formed in CO and CO_2 Using 193, 266, 355, 532, and 1064 nm Laser Radiation", Appl. Phys. B, Vol. 59, p. 1, 1994.

6) C.K. Williamson, R.G. Daniel, K.L. McNesby, and A.W. Miziolek, "Laser-Induced Breakdown Spectroscopy (LIBS) for Real-Time Detection of Halon Alternative Agents", Anal. Chem., Vol. 70, p. 1186, 1998.

7) E.D. Lancaster, K.L. McNesby, R.G. Daniel, and A.W. Miziolek, "Spectroscopic Analysis of Fire Suppressants and Refrigerants by Laser-Induced Breakdown Spectroscopy", Appl. Opt., Vol. 38, pp. 1476-1480, 1999.

Aniolek, Kenneth W. ■ PD6

Axner, Ove ■ PD1

Bisson, Scott E. ■ PD6

Carlsten, J.L. ■ PD4

Daniel, Robert G. ■ PD7

Di Teodoro, F. ■ PD2

Farrow, R. L. ■ PD2

Fiechtner, Gregory J. ■ PD3

French, Patrick D. ■ PD7

Gord, James. R. ■ PD3

Harmon, Russell ■ PD7

Henderson, Angus ■ PD3

Kluczynski, Pawel ■ PD1

Kulp, Thomas J. ■ PD6

Lindberg, Asa M. ■ PD1

McNesby, Kevin L. ■ PD7

Mead, Roy D. ■ PD3

Meng, L.S. ■ PD4

Miziolek, Andrzej W. ■ PD7

Repasky, K.S. ■ PD4

Rehm, J.E. ■ PD2

Roos, P.A. ■ PD4

Roper, Pam ■ PD3

Sagan Frank ■ PD7

Thantu, Napoleon ■ PD5

Tietz, George E. ■ PD3

Wainner, Richard T. ■ PD7

Yeralan, Serdar ■ PD6

Laser Applications to Chemical and Environmental Analysis

Technical Program Committee

Mark G. Allen, *Physical Sciences Inc., USA, General Chair*
Robert W. Shaw, *Oak Ridge Natl. Lab., USA, General Chair*
Volker Sick, *Univ. of Michigan, USA, General Chair*
David J. Rakestraw, *Sandia Natl. Labs., USA, Program Chair*
Markus Sauer, *Univ. of Heidelberg, Germany, Program Chair*
Alan C. Stanton, *Southwest Sciences, Inc., USA, Program Chair*
William P. Ambrose, *Los Alamos Natl. Lab., USA*
Douglas S. Baer, *Stanford Univ., USA*
Jay B. Jeffries*, *SRI Intl., USA*
Kevin L. McNesby, *ARL, USA*
Peter Werle, *Fraunhofer Inst. for Atmospheric Environmental Res., Germany*

**Denotes OSA Technical Council Representative*